

**EXPERIMENTAL AND THEORETICAL
FLOW STUDIES IN THE RETURN CHANNEL PASSAGES
OF A CENTRIFUGAL COMPRESSOR STAGE**

A Thesis

Submitted

*in the partial fulfillment of the requirements for
the award of the degree of*

DOCTOR OF PHILOSOPHY

in

FACULTY OF MECHANICAL ENGINEERING

By

**K. SRINIVASA REDDY
(REG. NO: 0503PH1522)**



**RESEARCH AND DEVELOPMENT CELL
JAWAHARLAL NEHRU TECHNOLOGICAL UNIVERSITY HYDERABAD
KUKATPALLY, HYDERABAD – 500 085
INDIA
AUGUST 2010**

DECLARATION

I hereby declare that the work described in this thesis, entitled ***"Experimental and Theoretical Flow Studies in the Return Channel Passages of a Centrifugal Compressor Stage"*** which is being submitted by me in partial fulfillment for the award of **Doctor of Philosophy (Ph.D.)** in the **Dept. of Mechanical Engineering** to the **Jawaharlal Nehru Technological University Hyderabad**, Kukatpally, Hyderabad (A.P.)-500 085, is the result of investigations carried out by me under the Guidance of **Dr. G.V.Ramana Murty**, Professor and Head, Department of Mechanical Engineering, Vasavi College of Engineering, Hyderabad, and **Dr.K.V.Sharma**, Professor, Faculty of Mechanical Engineering, University Malaysia, Pahang, Malaysia.

The work is original and has not been submitted for any Degree/Diploma of this or any other university.

Place:

Date:

Signature

(K.Srinivasa Reddy)

(Reg.No. 0503PH1522)

CERTIFICATE

This is to certify that the thesis entitled "***Experimental and Numerical Flow Studies in the Return Channel Passages of a Centrifugal Compressor Stage***", that is being submitted by **Sri K.Srinivasa Reddy**, in partial fulfillment for the award of **Ph.D.** in **Mechanical Engineering** to the **Jawaharlal Nehru Technological University, Hyderabad** is a record of bonafide work carried out by him under our guidance and supervision. The results embodied in this thesis have not been submitted to any other University or Institute for the award of any degree or diploma.

Signature of Supervisor

**Dr.G.V.Ramana Murty
Professor and HoD
Vasavi College of Engineering
Hyderabad, India**

Signature of Co-Supervisor

**Dr.K.V.Sharma
Faculty of Mechanical Engineering,
Universiti Malaysia, Pahang
Malaysia**

CERTIFICATE

This is to certify that the thesis entitled "***Experimental and Theoretical Flow Studies in the Return Channel Passages of a Centrifugal Compressor Stage***", that is being submitted by Sri **K.Srinivasa Reddy**, in partial fulfillment for the award of Ph.D. in Mechanical Engineering to the **Jawaharlal Nehru Technological University** is a record of bonafide work carried out by him while working at our institution.

Signature of Head of Institution

**Dr.U.M.Chaudhari
Principal,
Aurora's Engineering College,
Bhongir, India**

ACKNOWLEDGEMENTS

At the outset I express my profound gratitude and sincere thanks to **Dr.U.M.Chaudhari, Principal** and the **Management of Aurora's Engineering College, Bhongir** for encouraging me and granting permission to register for PhD and pursue the research work.

I express my deep sense of gratitude to the management of **Corporate R&D Division, BHEL, Vikasnagar, Hyderabad** for according permission to carry out the experimental and numerical work.

I owe my deepest gratitude to **Dr.G.V.Ramana Murty, Professor & Head, Department of Mechanical Engineering, Vasavi College of Engineering, Hyderabad**, (formerly, General Manager, Turbomachinery Laboratory, Corporate Research and Development, B.H.E.L, Hyderabad), for his supervision, advice, guidance, unflinching encouragement and support in various ways throughout this research work. I gratefully acknowledge **Dr.K.V.Sharma, Professor, Faculty of Mechanical Engineering, UMP, Malaysia, Pahang**, for his advice, inspiration and supervision in completing the project work.

I express my sincere thanks to **Sri A. Dasgupta** for his suggestions during the experimental programme. The cooperation and assistance rendered by the Turbomachinery Laboratory staff is gratefully acknowledged. I would like to thank **AGM / HRD** and **Sri S.Prithviraj, Sr.Manager/ HRD**, for providing all the necessary support in carrying out the project at Corporate R&D, BHEL.

I express my sincere thanks to the **Dr.D.N.Reddy**, Vice-Chancellor JNTUH, Kukatpally and **Dr.K.Lal Kishore, Director I/c**, Research and Development Cell for enabling me to register for PhD and facilitating the completion of my research work. The support received from **Dr.T.Ch.Siva Reddy**, Professor, SNIST and **Faculty and staff** of Mechanical Engineering Department, **Aurora's Engineering College, Bhongir**, is gratefully acknowledged.

This thesis would not have been possible but for the invaluable and great support I received from my family members, **Suneetha (wife), Naga Jahnavi (daughter) and Sri Shiva Charan Reddy (son)** and my friend **VASU**, who have always stood by me throughout the period.

ABSTRACT

The flow through the crossover components of a stage in a multi-stage centrifugal compressor consisting of U-bend, radial cascade of return channel passages and L-turn ducting, presents a complex fluid dynamic problem. In the present study a 1:1 experimental model test rig simulating the flow path through the crossover bend, cascade of return channel vanes and L-turn ducting is fabricated for conducting flow studies with two different configurations of return channel passages namely RCV1 and RCV2. The two configurations differ in their inlet flow angles, chord length and thickness distribution. The aerodynamic performance of the return channel passages is obtained through experiments and presented in terms of total pressure loss coefficient, static pressure recovery coefficient, exit swirl angle and vane surface pressure distribution and compared with each other. The experimental results indicated a lower total pressure loss and better static pressure recovery in RCV1 configuration than in RCV2. However the average swirl angle distribution at the L-turn exit in RCV2 configuration is observed to be less than in RCV1, the reason being attributed to the influence of secondary flows in L-turn section.

Also numerical studies were conducted in the two return channel vane configurations RCV1 and RCV2 with the same operating conditions used in the experiments using the commercial flow solver FLUENT. The

turbulence was handled with standard $k-\varepsilon$, model and standard wall functions. The numerical results obtained were compared with the experimental results. A qualitative agreement between the experimental and numerical results was observed. The flow separation phenomenon on the suction side of the vane in RCV1 and RCV2 configurations and the development of secondary flows in the flow path were visualized through CFD studies.

An attempt has been made to design a new return channel vane configuration, RCV3 to overcome the flow separation on the suction side of the vane and to reduce the average exit swirl angle. The inlet vane angle is reduced to 25° while keeping the exit flow angle of 82° (with respect to tangential direction), same as that of RCV1 and RCV2. CFD studies were conducted to obtain the aerodynamic performance of the crossover system with RCV3 configuration. The results were found to be very encouraging as the total pressure loss coefficient is observed to be least for RCV3 and the static pressure recovery the highest. The exit swirl angle is also found to be well distributed and almost same as that of RCV2. Further numerical studies conducted by varying the U-bend exit flow path width with decreased return channel vane shroud wall divergence angle from 6° to 3.44° , showed a drastic improvement in the aerodynamic performance in terms of 22% decrease in total pressure loss coefficient and about 69% increase in static pressure recovery coefficient when compared with RCV1 configuration.

CONTENTS

Declaration.....	i
Certificate from Supervisors.....	ii
Certificate from the Head of the Institution.....	iii
Certificate from B.H.E.L R&D, Hyderabad.....	iv
Acknowledgements.....	v
Abstract.....	vi
Table of Contents.....	viii
List of Plates.....	xv
List of Tables.....	xvi
List of Figures.....	xvii
Nomenclature.....	xxi
List of publications based on the present Work.....	xxiii

Ch.			Page No
No	Title		
1	INTRODUCTION		1-11
1.1	General.....	1	
1.2	Working principle of a centrifugal compressor...	2	
1.3	Flow mechanism in a centrifugal compressor stage.....	3	
1.4	Key issues in the design of return channel passages.....	5	
1.5	Background and motivation for the present work.....	6	
1.6	Objectives of the present study.....	8	
1.7	Scope of the present study.....	9	
1.8	Presentation of the thesis.....	10	

2	REVIEW OF LITERATURE	12-37
2.1	General.....	12
2.2	Nature of flow mechanism in crossover system....	13
2.2.1	Flow mechanism in U-bend.....	14
2.2.2	Flow mechanism in return channel passages.....	15
2.2.3	Flow mechanism in L-turn ducting.....	15
2.2.4	Secondary flows in a centrifugal compressor stage.....	16
2.3	Design guide lines for crossover system components.....	17
2.3.1	Design guidelines by Aungier (2000).....	18
2.3.2	Design guidelines by Lüdtke (2004).....	19
2.4	Experimental and Numerical Investigations.....	20
3	EXPERIMENTAL TEST SETUP AND INSTRUMENTATION	38-55
3.1	Description of the test setup.....	38
3.2	Assembly of the test section.....	39
3.2.1	Swirl Vane Assembly.....	40
3.2.2	Variable angle mechanism.....	40
3.2.3	Return channel vanes assembly.....	44
3.2.4	Outer casing assembly.....	46
3.2.5	Centre body assembly.....	47
3.2.6	Exit diffuser cone.....	48
3.3	Instrumentation.....	48
3.3.1	Measurement of pressure.....	48

3.3.2	Measurement of temperature.....	48
3.3.3	Measurement of flow rate using a venture nozzle.....	49
3.3.4	Probe traversing mechanism.....	50
3.3.5	Measurement with 3-hole wedge probe....	51
3.3.6	Calibration of wedge probe.....	51
3.3.7	Vane surface pressure measurement.....	53
4	EXPERIMENTAL PROGRAMME AND PROCEDURE	56-67
4.1	Basis for Selection of Vane Profiles RCV1 And RCV2.....	56
4.2	Experimental programme.....	59
4.2.1	Operating conditions.....	60
4.2.2	Leakage testing.....	62
4.3	Experimental procedure.....	64
4.4	Graphical presentation of results.....	66
4.4.1	Meridional velocity distribution.....	66
4.4.2	Flow angle distribution.....	66
4.4.3	Vane surface pressure distribution.....	66
4.4.4	Total pressure loss coefficient.....	66
4.4.5	Static pressure recovery coefficient.....	67
5	NUMERICAL SOLUTION AND PROBLEM SETUP	68-76
5.1	Introduction.....	68
5.2	Steps for numerical solution.....	69
5.3	Grid generation.....	70
5.4	Boundary conditions.....	73

5.5	Solver settings.....	73
5.6	Grid independence study.....	75
5.7	Post processing of results.....	75
6	EXPERIMENTAL RESULTS AND DISCUSSION	77-111
6.1	General.....	77
6.2	Experimental Flow investigations in RCV1.....	77
6.2.1	Meridional velocity and flow angle distribution at U-bend inlet.....	78
6.2.2	Meridional velocity and flow angle distribution at U-bend exit.....	80
6.2.3	Meridional velocity and flow angle distribution at L-turn exit.....	82
6.2.4	Vane surface pressure distribution.....	86
6.2.5	Performance of the stage.....	89
6.2.6	Performance of the U- bend.....	91
6.3	Experimental investigations in RCV2.....	93
6.3.1	Meridional velocity and flow angle distribution at U-bend inlet.....	93
6.3.2	Meridional velocity and flow angle distribution at U-bend exit.....	95
6.3.3	Vane surface pressure distribution.....	97
6.3.4	Variation of Meridional Velocity and Swirl Angle at L-turn exit.....	97
6.3.5	Performance of the stage.....	102
6.3.6	Performance of the U-bend.....	103
6.4	Comparison of experimental results of RCV1 and RCV2.....	106

6.4.1	Meridional Velocity and Flow Angle Distribution at U-Bend exit.....	106
6.4.2	Comparison of meridional velocity and flow angle distribution at the stage exit... ..	107
6.4.3	Comparison of Vane surface pressure distribution.....	109
6.4.4	Performance comparison for the stage and U-bend.....	111
7	NUMERICAL RESULTS AND DISCUSSION	116-217
7.1	Introduction.....	116
7.2	Numerical results in RCV1.....	116
7.2.1	Variation of Meridional Velocity and Flow Angle at U-Bend Exit.....	117
7.2.2	Vane surface pressure distribution.....	119
7.2.3	Iso-Mach contour plots.....	124
7.2.4	Variation of meridional velocity and swirl angle at the L-turn exit.....	127
7.2.5	Performance of the stage and U-bend	132
7.3	Comparison of experimental and numerical results in RCV1 configuration.....	135
7.3.1	Comparison of meridional velocity and flow angle at U-bend exit.....	135
7.3.2	Comparison of Vane surface pressure distribution.....	135
7.3.3	Comparison of Meridional Velocity and Swirl Angle at the L-Turn Exit.....	138
7.3.4	Comparison of Performance of the stage and U-bend.....	141

7.4	Numerical Results in RCV2 Configuration.....	144
7.4.1	Variation of meridional Velocity and flow angle at U-bend exit.....	144
7.4.2	Vane surface pressure distribution.	145
7.4.3	Variation of meridional velocity and Swirl angle at L-turn exit.....	149
7.4.4	Performance of the stage and U-bend.....	155
7.4.5	Iso-Mach contour plots	158
7.5	Comparison of experimental and numerical results in RCV2 configuration.....	162
7.5.1	Comparison of Meridional Velocity and flow angle at U-bend exit.....	162
7.5.2	Comparison of vane surface pressure distribution.....	164
7.5.3	Meridional velocity at the L-turn exit.....	165
7.6	Numerical results in RCV3 configuration.....	171
7.6.1	Variation of meridional velocity and flow angle at U-bend exit.....	174
7.6.2	Vane surface pressure distribution.....	174
7.6.3	Variation of meridional velocity and flow angle at the L-turn exit.....	178
7.6.4	Stage performance with RCV3 configuration.....	181
7.6.5	Performance of U- bend.....	184
7.7	Comparison of Numerical Results of RCV1, RCV2 and RCV3 configurations.....	187
7.7.1	Variation of Meridional Velocity at U-bend exit.....	187

7.7.2	Vane surface pressure distribution at the design flow rate.....	189
7.7.3	Variation of Total Velocity in the RCV mid-span plane.....	189
7.7.4	Meridional velocity distribution at the stage exit.....	191
7.7.5	Secondary flow pattern at the L-turn inlet.....	191
7.7.6	Variation of exit swirl angle.....	197
7.7.7	Performance of the stage.....	197
7.7.8	Performance of the U-bend.....	201
7.8	Further numerical studies in RCV3.....	203
7.8.1	Effect of U-bend exit flow path width on the stage performance.....	203
7.8.2	Effect of varying the U-bend radius of curvature on stage performance.....	210
7.8.3	Effect of varying the number of vanes on the stage performance.....	213
8	CONCLUSIONS AND SUGGESTIONS	219-223
8.1	Summary.....	219
8.2	Conclusions.....	220
8.3	Suggestions for Future Work.....	223
A-1	ERROR ANALYSIS	224-231
	REFERENCES	232-236

LIST OF PLATES

Plate. No.	Title	Page No
3.1	View showing the model test section.....	42
3.2	View showing location for vane surface static pressure measurement.....	55
4.1	View showing measuring station at the inlet of U-bend.....	63
4.2	View showing measuring station at the exit of U-bend and L-turn exit.....	64

LIST OF TABLES

Table No.	Title	Page No.
4.1	Average flow angles at the vane less diffuser exit.	56
4.2	Design parameters for RCV1 and RCV2.....	59
4.3	Operating conditions.....	60
5.1	Grid independence study.....	76
7.1	Incidence angle on the L.E of RCV1 configuration	122
7.2	Incidence angles on RCV2 vane.....	147
7.3	Vane design parameters for RCV3.....	171
7.4	Incidence angle information on the L.E of RCV3..	176
7.5	Comparison of angle of flow incidence at the design point.....	189
7.6	U-bend flow path parameters.....	205
7.7	Average flow angles at the U-bend exit for the design flow.....	208
7.8	Existing and modified U-bend parameters.....	210
7.9	Comparison of aerodynamic performance for RCV1 and RCV3	218

LIST OF FIGURES

Fig. No.	Title	Page No
2.1	Sectional view of multistage centrifugal compressor.....	13
2.2	Components of a multi-stage centrifugal compressor stage.....	14
3.1	Schematic diagram of the return channel test rig.....	41
3.2	Sectional view of the test setup in meridional plane.....	42
3.3	NACA Profile of the swirl vane.....	43
3.4	Swirl vanes assembly.....	43
3.5	Variable angle linkage mechanism.....	45
3.6	Return channel vanes assembly.....	45
3.7	Outer casing exit assembly.....	46
3.8	Centre body assembly.....	47
3.9	Venturi nozzle.....	50
3.10	Three hole wedge probe.....	52
3.11	Calibration chart for three-hole wedge probe.....	53
3.12	Locations of holes on return channel vane surface for pressure measurement.....	54
4.1(a)	Variation of mean streamline flow angle - RCV1, RCV2....	58
4.1(b)	Vane-to-vane nomenclature of return channel vanes.....	58
4.2	Overlapped profiles of RCV1 and RCV2.....	58
4.3	Measurement locations in the meridional plane	61
4.4	Measurement locations along the circumference at the L-turn exit.....	63

5.1	Computational model.....	72
5.2	Computational mesh for U- bend, 90 deg bend and RCV2	74
6.1(a)	Variation of meridional velocity at U-bend inlet.....	79
6.1(b)	Variation of flow angle at U-bend inlet.....	79
6.2(a)	Meridional Velocity distribution at U-bend exit.....	81
6.2(b)	Absolute Flow Angle distribution at U-bend exit.....	81
6.3(a)	Measurement locations at the L-turn exit.....	83
6.3(b)	Meridional Velocity Distribution at stage exit ($\alpha_1 = 29^\circ$)....	83
6.4(a)	Swirl angle Distribution at final exit ($\alpha_1 = 29^\circ$).....	85
6.4(b)	Average swirl angle distribution at final exit	85
6.5	Average Meridional Velocity Distribution at L-turn exit....	86
6.6	Return Channel Vane surface pressure distribution.....	88
6.7(a)	Variation of total pressure loss coefficient	90
6.7(b)	Variation of static pressure recovery coefficient	90
6.8(a)	Variation of total pressure loss coefficient (U-bend).....	92
6.8(b)	Variation of static pressure recovery coefficient (U-bend)..	92
6.9(a)	Variation of meridional velocity at U-bend inlet.....	94
6.9(b)	Variation of flow angle at U-bend inlet.....	94
6.10(a)	Variation of meridional velocity at U-bend exit.....	96
6.10(b)	Variation of flow angle at U-bend exit.....	96
6.11	Vane surface pressure coefficient (RCV2).....	98
6.12(a)	Variation of meridional velocity at L-turn exit (circumferential average).....	100
6.12(b)	Meridional velocity distribution at the design flow rate....	100
6.13(a)	Variation of swirl angle at the L-turn exit (design flow)....	101

6.13(b) Average swirl angle at the L-turn exit (RCV2).....	101
6.14(a) Variation of total pressure loss coefficient for stage (RCV2).....	104
6.14(b) Variation of static pressure recovery coefficient for stage (RCV2).....	104
6.15(a) Variation of total pressure loss coefficient for the U-bend (RCV2).....	105
6.15(b) Variation of static pressure recovery coefficient for the U- bend (RCV2).....	105
6.16 Comparison of meridional velocity and flow angle distributions for RCV1 and RCV2 at U-bend exit.....	108
6.17 Variation of Meridional velocity and swirl angle at stage exit At the design point	110
6.18 Comparison of vane surface pressure distribution.....	112
6.19(a) Variation of total pressure loss coefficient (stage).....	114
6.19(b) Variation of static pressure recovery coefficient (stage)....	114
6.20(a) Variation of total pressure loss coefficient (U-bend).....	115
6.20(b) Variation of static pressure recovery coefficient (U-bend)..	115
7.1(a) Variation of meridional velocity at U-bend exit.....	118
7.1(b) Variation of flow angle at U-bend exit.....	118
7.2 Velocity vectors in the meridional plane of U-bend.....	119
7.3 Contour plots of meridional velocity in the U-bend exit plane.....	120
7.4 Calculated vane surface pressure distribution (RCV1).....	121
7.5 Velocity contours on a plane passing through the mid span of RCV1.....	123
7.6 Plane nomenclature used for qualitative plots.....	125

7.7	Calculated Iso contours of Mach number ($\alpha_1 = 29^\circ$).....	126
7.8	Calculated cross flow velocity vector plot on plane 5 ($\alpha_1 = 29^\circ$).....	128
7.9	Variation of meridional velocity at the L-turn exit (Circumferential average).....	129
7.10(a)	Variation of meridional velocity at the L-turn exit.....	130
7.10(b)	Variation of average swirl angle at the L-turn exit.....	130
7.11	Contours of meridional velocity at L-turn exit.....	131
7.12	Variation of total pressure loss coefficient (stage).....	133
7.13	Variation of static pressure recovery coefficient (stage).....	133
7.14(a)	Variation of total pressure loss coefficient for U-bend.....	134
7.14(b)	Variation of static pressure recovery coefficient for U-bend.....	134
7.15	Variation of meridional velocity and flow angle at U-bend exit	136
7.16	Comparison of Vane surface pressure distribution (RCV1)	137
7.17(a)	Meridional Velocity distribution at the L-turn exit (70% of design flow).....	139
7.17(b)	Meridional Velocity distribution at the L-turn exit (100% of design flow).....	139
7.17(c)	Meridional Velocity distribution at the L-turn exit (120% of design flow).....	140
7.18	Comparison of average swirl angle distribution.....	140
7.19	Variation of total pressure loss coefficient for the stage....	142
7.20	Variation of static pressure recovery coefficient (stage).....	142
7.21	Variation of static total pressure loss coefficient for U-bend.....	143

7.22	Variation of static pressure recovery coefficient for U-bend.....	143
7.23(a)	Variation of meridional velocity at U-bend exit.....	146
7.23(b)	Variation of flow angle at U-bend exit.....	146
7.23(c)	Contour plot of meridional velocity distribution at the U-bend exit.....	147
7.24	Vane surface pressure distribution (RCV2).....	148
7.25	Velocity contours on a plane passing through the mid span of RCV2.....	150
7.26(a)	Variation of meridional velocity at the L-turn exit (circumferential average).....	152
7.26(b)	Variation of Meridional velocity at the L-turn exit (Design flow rate).....	152
7.27(a)	Variation of swirl angle at the L-turn exit (Design flow rate).....	153
7.27(b)	Variation of average swirl angle at the L-turn exit.....	153
7.28	Contour plots of Meridional velocity at the L-turn exit.....	154
7.29(a)	Variation of total pressure loss coefficient.....	156
7.29(b)	Variation of static pressure recovery coefficient.....	156
7.30(a)	Variation of total pressure loss coefficient (U-bend).....	157
7.30(b)	Variation of static pressure recovery coefficient (U-bend)..	157
7.31	Plane nomenclature used for iso-Mach contour plots.....	159
7.32	Iso-Mach contour plots on different planes.....	160
7.33(a)	Iso-Mach contour plot on a plane passing through mid-span of RCV2.....	161
7.33(b)	Secondary flow pattern on plane- 5	161
7.34	Comparison of meridional velocity and flow angle at U-bend exit ($\alpha_1 = 29^0$).....	163

7.35	Comparison of Vane Surface Pressure Distribution.....	164
7.36(a)	Circumferentially averaged meridional velocity at the L-turn exit ($\alpha_1 = 21^\circ$).....	165
7.36(b)	Circumferentially averaged meridional velocity at the L-turn exit ($\alpha_1 = 29^\circ$).....	166
7.36(c)	Circumferentially averaged meridional velocity at the L-turn exit ($\alpha_1 = 34^\circ$).....	166
7.37	Average swirl angle at the L-turn exit.....	167
7.38(a)	Variation of total pressure loss coefficient (stage).....	168
7.38(b)	Variation of static pressure recovery coefficient (stage)....	169
7.39(a)	Variation of total pressure loss coefficient (U-bend).....	169
7.39(b)	Variation of static pressure recovery coefficient (U-bend).....	170
7.40(a)	Geometrical details of RCV3 configuration.....	172
7.40(b)	Variation of flow angle along the mean stream line (RCV3)	172
7.41(a)	Comparison of return channel vane profiles RCV1 and RCV3.....	173
7.41(b)	Comparison of return channel vane profiles RCV2 and RCV3.....	173
7.42(a)	Meridional Velocity Distribution at U-bend exit.....	175
7.42(b)	Flow Angle Distribution at U-bend exit.....	175
7.43	Contour plot of meridional velocity at U-bend exit.....	176
7.44	Vane surface pressure distribution for RCV3 configuration.....	177
7.45(a)	Meridional Velocity Distribution at L-turn exit (Circumferential average).....	179
7.45(b)	Meridional Velocity Distribution at L-turn exit ,100% flow	179

7.46(a)	Swirl angle distribution at L-turn exit (Design flow rate)...	180
7.46(b)	Average swirl angle distribution at L-turn exit.....	180
7.47	Contours of meridional velocity at L-turn exit.....	182
7.48	Contours of swirl angle at L-turn exit.....	183
7.49(a)	Variation of total pressure loss coefficient (stage).....	185
7.49(b)	Variation of static pressure recovery coefficient (stage)....	185
7.50(a)	Variation of total pressure loss coefficient, U-bend.....	186
7.50(b)	Variation of static pressure recovery coefficient, U-bend...	186
7.51(a)	Variation of meridional velocity at U-bend exit.....	188
7.51(b)	Contours of meridional velocity at U-bend exit.....	188
7.52	Vane surface pressure distribution at the design point....	190
7.53	Variation of total velocity in a plane passing through the mid-span of the RCV (flow angle at U-bend inlet = 21 deg)	192
7.54	Variation of total velocity in a plane passing through the mid-span of the RCV (flow angle at U-bend inlet = 24 deg)	193
7.55	Variation of total velocity in a plane passing through the mid-span of the RCV (flow angle at U-bend inlet = 29 deg)	194
7.56	Variation of total velocity in a plane passing through the mid-span of the RCV (flow angle at U-bend inlet = 32 deg)	195
7.57	Variation of total velocity in a plane passing through the mid-span of the RCV (flow angle at U-bend inlet = 34 deg)	196
7.58	Variation of Meridional Velocity at the stage exit (100%)...	198
7.59	Secondary flow pattern on the L-turn inlet plane (design point).....	198
7.60	Variation swirl angle at the stage exit (off-design conditions).....	199
7.61(a)	Variation of total pressure loss coefficient (stage).....	200

7.61(b)	Variation of static pressure recovery coefficient (stage).....	200
7.62(a)	Variation of total pressure loss coefficient (U-bend).....	202
7.62(b)	Variation of static pressure recovery coefficient (U-bend)..	202
7.63	Geometrical details of the flow path modifications with varying (b_2 / b_1) ratios.....	204
7.64(a)	Variation of total pressure loss coefficient for the stage for different (b_2 / b_1) ratios.....	206
7.64(b)	Variation of static pressure recovery coefficient for the stage for different b_2/b_1 ratios.....	206
7.65(a)	Variation of total pressure loss coefficient for U-bend for different (b_2 / b_1) ratios.....	207
7.65(b)	Variation of average swirl angle at the stage exit for different (b_2 / b_1) ratios.....	207
7.66	Velocity contour plots on a plane passing through the mid-span of RCV3 for $(b_2/b_1) = 1.163$	209
7.67	Modified U-bend geometry configurations	211
7.68(a)	Variation of total pressure loss coefficient for varying R^* ...	213
7.68(b)	Variation of static pressure recovery coefficient for varying R^*	213
7.69	Variation of swirl angles for varying R^* values	214
7.70(a)	Variation of total pressure loss coefficient with number of vanes.....	216
7.70(b)	Variation of static pressure recovery coefficient with number of vanes	216
7.71	Variation of average swirl angle with number of vanes	217

NOMENCLATURE

Symbol	Description	units
b	Width from hub wall to shroud wall	(m)
C	Velocity	(m/s)
C_p	Static pressure recovery coefficient	
C_{pv}	Vane surface static pressure coefficient	
D	Diameter	(m)
g	Acceleration due to gravity	(m/s ²)
i	Angle of incidence on RCV ($\beta_2 - \alpha_2$)	
L	Mean stream line length from the throat of vane to vane	(m)
LE	Leading edge	
m	Mass flow rate	(kg/s)
N	Speed	(rpm)
P,p	Pressure	(Pa)
Q	Volume flow	(m ³ /s)
r	Radius	(m)
t	Throat length of vane to vane	(m)
TE	Trailing edge	
U	Impeller tip speed = $(\pi DN / 60)$	(m/s)
x	Distance from hub	(m)
ρ	Inlet total density	(kg/m ³)
ϕ	Flow coefficient = $(m/\rho) / (U\pi R^2)$	
φ	Return channel vane shroud wall divergence angle	(deg)
α	Average flow angle, measured with respect to tangential direction	(deg)
β	Vane angle, measured with respect to tangential direction	(deg)

Subscripts	Description
1	Stage inlet /U-bend inlet
2	U-bend exit /return channel vane inlet
3	Return channel vane exit/ L-turn inlet
4	L-turn exit/stage exit
t	Total condition
s	Static condition
av	Average
wL	Wall condition on left side
wR	Wall condition on right side

PUBLICATIONS BASED ON THE PRESENT WORK

International Journal (01)

1.“Flow Investigations in the Crossover System of a Centrifugal Compressor Stage” K. Srinivasa Reddy, G. V. Ramana Murty, A Dasgupta and K. V. Sharma, International Journal of Fluid Machinery and Systems, Vol. 3 (2010) , No. 1 (January-March) pp.11-19, ONLINE ISSN : 1882-9554 , <http://ess.jstage.jst.go.jp/>

International Conferences (02)

1. “Experimental Investigations in the Return Channel Vanes of a Centrifugal Compressor Stage” K. Srinivasa Reddy, G. V. Ramana Murty, A Dasgupta and K. V. Sharma, Proc. of the 3rd International Conference on Advances in Mechanical Engineering, January 4-6, 2010, PP 144-148, S.V. National Institute of Technology, Surat – 395 007, Gujarat, India.
2. “Aerodynamic Studies in the Static Components of a Centrifugal Compressor Stage” K. Srinivasa Reddy, G.V.Ramana Murty, K.V.Sharma, National Conference in Mechanical Engineering for Research & Postgraduate Studies (NCMER'10), 26th May, ISBN:978-967-5080-95-1, Universiti Malaysia Pahang, 2010.

National Conferences (03)

1. "A Numerical Study Of Effect of Return Channel Wall Divergence Angle on The Crossover System Performance In Centrifugal Compressors", K. Srinivasa Reddy, G. V. Ramana Murty K. V. Sharma, Proceedings of National conference on " Emerging trends in Mechanical Engineering" July 1-2, 2009, SNIST, Hyderabad, , pp 261-268
2. "Numerical Studies in the Return Channel Passages of a Centrifugal Compressor Stage", K. Srinivasa Reddy, G. V. Ramana Murty, A Dasgupta and K. V. Sharma, Proceedings of 2nd National conference on "CFD Applications in Power and Industry Sectors", 28th-29th January 2009, Corporate R&D, B.H.E.L, Hyderabad.
3. "CFD Studies in the Return Channel Vanes Of a Centrifugal Compressor Stage", K. Srinivasa Reddy, G. V. Ramana Murty, A Dasgupta and K. V. Sharma, , Fluid Mechanics and Fluid Power (FMFP), December 10-12, 2007, BITS Ranchi.

Chapter 1

INTRODUCTION

1.1 GENERAL

Centrifugal compressors are classified under radial turbo machines, which are used for supplying pressurised air for industrial plant uses. They find applications in various industrial plants like petrochemical, fertilizer, pharmaceutical, automotive, aerospace, electronics, textile and chemical processing industries. Depending upon the delivery pressure requirement, they are categorized into single stage or multi stage machines. In a multi-stage centrifugal compressor, the working fluid is passed through many impeller stages arranged in series. They are robust, compact, have better resistance against foreign object damage and are less susceptible to performance degradation through fouling effect. Centrifugal compressors are widely used because of their smooth operation, large tolerance of process fluctuations, and their higher reliability compared to other types of compressors. These are in general used for higher pressure ratios and lower flow rates compared to lower stage pressure ratios and higher flow rates in axial flow compressors. The main difference between the centrifugal and axial flow compressors is the variance in the diameters of the inlet and the outlet. The working principle of a centrifugal compressor and its flow physics are described in the following sections.

1.2 WORKING PRINCIPLE OF A CENTRIFUGAL COMPRESSOR

The main components of a single stage centrifugal compressor are inlet guide vanes, an impeller, vane or vaneless diffuser and volute casing. The fluid enters the compressor through an intake duct in the axial direction and is given pre-whirl by the inlet guide vanes and then flows into the inducer without any incidence angle. The flow as it enters the impeller, changes its direction from axial to radial. The fluid is then passed through the impeller by rapidly rotating impeller blades. The impeller imparts kinetic energy to the fluid at this stage. The static pressure rise occurs partially as the fluid moves from inlet radius to exit radius of the impeller. The fluid is then discharged into a diffuser, where its kinetic energy is converted into static pressure. The flow enters collecting chamber which is a volute casing from where it is discharged. The inlet guide vanes are employed in higher pressure ratio compressors. Though vane diffusers enhance the efficiency of the centrifugal compressor its operating range is narrowed due to the fixed vane angle of the diffuser.

In a multistage centrifugal compressor volute chamber of the single stage centrifugal compressor is replaced with an 180° circumferential crossover bend (U-bend) followed by a cascade of return channel vanes (deswirl vanes) and L-turn exit ducting (90° bend). Many number of such components are assembled together to form a multistage centrifugal compressor. In the present study the flow conducting components

starting from circumferential crossover bend followed by the cascade of return channel vanes and the L-turn exit ducting together is termed as "Crossover System". The compressed air leaving the diffuser passes through the circumferential U-bend, return channel vanes and exit ducting before it is passed on to the subsequent stage.

1.3 FLOW MECHANISM IN A CENTRIFUGAL COMPRESSOR STAGE

David Japikse (1996), of Concepts ETI, Inc, described the impeller flow physics in detail. The growth of boundary layers occurs on all wall surfaces like blade, hub, and shroud. In the passage through the impeller, the core flow and the boundary layers interact and more complicated flow patterns develop. Later in the downstream direction, the boundary layers and the core flow are affected by the very strong cross-passage Coriolis force field. Subsequently, a secondary flow develops around the core with the low momentum fluid collected near the shroud suction surface and the high momentum fluid located near the hub pressure area. Secondary flow does not show the basic flow pattern of the principal or primary flow core. The flow leaves the impeller with some tangential flow component of velocity whose magnitude and direction depends upon the flow coefficient and the operating condition of the compressor.

The vaneless diffuser which is widely used in process compressors, refrigeration compressors and turbocharger compressors consists of parallel walls forming an open annular passage in the radial direction.

The changes in the velocity and static pressure rise occur as per the conservation of angular momentum principle. The static pressure recovery occurs in the vaneless diffuser with little change in the flow angle. In general the reverse flow that place on the shroud wall of the vaneless diffuser contributes the losses. The flow in the vaneless diffuser is also prone to dynamic instabilities particularly under unsteady state flow conditions.

In a multistage centrifugal compressor the crossover system comprises of 180° U-bend followed by a radial cascade of return channel vanes and L-turn exit ducting. The circumferential crossover bend receives the fluid from the diffuser with some tangential component of velocity, complicating the flow pattern while turning it by 180° . The flow distribution at the exit of U-bend is influenced by its radius of curvature. A small radius of curvature causes flow separation on the hub wall and induces secondary flows, while a bend with large radius of curvature causes more frictional losses.

The function of return channel vanes is to guide the flow with strong tangential component of flow leaving the diffuser elements to the eye of the subsequent impeller stage, which it must enter with zero or near-zero swirl. The removal of tangential swirl process should occur with as little loss in total pressure and as high static pressure recovery as possible. The flow field through the return channel passages is strongly associated with secondary flows due to the sharp turning with deceleration.

1.4 KEY ISSUES IN THE DESIGN OF RETURN CHANNEL PASSAGES

The present day requirement is to reduce the consumption of power, which requires the enhancement of efficiency of individual components of a stage. The power consumption in a centrifugal compressor stage can be reduced significantly by improving its overall efficiency which depends upon the performance of individual components. The efficiency of the impeller has reached its near maximum. Any further improvement in the efficiency and the performance of a centrifugal compressor stage has to be obtained from improvements achievable in its stationary components, especially the diffuser and the return channel vanes. In a multi-stage centrifugal compressor stage, the stage efficiency can be further improved by reducing the pressure losses in return channel vanes. Also the flow through crossover U-bend and exit ducting with a 90° bend needs to be improved by minimizing the losses.

The performance of the crossover system of a typical centrifugal compressor stage is expressed in terms of non-dimensional pressure coefficients namely, total pressure loss coefficient, static pressure recovery coefficient. Another very important parameter considered in the design of return channel passages is the swirl angle distribution at the stage exit.

The important design parameters of the return channel vanes are the inlet and exit flow angles, variation of mean flow angle along the mean stream line curvature, vane thickness and vane height distributions. In

the return channel passages the fluid having some tangential component is to be turned in to radial direction, during the process of swirl removal. The key issue is to decide where and how the turning of the fluid is to be achieved without causing flow separation and induction of secondary flows. In turn the above mentioned parameters influence the swirl angle distribution at the stage exit.

1.5 BACKGROUND AND MOTIVATION FOR THE PRESENT WORK

The research literature available on the design and performance of the return channel passages is limited. Aungier (2000) and Lüdtke (2004) have given some design recommendations for the crossover system components like U-bend and return channel passages. Model testing of return channel vane passages was reported by Simon and Rothstein (1983). The flow through the actual centrifugal compressor stage was simulated in a static test setup. The swirling flow at the exit of actual impeller was simulated by a set of static vanes. The flow through the return channel vanes was investigated for three different configurations. Inoue and Koizumi (1983) carried out experimental investigations on a similar test bed with three different return channel vane configurations. They also reported some theoretical models for predicting the pressure losses in the return channel passages. Tomitaro Toyokura and Toshiaki Kanemoto (1986) reported about the performance of a radial cascade of return channel vanes designed by inverse method. The interference of

secondary flows on the end wall with flow separation on the vane surface was identified which made the flow more complex.

Lenke and Simon (2000) conducted Computational Fluid Dynamics (CFD) studies and reported the aerodynamic analysis of return channels of multistage centrifugal compressors. They conducted the studies on return channel geometries that were used for experimentation by Simon and Rothstein (1983). Oh. et al. (2005) reported a qualitative numerical study of the 2-dimensional U-bend in return channel systems for multistage centrifugal compressors. For the purpose of flow simulation, the U-bend geometry used by Inoue and Koizumi (1983) was used and the results were compared with the experimental values.

Árpád Veress and Braembussche R (2004) presented inverse design and optimization method of a return channel for a multistage centrifugal compressor. They observed that in a traditional 2-dimensional return channel, the flow separation on the shroud side of the U-bend inlet and on the return channel vane suction side of the hub contribute to increased stage losses; hence there is a need for designing 3-dimensional return channel vanes extending right from the inlet of crossover bend.

However the complex flow mechanism existing in the return channel passages is not well understood. The effect of U-bend curvature, vane height distribution and the number of vanes on the crossover system performance is not reported. It is felt that experimental model testing on

return channel passages coupled with extensive Computational Fluid Dynamics (CFD) studies be conducted in order to get more insight in to the flow mechanism in the U-bend, return channel passages and L-turn ducting and also to establish the effect of U-bend curvature, vane height distribution and the number of vanes on the crossover system performance.

1.6 OBJECTIVES OF PRESENT STUDY

It is envisaged to conduct detailed flow studies to understand the flow mechanism in the crossover system of a typical centrifugal compressor stage having a flow coefficient of 0.053. For this purpose a two-pronged approach in terms of experimental and numerical studies was proposed.

It is proposed to design, manufacture and assemble a model test rig with two different return channel vane configurations namely RCV1 and RCV2 and conduct experimental flow investigations. The objective of experimental investigations is to evaluate the aerodynamic performance of the two return channel vane configurations and compare them to get an insight into the influencing parameters in terms of total pressure loss coefficient, static pressure recovery coefficient, vane surface pressure coefficient and exit swirl angle distribution.

Also it is proposed to establish a proper numerical solution procedure using commercial flow solver FLUENT to conduct numerical investigations in the same geometry used for experimental investigations and obtain the performance of the two return channel vane

configurations for the purpose of comparison. This model will help in conducting further numerical studies with varying parameters such as vane flow angles, vane thickness distribution, U-bend curvature, vane height distribution, and number of vanes to make design recommendations for the crossover system components with a view to improve the performance.

1.7 SCOPE OF THE PRESENT STUDY

1. Design and setting up of a static 1:1 model test rig for the evaluation of performance of the crossover system.
2. Experimental study on two configurations of return channel vanes designated as RCV1 and RCV2.
3. Numerical studies on the same geometry simulating the experimental flow conditions for comparison of results.
4. Based on the experimental and numerical studies in RCV1 and RCV2 configurations, a new modified RCV3 configuration for the return channel passages to be suggested for improving the aerodynamic performance of the stage.
5. Numerical study to evaluate the influence of the U-bend curvature with four different curvature factors, R^* on the stage performance with RCV3 configuration.
6. The effect of varying the vane height, by varying the U-bend exit flow path width on the stage performance with RCV3 configuration.
The numerical study to cover two different b_2/b_1 ratios.

7. The effect of varying the number of return channel vanes on the performance of the stage with RCV3 configuration. The numerical study to cover 16, 18, 20 vanes.

1.8 PRESENTATION OF THE THESIS

The thesis is presented with the following arrangement of chapters.

Chapter 1 gives the introduction to centrifugal compressors and its types. The flow mechanism through centrifugal stage components is described. The background and motivation for the present work is described. The objectives and scope of present study is mentioned.

A detailed review of research literature available in the area of aerodynamic performance estimation of return channel passages is presented in chapter 2. The complex flow mechanism in the return channel passages, their design parameters and design recommendations are described. The experimental test rig component drawings, its constructional features, instruments used and their calibration is presented in chapter 3. The design features of RCV1, RCV2 are also described in this chapter. The detailed experimental procedure followed is explained in chapter 4.

The geometric modeling, meshing of the flow conducting components as a part of numerical study is described in chapter 5. The boundary conditions and the solver settings applied are discussed.

Detailed discussion of experimental and numerical results is presented in chapter 6. The experimental results in RCV1 and RCV2 configurations are compared and discussed.

The numerical results obtained through CFD studies on RCV1 and RCV2 are presented separately and with comparison of experimental results in chapter 7. Also the numerical results in RCV3 compared with numerical results of RCV1 and RCV2 are presented. The numerical results obtained with varying U-bend curvature, number of vanes, U-bend exit flow path width are presented in this chapter.

The conclusions from the present study and suggestions for future work are presented in Chapter 8. The list of references is given at the end. Uncertainty analysis of the experimental work is presented in Appendix-I.

Chapter 2

REVIEW OF LITERATURE

2.1 GENERAL

The flow through the crossover system components of a multistage centrifugal compressor stage is quite complex owing to the sharp turning of the swirling fluid through the 180° bend and return channel vanes. The main problem that is faced in the design of return channel vanes is to prevent the flow separation on the vane surface and development of secondary flows while turning the fluid into the radial direction (removal of tangential swirl). The diffuser exit flow has a tangential component of velocity which is passed on to the U-bend inlet. The circumferential U-bend turns the fluid by 180° and therefore the radius of curvature of the U-bend influences the flow pattern. The inlet flow angle, exit flow angle, variation of flow angle along the mean streamline curvature, height and thickness distributions of the return channel vanes influence the flow through the return channel passages. Experimental investigations and numerical studies that were reported in open literature in the said area are limited. Aungier (2000) and Lüdtke (2004) presented some design guide lines for the crossover bend and return channel vanes. The description of flow mechanism in the crossover system, recommended crossover system design guidelines, literature available on experimental and numerical investigations are presented in the following sections.

2.2 NATURE OF FLOW IN A CROSSOVER SYSTEM

The sectional view of a multistage centrifugal compressor depicting the components like impeller, vane-less diffuser and return channel vanes is shown in Fig. 2.1. The meridional view of the first stage of a typical multistage centrifugal compressor is shown in Fig. 2.2. The flow mechanisms in U-bend, return channel vanes and L-turn exit comprising of a stage in a multistage centrifugal compressor are briefly described below. The loss mechanisms in each of these individual components and the nature of secondary flows and its origin are discussed.

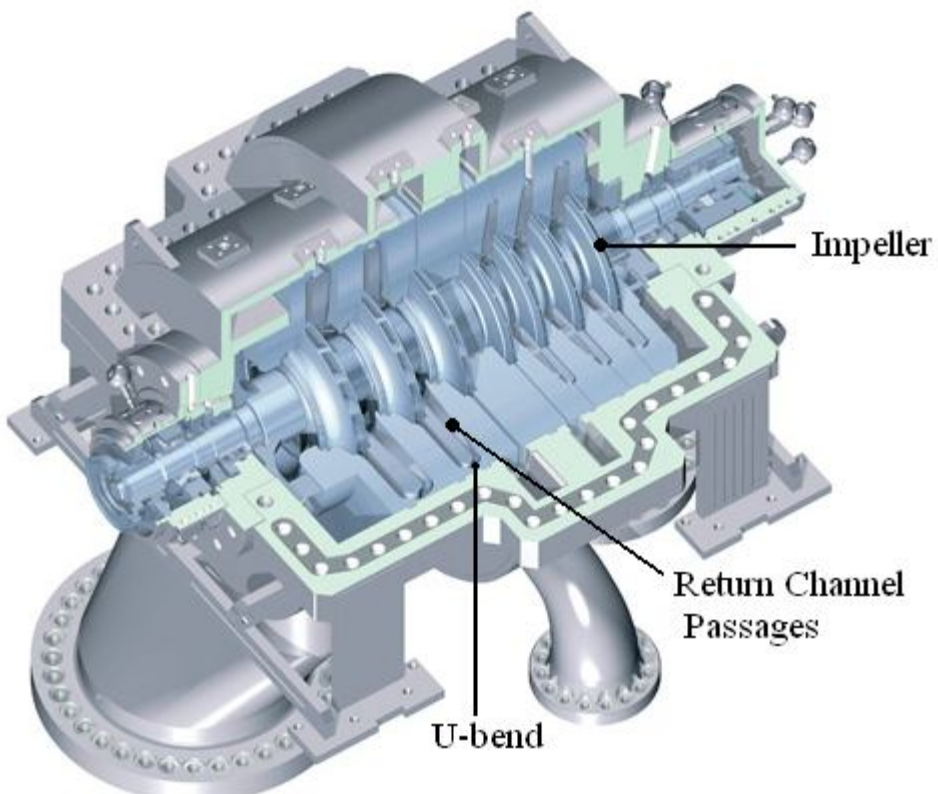


Fig. 2.1 Sectional view of multistage centrifugal compressor

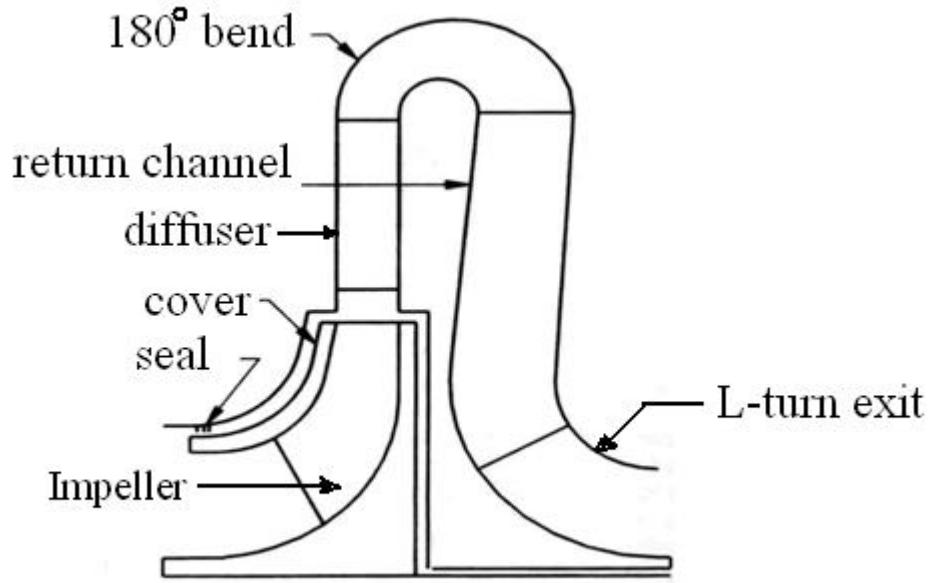


Fig. 2.2 Components of a multi-stage centrifugal compressor stage
(Aungier, 2000)

2.2.1 Flow Mechanism in U-Bend

The flow from the exit of the impeller enters the diffuser with some tangential component of velocity. The flow angle may slightly increase towards the exit of vaneless diffuser. The circumferential crossover bend receives the fluid with this tangential component, complicating the flow pattern while turning it by 180° . The flow distribution at the exit of U-bend is influenced by its radius of curvature. A small radius of curvature causes flow separation and induces secondary flows, while a bend with large radius of curvature gives uniform velocity distribution at the exit but with more frictional losses. Therefore proper selection of crossover bend is an important design consideration in improving the overall efficiency of crossover system.

2.2.2 Flow Mechanism in Return Channel Passages

The role of return channel vanes is to guide the strongly swirling flow leaving the diffuser elements to the eye of the subsequent impeller stage which it should enter with zero or nearly zero inlet swirl. The swirl removal process should take place with as little loss as possible. In certain cases, this represents a mild diffusion of the flow field. In other cases, it corresponds to acceleration. The rate of turning of flow along the mean stream line coupled with deceleration might influence the flow separation and induction of secondary flows. The flow field through the return channel vanes is strongly dominated by secondary flows.

2.2.3 Flow Mechanism in L-turn Ducting

The return channel exit flow should be nearly radial in direction. However with positive incidence flows on the return channel vane leading edge and steeper mean stream line curvature, the flow is likely to get separated on the suction side near the trailing edge. The low pressure region at the trailing edge on suction side of the vane causes the flow to migrate from pressure side to suction side of the vane, inducing cross-flow. Therefore at the inlet of L-turn section, the 90° turn should be designed with proper radius of curvature to handle this flow. The flow, as it enters the 90° bend is likely to be concentrated towards the hub and away from shroud. However the losses associated with L-turn section are very less when compared to return channel and U-turn passages.

2.2.4 Secondary Flows in a Centrifugal Compressor Stage

Edward S Taylor (1968) of MIT described the development of secondary flows in a stationary curved channel. It was noted that secondary circulation appears after fluid with a non-uniform velocity distribution passes round a bend. The secondary flow changes the character of the core flow and is a source of loss. Secondary flow in a stationary curved channel replaces the slow-moving fluid near the walls with faster moving fluid, thereby increasing viscous friction near the walls. These secondary flows cause further losses in the downstream direction in the channel.

Japikse (1996) described the flow pattern complexity in a typical return channel path. A vortex is formed at the leading edge of the return channel vane as the end wall boundary layer rolls up in front of the vane. These vortices can be large enough to dominate the complete span of the vane. Also stream-wise passage vortices are formed as a result of the overturning of the slow-moving fluid in the end wall boundary layers inside the passage. These factors tend to drive the boundary layer fluid towards the vane suction surface and hence the development of secondary flows. The presence of secondary flows increases the fluid friction losses and hence the cause of their development should be identified and alleviated. Klaus Brun and Rainer Kurz (2005) described the secondary flows in impeller passage of centrifugal compressors. Secondary flows are observed in mixed-flow impellers such as centrifugal

pumps and compressors. These circulatory flows are undesirable as they cause head losses, non-uniformity of flow. The imbalance between static pressure field and the kinetic energy field in the flow induces the circulatory vortex flows. When an incoming boundary layer flow meets a stagnation line which causes a motion of the fluid along the wall, a vortex is formed in the shape of a horse shoe. The strength of the vortex depends upon the starting conditions and its further growth is determined by the conservation of angular momentum. In a rotating system the analogy is that the vortex flows are principally generated by the meridional flow field while the centrifugal and coriolis forces only act to change the vortex vector direction (tilting of the vortex plane).

2.3 DESIGN GUIDELINES FOR CROSSOVER SYSTEM COMPONENTS

The performance parameters considered in the design of U-bend and return channel section are the static pressure recovery coefficient, total pressure loss coefficient and vane loading patterns. Throughout the flow passage right from the U-bend inlet to the L-turn exit, the total pressure loss should be minimized. The total pressure loss might occur due to the presence of friction between the fluid and the wall surfaces. Also, locally induced secondary flows contribute to friction within the core flow. Therefore a better design should alleviate or minimize the frictional losses arising due to above mentioned reasons. The recommended design guidelines are discussed in the following sections.

2.3.1 Design guidelines by Aungier (2000)

Aungier (2000) proposed some guidelines for the design of crossover system of a typical centrifugal compressor stage. A circular-arc for hub contour and an elliptic-arc for shroud contour are recommended in the design of 180° U-bend. For the construction of 90° L-turn exit, an elliptic-arc for hub contour and circular-arc for shroud contour are preferred. Straight line contours are preferred for the hub and shroud walls of return channel section, connecting the 180° U-bend and 90° L-turn exit. It is emphasized that the U-bend and L-turn bend design should control the ratio of passage width-to-mean streamline radius of curvature. For the crossover bend a ratio less than 0.8 was recommended. In the design of return channel vanes, blade loading is an important parameter to be considered. A return channel vane loaded in the front is recommended in the vane construction. The vane should have higher loading near the leading edge than at the trailing edge to avoid flow deviation at the discharge. The maximum thickness of the vane, and its position along the chord line, is used to control the vane to vane flow path width. They should be used to reduce the local gradients of the velocity through the vane to vane flow path. The return channel vane is usually designed for incidence angle of 2° to 4° . Periodic evaluation of performance during the design process was emphasized in finalizing the design parameters.

2.3.2 Design guidelines by Lüdtke (2004)

According to Lüdtke (2004), the inlet flow angle for the return vane channel shall be kept in the range of 26° to 32° . This angle depends on the flow coefficient of the compressor, impeller exit angle and diffuser radius ratio. The outlet flow angle should be 90° with respect to tangential direction. For about 60° turning of fluid flow in the return vane channel passages, there should be least aerodynamic losses. To keep the frictional losses to minimum, the lower average velocity shall be maintained, particularly, where the streamline curvature is maximum. Since the velocities at the return channel inlet section and exit section are given by diffuser exit and inlet to the next impeller respectively, it is more meaningful to decrease the velocity initially and then accelerate towards the exit. This can be achieved by increasing the vane-to-vane flow path width, up to $2/3$ of the mean stream line length of the channel and thereafter decreasing in the remaining portion, where the vanes approach the required flow angle of 0° with respect to axial direction. The meridional flow path width has to be increased from inlet to outlet of the return channel vane and is dictated by the opening of the subsequent impeller stage. The increase of wall-to wall width along the return channel vane is usually kept in the range of 20% to 40%. The flow channel area in the first two thirds of the channel increases by some 30% to 50%, which is used for reducing the velocities and increase in static pressure. The static pressure recovery coefficient for the return

vane channel passage should range from 0.4 to 0.5. The total pressure loss coefficient should be equal to 0.25. These values are realized only when the incidence on the return channel vane is almost zero. The static pressure recovery coefficient decreases in part and excess loads and the total pressure loss coefficient increases in part and excess loads. The radius ratio of the vaned / vaneless diffuser influences the loss behavior of return channel passages; the longer the radius of the diffuser, the higher will be the stage efficiency, because it has been established that return vane channel losses reduce by 2% for every one percent of diffuser length increase. Therefore in spite of a longer path for the diffuser, the one with a greater radius ratio is more efficient than a compact package with small radius ratio.

2.4 EXPERIMENTAL AND NUMERICAL INVESTIGATIONS

Simon and Rothstein (1983), conducted experiments on the performance of three types of return channel vanes, on a static test rig. The flow path was constructed to resemble that of a complete stage in a multi-stage centrifugal compressor. Static swirl vanes were used in the place of an impeller, to give the flow the necessary whirl. The use of an adjustable guide vane unit permitted infinitely variable adjustments of the flow angle to the return channel passages. The fundamental character, however of the flow at the exit of an impeller and at the exit of a guide vane unit differs greatly. The impeller displays an unsteady discharge flow with regard to the absolute system, the flow after a fixed

guide vane unit is characterized by quasi-stationary wakes. The comparison of the two forms of flow is justified approximately at the inlet of U-bend but above all at the exit of the 180° bend because of the intensive energy exchanges taking place while turning. This was confirmed by comparative measurements on stage test beds. The return channel vanes start just after the exit of 180° U-bend.

The experimental investigations were conducted on three different return channel geometries with low flow coefficient namely Rfb 1.11, Rfb 1.12 and Rfb 1.13. These configurations differ in terms of number of vanes, chord length, vane thickness distribution and inlet flow angles. The return guide vanes Rfb1.11 were so designed that the flow is initially decelerated with a relatively small deflection. The deflection into the radial direction should then take place relatively quickly in a region in which the flow separation on the suction side of the vane would be inevitable. The flow at the exit should be directed radially in a relatively short, straight section of the channel, in order to obtain swirl-free flow. The configuration Rfb1.13 with 20 vanes and an inlet flow angle of 25° was shown to have minimum total pressure loss, better static pressure recovery, uniform vane loading and minimum exit swirl compared to Rfb1.11 and Rfb1.12. They could reduce the pressure-side separation phenomena in Rfb 1.12 and Rfb 1.13, which was more in case of Rfb1.11. Flow visualization with dye injections in low flow coefficient stages was done to visualize the development of secondary flows close to

the wall in the return vane channel in all the three tested configurations. The intensity of secondary flows with Rfb1.13 was observed to be less. They attributed the reason for this to the more favorable height/width ratio of return channel Rfb 1.13 and in the overall shorter flow path with longer straight section.

They also conducted experimental investigations in high flow coefficient stage with two different return channel geometries namely Rfb 2.11 and Rfb 2.12. In the high flow coefficient stages, both the tested return channels display a loss minimum approximately at the design point, but the largest values for the pressure recovery was obtained at flatter flow angles, since the flow with flatter angles is decelerated to a greater degree. The loss curve of Rfb2.12 was reported to be flatter than Rfb2.11, the reason being lower load caused by the smaller diffusion. They reported that a further improvement in the uniformity of the exit flow was achieved by splitting the tasks of the return guide vanes into two rows of vanes. The first vane row deflects and decelerates the flow, whereas the second row assures swirl-free exit flow. This concept was implemented in conjunction with a relatively widely curved 180^o bend in the four-stage compressor. Compared with a conventionally designed return passage, an increase of about 1.55% in the stage efficiency was obtained with, at the same time an improvement in the characteristic. It was concluded that, given the complex flow conditions in return passages, a reliable calculation of flow was not possible with the methods

available then. The comparison between the results obtained on the test bed presented here and results from stage test beds confirm the extensive similarity of the flow and hence the transferability of the results. It was also concluded that in order to keep the costs of experimental investigations within reasonable limits, attempts must be made to describe the relatively complex flow conditions in return channels with the aid of simplified calculation models.

Inoue and Koizumi (1983) studied experimentally the flow patterns and losses in three different return passages using a flow model. They also used static swirl vanes in the test rig in the place of impeller of an actual compressor stage. The test bed consists of parallel walled vaneless diffuser followed by 180° bend, a radial cascade of return channel vanes and L-turn exit. They felt that three dimensional blades were not necessary as the flow angle at U-bend exit shows uniform trend. It was concluded that there were secondary flows in the U-turn and L-turn sections, which causes the flow to be uniform across the passage section. The flow may be made uniform at the expense of total pressure losses due to secondary flow. The two dimensional blades are adequate for the deswirl vanes. The presence of some swirl at the stage exit is attributed to the secondary flow in the deswirl vanes. The pressure loss can be predicted using Eckert's equation with the friction coefficient 3.5 times larger than that of pipe flow. The large friction coefficient is attributed to the secondary flows. The losses in return channel can be explained for

inlet flow angles with the proposed model. However for the large flow angles, the calculation estimates are 50% lower than the experimental results.

Árpád Veress and Braembussche R (2004), presented inverse and optimization method of a return channel for a multistage centrifugal compressor. They observed that in a traditional 2D return channel, the flow separation on the shroud side of the U-bend inlet and on the return channel vane suction side of the hub contribute to increased stage losses, hence there is a need for designing 3D return channel vanes extending right from the inlet of crossover bend. An inverse design method of 3D vanes was used to control the flow separation and obtain better blade loading. The concentration is laid on obtaining uniform loading and controlling the vane lean to reduce the effect of secondary flows. With the obtained new design, it was concluded that extension of vanes upstream of the crossover might result in a considerable improvement of the performance and permits a larger operating range. It is observed that the positive lean results in larger losses and a substantial decrease of the turning. Optimum vane leaning further contributes to a performance increase by reducing the vorticity resulting from secondary flows. However the effect of crossover bend curvature, divergence of return channel with the newly designed configuration was not studied.

Oh, *et al.* (2005) reported a qualitative numerical study of the 2D U-bend in return channel systems for multistage centrifugal compressors. For the purpose of flow simulation, the U-bend geometry used by Inoue and Koizumi (1983) was taken and the results were compared with the experimental values. The commercial flow solver, FLUENT was used in the flow simulation. In the simulation the standard k- ϵ turbulence model and Reynolds stress model were used to predict the flow conditions. The results obtained with standard two equation k- ϵ turbulence model were observed to be closer to the experimental values than with Reynolds stress model. The near wall treatment was handled with standard wall functions. At the inlet of the U-bend the experimental velocity profile was specified along with fluid density and static pressure. They extended the U-bend geometry further in the downstream direction, though the actual domain of interest is up to the exit of U-bend. This was done to utilize the "outflow" exit boundary condition available in the solver. Steady and incompressible flow conditions were assumed. A turbulent intensity of 7% of the characteristic length of U-bend (width of diffuser) was given. For each case grid independency was checked. The return channel geometry RC30-01 was chosen for simulation. At the U-bend exit good agreement was observed between the numerical and experimental values for meridional velocity distribution. A qualitative 3D study was also carried out with an artificial wake/jet generated at the inlet of the U-bend sector. The development of secondary flow pattern in the U-bend

was visualized. The secondary flow at the U-bend exit was observed to spread more than in the upstream direction. The loss mechanisms and the performance of the turbulence models were discussed. Owing to the complex flow phenomenon in the U-bend, the conventional turbulence models could not predict the U-turn bend flow well. They felt the need for development of better turbulence model to capture the turbulent behaviour.

Tomitaro Toyokura, Toshiaki Kanemoto and Moriaki Hatta (1986) reported an inverse design based on singularity method, to design a circular cascade for a return channel of centrifugal turbomachine, whose vane-height varies in the radial direction. The desirable vane has to suppress the flow separation well and to give the radial out-flow condition. The relation between the velocity distribution and the vane profile was examined using the inverse method. The optimum position of the rear stagnation point on the round trailing edge was also derived. Out of the five different profiles generated for return channel vanes, configuration V was selected for experimental investigations at a later stage.

Tomitaro Toyokura and Toshiaki Kanemoto (1986) conducted the experimental investigations also on configuration V. The flow condition at the cascade outlet is very complicated because the secondary flow on the end wall interferes with the flow separation on the vane surface in the cascade. They observed some deviation of the actual flow from the

predictions by singularity method. The secondary flow on the end wall affects markedly the flow along the suction surface of the vane. The flow along the suction surface begins to separate from the middle-span surface and its region spreads in to both vane sides. Accordingly, the pressure along the suction surface recovers slightly even in the region of separation. The maximum velocity defect and its region caused by the flow separation on the suction surface of the vane are remarkable near the middle-width section. As its displacement effect decreases with a decrease of the incidence angle, the boundary layer on the end wall was observed to become thick. The flow downstream of the cascade turns into the radial direction near the design point. The flow loss becomes minimum at a small positive incidence angle. They also reported later that the performance of the return channel may be improved more successfully by using the tandem cascades.

Lenke and Simon (2000) conducted Computational Fluid Dynamics studies and reported the aerodynamic analysis of return channels of multistage centrifugal compressors. They conducted the studies on return channel geometries used for experimentation by Rothstein and Simon (1983) and Rothstein (1984). In their numerical study they solved algebraic stress equation with standard $k-\epsilon$ equations which is extended by an additional production range time scale and a cross-diffusion term to improve the separation behaviour of the turbulence model. At the inlet boundary the averaged total pressure and total density were specified.

Furthermore, the distributions of the radial velocity component and the flow angle were taken from the measurements. At the outlet, a constant static pressure near the hub was used to establish a radial pressure distribution and the correct mass flow. The simulation studies were conducted on two configurations, one for low flow coefficient and the other for a high flow coefficient. The design blade angle at the inlet of the vane is 26° . In their study it was reported that the influence of vanes on the velocity within the 180° bend is small so that the averaged flow angle at its exit increases by 3° due to friction in the bend. Downstream of the 180° bend the calculations show a separation at suction side. This separation increases from hub to shroud and reattaches in the rear half of the vane. They observed that the secondary flow has no great influence on the flow and shows typical characteristics. A very small horseshoe vortex exists near the leading edge. The secondary flow that was observed at the rear half of the vanes is less than that at the mid region. They attributed this to the acceleration of flow in the second half of the flow channel. The loss behaviour of the investigated channel was observed to be favorable, particularly with steep flow angles. The measured exit flow was found to be swirl-free over the investigated operating range. Only in the region of very small inlet flow angles a deflection beyond 90° occurs in the measurements. The increasing losses with small inlet flow angles indicate that this separation at suction side must be very large. In their simulation study with low flow coefficient

stage both the turbulence models are not able to calculate exit flow angles beyond 90° due to the over prediction of flow separation and the underestimation of streamline curvature effects especially with the $k-\varepsilon$ turbulence model. In the case of small flow coefficient the frictional losses are more dominant and increase the loss coefficients over the whole channel. On the other hand higher flow coefficients increase secondary flow and care has to be taken to avoid small streamline radius of curvature within the crossover bend. A reduced ratio of passage width to mean streamline radius of curvature within the crossover bend has little effect on the losses produced within the bend. But it improves mainly the flow distribution between hub and shroud at the inlet of vanes, which reduces secondary flow within the channel and causes a smoother flow angle distribution between hub and shroud at the exit of the return channel. It was reported that the numerical simulations had shown their capacities to investigate the flow structure within the return channels and CFD became an effective tool for further investigations which are necessary to achieve further improvements particularly in the part load range near surge.

Sorokes, et. al (2003) of Dresser-Rand conducted field tests on a high pressure gas injection multistage centrifugal compressor. They decreased the gas flow path height in order to increase the inlet flow angle and succeeded partially in improving the stage performance.

Sorokes, *et al.* (2000) studied the side-stream optimization for industrial centrifugal compressors through the use of Computational Fluid Dynamics and model testing. Two side-stream configurations were model tested and analyzed. An experimental rig to simulate a typical industrial side-stream device was designed, fabricated and tested. Static swirl vanes were used to give some pre-swirl to the flow before it enters the vaneless diffuser. The flow then takes 180° turn in the crossover bend before it enters the return channel cascade. At the exit of these radial deswirl vanes, the core flow mixes with the side stream flow as it passes through a set of exit guide vanes around a 90° bend, and exits the test rig. In the CFD simulation the grid for each part was considered separately. To reduce the computational grid size and time, only a single swirl vane out of 23 was included in the swirl vane section grid. This was based on the assumption of an axi-symmetric core inlet flow at the top of the return channel bend. The other sections like U-bend and deswirl vanes were modeled full for 360° . The final grids for the original and modified side-stream inlet analyses combined the three parts: main, swirl vane and nozzle. The swirl vane section was connected to the main section by way of a circumferential averaging "stage" interface feature in the CFD solver. The total grid has approximately 8, 00,000 nodes in size. At the inlet of core flow uniform total pressure and temperature were specified along with flow components and their directions. At the exit sections "outflow" boundary condition with specified mass flow rate were

used. They observed that the qualitative agreement between CFD and measured data was fairly good, especially in the total pressure losses. Also the calculated performance difference configuration-to-configuration agreed fairly well with the measured difference. It was concluded that despite the lack of total agreement, CFD can serve as an effective comparative tool in assessing the advantages/disadvantages of design alternatives.

Pazzi *et al.* (2002) reported the use of artificial neural networks for performance prediction of return channels for industrial centrifugal compressors. An innovative procedure for the preliminary design and optimization of return channels for centrifugal compressors was explained. A typical configuration of return channel passages for industrial centrifugal compressors was studied by means of a well-known commercial Navier-Stokes solver. A set of geometrical parameter groups was chosen in order to represent the most significant changes in geometry with respect to the base configuration. A series of new return channel configurations is obtained as the result of variations of one or more geometrical parameters. Each of the geometry obtained with this procedure was analyzed by the flow solver which returns a set of accurately chosen performance indices quantifying aerodynamic losses and distortions at the eye of the downstream impeller. The results thus obtained are used to train a simple single-layer Neural Network which was afterwards interrogated to compute some performance maps linking

the performance indices to the three most related geometrical parameters. Further calculations were carried out on some return channel configurations which have not been previously analyzed. The results confirm that the interpolator is able to predict the return channels performances with a good accuracy. The resulting performance maps, validated by some random tests, seem to be a valid tool for performance prediction of this kind of return channels.

Suping WEN (2008) conducted numerical studies in the circumferential U-bend of a centrifugal compressor stage. A numerical investigation on the flow in a bend channel by coupling the impeller with the vaneless diffuser in a centrifugal compressor with different r/b ratios (bend radius r to bend channel width b) is presented. The jet-wake effect of the impeller outlet is considered and flow pattern in the bend channel and the performance of the centrifugal compressor stage are investigated. The results indicate that there is an optimal r/b ratio for increasing the stage efficiency to the highest for a specific compressor stage. The change in r/b ratio significantly affects the flow angle of the bend channel outlet. The prime reason for the total pressure loss in the bend channel is the wall friction in the bend channel.

Sorokes and Hutchinson (2000) reviewed the practical application of CFD in the design of industrial centrifugal compressors. The industrial designer using CFD as a tool should conform to accuracy of results. Qualitatively the code should reproduce the important flow features,

such as swirl, boundary layers, shocks, wakes separation zones, stagnation points, mixing layers etc. The code should also provide reliable information regarding quantitative data like efficiency, work input, pressure rise, hub-to-shroud profiles, component loss coefficients, flow distortion parameters, incidence, deviation or slip etc. In a case study on "Vaned Diffuser Optimization", it was mentioned that sector models were appropriate since the flow passages were axi-symmetric. This also minimized the computer memory requirement and allowed grid refinement in critical regions like the impeller and diffuser leading edge regions.

Meng and Jackson (1983) reported about the design of continuous-diffuser crossover systems. The continuous-diffusion crossover system serves as a connecting passage and diffuser between two centrifugal impeller stages. This system consists of identical continuous passages axi-symmetrically distributed on a disk plane. Every individual passage consists of two straight meanline diffusers with a turning channel in between. The advantage of this system is reduced diameter for large velocity reduction with reduced pressure loss. This report brings together numerous published experimental results and shows how these can be used together with relatively simple analytical approaches to achieve a high diffuser-crossover system performance. Design details that enhance the performance are discussed. Also, a stall model developed to handle the prediction of the occurrence of stall and the accompanying head loss

due to the diffuser inlet is presented. This model has been shown to correlate well with experimental data. The model can be successfully applied to any vane system, rotating or stationary, to predict the off-design flow that will cause the vane inlet to stall.

Akaike and Toyokura (1979) reported experimental investigations about the flow condition in the inter-stage return bend of a centrifugal compressor stage. The effects of the inlet flow condition and the bend profile on the flow in it were discussed by using five model bends. The flow variation in the bend is resulted from the behavior of a skewed boundary layer along the end walls. In the accelerated region of the downstream half of the bend, the flow shows a tendency to become uniform in general, but the boundary layer along the inner wall has a considerable influence on the flow condition in it.

Japikse (2009) presented detailed guidelines in the turbomachinery performance modeling using CFD. Three-dimensional CFD modeling solves the fluid dynamic equations directly, giving maximum detail. Referred to as Full Navier-Stokes (FNS) methods, they have grown significantly in popularity with the explosion of inexpensive computing power and memory. Historically, computational time and costs were the limiting factor in CFD. More recently, the dominant issue has become the human time for problem setup and interrogation. Specifically, generating the solution grid and post-processing solution results for meaningful data have become the most significant drivers. Software manufacturers

have realized this and have invested significant resources to reducing this aspect of cost, but much more work remains to be done. The calculations just shown were set up and run in a day using an O-grid and a Spallart-Allmaras algebraic turbulence model.

Theoretically, CFD can account for nearly all fluid dynamic phenomena that can potentially affect the performance of turbomachinery. In practice, many issues come into play that can compromise solution results. These issues include: turbulence modeling, numerical schemes, grid resolution, convergence criteria, and others. Virtually all of them can be reduced or even eliminated with sufficient time and computational resources. The trick is to minimize these effects within the practical limits of a real design problem.

The computing power available today has somewhat reduced the variation seen in the past from one turbulence model to the next. While this can be broadly stated for attached flow nominally near the design point, there remains substantial uncertainty for significantly separated flows typically found well off-design or nearing stall. Progress on this front may well come more from systematic study and comparison to test data and “tuning” the approach rather than through any revolutionary breakthrough in turbulence modeling. In this respect, the approach comes full circle back to heuristic methods pioneered in meanline modeling.

It was noted that best practice CFD and meanline models each achieve useful accuracy; it is not a question of one versus the other in most design problems. Rather, it is a matter of using the correct tool at the correct time to deal with the level of detail required.

Benvenuti (1977) presented some test data on return channel vanes at off-design conditions. The design point data is not specified in this particular work. A comprehensive study of the return channel design pertaining to a centrifugal pump was presented by Sulaiman (1975). With a vaneless diffuser, crossover bend has a free vortex flow field. He designed the return channel flow path according to forced vortex flow. The return channel section was designed according to cascade theory using meanline approach. Sulaiman set down the condition of linear change in the moment of momentum for the return channel.

Japikse and Osborne (1982) recommended for a linear change in tangential velocity and also a linear change in the moment of momentum for the return channel design. It was shown that the return passage flow was dominated by large viscous secondary flows and hence the classical two-dimensional cascade data would have little bearing on the return channel performance.

Details of return channel blade shape design were suggested by Ferretti and Pareschi (1977). The blade shapes considered were simple circular arc vanes but with different leading edge shapes. It was shown that the return channel had a minimum loss of 20% of the inlet kinetic

energy, which rises to much higher levels for off-design operation. The blade leading edge was shown to have an effect on the off-design performance.

Person and Wilhelm (1971) investigated three types of crossover systems, with an axial diffuser, radial diffuser and conical diffuser. The configuration with radial diffuser was shown to be most efficient.

Rothstein (1984) designed seven U-bends covering a wide range of geometric parameters and tested for flows swirling between 30° and 80° . He reported the test results of three of the seven U-bends. It was concluded that at higher flow angle of U-bend inlet the loss is dictated by frictional loss evidenced by the insensitivity of meridional velocity and flow angle at U-bend inlet to the U-bend curvature. On the other hand, a flow separation on the convex surface of the bend caused by excessively low values of r is the major reason for the U-bend with below optimum (r/b) values. The importance of Rothstein finding is that a certain extent of axial length constraint might be compensated by an increase of flow swirl.

Chapter 3

EXPERIMENTAL TEST SETUP AND INSTRUMENTATION

3.1 DESCRIPTION OF THE TEST SETUP

The return channel flow investigation is carried out with the development of a static return channel model representing the flow through the impeller, vaneless diffuser, U-bend and return channel passage. To obtain realism in the flow conditions in the area of return passages, the flow path is constructed to resemble that of a complete stage in a multi stage centrifugal compressor. Figure 3.1 shows the schematic sketch of the test setup. The air is drawn in from atmosphere by a blower, delivering design flow rate of $2.5\text{m}^3/\text{sec}$ imparting head of 440 mm of water column at 1500 rpm driven by induction motor of capacity 50 kW. Swirl vane unit is fitted before the inlet of U-bend to simulate the flow conditions at the exit of the rotating impeller of a centrifugal compressor stage. Downstream of the swirl vanes the flow enters a parallel walled vaneless passage to simulate the vaneless diffuser and subsequently into 180° U-turn bend. The radius ratio of diffuser, U-bend and return channel vane configuration is simulated corresponding to a centrifugal compressor stage with a design flow coefficient of 0.053. The fundamental nature of the flow at the exit of swirl vane unit differs from that of an impeller exit in that the impeller

displays an unsteady discharge flow with the mixing of the wakes. The flow after a fixed swirl vane unit is characterized by quasi-stationary wakes. Simon, H and Rothstein, E., 1983, reported that the comparison of the two forms of flow is justified more or less at inlet of the cross over bend, but almost certainly better at the exit of 180° bend because of rigorous energy exchanges taking place in vaneless diffuser and circumferential U-bend. The flow leaving the cross over bend, enters annular passages formed by de-swirl vanes (return channel vanes). From the 90° bend exit, the air enters an annular passage followed by a cone and a straight duct before entering a venturi nozzle for measurement of flow rate. Straight duct of diameter 500 mm carries the flow out of the venturi nozzle into the atmosphere. The mass flow rate through the test section is varied by varying the speed of the blower. The required flow angle at U-bend inlet is obtained by rotating the swirl vanes with the help of variable angle linkage mechanism. This mechanism helps in varying the flow angle at U-bend inlet over a wide range.

3.2 ASSEMBLY OF THE TEST SECTION

The magnified sectional view of the return channel model test section assembly in the meridional plane is shown in Fig. 3.2. The assembly consists of a swirl vane unit with 24 vanes, a return channel vane unit with 18 vanes, centre body, exit diffuser, outer casing inlet assembly and outer casing exit assembly. The crossover bend (180° U-bend), L-turn

exit (90° bend) are formed after assembling the components as shown in Fig. 3.2. The U-bend is sharp on the shroud side which should have been avoided but for the ease of manufacturing and assembling. Its effect on the flow performance is also studied numerically. The details of each component of the test section assembly are discussed below.

3.2.1 Swirl Vane Assembly

The swirl vanes are meant for giving a tangential swirl to the incoming air from the inlet section. The swirl vanes are designed such that they are able take the flow over a wide range of incidence without much disturbance at the leading edge. This is required to obtain the variation of flow angle by turning the vanes about a point passing through the camber line to simulate the corresponding flow angles at the inlet of U-bend. The NACA profile is used to make the swirl vane which is shown in the Fig. 3.3. The swirl vane assembly consisting of 24 vanes is shown in Fig. 3.4. All the swirl vanes are linked to the variable angle mechanism which is described in the following section.

3.2.2 Variable Angle Mechanism

The flow angle at the inlet of crossover bend is required to be changed during the experimental investigations to cover the most of the operating range of the actual centrifugal compressor stage. In the actual centrifugal compressor stage, the flow angle is a function of the flow coefficient.

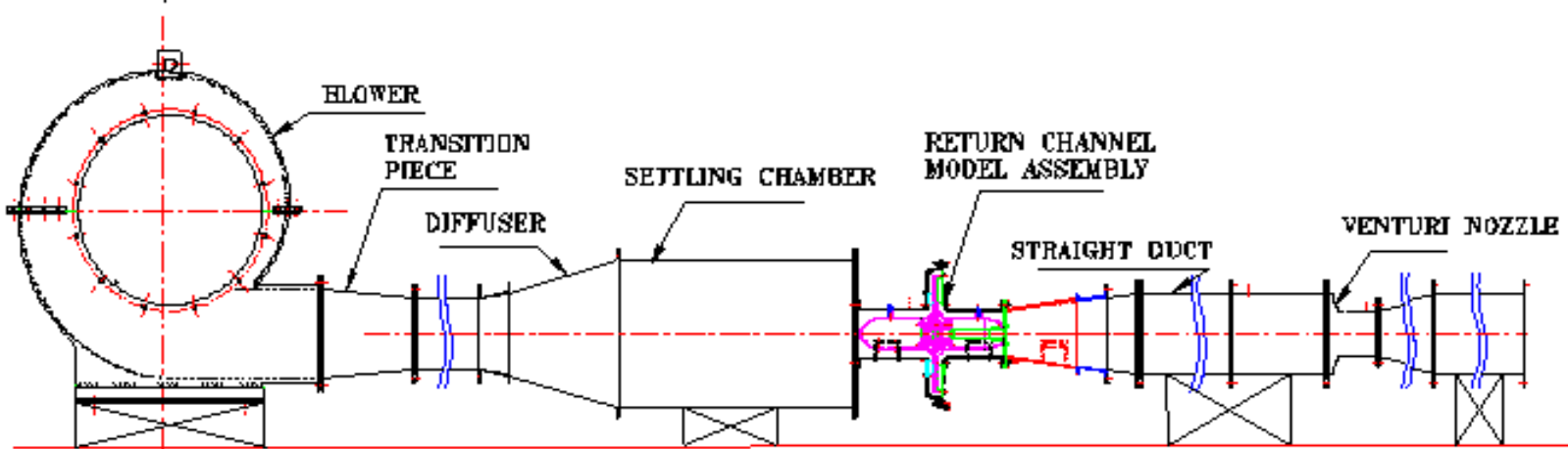


Fig. 3.1 Schematic diagram of the return channel test rig

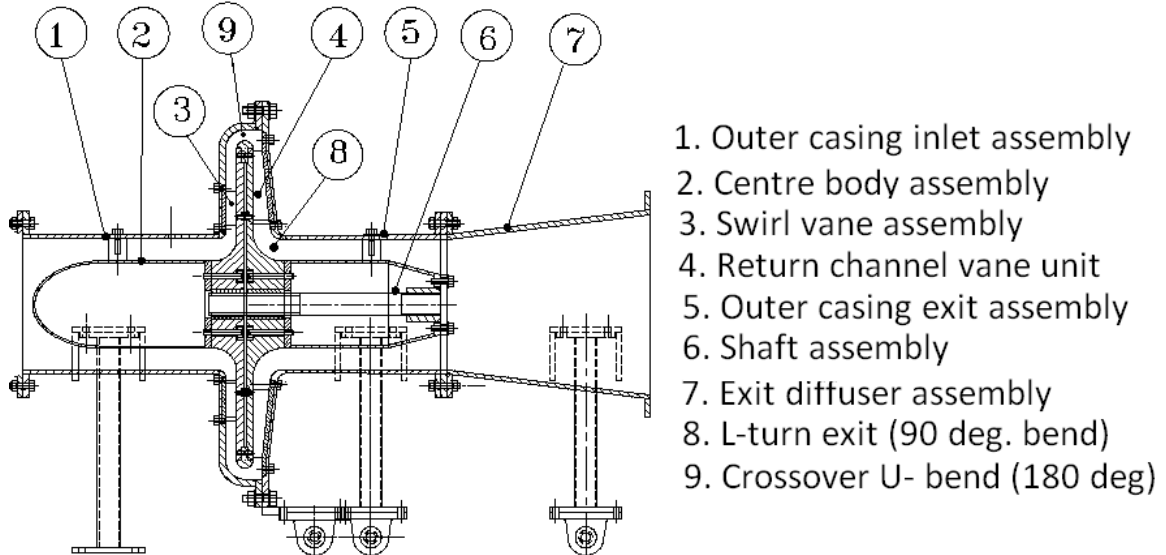


Fig. 3.2 Sectional view of the test setup in meridional plane

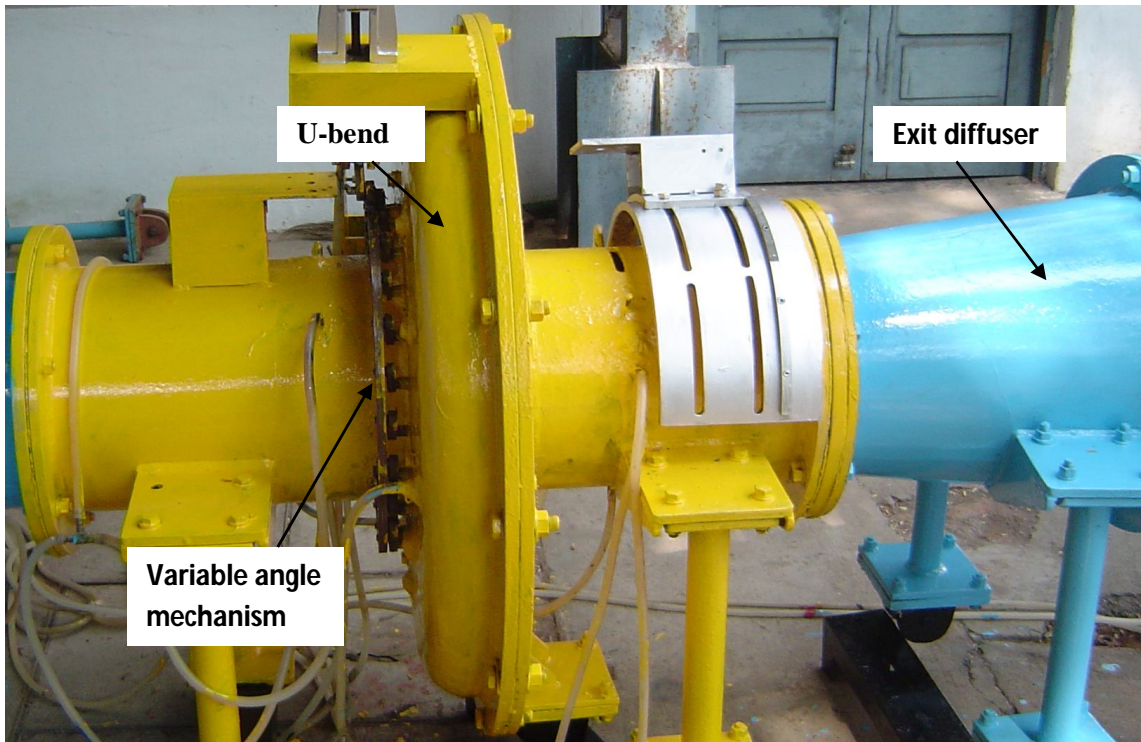


Plate No. 3.1 View showing the model test section

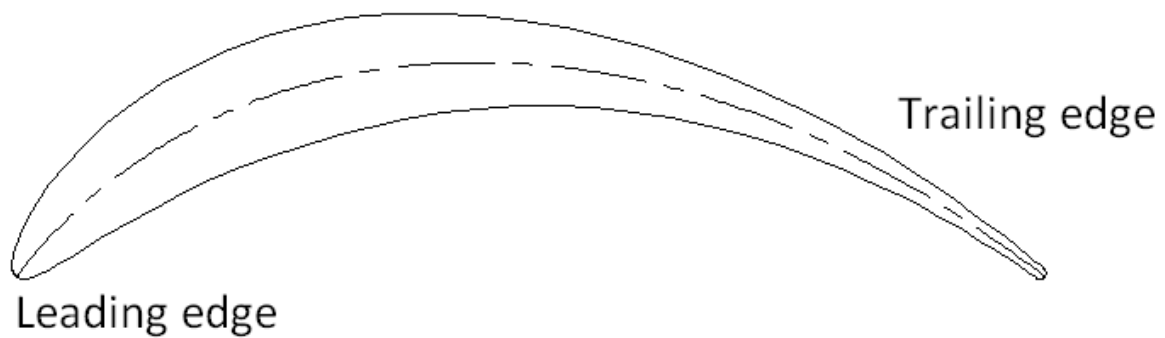


Fig. 3.3 NACA Profile of the swirl vane

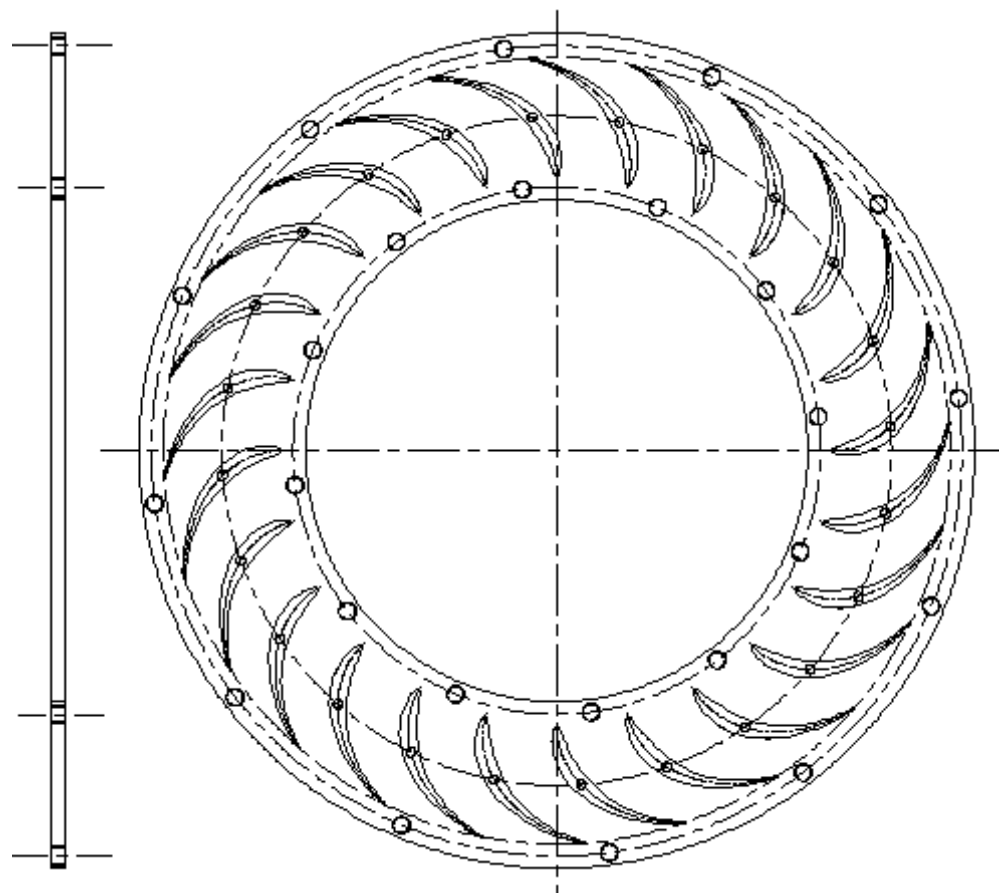


Fig. 3.4 Swirl vanes assembly

The flow angle at the vane less diffuser exit depends on tip speed of the impeller and also the mass flow rate of the fluid. In the present model a set of static swirl vanes are provided to give artificially the required swirl. It is therefore mandatory that the swirl vanes orientation must be altered to simulate the flow conditions covering the most of the operating range of the compressor. The linkage mechanism used for the changing of swirl vane orientation is shown in Fig. 3.5. Using this linkage mechanism all the vane can be rotated about a point on their camber line by the same angle. The swirl vanes are connected through studs to a common ring which has some eccentricity with the centre of the inlet pipe. It is possible to change the orientation of swirl vanes such that the average flow angle at U-bend inlet can be varied from 20° to 45° with respect to tangential direction. In the present study it is required to change the flow angles within the range of 21° to 34° .

3.2.3 Return Channel Vanes Assembly

The assembly of the return channel vanes is shown in Fig. 3.6. The return channel vane assembly consists of 18 number of vanes made up of mild steel and coated with nickel, rigidly fastened to a plate with the help of counter-sunk bolts. The plate fixed with the vanes is fitted in to the outer casing exit assembly. The return channel flow is formed with the central body as hub wall and return channel plate as shroud wall. It may be noted that there is a 6° taper provided to the plate.

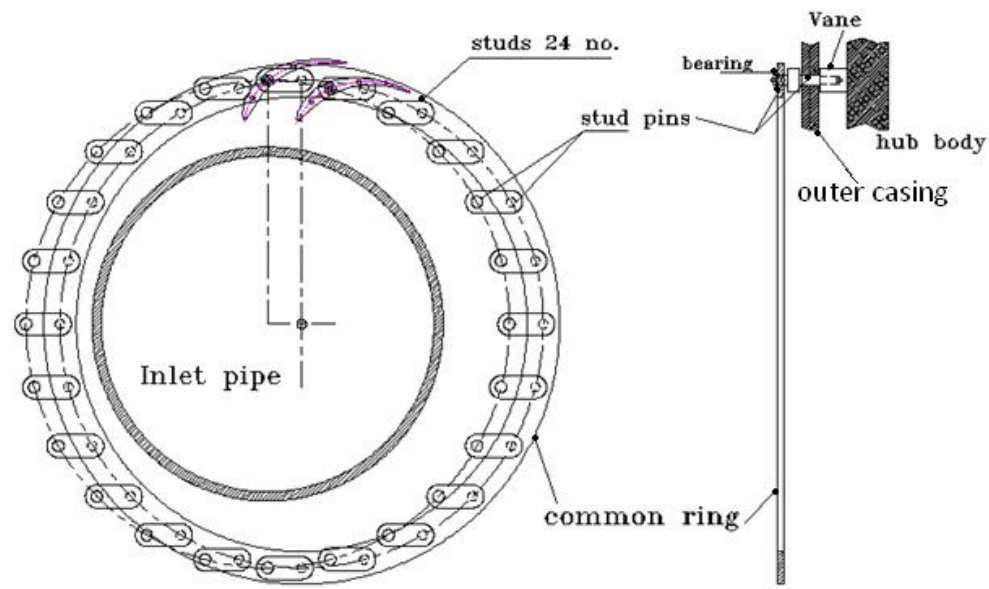


Fig. 3.5 Variable angle linkage mechanism

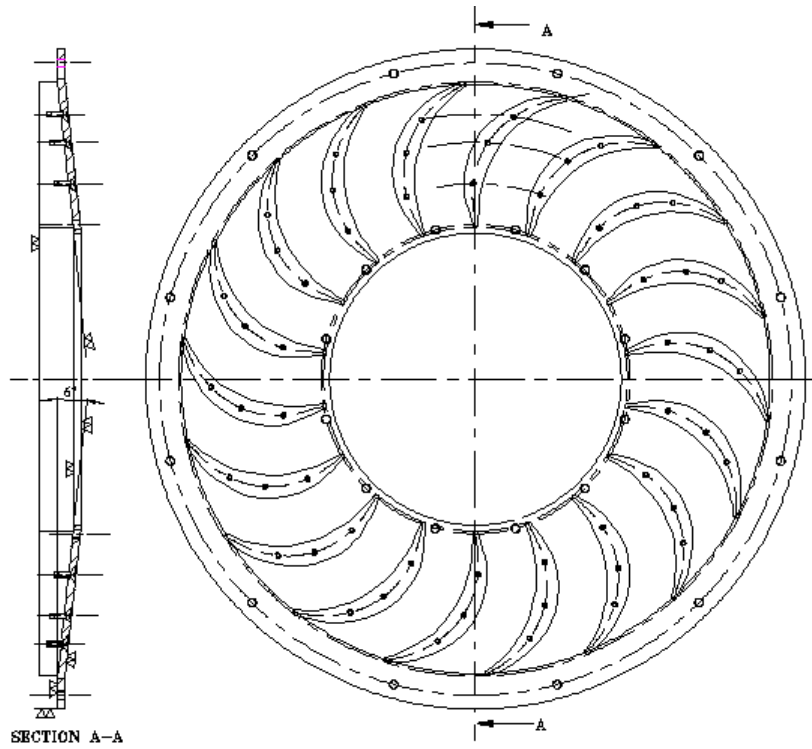


Fig. 3.6 Return channel vanes assembly

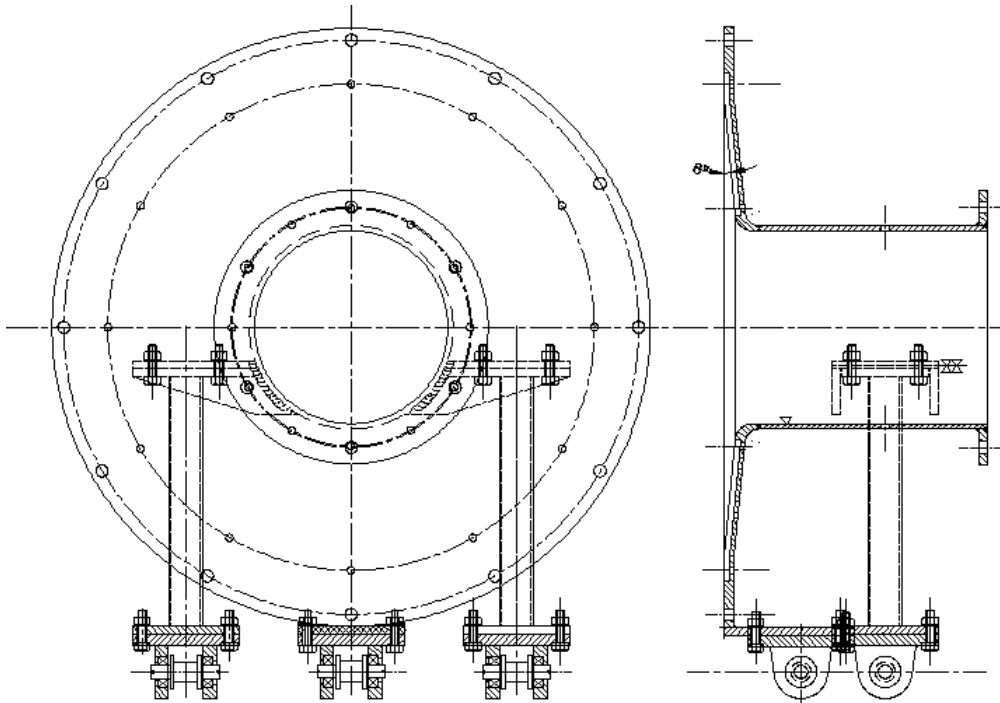


Fig. 3.7 Outer casing exit assembly

3.2.4 Outer Casing Assembly

The outer casing assembly consists of two parts. The first part is towards the inlet side and the second part is towards the exit side. The inlet side and exit side outer casings are rigidly fastened with bolts on their flanges, which form the required flow geometry when assembled with central body, swirl vane ring and deswirl vane ring. The outer casing exit assembly is shown in Fig. 3.7. The outer casing is supported on a stand.

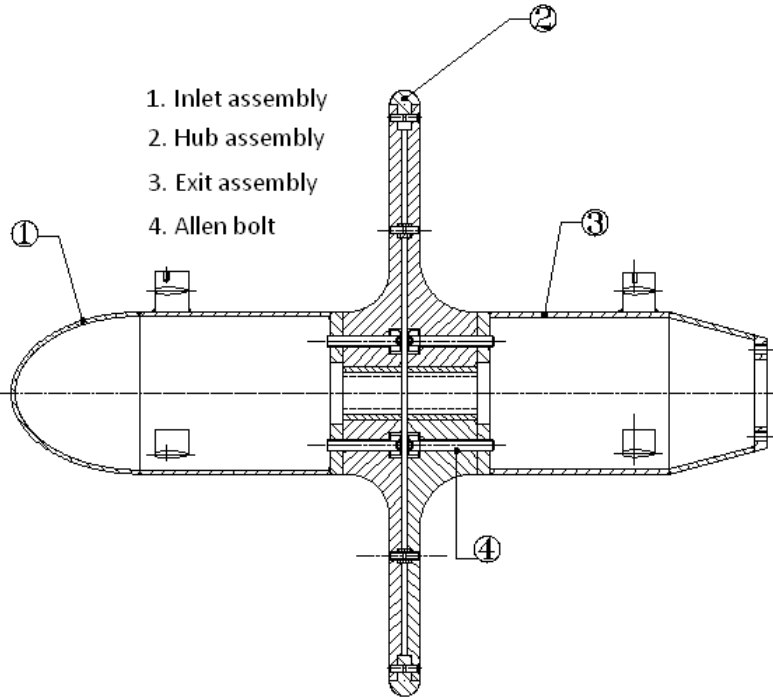


Fig. 3.8 Centre Body assembly

3.2.5 Centre body assembly

The Central Body assembly is shown in the Fig. 3.8. It occupies the space between the front and back support walls of the casing on swirl vane unit side and deswirl vane unit side. This is made up of aluminum alloy. The front wall should firmly touch the swirl vane blades to avoid leakage of the flow without swirl. There is a provision for aligning the wall firmly with the deswirl vanes. A hub is supported by bolts to prevent misalignment. The hub is made of mild steel. The back wall is provided to support deswirl vane unit. This is also firmly fixed to avoid leakage flow in deswirl vane unit. The back wall has been aligned firmly to avoid leakage and to see that all the flow passes through the deswirl vanes.

3.2.6 Exit Diffuser Cone

The exit flow from the deswirl vanes takes an L-turn and enters the exit diffuser cone. It is fixed rigidly to the outer case exit flange with bolts. This is made up of mild steel. It is a diverging section used for recovery of pressure after deswirl vane exit. Wheels are provided for easy alignment on to the test stand. A gasket is provided between the joining sections to prevent leakage of air. High tensile bolts and nuts are used for firm fixing without failure of joints.

3.3 INSTRUMENTATION

3.3.1 Measurement of Pressure

The pressure at different locations was measured using a digital micro manometer. It has measuring range of 0-199.9 and 0-1999 mm water column and a measuring accuracy of 0.1mm and 1mm water column respectively. A 20 channel differential scanning box was used in conjunction with the digital micro-manometer for recording the different pressure signals. The atmospheric pressure was measured using an absolute pressure transducer in conjunction with the micro-manometer.

3.3.2 Measurement of Temperature

Wet and dry bulb temperatures and atmospheric pressure are required for calculating density of medium. Wet bulb and dry bulb temperatures were measured with the help of two wet and dry bulb thermometers. In one of them a wick was placed around the mercury bulb. The wick was partially immersed in water with the bulb exposed to

atmospheric air to measure the wet bulb temperature. The ambient temperature was used in the calculation of density of atmospheric air. The temperature of air flow was measured by using resistance thermometer with a digital read out, having a least count of 0.1°C.

3.3.3 Measurement of Flow Rate using a Venturi Nozzle

The measurement of airflow rate through the test setup was carried out using a venturi nozzle which is shown in Fig. 3.9. The venturi is simplest type of flow meter and can be easily inserted into the existing pipeline with a minimum of alteration to the layout and can be used to measure the airflow. The flow rate was found by measuring the static pressure drop across the venturi nozzle. The static pressure drop was found by connecting the flexible pipe of 5mm bore to a micro manometer. This was calibrated and has an accuracy of 0.01 mm of water column. The mass flow rate was calculated by the equation given below.

$$m = \frac{\alpha * \varepsilon * \pi d^2}{4 * \sqrt{(2 * g * \rho_u * \Delta p)}} \quad \text{Eq.3.1}$$

Where,

m = Mass flow in kg/s

α = Flow coefficient

ε = Expansibility factor

d = Throat diameter of venturi nozzle in metres.

ρ_u = Density at the upstream of venturi in kg/m³

Δp = Pressure drop across the venturi nozzle in mm of water column

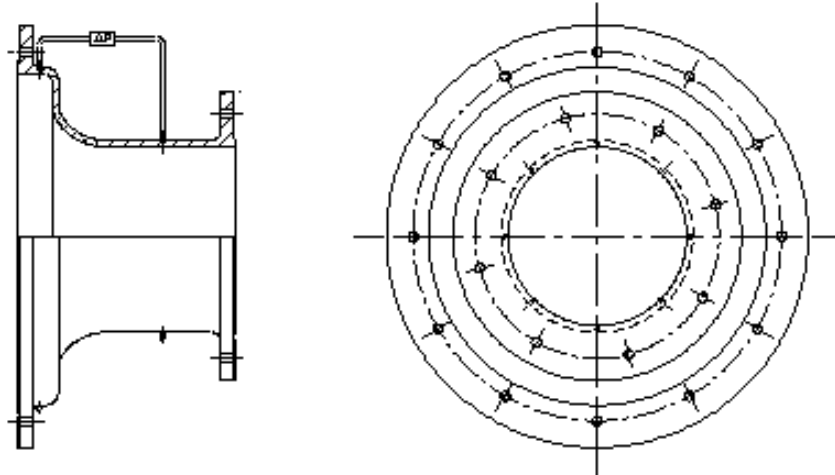


Fig.3.9 Venturi Nozzle

3.3.4 Probe Traversing Mechanism

For surveying of flow at various stations of test setup, the measuring probes should be supported in suitable holders to permit accurate linear and circumferential traverses and angular setting of the probe. The installation of actuator includes allotting mechanical space on the test rig sufficient to mount the actuator, heat avoidance problems and getting the proper electrical cables and transducers hooked up to the actuator and probe. One electric motor drives the lead screw for linear traverse called Traversing Motor and another rotates the barrel to which the probe is attached to give angular movement of the probe and is called Yaw Motor. The probe is held firmly in position by the probe collect. The probe collect is a split clamp collect. No collect insert is needed for 3/4" diameter probes. If a different diameter is to be used up to 3/4", then a

collect insert should be used. Actuator calibration consists of checking the traverse and angular motion position verses their respective electronic read outs at the control. Traversing mechanism is fixed firmly using screwed fasteners on a bracket, which is welded on the test setup periphery using arc welding process. Indications of the linear and the angular positions are obtained from the counter readings, which are provided on the traversing mechanism.

3.3.5 Measurements with Three-hole Wedge Probe

A pre-calibrated three-hole wedge probe is used to measure total pressure, static pressure, velocity and flow angle at various locations like U-bend inlet, U-bend exit and L-turn exit. A specially made traversing mechanism is used for longitudinal and rotational movements of the probe. This mechanism is fixed to an arm, which is pivoted at a location on the back wall of the casing.

3.3.6 Calibration of Wedge Probe

The wedge probe used for the measurement of flow at various locations of the flow geometry was calibrated in a calibration tunnel before the start of experimentation. The probe geometry is shown in the Fig 3.10. A 3-hole probe generally measures total and static pressures in the direction of flow in yaw position from which velocity components in 2-imensions can be computed. The probe is mounted in a special holding adjustment mechanism, which could be rotated in two mutually perpendicular planes.

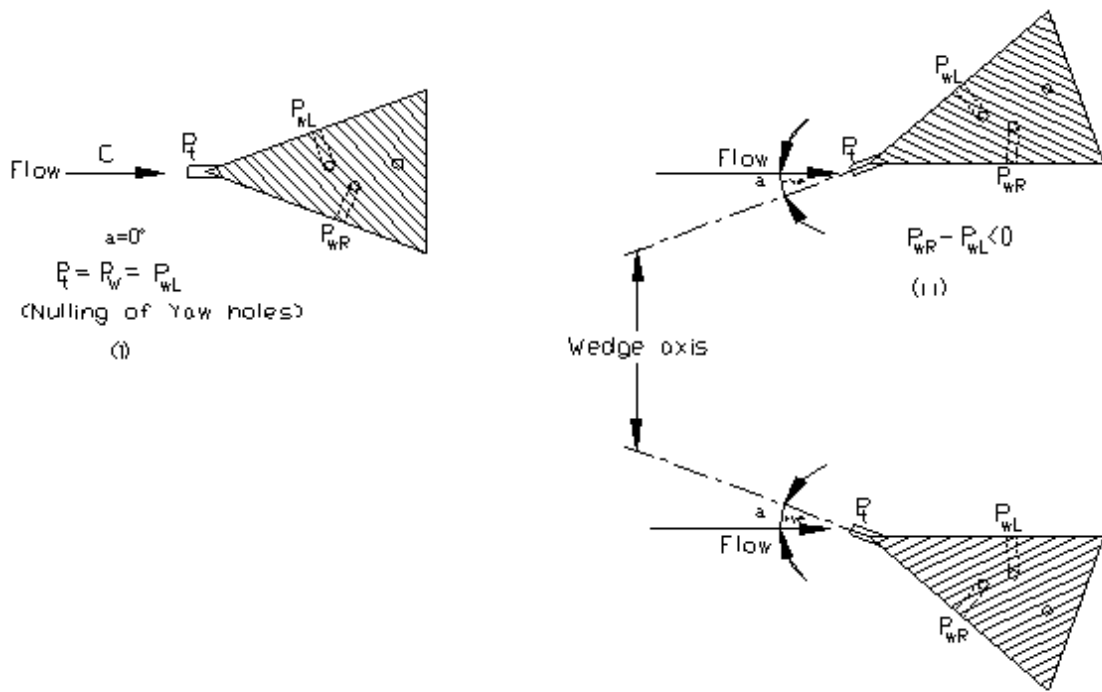


Fig.3.10 Three-Hole Wedge probe

The holding device is designed in such a way that, yaw angle and pitch angle could both be varied independently. Static pressure was noted from the wall static pressure taps, which were provided on the test section of the tunnel. Same procedure is followed for non-nulling method by varying the yaw angle in the range of $\pm 20^\circ$ in intervals of 3° . From the pressures taken, the following calibration coefficients are computed.

P_t = Center hole pressure.

P_s = Wall Static Pressure.

$$\text{and } P_{av} = (P_{wR} + P_{wL}) / 2 \quad \text{Eq3.2}$$

$$\text{Calibration factor for each data point} = (P_s - P_{av}) / ((P_t - P_{av}))$$

The average calibration factor is given by the slope of the curve fitted. Using above coefficients, the calibration curves are drawn. A typical Calibration curve is shown in Fig. 3.11.

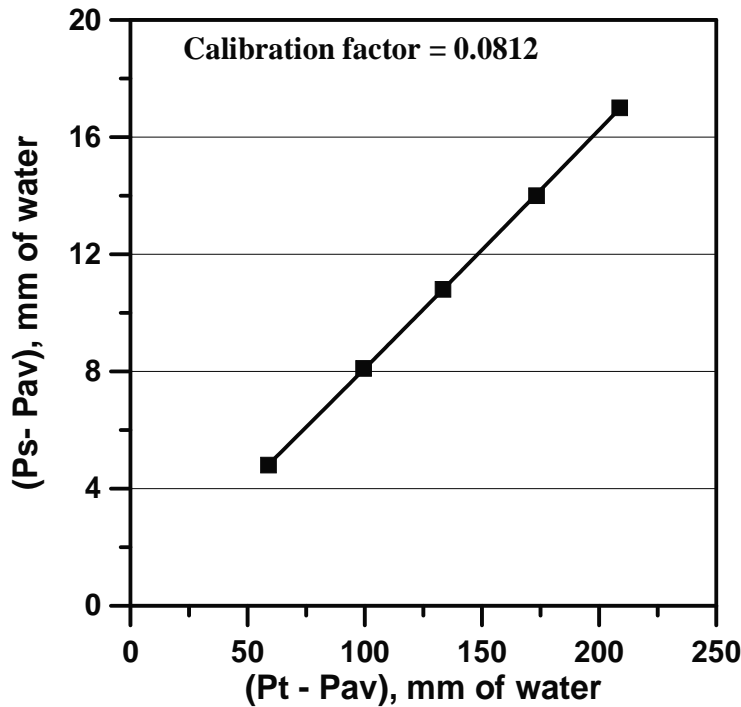


Fig.3.11 Calibration Chart for three-hole wedge probe

3.3.7 Vane Surface Pressure Measurement

On the return vane surface 1mm diameter holes were drilled to certain depth on the mid-span line of pressure side and suction side of the vane. Again 1.5 mm diameter holes were drilled through the casing in to the vane perpendicular to the 1mm diameter holes, until them meet each other. Stainless steel tubes were inserted in to the vane through the 1.5mm diameter holes from outside of the casing. A total of 34 holes of 1mm diameter were drilled on the vane surface for sensing the static

pressure. Figure 3.12 shows the locations of the drilled holes for the measurement of static pressure distribution on the vane surface. Plate 3.2 shows the vane surface static pressure measurement location and the circumferential plate for probe traverse at the stage exit. All the stainless steel tubes are connected with vinyl tubing to a multi channel scanner and selector box. The output from the scanner box is connected to a micro-manometer. The selected channel static pressure output is read through a micro-manometer with digital display.

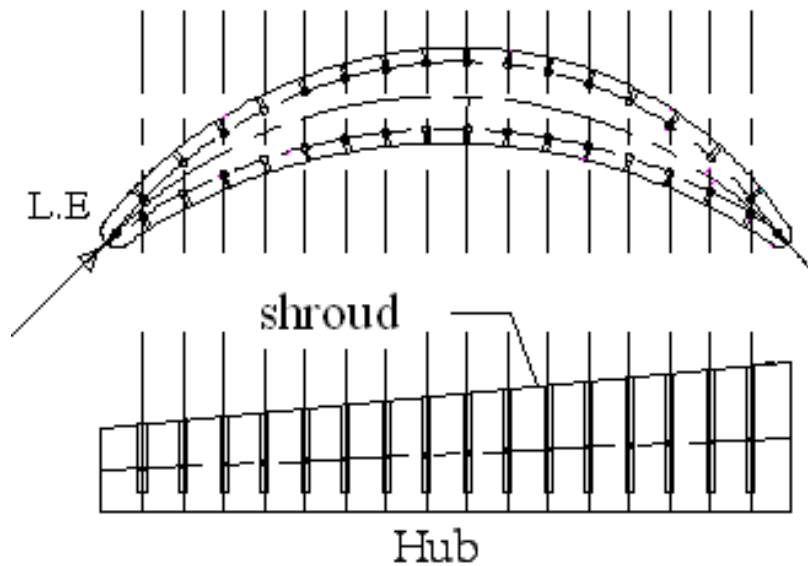


Fig.3.12 Locations of holes on return channel vane surface for pressure measurement

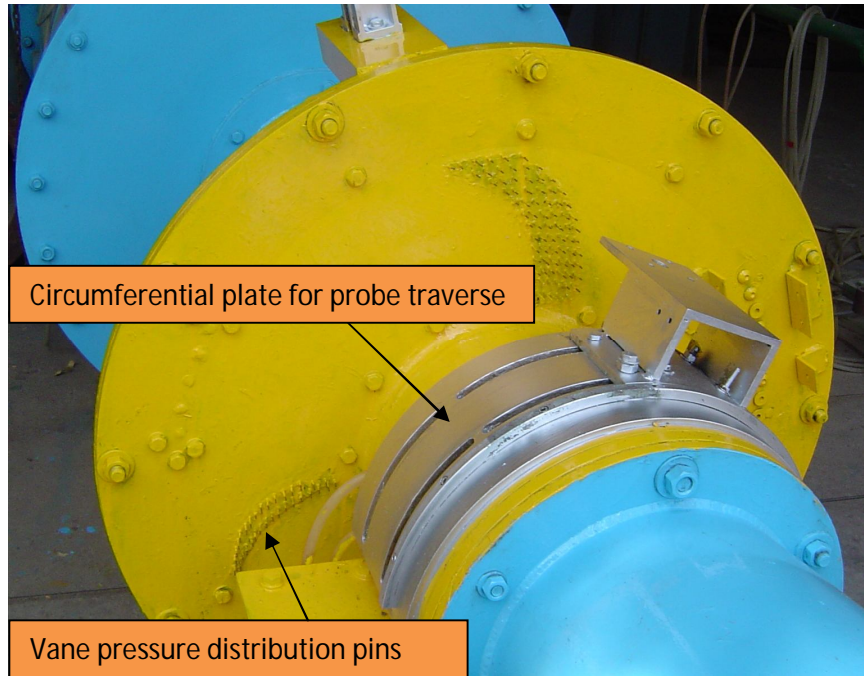


Plate 3.2 View showing location for vane surface static pressure measurement

Chapter 4

EXPERIMENTAL PROGRAMME AND PROCEDURE

4.1 BASIS FOR SELECTION OF VANE PROFILES RCV1 AND RCV2

Siva Reddy (2007) conducted experimental studies in a centrifugal compressor stage with a stage flow coefficient of 0.053. The flow angle distributions measured at the exit of vane-less diffuser and the corresponding mass flow rates formed the basis for the design of return channel passages RCV1 and RCV2 and the operating conditions in the present study. The average flow angles at the vane-less diffuser exit of the centrifugal compressor stage as reported by Siva Reddy (2007) are shown in the Table 4.1.

Table 4.1 Average flow angles at the vane less diffuser exit

S.No	Operating Condition	α_1
1	70% flow rate	21°
2	80% flow rate	24°
3	100%flow rate	29°
4	110% flow rate	32°
5	120% flow rate	34°

As the flow passes through the 180° crossover bend, for a decrease in the flow path width of U-bend exit, it is expected that the average flow angle at the exit should increase by 3° to 5° . Therefore there is a possibility of flow angle varying from 24° to 37° at the entrance of the

return channel passages throughout the operating range of the actual centrifugal compressor stage. The return channel vane L.E should be able to cope up with this type of flow angle variations while receiving the flow. For this reason RCV1 was given an inlet vane angle of 28.5° . For RCV2 an inlet vane angle of 27° was chosen. It is expected that the flow at the exit of the return channel passages should become purely radial and should not have any deviation (swirl) up to the L-turn exit.. This means that the flow should be turned through the return channel passages by 60° to 65° while making it swirl free. This whole process should occur with minimum losses. This is difficult to achieve without causing the flow separation particularly on the suction side with flow angles having positive incidence on the L.E of return channel vane. Any small amount of flow separation on the suction side would induce cross flows and an increase in the exit swirl angle. For this reason to avoid large swirl angles at the stage exit, the exit vane angle of the return channel vane for RCV1 and RCV2 is chosen as 82° with respect to tangential direction so that even when the flow is subjected to secondary flows in the L-turn ducting turning, the flow shall be closer to the axial direction. The next important design parameter is the mean stream line flow angle variation in the vane to vane flow path. The variation of mean stream line flow angle with % arc length for RCV1 and RCV2 and the nomenclature are shown in Fig. 4.1(a) and (b) respectively.

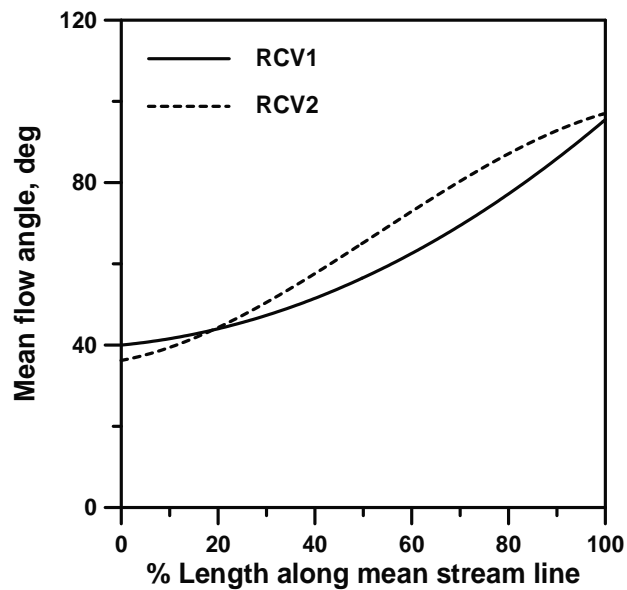


Fig. 4.1(a) Variation of mean streamline flow angle for RCV1 and RCV2

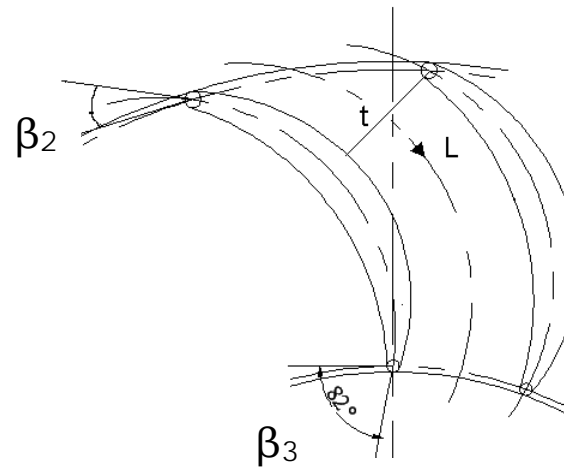


Fig. 4.1 (b) Vane-to-vane nomenclature of return channel vanes

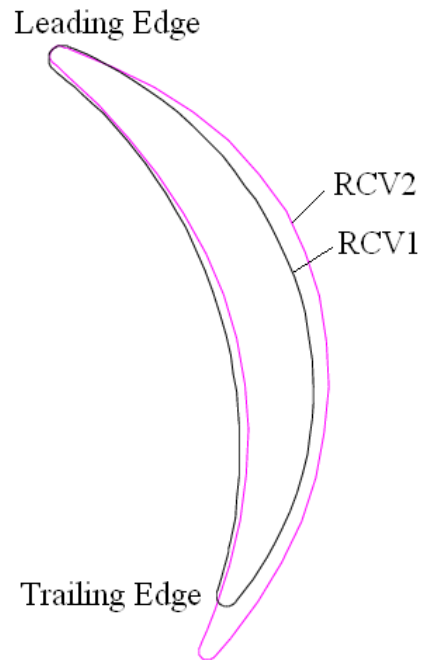


Fig. 4.2 Overlapped vane profiles of RCV1 and RCV2

The mean streamline flow angle for RCV1 is gradually increased up to 60% length and thereafter the rate of increase is higher. RCV2 is given higher rate of flow angle increase in the first half of its length while the rate of increase is reduced in the second half. The overlapped vane profiles for RCV1 and RCV2 are shown in Fig.4.2. The selected design parameters for RCV1 and RCV2 are shown in Table 4.2

Table 4.2 Design parameters for RCV1 and RCV2

S.No	Parameter	RCV1	RCV2
1	Vane inlet angle	28.5°	27°
2	Vane exit angle	82°	82°
3	Chord length	168.5 mm	182 mm

4.2 EXPERIMENTAL PROGRAMME

The experimental programme is planned for conducting flow investigations in the model test rig with two different return channel geometries designated as RCV1 and RCV2. The main aim of these experimental investigations is to assess the aerodynamic performance of the crossover system consisting of a crossover U-bend, a cascade of return channel vanes and exit L-turn ducting. The flow measurements are to be taken by traversing a three-hole wedge probe at U-bend inlet, U-bend exit and L-turn exit. The vane surface static pressure distributions (vane loading) on the mid-span are to be obtained in each case. The experimental investigations on each configuration of return

channel vane are to be covered for the most of the operating range of a centrifugal compressor. In the present study the testing is to be carried out with model test rig simulating the flow conditions of a centrifugal compressor with a stage flow coefficient of 0.053. The flow conditions under which measurements are taken in the model test rig are covering the operating conditions of the actual compressor at 70%, 80%, 100%, 110% and 120% of design flow rate.

4.2.1 Operating Conditions

The simulated flow conditions through the test rig are shown in Table 4.1. The flow angles mentioned are measured with respect tangential direction. The centrifugal blower is driven by a variable speed induction motor. The flow measurements were taken at three different locations namely, Location-1(U-bend inlet), Location-2(U-bend exit) and Location-4 (L-turn exit) as shown in Fig.4.3

Table 4.3 Operating conditions

S.No	Q (m ³ /sec)	α_1 (deg)
1	0.867	21°
2	0.988	24°
3	1.24	29°
4	1.35	32°
5	1.47	34°

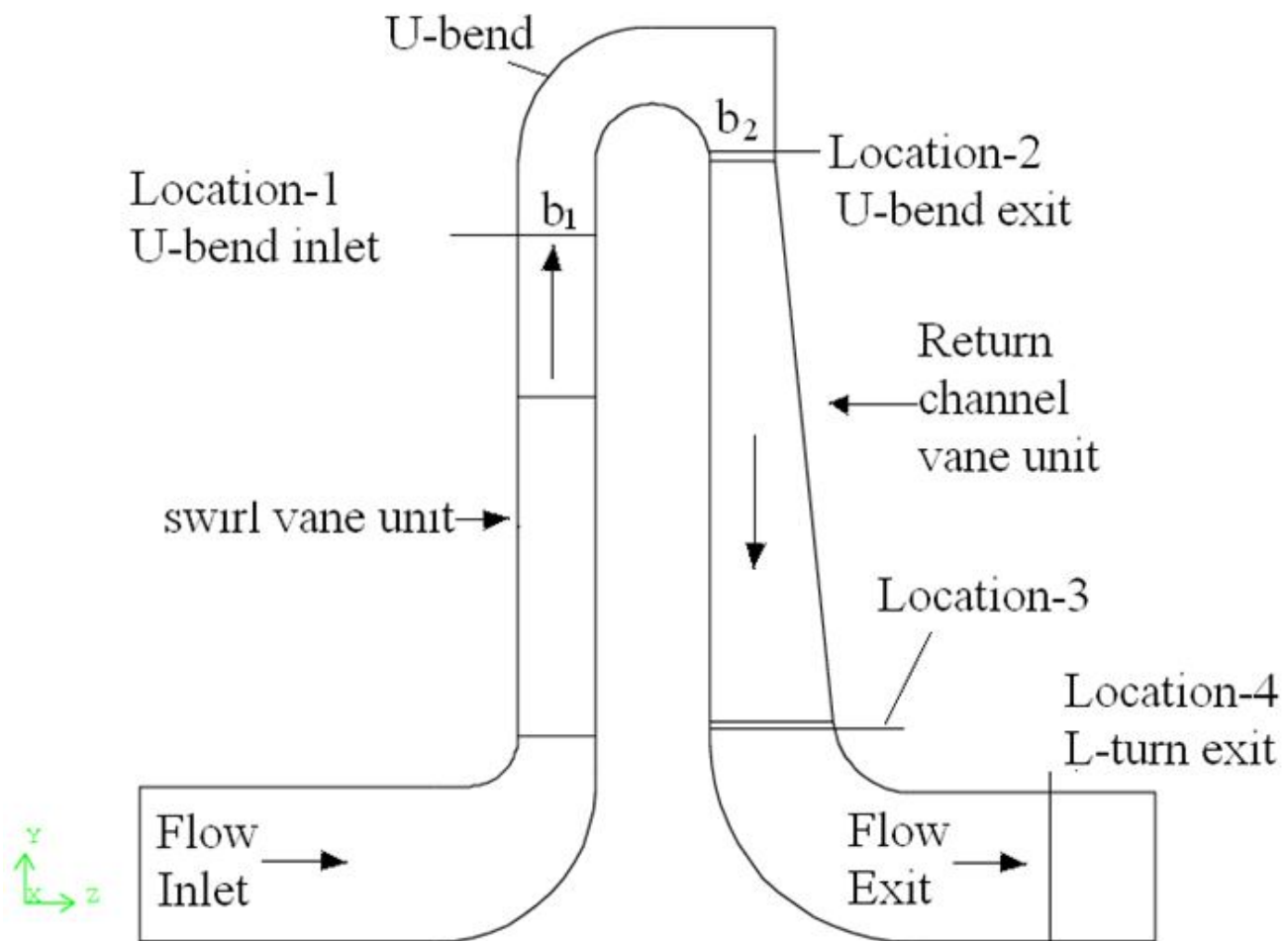


Fig. 4.3 Measurement locations in the meridional plane

No measurements were taken at Location-3 as it was not amenable for traversing the wedge probe using the traversing mechanism. The pre-calibrated wedge probe is traversed from shroud to hub at one station of U-bend inlet. The measurements at U-bend exit covered 11 stations circumferentially, covering two spans of the return channel vanes. At each station of U-bend exit the probe is traversed from hub to shroud. At the L-turn exit, the probe is traversed from shroud to hub at 9 circumferential locations as shown in Fig.4.4. These stations are corresponding to the angle made by the traversing direction with the vertical line. The stations are at -20° , -15° , -10° , -5° , 0° , $+5^\circ$, $+10^\circ$, $+15^\circ$ and $+20^\circ$ with respect to the vertical line (0°) at Location-4. To carry out flow measurements at the L-turn exit a circumferential slotted plate is manufactured and fixed. On the circumferential plate the probe traversing mechanism base is fixed which can be slided as per the requirement. The locations of measurement at the U-bend inlet is shown in Plate 4.1. The U-bend exit location, and L-turn exit on which circumferential plate is fixed are shown in Plate 4.2.

4.2.2 Leakage Testing

All the joints were tightened with suitable gaskets placed in between to prevent possible leakage of air at different flange joints along the flow path. The test rig was erected according to BS 848 standard (1997). A trial test was conducted before the start of each run of experiment to check the leakage flows at the flanged joints.

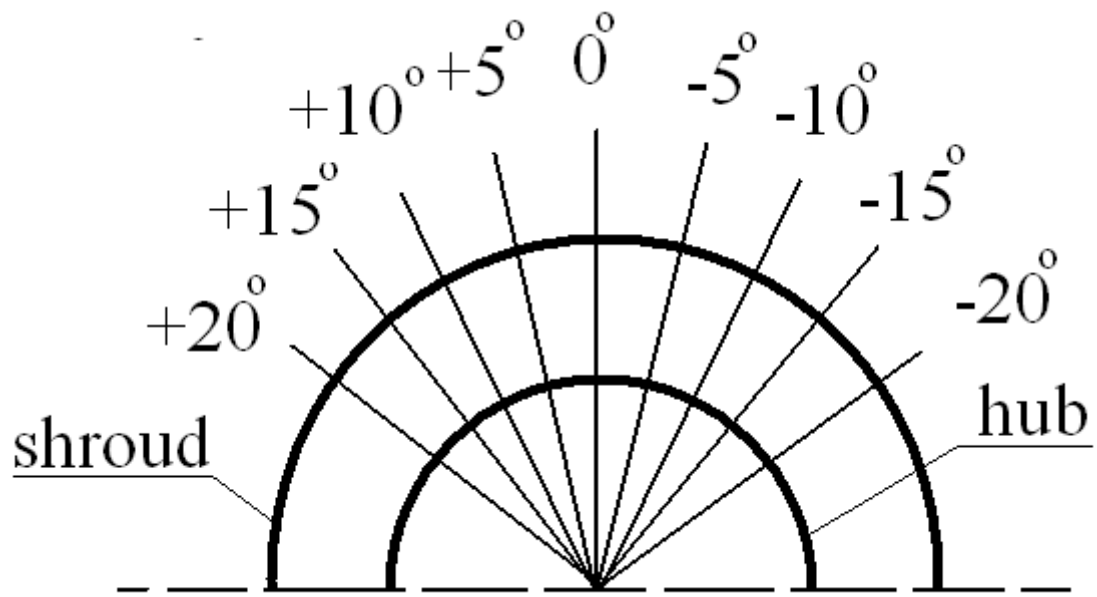


Fig.4.4 Measurement locations along the circumference at the L-turn exit

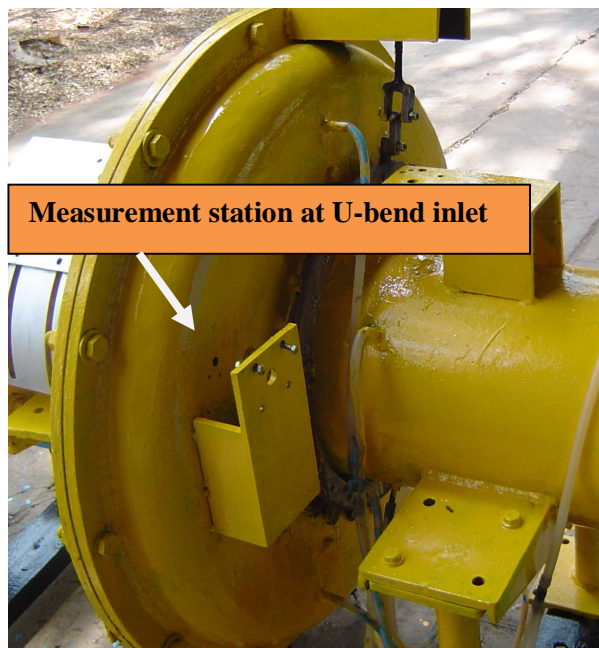


Plate 4.1 View showing measuring station at the inlet of U-bend

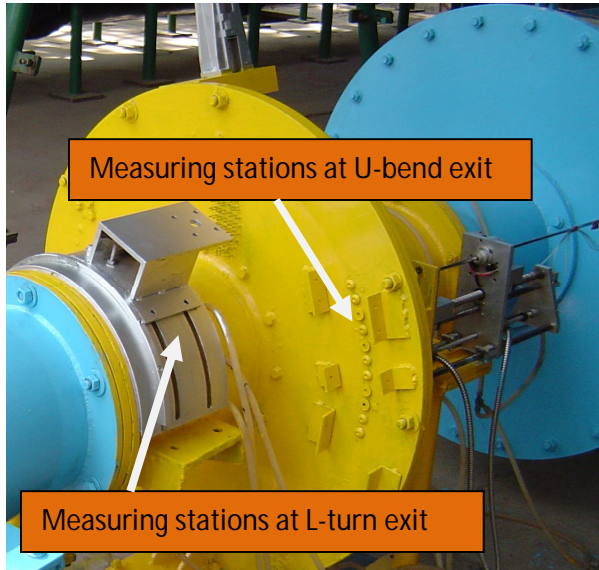


Plate 4.2 View showing measuring stations at the exit of U-bend and L-turn exit

4.3 EXPERIMENTAL PROCEDURE

The experimental procedure followed during the whole program is explained below:

1. The return channel configuration RCV1 was assembled in the test rig and the trial runs were conducted to check the leakage of flow.
2. The flow conditions at the design point of the actual compressor stage are simulated in the test rig. This is achieved by adjusting the swirl vane orientation with the help of variable angle mechanism and the speed of the blower. At the design point a flow angle of 29° with respect to tangential direction is achieved corresponding to a flow rate of $1.24 \text{ m}^3/\text{sec.}$.

3. Once the flow conditions are established, the wedge probe is traversed at U-bend inlet, U-bend exit and L-turn exit from hub to shroud and the static pressures and total pressure were noted. At the same time the wall static pressures at various locations of the flow path like, U-bend inlet, U-bend exit and L-turn exit were also noted.
4. The vane static pressure readings at the 34 locations on the return channel vane surface were noted.
5. The settling chamber pressure and temperature were noted. The ambient wet bulb and dry bulb temperatures were noted. The variations in the ambient conditions during the testing are taken care of by normalizing the recorded pressures with the chosen constant value of the settling chamber pressure.
6. The atmospheric pressure is measured using a pre-calibrated pressure transducer with a digital display.
7. The above experimental procedure is repeated for off-design operating conditions which were mentioned in Table 4.1.
8. The above said experimental procedure at the design and off-design conditions is repeated for RCV2 configuration
9. The velocity distribution, static pressure distribution and performance parameters were plotted for both RCV1 and RCV2 configurations.

4.4 GRAPHICAL PRESENTATION OF RESULTS

4.4.1 Meridional Velocity Distribution

The meridional velocity distribution from hub to shroud at U-bend inlet, U-bend exit and L-turn exit are presented in X-Y plots. The circumferentially averaged values are presented at U-bend exit and L-turn exit locations.

4.4.2 Flow Angle Distribution

The flow angles at all stations are measured with respect to tangential direction. The variation of flow angle is plotted from hub to shroud at all locations 1, 2 and 4. The flow angle at the exit ducting is also termed as "exit swirl".

4.4.3 Vane Surface Pressure Distribution (C_{pv})

The static pressures measured on the suction and pressure surfaces of the return channel vane are expressed as coefficient in the non-dimensional form by dividing with the average dynamic pressure at the inlet of U-bend as shown in Eq.4.1. The vane static pressure distribution is plotted against the percent chord length from the leading edge.

$$C_{pv} = \frac{\bar{p}_{sv} - \bar{p}_{s1}}{\bar{p}_{t1} - \bar{p}_{s1}} \quad \text{Eq 4.1}$$

4.4.4 Total Pressure Loss Coefficient

The total pressure loss between any two locations is expressed in the non-dimensional form by dividing with the average dynamic pressure

at the inlet of U-bend. Eq.4.2 and 4.3 give the expressions for U-bend and stage total pressure loss coefficients respectively. The total pressure loss coefficient is plotted against the average flow angle at the inlet of U-bend. This is one of the important parameters in assessing the stage performance.

$$\zeta_{14} = \frac{\bar{p}_{t1} - \bar{p}_{t4}}{\bar{p}_{t1} - \bar{p}_{s1}} \quad \text{Eq 4.2}$$

$$\zeta_{12} = \frac{\bar{p}_{t1} - \bar{p}_{t2}}{\bar{p}_{t1} - \bar{p}_{s1}} \quad \text{Eq 4.3}$$

4.4.5 Static Pressure Recovery Coefficient

The static pressure difference between any two locations is expressed in the non-dimensional form by dividing with the average dynamic pressure at the inlet of U-bend. Eq.4.4 and 4.5 give the expressions for U-bend and stage static pressure recovery coefficients respectively. The static pressure recovery coefficient is plotted against the average flow angle at the inlet of U-bend.

$$C_{p12} = \frac{\bar{p}_{s2} - \bar{p}_{s1}}{\bar{p}_{t1} - \bar{p}_{s1}} \quad \text{Eq 4.4}$$

$$C_{p14} = \frac{\bar{p}_{s4} - \bar{p}_{s1}}{\bar{p}_{t1} - \bar{p}_{s1}} \quad \text{Eq 4.5}$$

Chapter 5

NUMERICAL SOLUTION DETAILS

5.1 INTRODUCTION

The numerical studies procedure that is used in the present study of flow through return channel passages is described in this chapter. The commercial Computational Fluid Dynamics software FLUENT was used to perform numerical calculations. It solves the 3-D Reynolds-Navier-Stokes equations for the mass-averaged velocity and the time-averaged pressure, energy and density. The software has been used by many researchers in solving fluid dynamics problems like flow through turbomachines, combustion simulation and chemical reaction flows. The fluid flow solver provides solutions for incompressible, compressible, steady state, transient, laminar, turbulent, single-phase and multi-phase fluid flows in complex geometries. The software uses finite volume formulation in solving the governing equations.

The governing equations of Reynolds-averaged Navier-Stokes (RANS) solved by the code in relation to the present problem are given as follows.

1. Conservation of mass

$$\rho \frac{\partial \rho}{\partial t} + \frac{\partial}{\partial x_i} (\rho u_i) = 0 \quad --- \quad \text{Eq-5.1}$$

2. Conservation of momentum

$$\rho \frac{D u_i}{D t} = - \frac{\partial p}{\partial x_i} + \frac{\partial}{\partial x_i} \left[\mu \left(\frac{\partial u_i}{\partial x_j} + \frac{\partial u_j}{\partial x_i} - \frac{2}{3} \delta_{ij} \frac{\partial u_k}{\partial x_k} \right) \right] + \frac{\partial}{\partial x_j} (- \rho \bar{u}_i' \bar{u}_j') \quad --- \quad \text{Eq-5.2}$$

5.2 STEPS FOR NUMERICAL SOLUTION

The numerical solution was obtained through the following steps.

1. Identification of flow domain
2. Reading the coordinates for hub, shroud and return channel vane profile.
3. Creation of 3D sector models for the U-bend and L-turn exit
4. Mesh generation for U-bend and L-turn ducting
5. Specifying the boundary conditions for the U-bend and L-turn ducting
6. Importing the mesh for U-bend and L-turn ducting
7. Creation of 3D sector model for return channel vane using TURBO TOOLS option in GAMBIT
8. Creation of boundary layers on the return channel vane surface
9. Mesh generation for the return channel vane sector
10. Defining the boundary conditions for the return channel vane sector
11. Importing the return channel vane mesh
12. Merging the U-bend, L-turn mesh file and the return channel vane mesh files using TGRID
13. Reading the merged mesh file in to FLUENT solver
14. Defining the interface boundaries
15. Specifying the boundary condition values at the inlet of U-bend and exit of L-turn

16. Specification of solver settings like turbulence model, type of solver, discretization method, relaxation parameters
17. Setting the residual parameters
18. Initialization of the solution
19. Running the solution till convergence
20. Post-processing of the data

5.3 GRID GENERATION

The first step of grid generation is to define the flow domain through which fluid flow needs to be simulated. The present study is carried out in the flow domain starting from the inlet of crossover bend followed by a cascade of return channel vanes and an L-turn exit. The experimental values of velocity distribution and total pressure obtained at the inlet of U-bend are given as inlet boundary conditions in the numerical study.

The three dimensional sector models are considered appropriate for this analysis as the flow passages are axi-symmetric. This procedure also minimized the computer memory requirement and allowed grid refinement in critical regions. The grid generated for the entire stage starting from U-bend inlet to L-turn exit consists of three separate blocks. They are a sector of U-bend, a sector of deswirl vane and a sector of L-turn exit. There are 18 deswirl vanes in the return channel geometry, of which only one deswirl vane covering a rotational angle of 20° is considered for simulation. Similarly the circumferential U-bend and L-turn ducting were also modeled as sector elements covering a

rotational angle of exactly 20° . The grid is generated using GAMBIT preprocessor, which is an in-built modeling tool that comes along with FLUENT package. The steps involved in the grid generation process are explained in the following sections.

The dimensions and coordinates for casing and hub curves of circumferential crossover bend are read from the 2D drawings of AutoCAD from the sectional view of the test setup assembly. For each block, the vertices are created in GAMBIT using the coordinates. From these vertices, straight lines and circular arc edges were created. The closed edges were converted into planes. These planes are revolved about the Z - axis to form sectorial solids of circumferential U-bend and L-turn exit. The circumferential U-bend and L-turn exit sectors were created as .dbs file. The sector for deswirl vane was created using the TURBO TOOLS option as another .dbs file. The modeled geometries for RCV2 are shown in Fig. 5.1. The grid is generated for the U-bend and L-turn sectors using structured hexahedral volumes. Near the walls of flow geometry the grid is refined by resolving the grid into finer cell volumes.

The modeling and grid generation for deswirl vane sector is more involved. The return channel vane profile coordinates are read from its 2-dimensional AutoCad drawing. The vertices were created for deswirl vane profile by importing vertex data from .txt file in which they were stored in specified format. Even numbers of edges were created for the vane profile by means of NURBS.

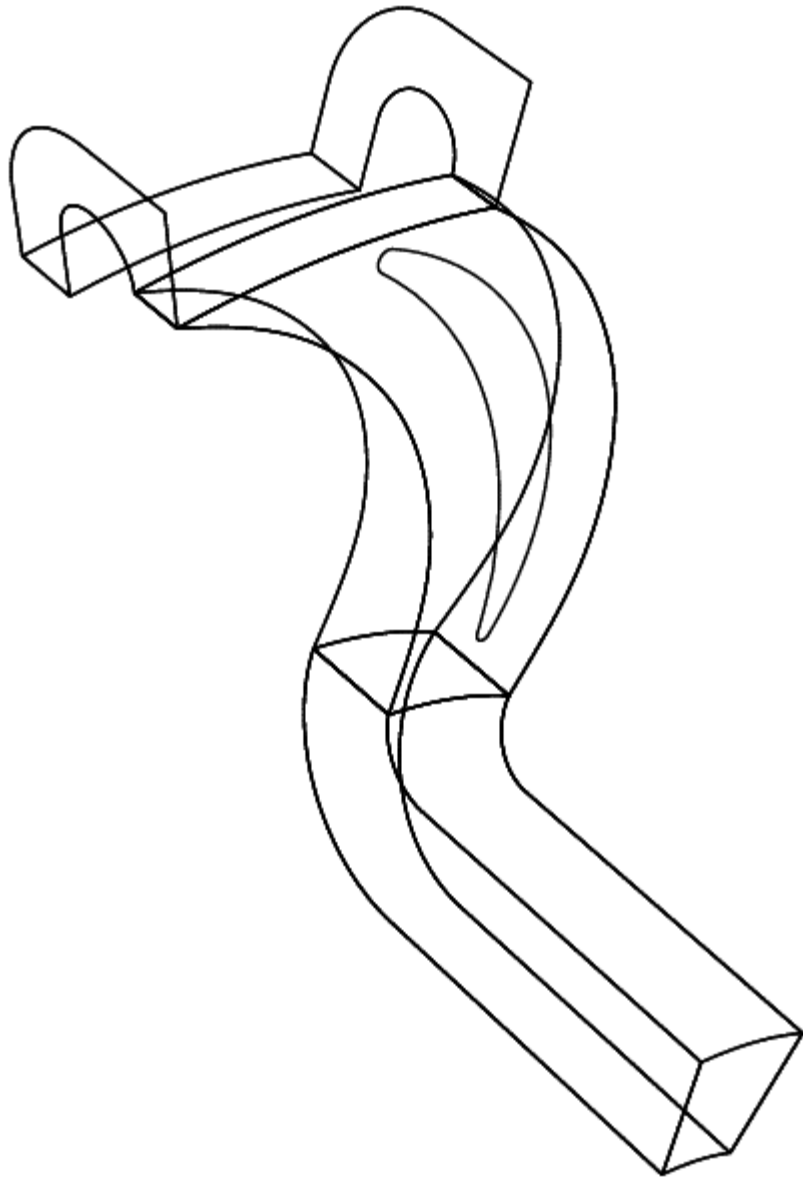


Fig. 5.1 Computational model

The hub curve and casing curve for deswirl vane section, were drawn. Using the TURBO TOOLS, a turbo volume was created. An unstructured grid with hex/wedge elements was created for this vane geometry. To capture the flow separation, fine grid features were used on the return channel vane surface. On the vane suction and pressure sides, leading

and trailing edges, boundary layers were created to resolve the flow details in the boundary layers. The details of computational mesh generated for U-bend, L-turn exit and return channel vanes are shown in Fig. 5.2.

5.4 BOUNDARY CONDITIONS

The inlet of U-bend was defined as "Pressure Inlet" boundary, while L-turn exit was specified as "Pressure Outlet", with target mass flow rate and "Radial Equilibrium Pressure Distribution" option. The exit of U-bend and inlet of L-turn section were specified as "INTERFACE" boundaries.

The inlet and exit of the vane sector were defined as "INTERFACE" boundaries. Since sector slices were used in the simulation, the periodic faces were defined with appropriate "Periodic" boundary condition. The two .msh files were called into TGRID tool of FLUENT and merged into one .msh file.

5.5 SOLVER SETTINGS

The total grid size consists of 2, 51,460 hexahedral cell volumes. The exit section of 180^o U-bend and inlet section of return channel vanes are coupled with "interface" feature available in the program. Similarly the exit section of return channel vanes and inlet section of 90^o bend are coupled with interface feature. At the inlet section, the fluid properties and the total pressure along with flow angle were specified.

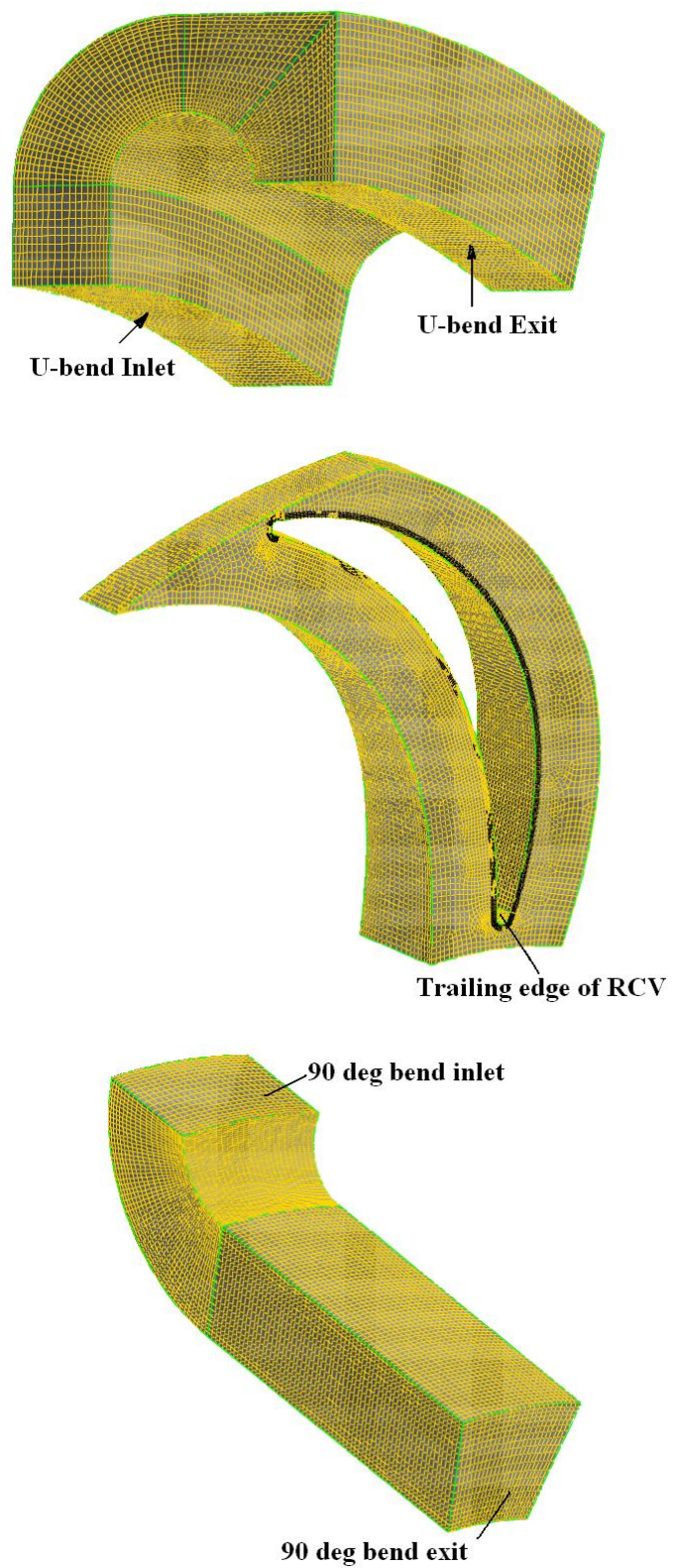


Fig. 5.2 Computational mesh for U- bend, 90^o bend and RCV2

The data obtained from experimental investigations were specified as inlet boundary conditions in the present study for ease of comparison. At the exit section of 90° bend, the static pressure with radial equilibrium pressure distribution option with target mass flow rate was used as outlet boundary condition. The pressure based solver with implicit formulation under 3-dimensional steady flow conditions with absolute velocity formulation is chosen. In the present study the standard k- ϵ model is used to predict the turbulence. The near wall treatment is handled with standard wall functions. The second order upwind scheme is used for discretization of convection terms. The solution was obtained with the maximum residual values equal to 1e-06.

5.6 GRID INDEPENDENCE STUDIES

To ensure that the solution is obtained with sufficient grid spacing for accuracy, grid sensitivity studies were conducted with different interval spacing. The total pressure loss coefficient is chosen as the basic parameter to decide the optimal grid size. Based on the study, the solution was found to be grid independent with an interval size of 0.002 meters. The details of grid sensitivity study are shown in Table 6.1. Thereafter all the solution runs were conducted at this grid size of 2,51,460 for the chosen geometry.

5.7 POST PROCESSING OF RESULTS

The solution runs were taken for a total of 5 different operating conditions for each of RCV 1 and RCV 2. The post processing of results

Table 5.1 Grid independence study

S no	Grid interval size	Total number of elements	Total pressure loss coefficient
1	0.003	72610	0.50185
2	0.0025	131950	0.45027
3	0.002	251460	0.4259
4	0.0015	497232	0.4230

was carried out and the results are depicted in the form of X-Y plots, contour plots and vector plots. The quantitative data at the locations of U-bend inlet, U-bend exit, L-turn exit and on the return channel vane surface was extracted by creating line and point surfaces. Circumferential averaging of the data was done at U-bend exit and L-turn exit locations. Bounded planes were created along the flow path through the return channel vanes. The contour plots for Mach number were plotted on these planes along the flow path through the return channel vanes. The vane loading graphs were plotted on X-Y plane with vane surface pressure coefficient on Y-axis and % chord length on X-axis.

Chapter 6

EXPERIMENTAL RESULTS AND DISCUSSION

6.1 GENERAL

The experimental investigations were carried out in two phases. In the first phase the return channel vane configuration RCV1 was assembled for testing. The flow measurements were taken at different locations of the flow path as explained in chapter 4. Similarly in the second phase of experiments, the return channel configuration RCV2 was assembled and flow investigations were carried out in a similar fashion to assess its performance. The various performance parameters of the crossover system with RCV1 and RCV2 configurations are presented in the graphical form. The performance of RCV1 and RCV2 are presented in separate sections followed by their comparison.

6.2 EXPERIMENTAL FLOW INVESTIGATIONS IN RCV1

The variation of meridional velocity, flow angle distribution from hub to shroud at the inlet of U-bend, exit of U-bend, exit of L-turn ducting with RCV1 configuration are presented and discussed in the following sections. The vane loading patterns, aerodynamic performance of the stage and the crossover bend in terms of total pressure loss and static pressure recovery coefficients at all the tested operating conditions are presented and discussed. All the flow calculations are presented as circumferential averages unless otherwise mentioned.

6.2.1 Meridional Velocity and Flow Angle Distribution at U-Bend

Inlet

The meridional velocity distribution at U-bend inlet measured from hub to shroud is shown in Fig. 6.1(a). From the figure it is seen that at a particular average U-bend inlet flow angle, the meridional velocity increases to a peak value with increase in distance from hub and reduces towards shroud. Due to the development of the boundary layer along the walls, the velocity is reduced near hub and shroud walls. This type of variation is generally observed for all the flow angles studied except for 34° corresponding to 120% flow rate. The variation of meridional velocity for 120% flow rate is showing double peaks. The kind of variation in meridional velocity for different operating conditions obtained in the present model test rig is similar to the actual compressor stage. The peak value of meridional velocity is observed to be nearer to the hub, which may be due to the effect of crossover bend. With the increase in flow angle at U-bend inlet the mass flow rate is increasing due to which higher magnitude of meridional velocities are observed. This variation is generally in agreement with the trends reported by Inoue and Koizumi (1983) in which a similar test rig was used. Figure 6.1(b) shows the distribution of flow angle measured with respect to the tangential direction at the inlet of U-bend. In all the 5 cases of flow, the flow angles are observed to decrease towards the shroud due to the effect of U-bend. For each curve the average flow angle is computed from the

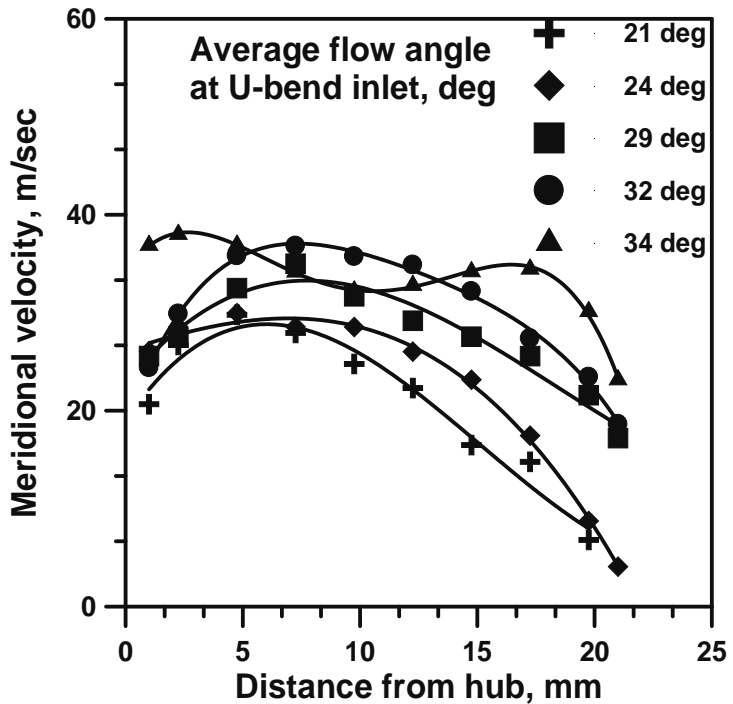


Fig.6.1 (a) Variation of meridional velocity at U-bend inlet

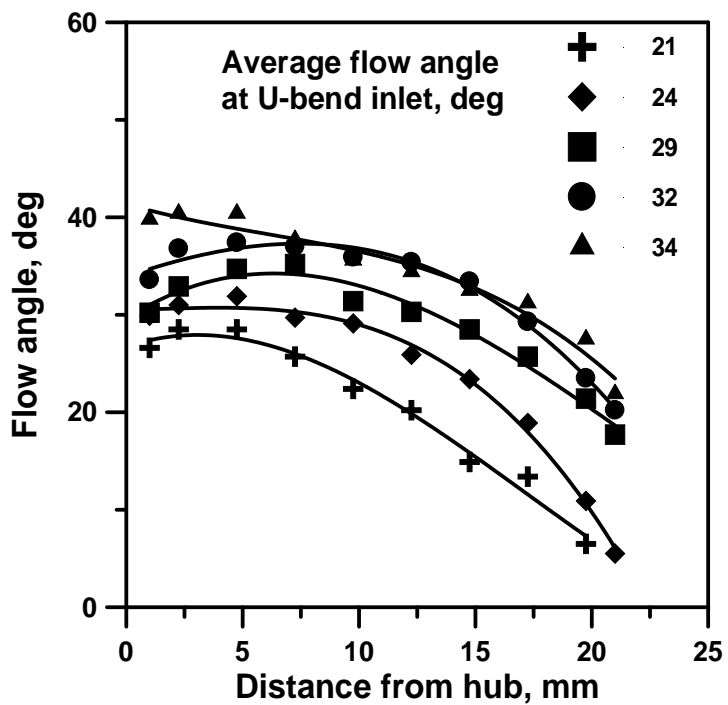


Fig. 6.1(b) Variation of flow angle at U-bend inlet

measured values from hub to shroud. The average flow angles computed are shown in the legend. The variation in average flow angle from curve to curve is achieved with the help of variable angle mechanism fitted to the swirl vanes. The flow is more concentrated towards the hub which is the reason for the flow having higher flow angles towards the hub.

6.2.2 Meridional Velocity and Flow Angle Distribution

at U-Bend Exit

Figure 6.2(a) shows the variation of meridional velocity from hub to shroud at the U-bend exit. The meridional velocity is seen to increase in magnitude from hub wall to shroud wall. The main flow is directed towards the shroud while the inner flow is reduced due to the sharp turning in the U-bend. The radius of curvature of the U-bend influences the extent of migration of flow towards the shroud. Though a larger radius of curvature tends to give uniform meridional velocity distribution at the U-bend exit, the frictional losses increase resulting in higher total pressure losses. The smaller radius of curvature results in the higher concentration of flow towards the shroud and flow separation on the hub wall towards the exit of U-bend. Therefore a compromise is required between the two in obtaining uniform meridional velocity distribution with minimum pressure losses. In the present study the U-bend has a curvature factor of $R^* = (2r)/(b_1+b_2) = 0.8$. The return channel flow path becomes narrower at the U-bend exit by about 16% than at inlet, due to which an increase in the magnitude of meridional velocity is observed

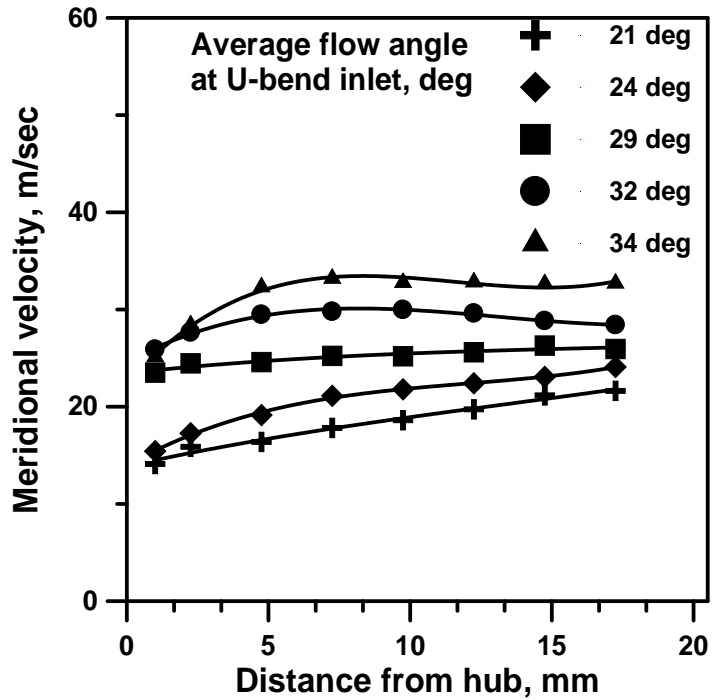


Fig. 6.2(a) Meridional Velocity distribution at U-bend exit

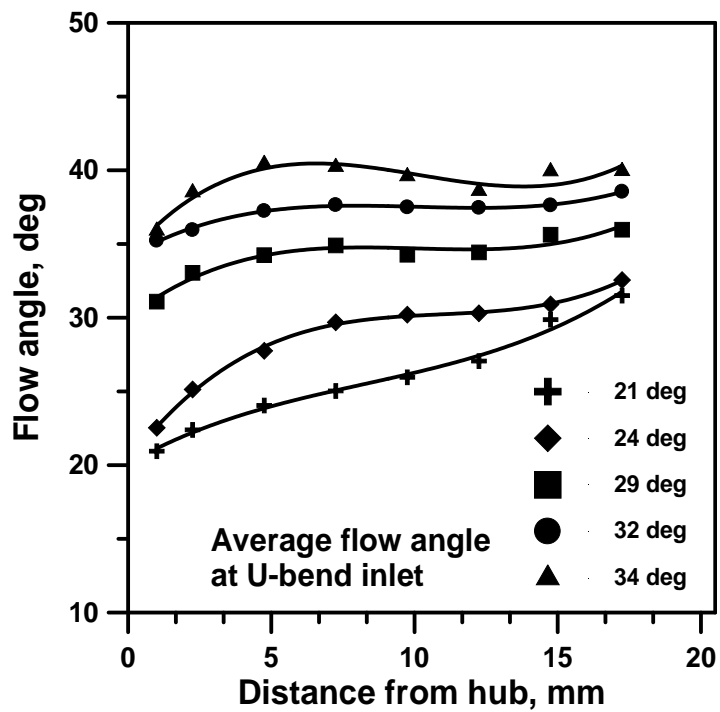


Fig. 6.2(b) Absolute Flow Angle distribution at U-bend exit

than at inlet. Figure 6.2(b) shows the distribution of flow angle from hub to casing walls at the U-bend exit. The average flow angles are approximately 4° to 5° higher in magnitude than at U-bend inlet. The increase in flow angle may be attributed to the decrease in the flow path width resulting in the increased meridional velocity.

6.2.3 Variation of Meridional Velocity and flow angle at the L-Turn

Exit

The distribution of meridional velocity at the L-turn exit (the exit of 90° bend) at the design flow rate and the variation of swirl angle are presented in this section. The probe is traversed from hub to shroud at chosen circumferential stations of location 4. The measurements covered two return channel vanes over an angle of 40° along the circumference as shown in Fig 6.3(a). The variation of meridional velocity distribution at the design flow rate along the circumferential direction at different distance ratios (x_4/b_4) is shown in 6.3(b). From the present study it is observed that the trailing edge of the return channel vanes influences the meridional velocity distribution at the stage exit. The magnitude of the velocity is seen to be larger at hub and decrease towards the shroud indicating the migration of the flow towards the hub surface due to the flow taking a 90° turn. The meridional velocity along the circumferential direction at a given distance ratio (x_4/b_4) is observed to vary in a wavy fashion near the shroud. The meridional velocity is observed to become uniform with higher magnitude towards the hub.

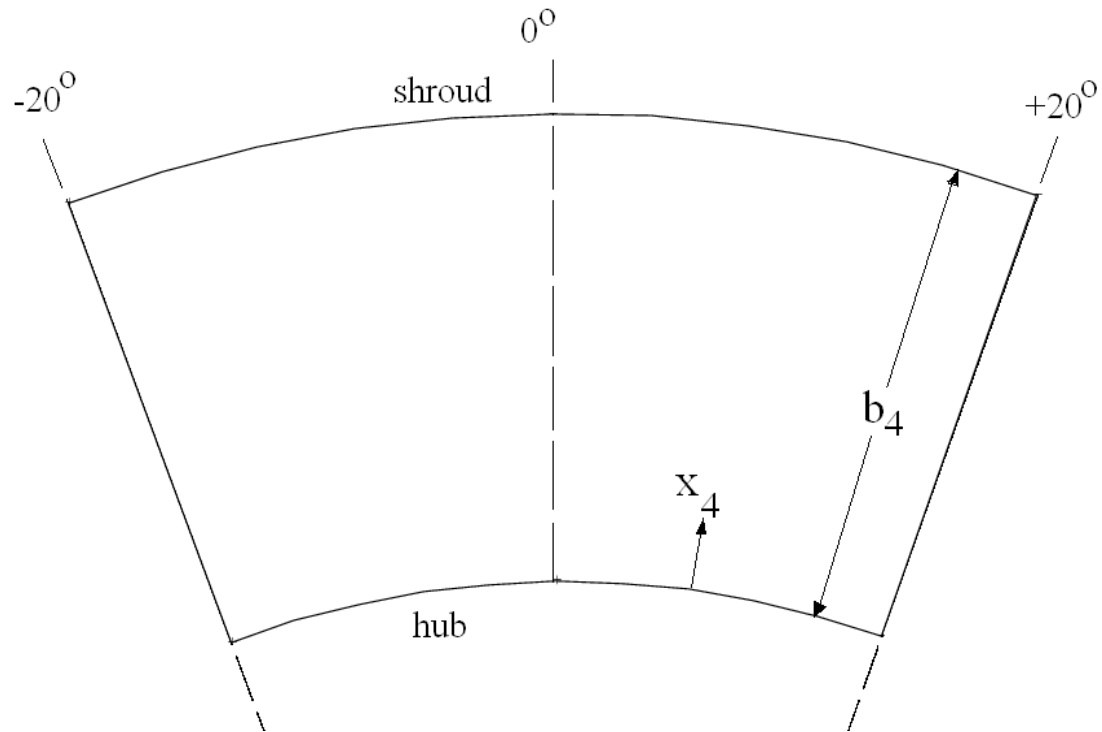


Fig. 6.3(a) Measurement Locations at the L-turn exit

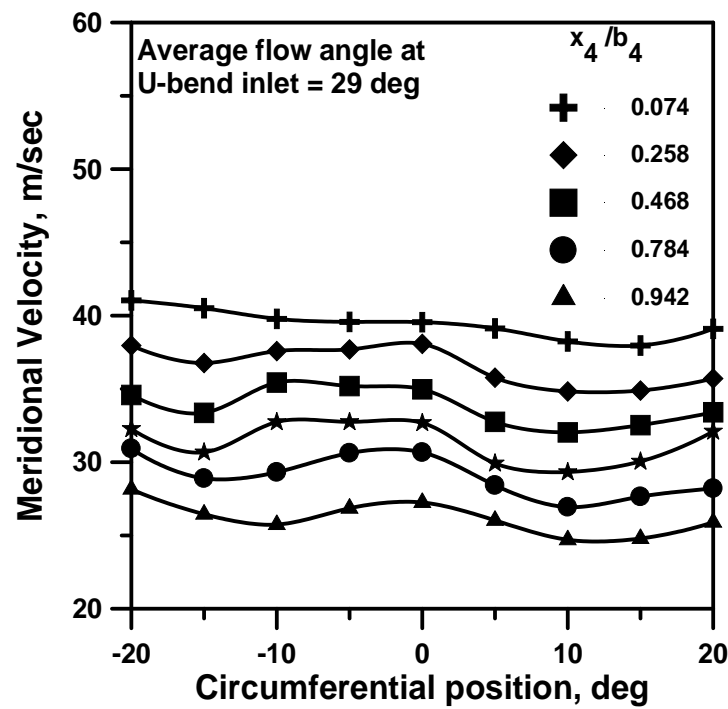


Fig. 6.3(b) Meridional Velocity Distribution at stage exit ($\alpha_1 = 29^\circ$)

The swirl angle variation at the L-turn exit for the design flow operating condition is shown Fig 6.4(a). The swirl angle indicates the extent of flow deviation expressed either with reference to tangential direction or axial direction. When the swirl angle is measured with respect to tangential direction, zero-swirl corresponds to 90° . When it is expressed with respect to axial direction zero-swirl corresponds to 0° . It is observed to vary from 93° to 100° (a deviation of 3° to 10° with respect to axial direction). The trailing edge wake effect on the swirl angle distribution is seen as it is observed to vary in wavy fashion. The variation of average swirl angle at the L-turn exit, measured with respect to the tangential direction for the whole operating range is shown in Fig. 6.4(b). It is observed to be in the range of 98° to 106° meaning which there is a swirl of 6° to 13° with respect to axial direction at the exit section. At the trailing edge of the return channel vanes there is a possibility of boundary layer separation on the suction side particularly with positive incidence angles on the L.E of RCV1, due to the deflection of fluid owing to the sharp curvature of the vane. Also the deceleration of flow with higher tangential velocities (positive incidence) may lead to the development of secondary flows (cross-flows) leading to pressure losses and increase in exit swirl angle.

The variation of circumferentially averaged meridional velocity from hub to shroud at the L-turn exit for different operating conditions is shown in Fig.6.5. The peak values of meridional velocity are observed

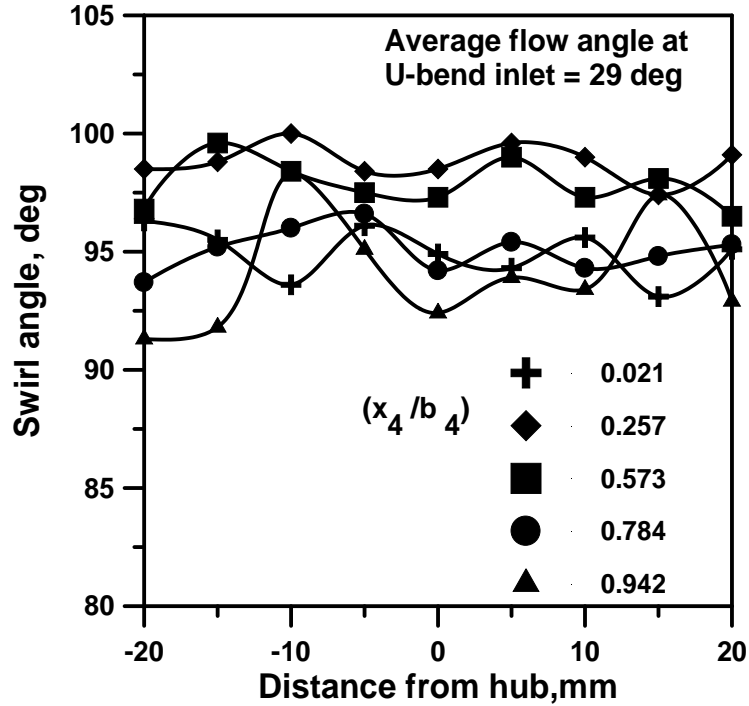


Fig. 6.4(a) Swirl angle Distribution at final exit ($\alpha_1 = 29^\circ$)

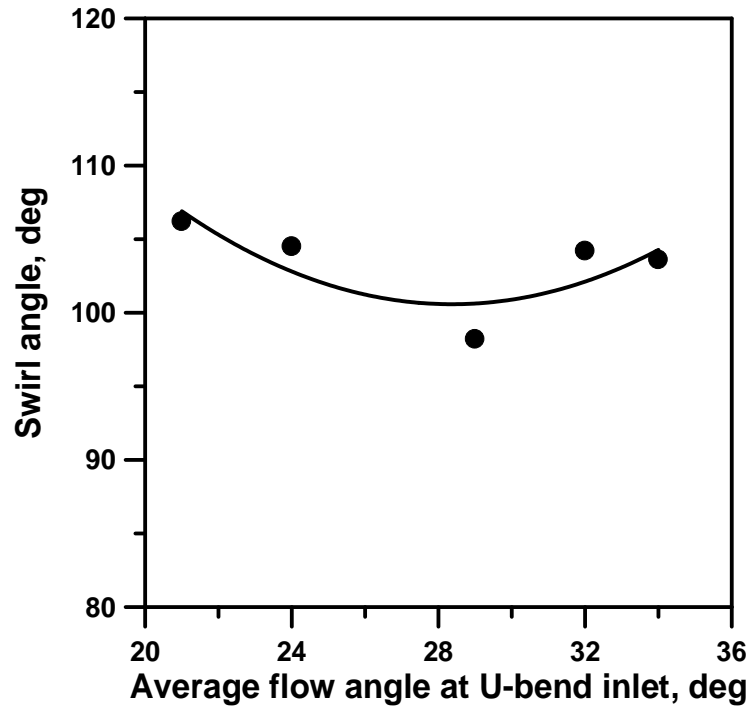


Fig. 6.4(b) Average swirl angle distribution at final exit

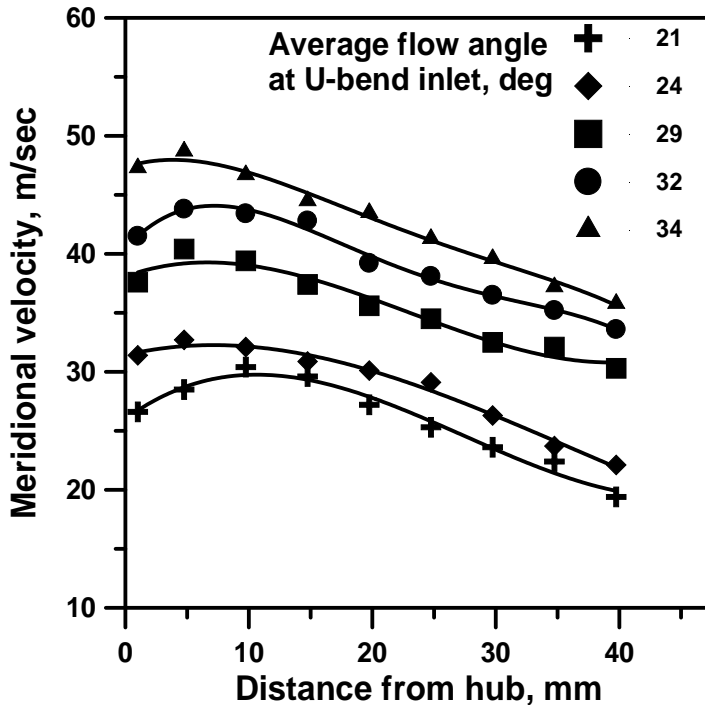


Fig. 6.5 Average Meridional Velocity Distribution at the L-turn exit

nearer to the hub. The meridional velocity is seen to decrease with increase in distance from hub. The 90° turn appears to cause the migration of flow towards the hub.

6.2.4 Vane Surface Pressure Distribution

Figure 6.6 shows the vane surface pressure distribution obtained through measurements for different average flow angles at U-bend inlet. The exit blade angle of the tested return channel vane RCV1 is 82° , measured with respect to tangential direction. If there had been no turning of flow after the exit from RCV1, the exit swirl angle should be 82° with respect to tangential direction. However in the present case the average swirl angle measured is in the range of 96° to 103° , indicating a

total turning of 14° to 21° . The vane surface pressure coefficient is plotted against the % chord length from the leading edge of the vane. From the present study it is observed that the vane surface pressure coefficient is nearly constant beyond 50% chord length on the suction side at 21° U-bend inlet flow angle. This effect may be attributed to the curvature distribution of the return channel vane coupled with positive incidence on the leading edge of the vane. With the increase in average flow angle at the inlet of U-bend and hence with the change in incidence angle on the leading edge of the return channel vane, considerable gradient has been observed on suction side. Therefore the reason for constant pressure coefficient on suction side may be attributed to possible flow separation beyond 50% chord length, which needs to be visualised through either CFD studies or experimental flow visualization methods. There is a sudden drop in pressure observed immediately after the leading edge on the pressure surface of the vane for U-bend inlet flow angle of 29° and higher. This may be due to the separation and reattachment on the pressure surface near the leading edge with negative incidence angles. Later there is some pressure recovery on the pressure side owing to the curvature of the vane. Some pressure recovery on the pressure surface of the vane beyond 40% chord length is also observed.

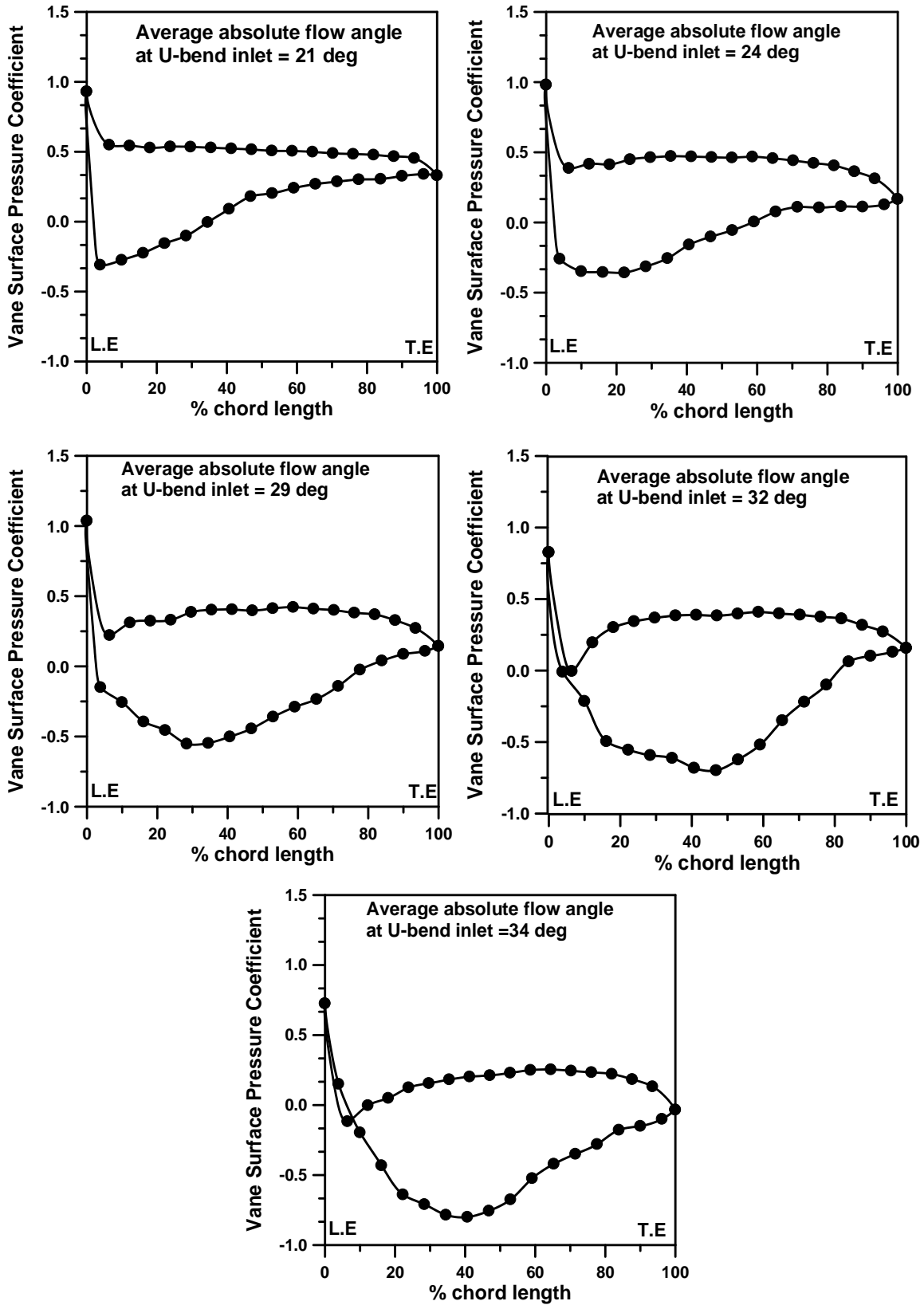


Fig.6.6 Return channel vane surface pressure distribution

6.2.5 Performance of the Stage

The variation of total pressure loss coefficient and static pressure recovery coefficient at different operating conditions for the stage is shown in Fig. 6.7(a) and (b) respectively. It is seen from Fig. 6.7 (a) that the total pressure loss coefficient is minimum for an average absolute flow angle at inlet to U-bend of 23° . If the flow angle is reduced or increased from this value, the total pressure loss coefficient is seen to increase; the increase is rapid as the flow angle increases beyond 23° . The increase in total pressure loss coefficient can be attributed to the separation of flow as well as the frictional losses in the flow path coupled with losses associated with secondary flows. The flow separation may be occurring both on suction and pressure surfaces causing higher total pressure loss. It is seen from Fig. 6.7(b) that the static pressure recovery coefficient increases with decrease in absolute flow angle at U-bend inlet. A return channel vane removes the swirl velocity at inlet, but accelerates the meridional velocity as the flow moves to a lower radius with a smaller area. So it has a combination of deceleration of the swirl velocity with an acceleration of the meridional component of velocity. Whether the absolute velocity decreases (which is needed for a static pressure rise) then depends on the geometry and the inlet flow angle. A one-dimensional consideration of this indicates that one cannot expect a static pressure recovery with an overall deceleration at high flow angles. At higher negative incidence angles on the L.E of RCV1 the tangential

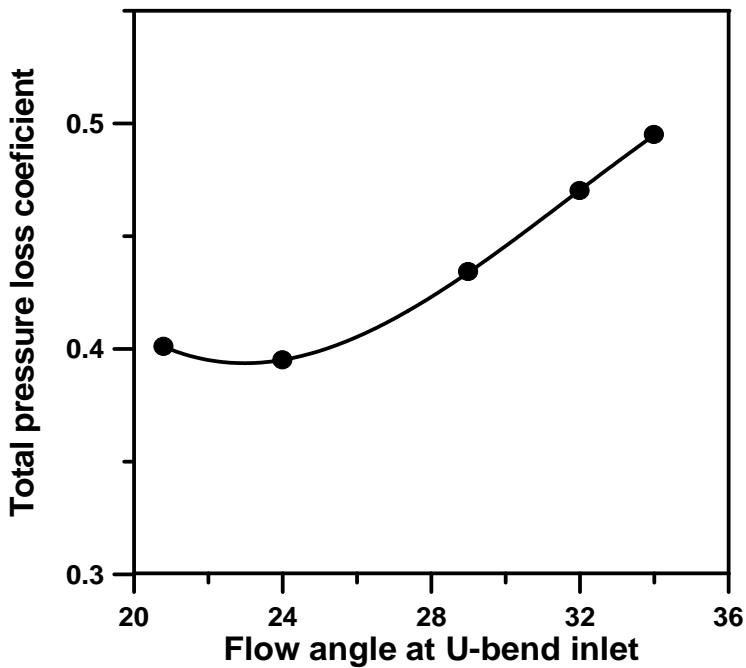


Fig. 6.7(a) Variation of total pressure loss coefficient (stage)

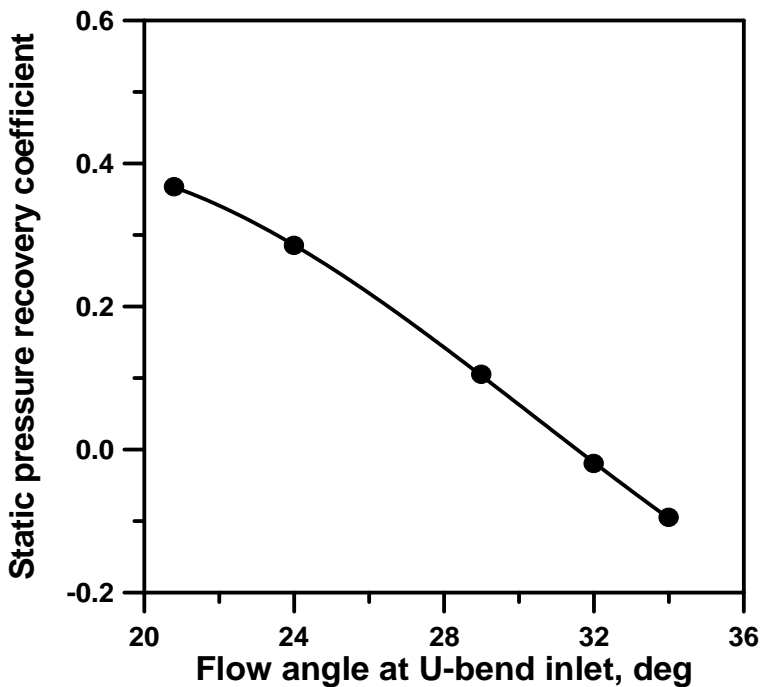


Fig. 6.7(b) Variation of static pressure recovery coefficient (stage)

component of velocity (swirl component) decreases. Therefore there is little deceleration of the swirl velocity due to the smaller swirl to be removed, but a strong acceleration of the meridional velocity due to the high mass flow. Similar variation of total pressure loss coefficient and static pressure recovery coefficient was reported in the literature by Simon and Rothstein (1983).

6.2.6 Performance of the U-bend

The variation of total pressure loss coefficient and static pressure recovery coefficient with the increase in U-bend inlet flow angle for the crossover bend alone is shown in Fig. 6.8(a) and 6.8(b) respectively. The total pressure loss coefficient for the U-bend is observed to be higher for lower U-bend inlet flow angles and decreasing with increase in flow angle up to the design point and thereafter increasing. The U-bend losses are seen to be less than 0.2 which is a favorable feature. It is inferred that the losses in return channel vanes are more predominant than in U-bend which is evident by comparing with the stage performance as shown in Fig. 6.7(a). The static pressure recovery coefficient is observed to be negative at higher U-bend inlet flow angles. As stated earlier, the static pressure recovery with higher flow angles shall be zero or negative. Not much static pressure recovery is noted even with lower flow angles because of the reduction in area at U-bend exit which caused increase in total velocity. The total pressure loss coefficient is within the desirable range (less than 0.3) as recommended by Lüdtke (2004).

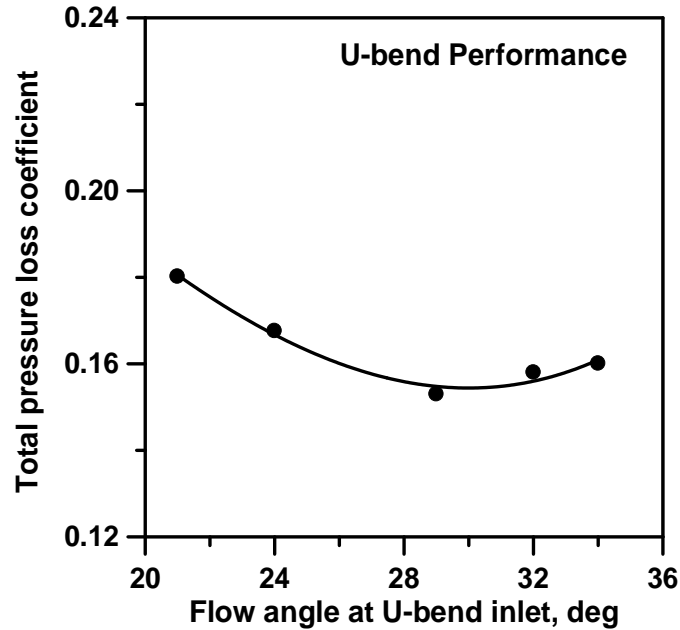


Fig. 6.8(a) Variation of total pressure loss coefficient (U-bend)

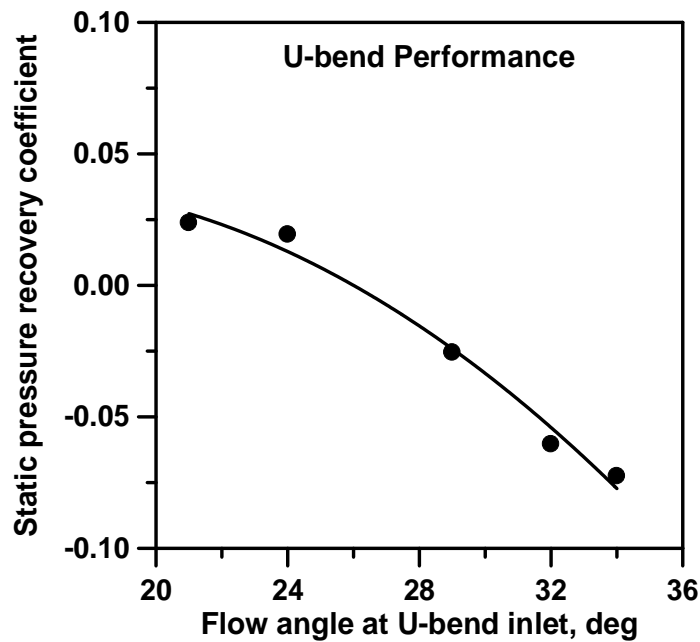


Fig. 6.8(b) Variation of static pressure recovery coefficient (U-bend)

6.3 EXPERIMENTAL INVESTIGATIONS IN RCV2

In the second phase of experiments the return channel configuration RCV1 was dismantled and reassembled with second return channel vane configuration RCV2. The RCV2 configuration is different from RCV1 in terms of inlet vane angle, chord length and vane thickness distribution. The number of vanes was kept unaltered. The vane inlet angle is changed to 27° and chord length is increased to 182 mm. The experimental investigations were carried out with the similar operating conditions of RCV1. The required flow angle and mass flow rate were obtained by adjusting the swirl vane positions and the speed of the blower. The results obtained are discussed in the following sections.

6.3.1 Variation of Meridional Velocity and Flow Angle at U-bend Inlet

The variation of meridional velocity obtained at the inlet of U-bend with RCV2 return channel configuration is shown in Fig.6.9 (a). The meridional velocity is observed to reach a peak and then decrease later with the increase in distance from hub. The peak value of meridional velocity is observed nearer to the hub. The flow angle distribution measured with respect to tangential direction at the U-bend inlet is shown in Fig 6.9(b). Similar to the flow angle distributions observed in RCV1 case, the magnitude is observed to decrease towards the shroud. The U-turning of the fluid is seen to effect the flow distribution.

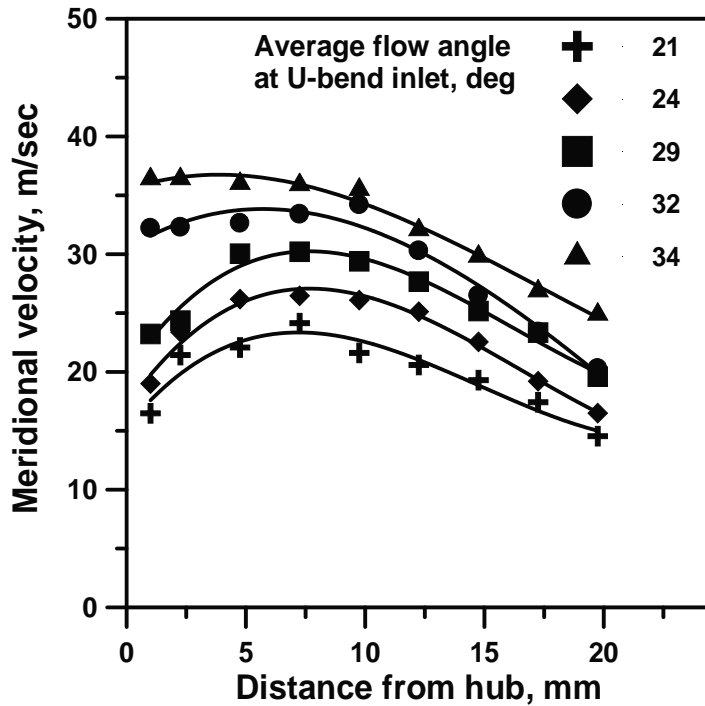


Fig. 6.9(a) Variation of meridional velocity at U-bend inlet

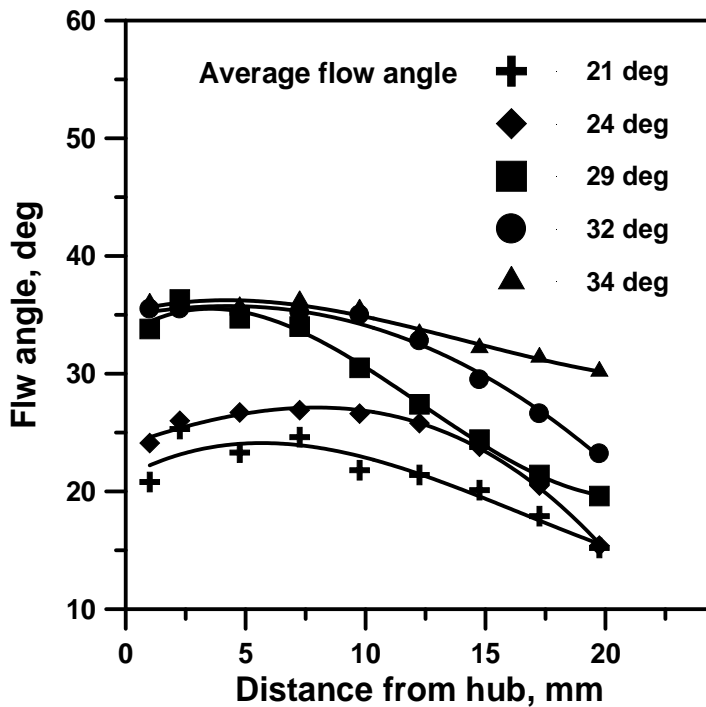


Fig. 6.9(b) Variation of flow angle at U-bend inlet

6.3.2 Meridional Velocity and Flow Angle Distribution at U-bend exit

The meridional velocity distribution obtained through measurements at the U-bend exit is shown in Fig. 6.10(a). The meridional velocity at the exit of U-bend is observed to be somewhat uniform compared to inlet at the U-bend exit exhibiting the similar variations to that of RCV1 results. Due to turning in the U-bend the flow appears to be slightly concentrated towards the shroud wall. The meridional velocity magnitude is seen to be increasing with the increase in the average flow angle at U-bend inlet due to increased mass flow rate.

The distribution of flow angles at U-bend exit is shown in Fig. 6.10(b). The flow angles measured with respect to tangential direction are seen to increase towards shroud wall. The average flow angle at a given operating condition is seen to be higher in magnitude than the corresponding average flow angle at U-bend inlet. The same trend was observed in the case of testing with RCV1 configuration.

The reason for increased meridional velocity and hence the increased flow angle is attributed to the decreased flow path width at U-bend exit. In the present study the flow path width at U-bend exit is 20.5 mm where as the width at U-bend inlet being 24.5 mm. A sharp edge on the shroud wall of U-bend is present, which is provided to make the manufacturing and assembly easier. However its influence on the stage performance is studied numerically and the results are presented in Chapter 7.

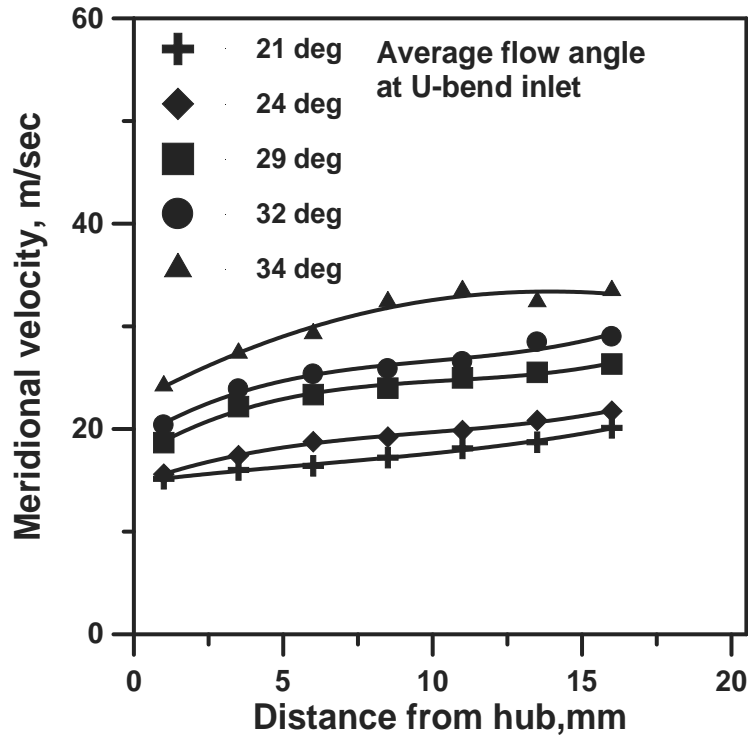


Fig. 6.10(a) Variation of meridional velocity at U-bend exit

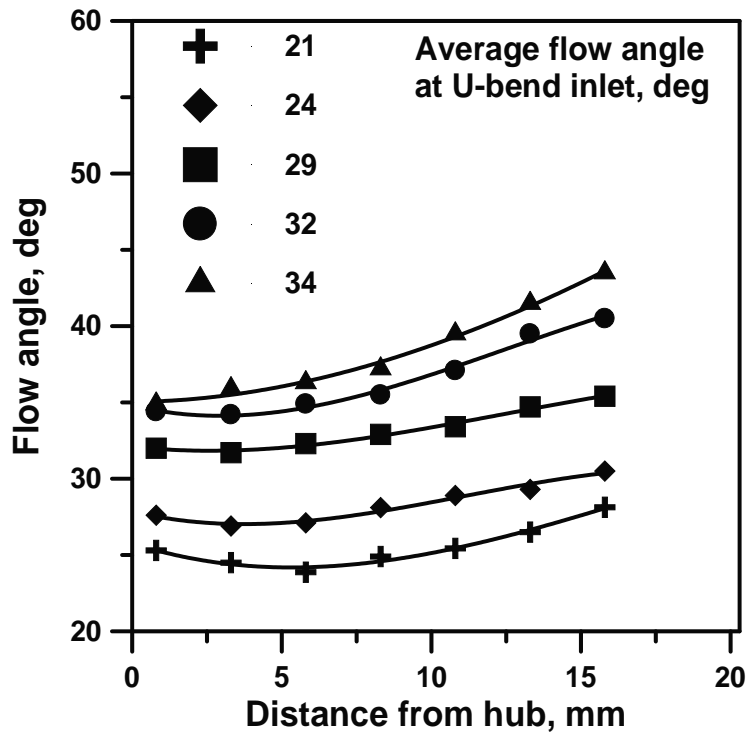


Fig. 6.10(b) Variation of flow angle at U-bend exit

6.3.3 Vane Surface Pressure Distribution

The static pressure measured on the mid span of the RCV2 vane surface is expressed as vane surface pressure coefficient (C_{pv}) and is plotted against % chord length from the leading edge. The variation of C_{pv} with % chord length for all tested operating conditions is shown in Fig.6.11. The static pressure coefficient on the suction side is observed to decrease up to some distance from the leading edge (L.E) and thereafter recovering towards the trailing edge (T.E). This indicates the acceleration of flow with decrease in static pressure. On the pressure side the static pressure coefficient is observed to drop suddenly at about 5% chord length from the L.E and thereafter recovering to positive values for the 110% and 120% of design flow conditions (higher U-bend inlet flow angles). With the increase in average flow angle at U-bend exit, the negative incidence on RCV2 vane L.E increases. This causes the flow to detach and thereafter reattach to the vane surface on the pressure side immediately after the L.E. The vane is seen to be loaded in a uniform way for the operating conditions with 70%, 80% of design flow rates.

6.3.4 Variation of Meridional Velocity and Swirl Angle at L-turn exit

The circumferentially averaged meridional velocity distribution from hub to casing at the L-turn exit is shown in Fig. 6.12(a). The meridional velocity is observed to decrease from hub to casing for all tested operating conditions. The flow is seen to be concentrated more towards the hub due to L-turn (90° turn).

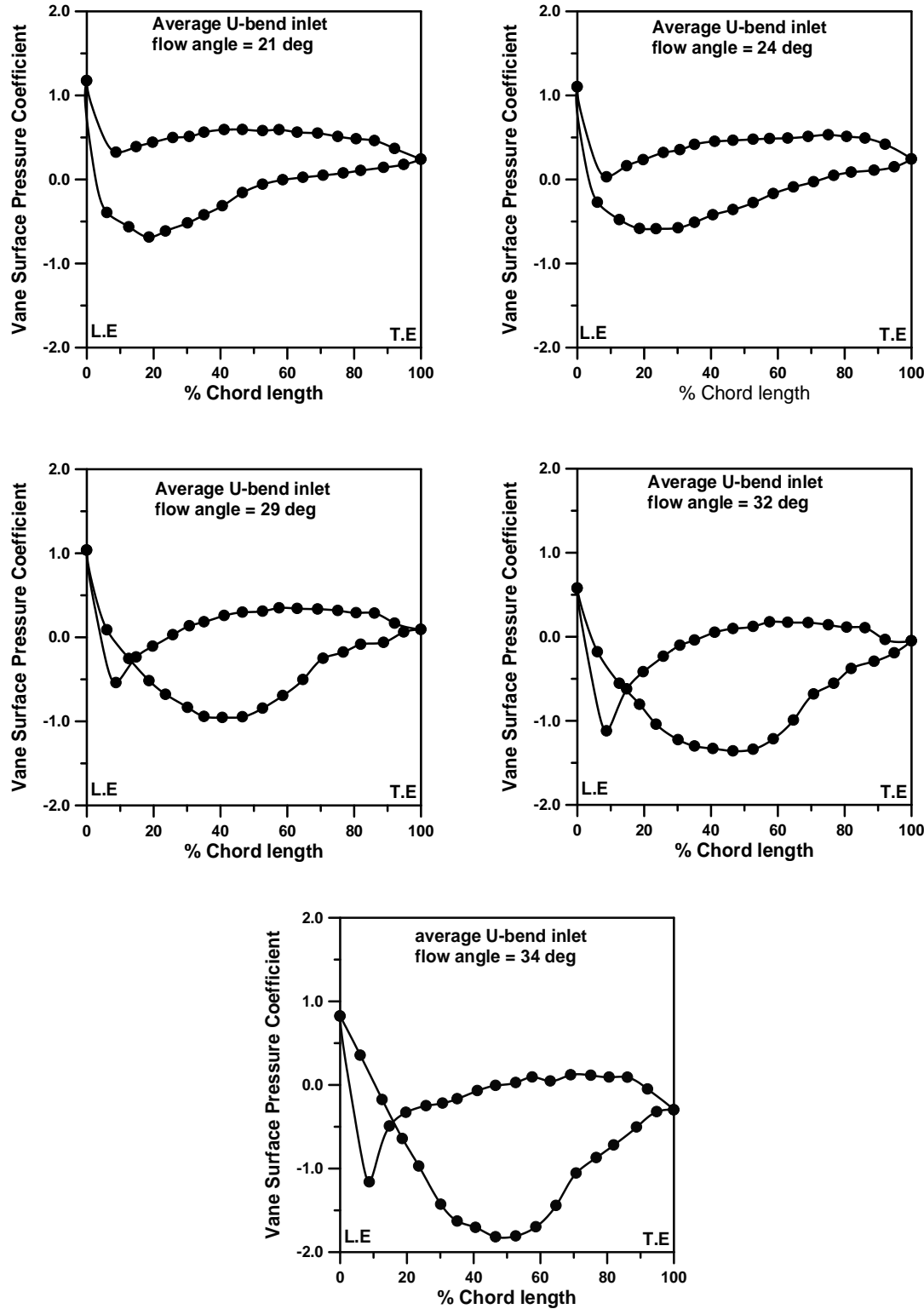


Fig.6.11 Vane surface pressure coefficient (RCV2)

The design point meridional velocity distribution in the circumferential direction as a function of non-dimensional distance at the L-turn exit (x_4/b_4) is shown in Fig.6.12 (b). The meridional velocity variation is showing wavy nature near the shroud while it is becoming almost uniform near the hub. Also the magnitude of meridional velocity is observed to be maximum near the hub and is decreasing towards the shroud. The wake effect of trailing edge of return channels vanes on the meridional velocity and swirl angle distributions at the L-turn exit is seen to be the reason for the wavy nature near to the shroud where the flow is actually concentrated towards the hub.

The swirl angle distribution at the L-turn exit in circumferential direction with varying (x_4/b_4) for the design flow rate operating condition is shown in Fig 6.13(a). The swirl angle at the hub is observed to be somewhat uniform and nearer to zero-swirl. Near to the shroud the swirl angle is observed to be varying in a wavy fashion in the circumferential direction. The averaged swirl angle distribution for all the tested operating conditions is plotted against the average flow angle at U-bend inlet as shown in Fig 6.13(b). A very small average swirl of about 91.5° is observed at the design flow rate condition, while the higher average swirl angles are observed at the off-design conditions. Compared to RCV1, lesser average swirl angles are observed for RCV2 at the design and off-design operating conditions which is discussed in more detail in the comparison section.

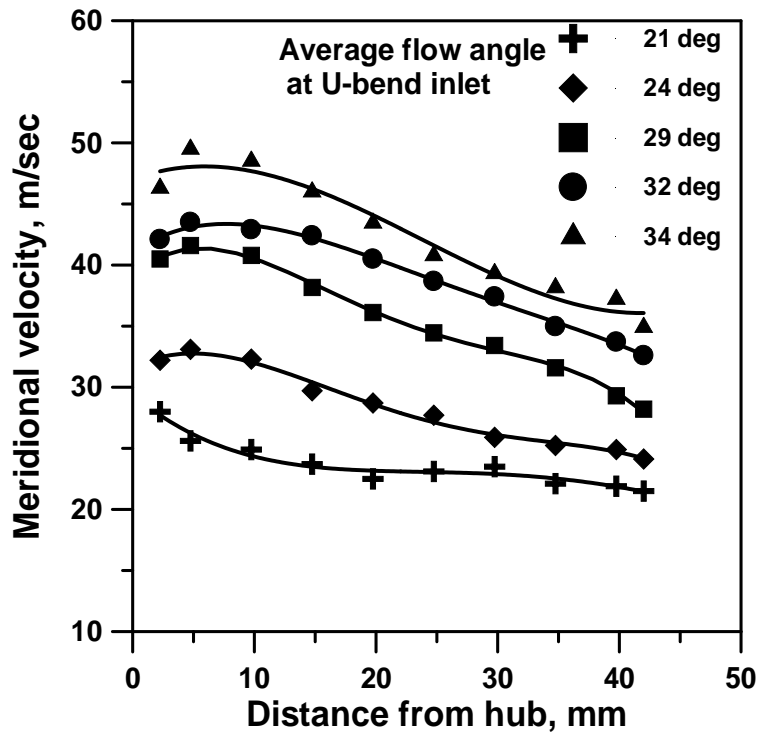


Fig. 6.12(a) Variation of meridional velocity at L-turn exit
(circumferential average)

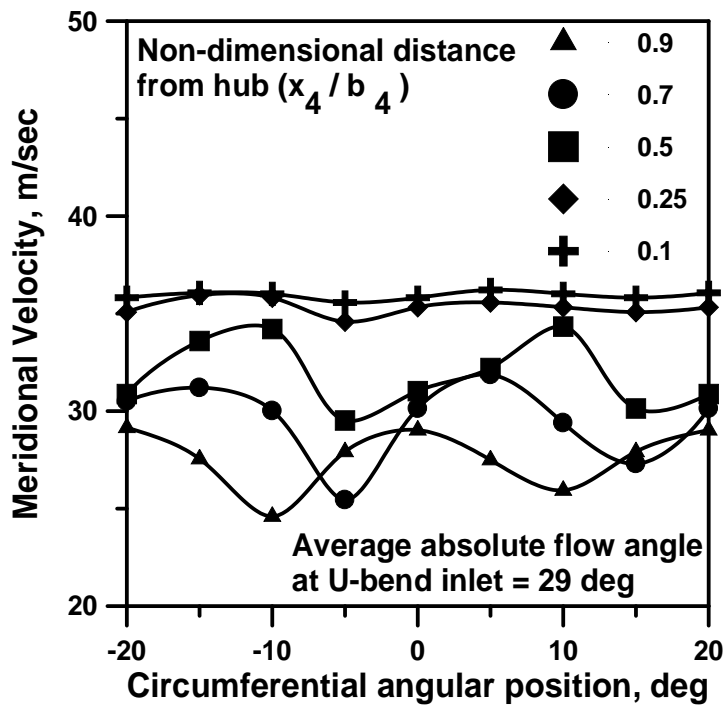


Fig. 6.12(b) Meridional velocity distribution at the design flow rate

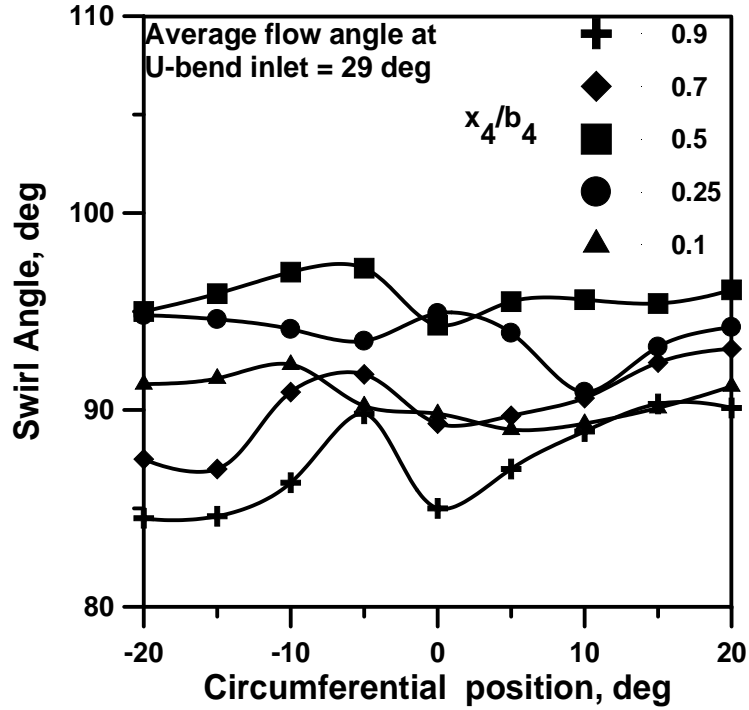


Fig. 6.13(a) Variation of swirl angle at the L-turn exit
(Design flow)

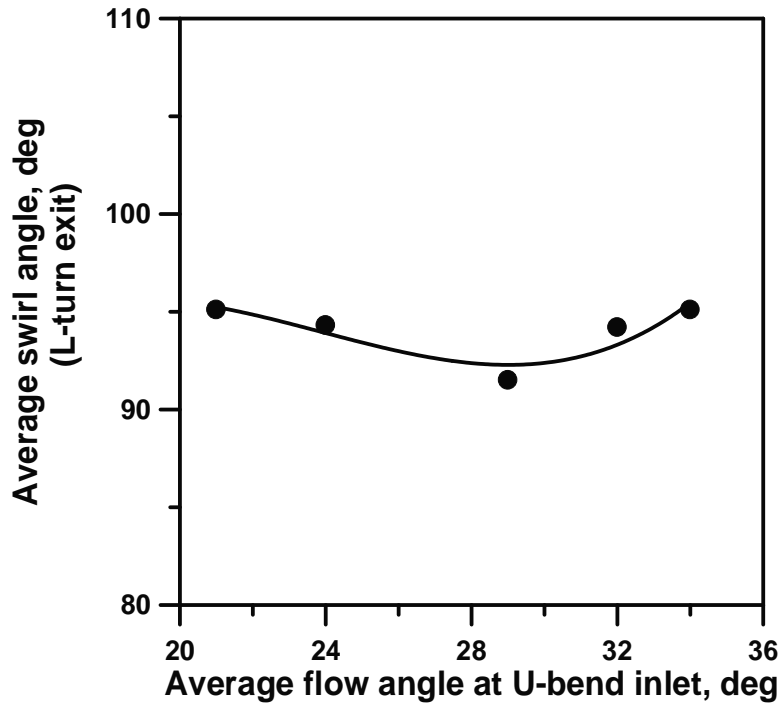


Fig. 6.13(b) Average swirl angle at L-turn exit (RCV2)

6.3.5 Performance of the Stage

The performance of the stage in terms of total pressure loss coefficient and static pressure recovery coefficient is discussed in this section. The variation of total pressure loss coefficient with the average flow angle at U-bend inlet is shown in Fig. 6.14(a). The total pressure loss is observed to be lower at lower flow angles and is seen to increase with the increase in average flow angle at U-bend inlet. The total pressure loss coefficient is seen to be minimum when the average flow angle at U-bend inlet is 21° . It is observed to increase from 0.38 to 0.67. The total pressure loss is considerably higher with higher average flow angles at U-bend inlet. The increased negative incidence on the vane with the increase in flow angle at U-bend inlet coupled with higher fluid velocities is the reason for increased total pressure losses.

The variation of static pressure recovery coefficient with the increase in average flow angle at U-bend inlet is shown in Fig. 6.14(b). The static pressure is observed to recover well at lower flow angles for the reasons explained in the case of RCV1 configuration. There is no recovery at higher average flow angle at U-bend inlet due to the lower tangential component of velocity.

Similar type of variations in the total pressure loss coefficient and static pressure recovery coefficient were reported in literature by Simon and Rothstein(1983), Inoue and Koizumi (1983) and Lenke and Simon (2000).

6.3.6 Performance of the U-bend

The performance of U-bend in terms of total pressure loss coefficient and static pressure recovery coefficient is presented in this section. The variation of total pressure loss coefficient for U-bend is shown in Fig. 6.15(a). The total pressure loss is seen to be minimum near the design point operating condition. It is observed to increase symmetrically on either side of the design point. However the magnitude of U-bend loss is smaller (0.12 to 0.14) when compared to the stage loss (0.38 to 0.67). This is clearly indicating that the return channel passage losses are dominant than the U-bend losses. However the static pressure recovery is seen to be poor in the U-bend throughout the operating range as can be seen from Fig. 6.15(b).

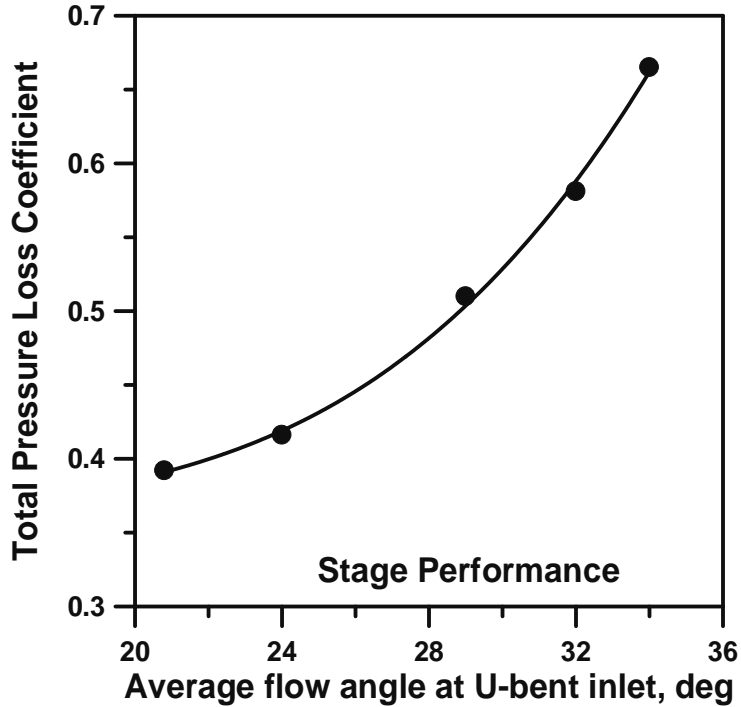


Fig. 6.14(a) Variation of total pressure loss coefficient for the stage (RCV2)

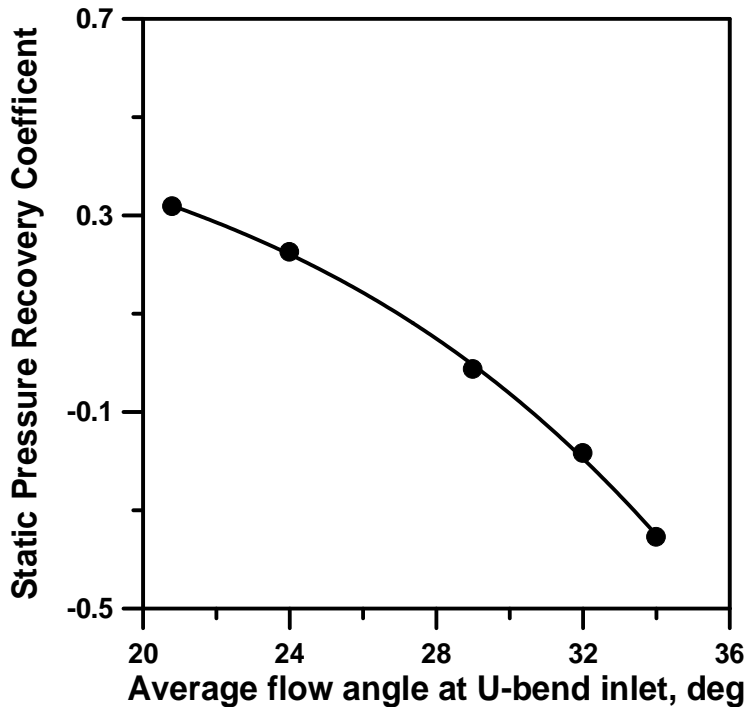


Fig. 6.14(b) Variation of static pressure recovery coefficient for the stage (RCV2)

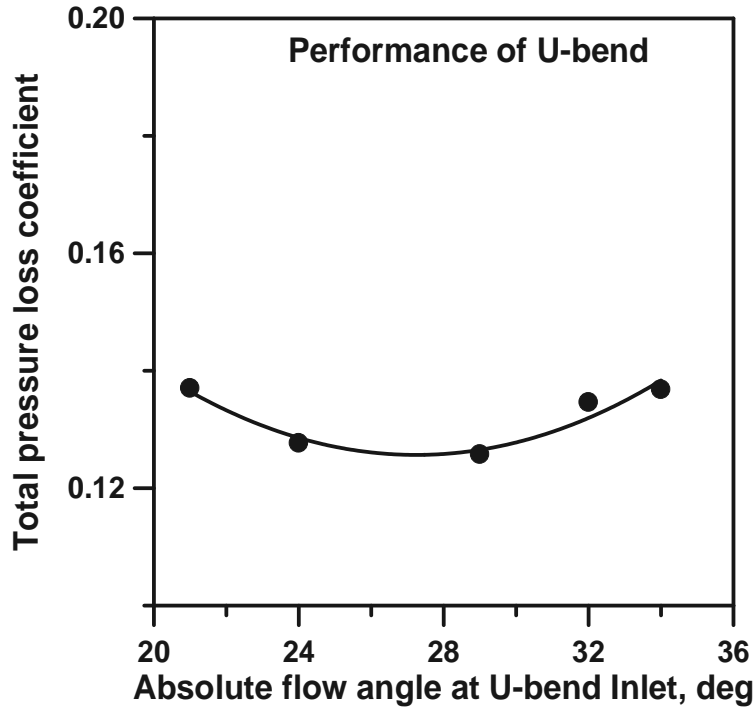


Fig. 6.15(a) Variation of total pressure loss coefficient for the U-bend (RCV2)

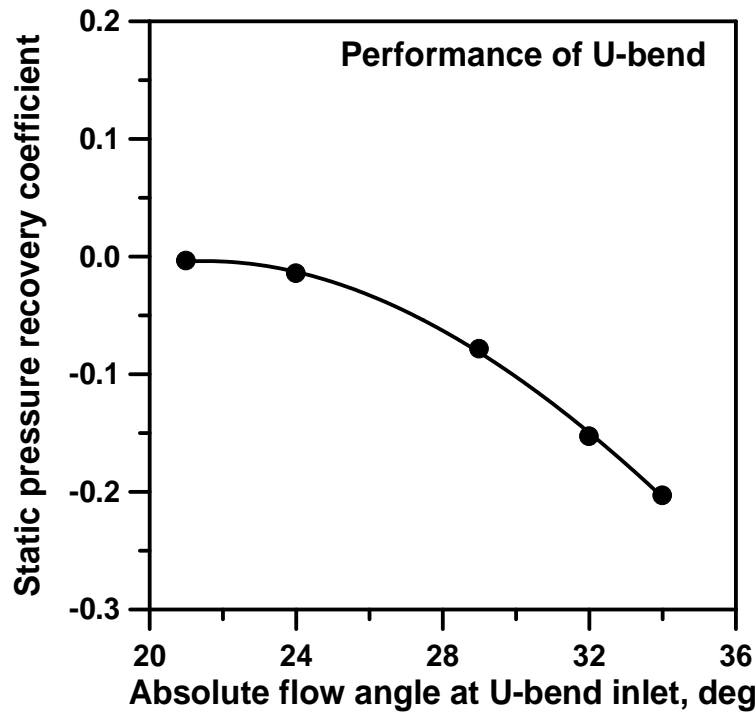


Fig. 6.15(b) Variation of static pressure recovery coefficient for the U-bend (RCV2)

6.4 COMPARISON OF EXPERIMENTAL RESULTS OF RCV1 AND RCV2

The experimental results obtained in RCV1 and RCV2 configurations are compared and presented in this section. The entire flow path of U-bend, L-turn section, return channel vanes height and the number of vanes were kept the same for the experimental studies using RCV1 and RCV2. The differences that were brought in RCV2 are in the vane profile, the inlet flow angle and the chord length. The operating conditions that were used in RCV1 studies are repeated during the testing of RCV2 also. The velocity and flow angle distributions at U-bend inlet, U-bend exit and L-turn exit are presented. Also the performance of the U-bend and the whole stage in terms of total pressure loss coefficient, static pressure recovery coefficient and vane surface pressure coefficient are presented and discussed.

6.4.1 Comparison of Meridional Velocity and Flow Angle Distribution at U-Bend Exit

The comparison of circumferentially averaged meridional velocity and the corresponding flow angle distribution at the exit of 180° U-turn bend is shown in Fig. 6.16. The meridional velocity for RCV1 at the design flow rate is seen to be nearly uniform from hub to shroud while there is a monotonic increase of meridional component of velocity from hub to shroud for RCV2. The shape of the return channel vane appears to have an effect on the incoming flow at the L.E of return channel vane. The

average flow angle at the exit of U-bend for both the configurations is observed to be higher than at the inlet. The average flow angle is observed to decrease towards the hub for both the configurations. The main flow is directed towards the shroud while the inner flow is reduced due to sharp turning. The flow angles are measured with respect to tangential direction at U-bend inlet and exit. The flow enters the U-bend with a tangential swirl and undergoes sharp 180° turning before it enters the return channel vanes. The increase in the average flow angle from U-bend inlet to U-bend exit is due to the decrease in passage width by about 16% which results in the increase of meridional component of velocity for satisfying the continuity equation. The measured average flow angles at U-bend exit are observed to be approximately 4° higher in magnitude than at the U-bend inlet.

6.4.2 Comparison of Meridional Velocity and flow angle distribution at the L-Turn Exit

The circumferentially averaged meridional velocity and swirl angle distribution from hub to shroud at three circumferential locations of stage exit corresponding to -20° , 0° and $+20^{\circ}$ at the design flow rate are shown in Fig. 6.17. The 0° position corresponds to vertical traverse at this plane which coincides with the trailing edge of the vane. The angular pitch of the vanes is 20° and as such the circumferential traverse covered two vane pitches. The meridional velocity is observed to decrease from hub to shroud for both the configurations and the magnitudes are

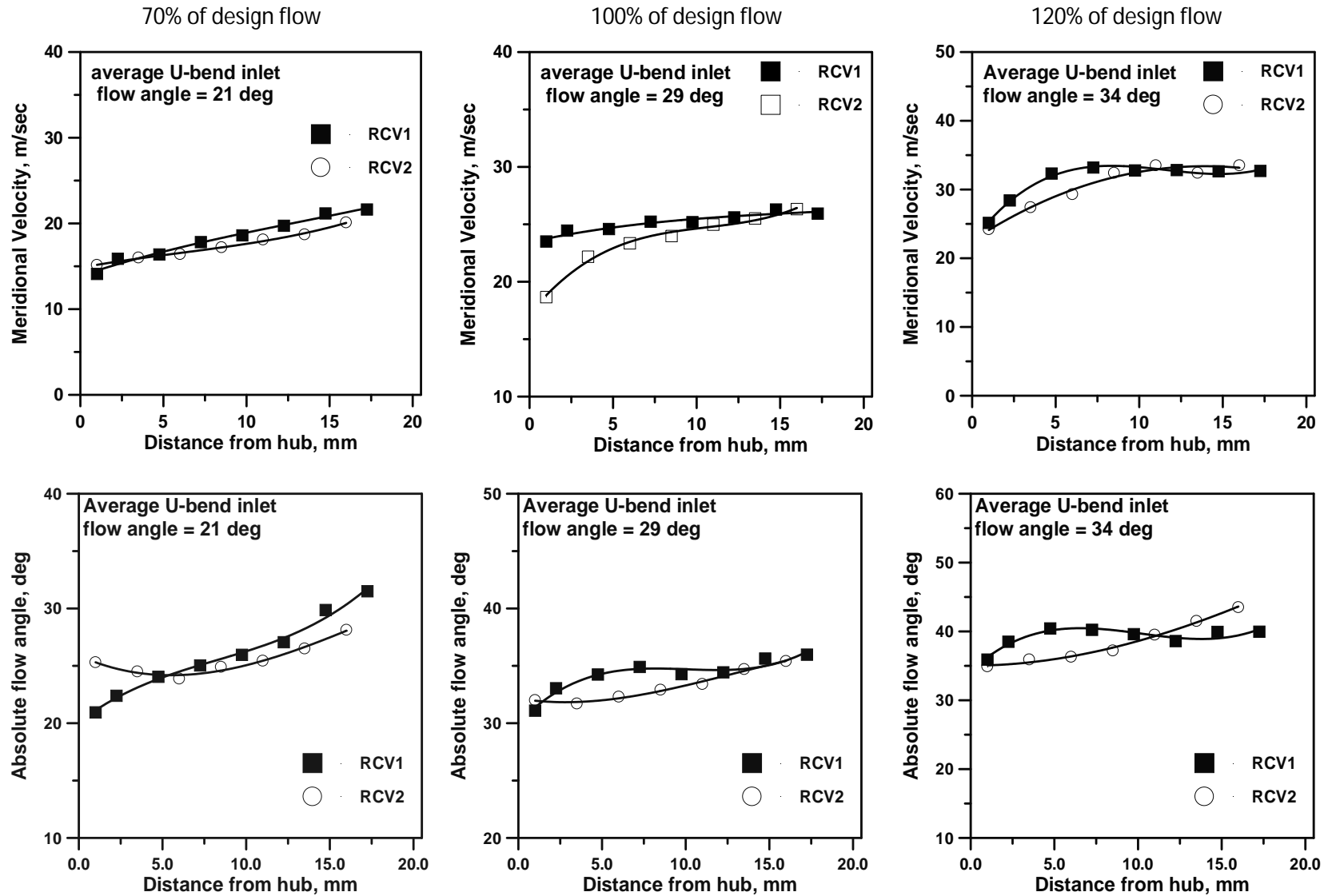


Fig. 6.16 Comparison of meridional velocity and flow angle distributions for RCV1 and RCV2

At U-bend exit

almost same at -20° and 0° circumferential locations. At $+20^{\circ}$ circumferential location, the meridional velocity for RCV2 is seen to be higher than RCV1. The magnitude of meridional velocity is more towards the hub, suggesting that the flow on turning is moved away from shroud. The exit swirl angle for RCV1 is seen to be varying between 93° and 100° , measured with respect to tangential direction. The swirl angle for RCV2 is observed to be smaller near the hub as well as shroud, while it is found to be higher in the core flow region. Due to the curvature of the vane there is a possibility of flow getting separated on the suction side, towards the trailing edge, particularly with positive incidence on return channel vane leading edge. As the flow enters the inlet of 90° bend immediately after the exit from return channel vanes, it may be subjected to development of secondary flows oriented from pressure side to suction side. These secondary flows cause not only increase in fluid friction losses but also the exit swirl to increase. The magnitude of swirl angle distribution for RCV1 is observed to be higher than RCV2, indicating more deviation from the axial direction.

6.4.3 Comparison of Vane Surface Pressure Distribution

The static pressures measured on the return channel vane surface for both the configurations and expressed as vane surface pressure coefficient (C_{pv}) are plotted against the percentage chord length from the leading edge (L.E) at the design and off-design flow rates as shown in Fig. 6.18.

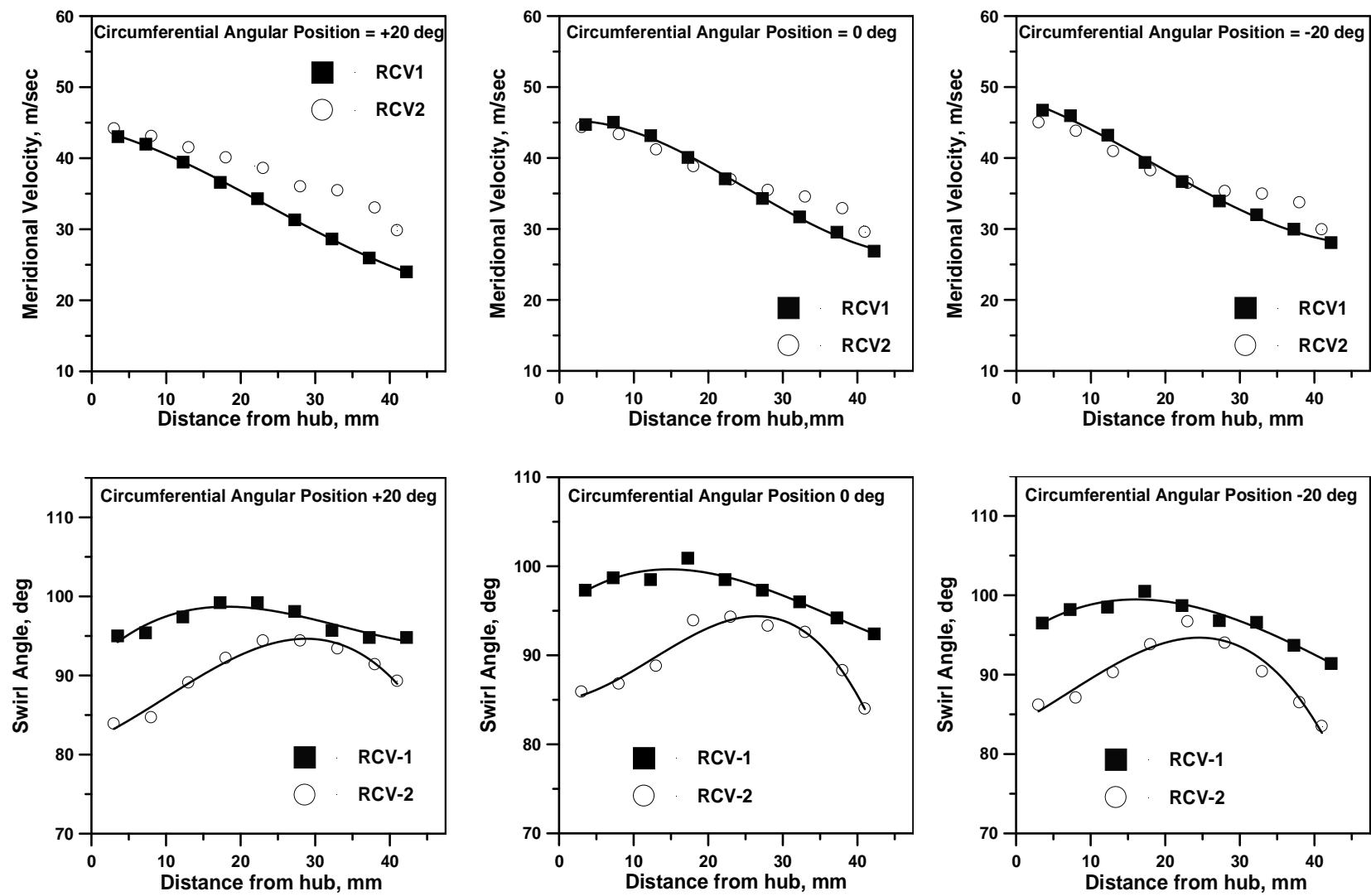


Fig. 6.17 Variation of Meridional velocity and swirl angle distributions at stage exit
At the design flow rate (RCV1 and RCV2)

The loading pattern at the design flow rate for RCV1 and RCV2 is the same on pressure side (PS) of the vane from 50% to 100% of the chord length. Similarly on the suction side (SS) of the vane the loading is similar from 70% to 100% of the chord length for both the configurations. A significant difference in the loading on PS is observed up to 50% of the chord length for the two return channel geometries. RCV1 appears to be more uniformly loaded on the PS as compared to RCV2. On the PS of RCV2, a sudden drop in static pressure from positive to negative values and there after recovering again to positive values is observed, indicating possible flow separation and reattachment on the PS towards the leading edge. The comparison at the off-design conditions also is shown in the Fig.6.18.

6.4.4 Performance Comparison for the Stage and U-bend

The aerodynamic performance of the stage for RCV1 and RCV2 is carried out in terms of total pressure loss coefficient and static pressure recovery coefficient as shown in 6.19(a) and 6.19(b) respectively . The total pressure loss coefficient (ζ) is observed to increase with increase in average flow angle at U-bend inlet for both RCV1 and RCV2, though the rate of increase is faster for RCV2 configuration. It may also be seen that the performance is nearly identical at 21° U-bend inlet flow angle. The static pressure recovery coefficient (C_p) for RCV1 and RCV2 is seen to decrease with increase in the U-bend inlet flow angle. There is no pressure recovery beyond 30° of U-bend inlet average flow angle.

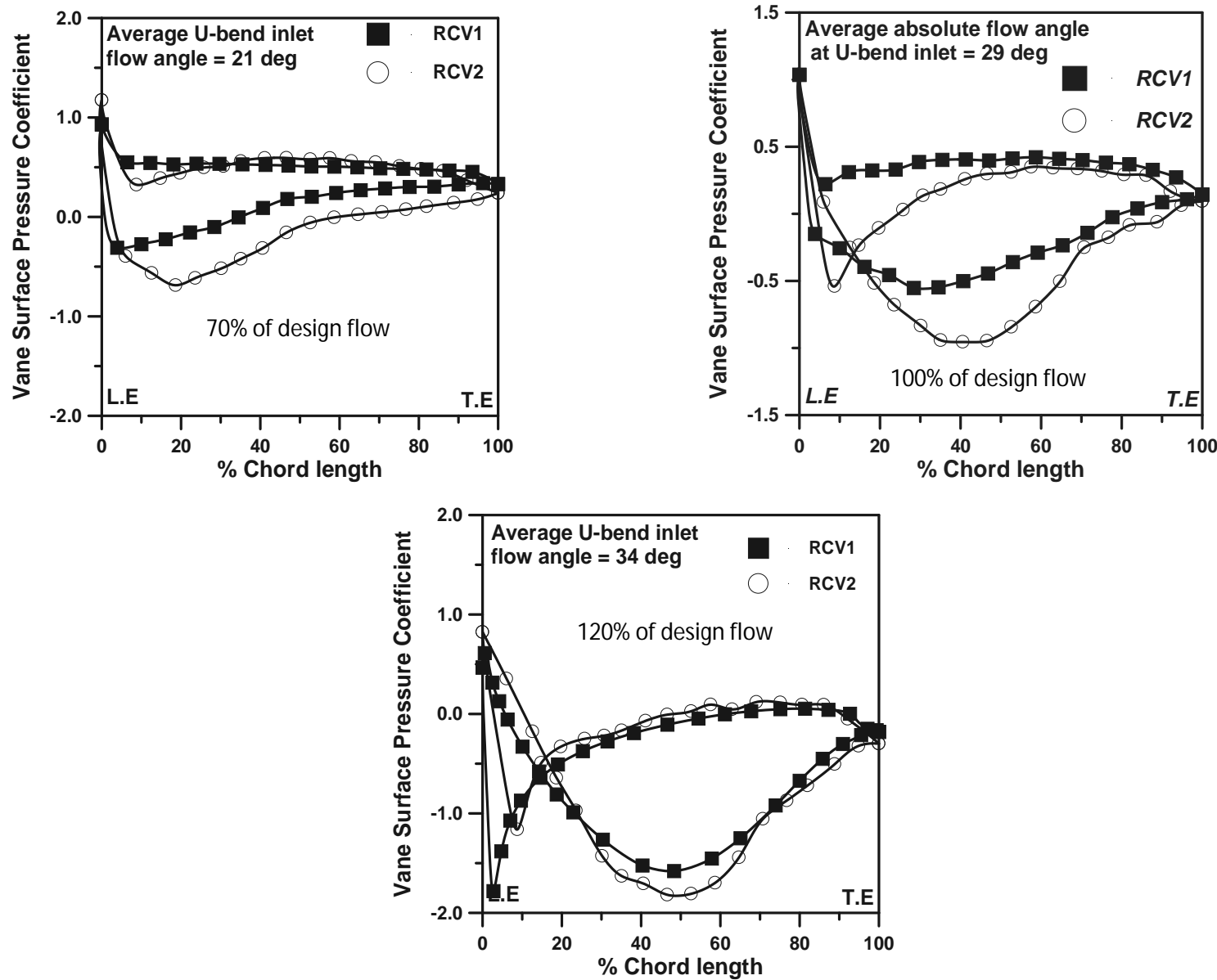


Fig. 6.18 Comparison of Vane surface pressure distribution

The pressure recovery is observed to be higher over the tested range for RCV1 than RCV2.

The aerodynamic performance comparison of the crossover bend with the tested two different return channel vanes is shown in Fig. 6.20(a) and (b). Though the operating conditions are kept same for both the configurations, the total pressure loss in the crossover bend is seen to be more with RCV1 than with RCV2. After the exit of crossover bend, the return channel proper starts, which seem to have an effect on the U-bend performance. However in terms of static pressure recovery the crossover bend is found to be better with RCV1 than RCV2. Based on these two coefficients, it may be concluded that the RCV2 configuration performance is inferior to RCV1.

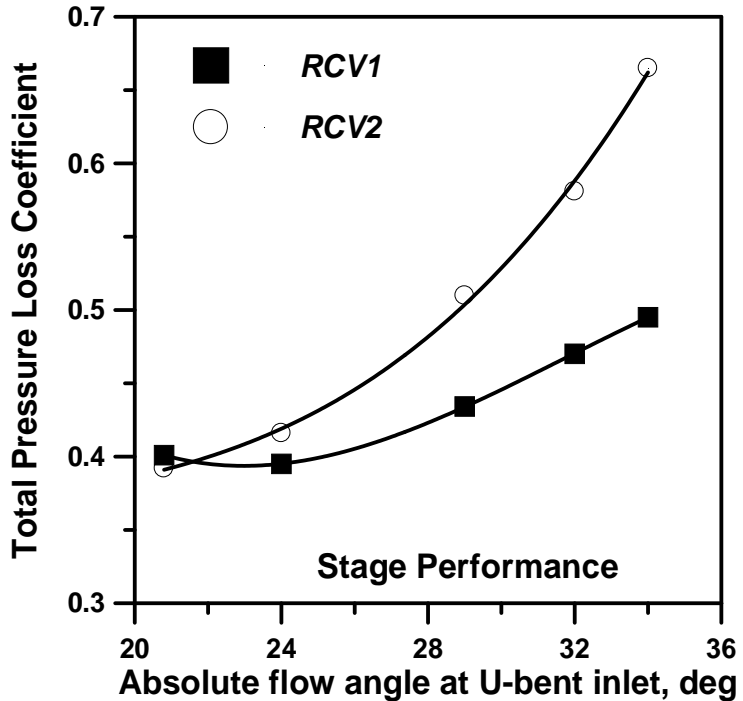


Fig. 6.19(a) Variation of total pressure loss coefficient (stage)

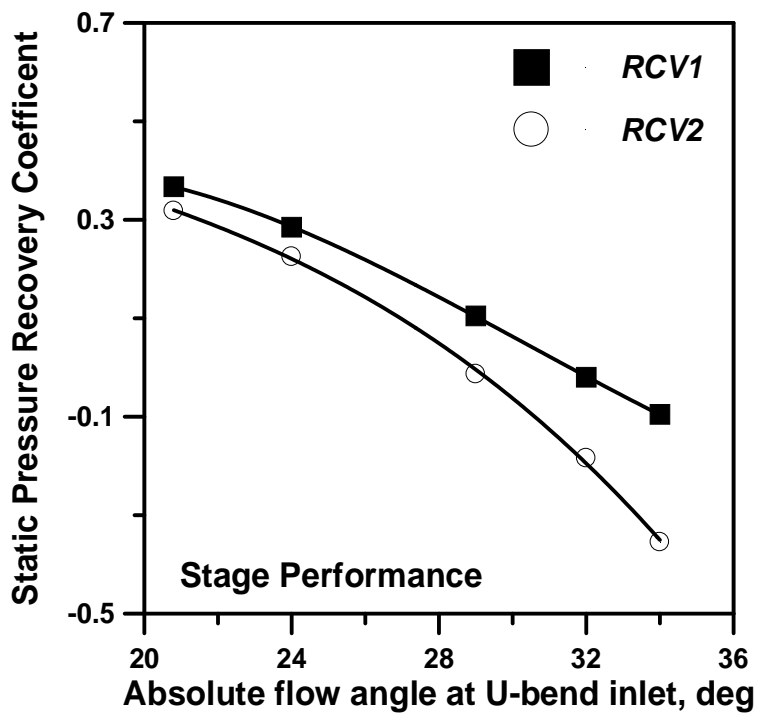


Fig. 6.19(b) Variation of static pressure recovery coefficient (stage)

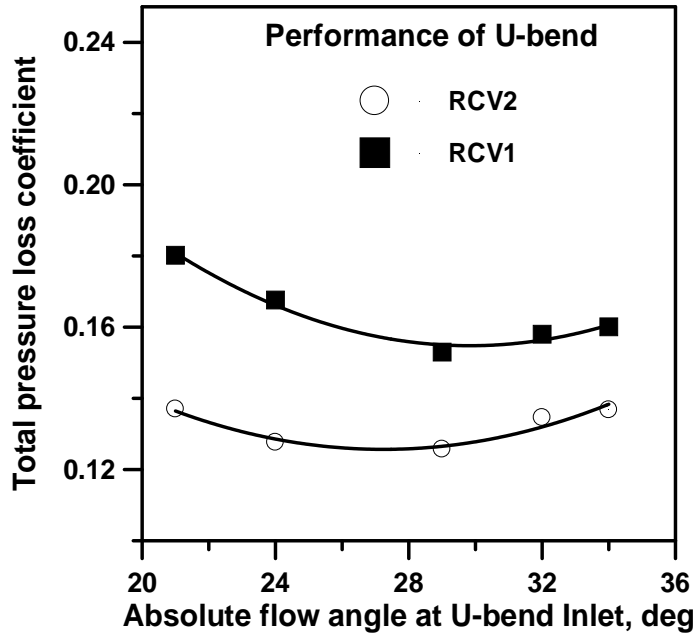


Fig. 6.20(a) Variation of total pressure loss coefficient (U-bend)

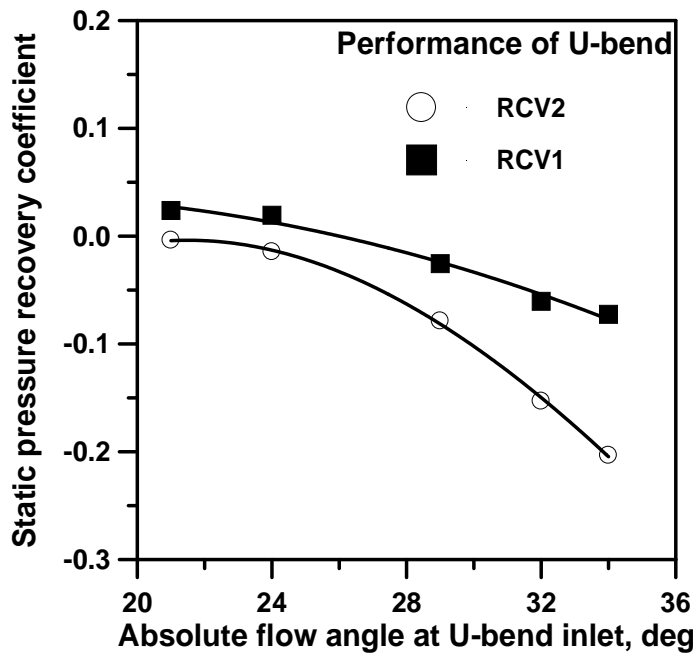


Fig. 6.20(b) Variation of static pressure recovery coefficient (U-bend)

Chapter 7

NUMERICAL RESULTS AND DISCUSSION

7.1 INTRODUCTION

The numerical results obtained with RCV1 and RCV2 configurations are presented in this section. The flow path geometry of the crossover system used in the experiments is modeled and meshed for the purpose of computational study. The flow angle and velocity distribution obtained through experimental measurements at the inlet of crossover bend (U-bend) is imposed as "inlet" boundary condition. The mass flow rate and static pressure are specified as "exit" boundary condition. The quantitative data obtained through numerical solution is presented in the form of X-Y plots. Also qualitative data is presented in the form of vector plots and contour plots for better understanding and later for the purpose of interrogation with the experimental results. Further numerical studies were carried out with variations return channel vane height and number of return channel vanes. The flow path modifications were studied with the sole objective of minimizing the losses in the crossover system.

7.2 NUMERICAL RESULTS IN RCV1

The numerical results obtained through simulation studies in RCV1 configuration are presented in this section.

7.2.1 Variation of Meridional Velocity and Flow Angle at U-Bend Exit

The calculated circumferentially averaged meridional velocity and flow angle distributions at the exit of U-bend are shown in Fig.7.1 (a) and 7.1(b) respectively. The meridional velocity and flow angle and distributions from hub to shroud are seen to be uniform. However near the hub lower meridional velocities are observed than towards the shroud which may be attributed to the U-turning of flow taking place in the 180^0 crossover bend. Fig. 7.2 shows the meridional velocity vectors in the meridional plane of U-bend at the design flow rate. It is very clearly seen that almost a uniform meridional velocity is present at the exit.

The filled contour plots of meridional velocity in the U-bend exit plane for all the studied operating conditions are shown in Fig. 7.3. In these filled contours the meridional velocities are shown on the scale as negative indicating that it is in the radially inward direction. The maximum meridional velocities are observed towards the two extremes in the circumferential direction while lower meridional velocities are seen in the mid-region space above the vane. This trend is attributed to the vane blockage effect. Also within nearer to the two extreme sides higher meridional velocities are noted in the space above the pressure side of the RCV1 than the suction side. However at any location on the U-bend exit plane the meridional velocity from hub to shroud is seen to be more or less uniform with slight decrease towards the hub wall which is also indicated in the X-Y plot of Fig. 7.1(a).

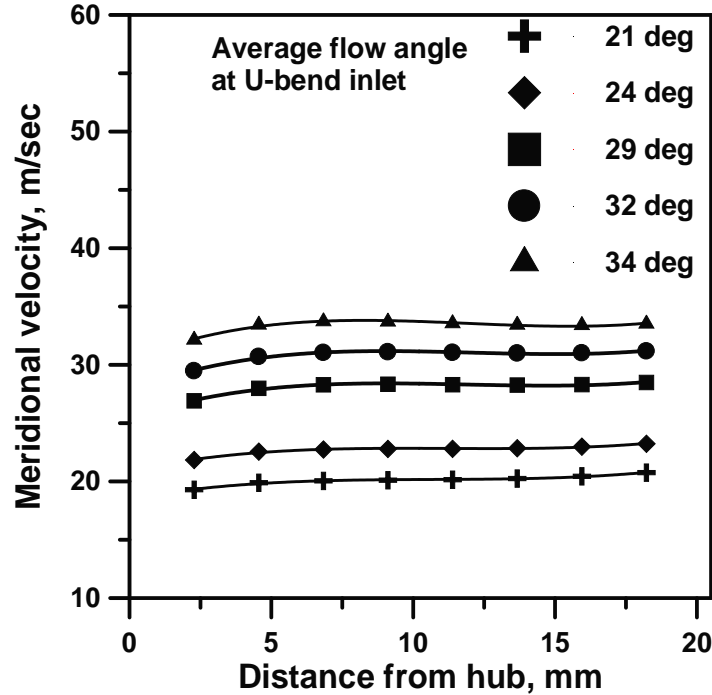


Fig. 7.1(a) Variation of meridional velocity at U-bend exit

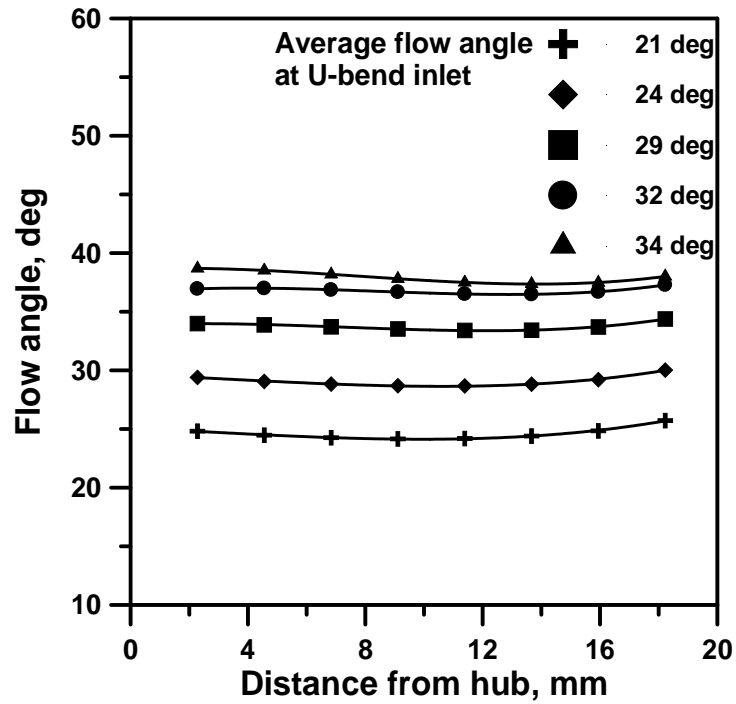


Fig. 7.1(b) Variation of flow angle at U-bend exit

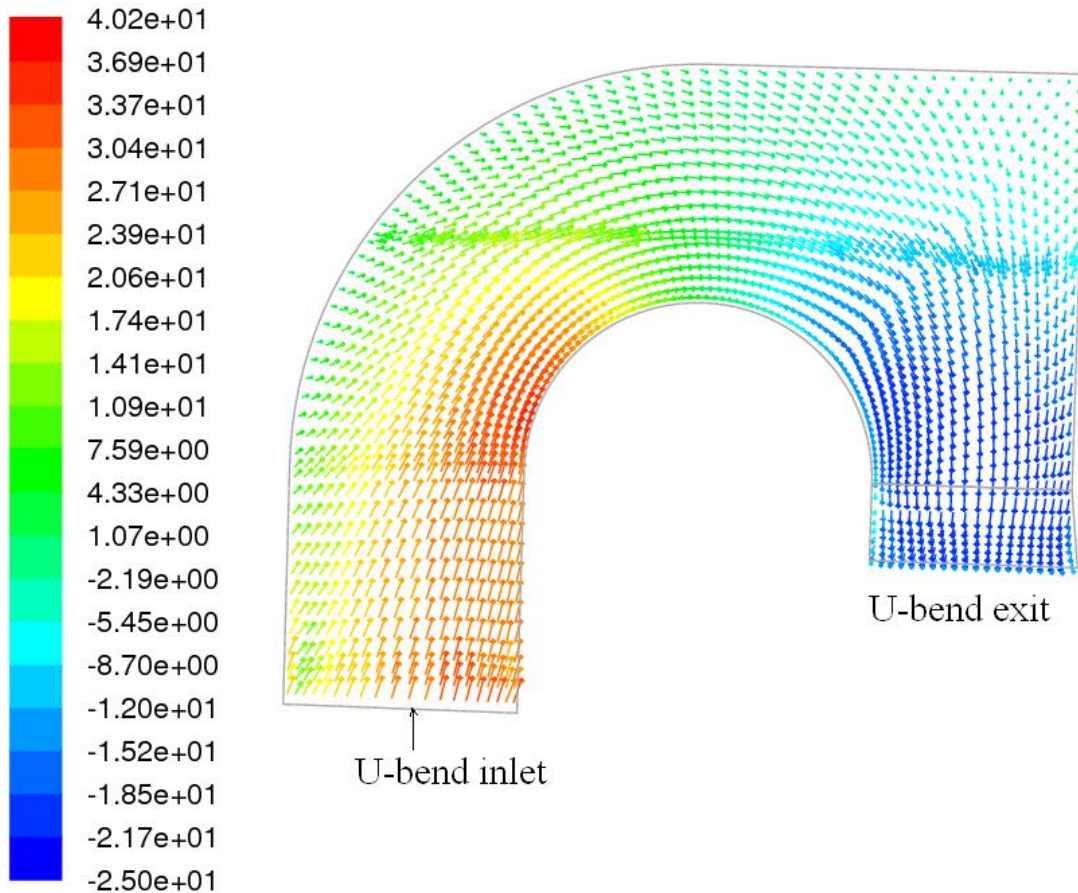


Fig. 7.2 Velocity vectors in the meridional plane of U-bend

7.2.2 Vane surface pressure distribution

The numerically calculated static pressure on the mid span of the return channel vane RCV1 configuration is expressed as a coefficient (C_{pv}) and is plotted against its chord length on X-axis. Figure 7.4 shows the vane surface static pressure distribution for all studied operating conditions. The average flow angle at the exit of crossover bend and its resulting incidence on the L.E of the RCV1 configuration is shown in the Table 7.1.

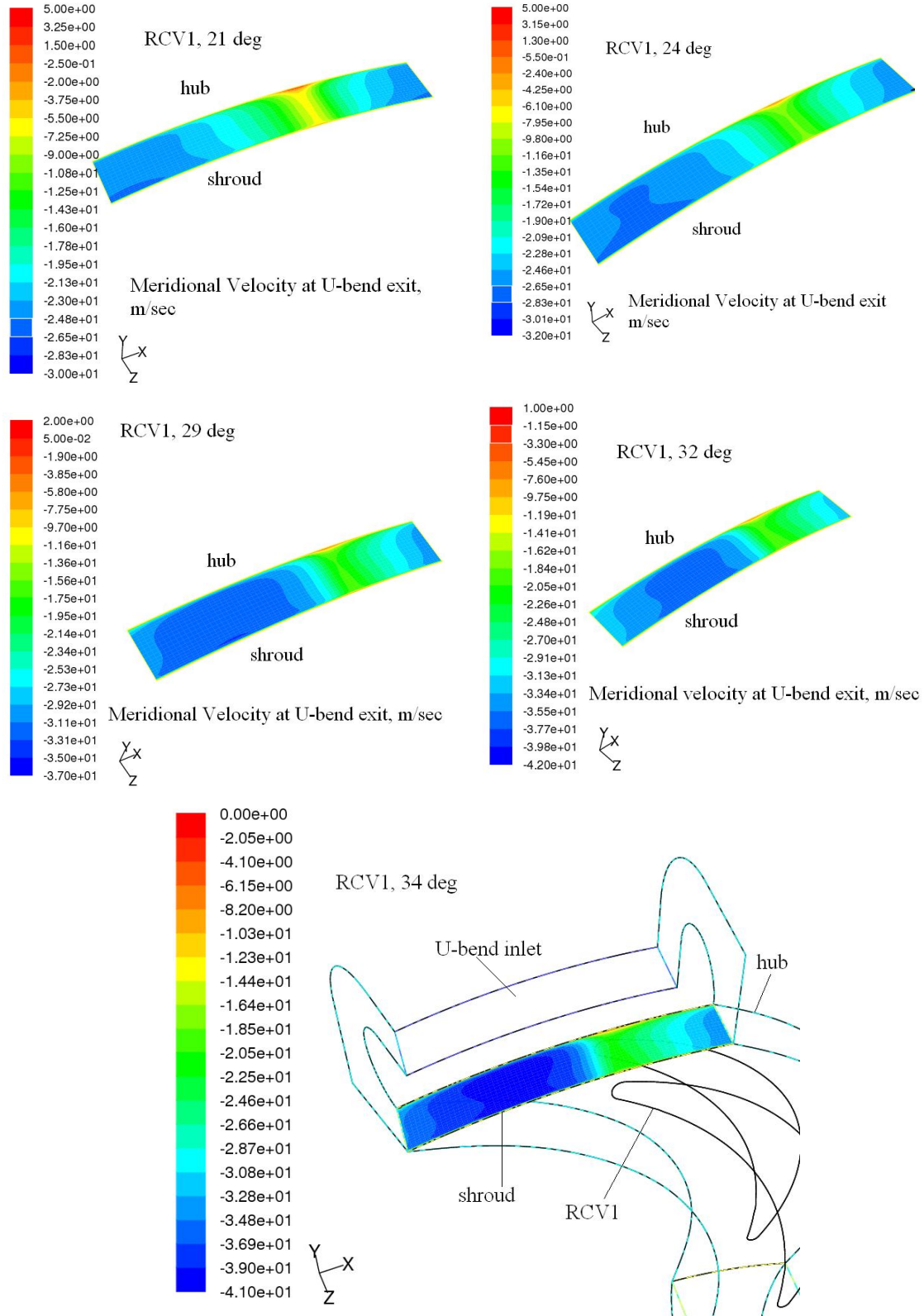


Fig. 7.3 Contour plots of meridional velocity in the U-bend exit plane

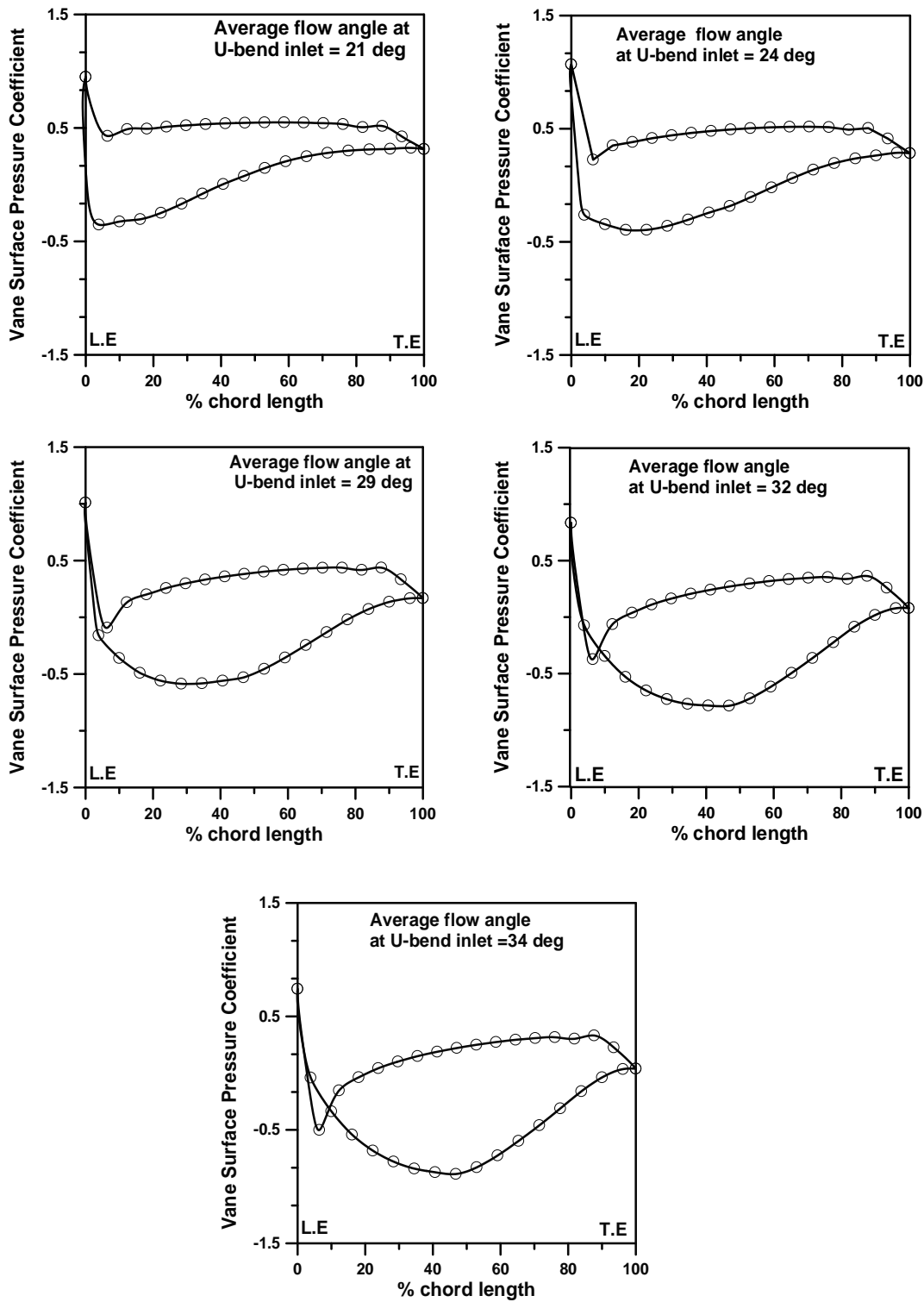


Fig. 7.4 Calculated vane surface pressure distribution (RCV1)

Table 7.1 Incidence angles on the L.E of RCV1 configuration

S.No	Average flow angle at U-bend inlet(α_1), deg	Average flow angle at U-bend exit(α_2), deg	Incidence on the L.E of RCV1 (i),deg
1	21	24.6	+3.9
2	24	29.08	-0.58
3	29	33.75	-5.25
4	32	36.8	-8.3
5	34	37.94	-9.44

With positive and near zero incidences on the L.E, it is observed that on the pressure side the static pressure is remaining constant for most of the chord length except near the L.E and T.E of RCV1. However with negative incidence a sudden drop in static pressure near the L.E on pressure side and there after some recovery is observed. On the suction side due to acceleration of flow a gradual decrease in static pressure and there after some rise is observed owing to the flow channel width variations. From the figure it is seen that the vane loading patterns for 80% and 100% flow conditions are more uniform when compared with 70%, 110% and 120% flow conditions. The filled velocity contour plots for RCV1 configuration at the all studied operating conditions on a plane passing through the mid span of the vane is shown in Fig. 7.5. When the average flow angle at the inlet of U-bend is 21 degrees a wide low velocity region is formed on the suction side towards the T.E indicating flow separation in that zone.

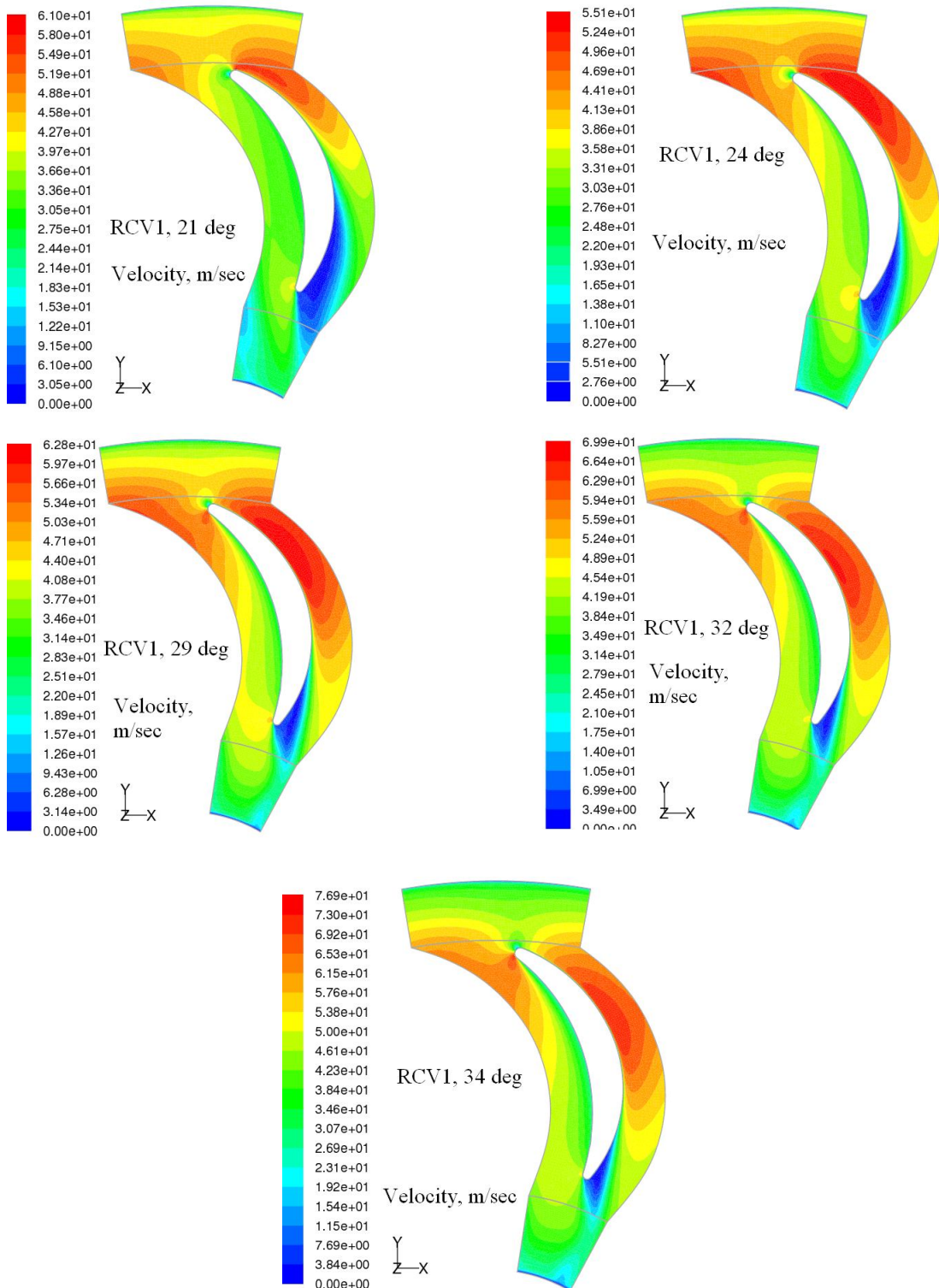


Fig. 7.5 Velocity contours on a plane passing through the mid span of RCV1

On the suction side an acceleration of flow, followed by deceleration is seen for all studied flow conditions. The intensity of low velocity zone and possible flow separation is reduced with increased flow angles at U-bend inlet. Therefore from the figure it is evident that the flow losses might be occurring which needs to be reduced especially with positive incidence angles on the RCV1 configuration. The inability of flow not to conform to the vane contour due to flow separation leads to local pressure differences and induction of cross flows (secondary flows). These low velocity zone is seen to spread in to the inlet of L-turn duct influencing the flow pattern in the downstream direction. The flow is likely to gain some swirl angle due to the flow separation phenomena observed particularly at positive incidence angles on the RCV1 configuration.

7.2.3 Iso-Mach Contour Plots

Figure 7.6 shows the nomenclature of different planes on which iso-Mach contour plots are presented. Figure 7.7 shows the Iso-Mach number contour plots on different planes along the flow path through the return channel vane passage. Plane-1 corresponds to radius ratio (ratio of radius at which the plane is selected to the radius at which LE is placed) of 0.96, which is very near to the leading edge. The iso contours of Mach number at this plane indicate acceleration of flow towards suction surface of the vane. Deceleration is seen to occur at Plane-2 which corresponds to a radius ratio of 0.86 as the flow progresses within the vane passage from Plane 1.

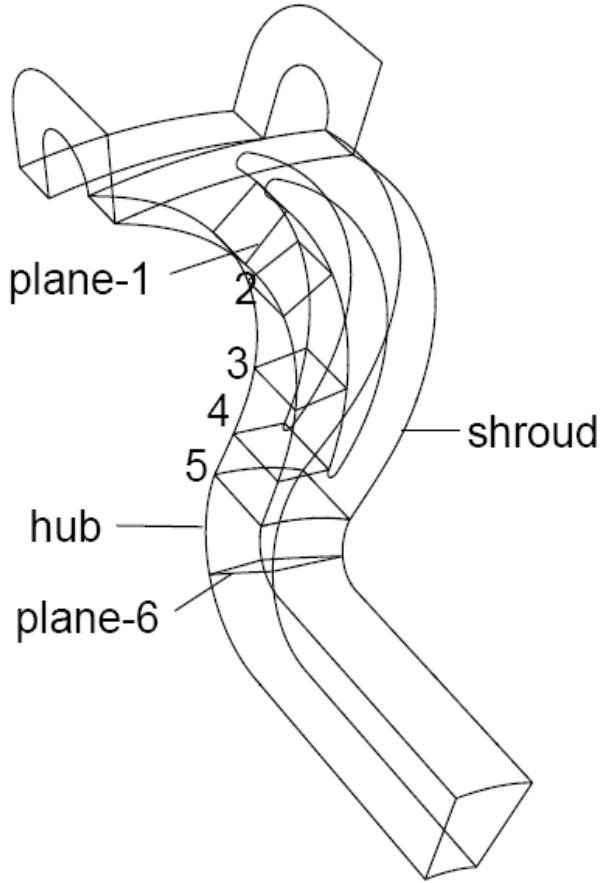


Fig.7.6 Plane nomenclature used for qualitative plots

Considerable pressure gradient has been observed at Plane 3 (radius ratio of 0.69) from SS to PS. Regions of low flow is seen to occur at plane 3 near the suction surface represented by iso mach shown in Plane 4. It is observed that near the SS the low flow regions are widened as represented by iso-Mach contours of low magnitude. The flow at the downstream region of the vane is represented in Plane5. The flow is seen to be concentrated towards the shroud at this plane. The spread of the low velocity region at inlet to 90° bend is seen on this plane. Plane 6 represents the flow configuration in the bend region and the flow is still

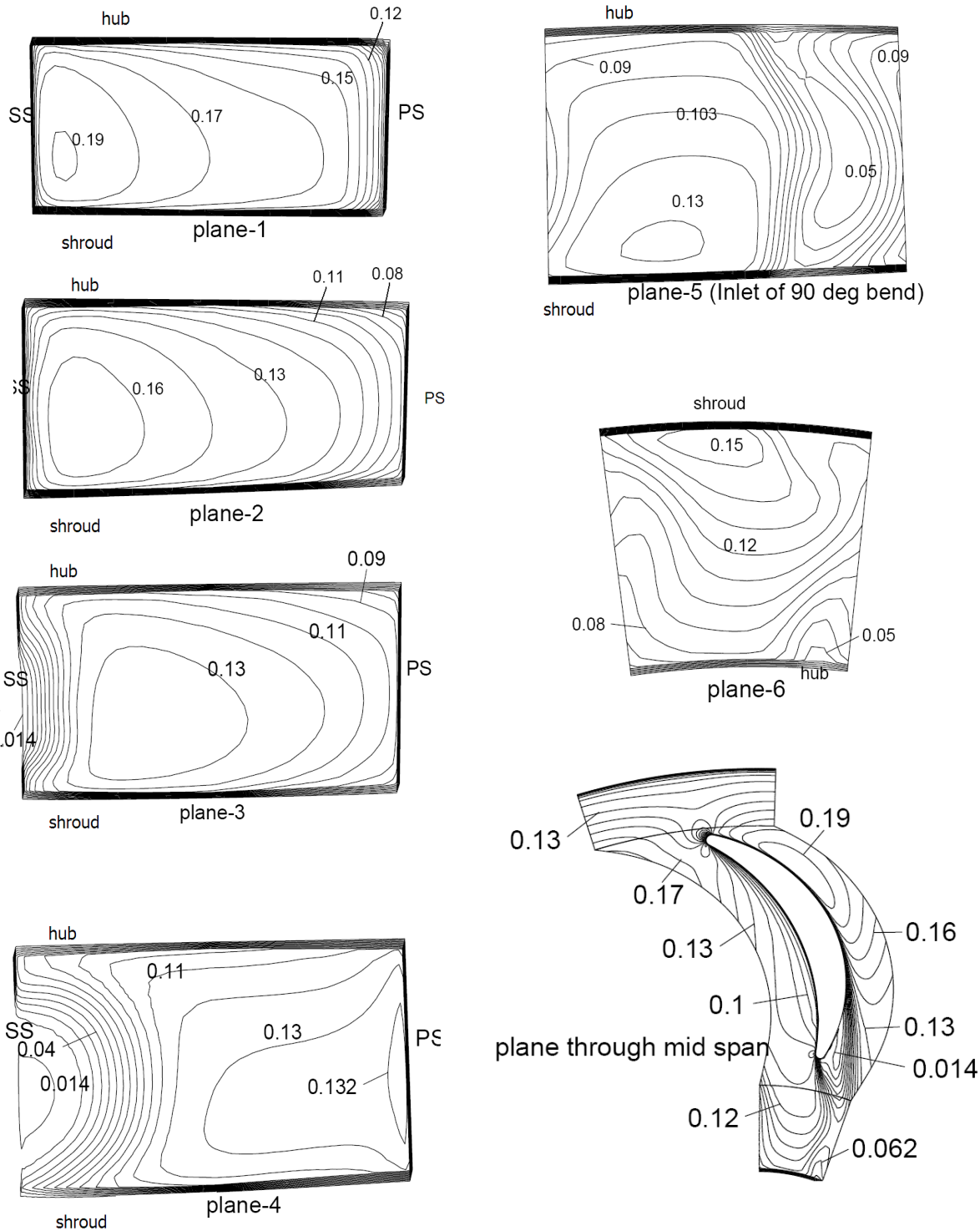


Fig. 7.7 Calculated Iso contours of Mach number ($\alpha_1 = 29^\circ$)

observed to be concentrated towards the shroud. The Iso-Mach contours on a plane through the mid span of the flow channel width in which the low Mach number contours are clearly seen on the downstream of suction side of the vane. This low velocity region is spreading in to the inlet of the 90° bend as also can be seen on plane-5 of Fig 7.7. The calculated cross flow velocity vectors at entrance to L-turn ducting are shown in Fig. 7.8. The secondary flow is observed to migrate from suction side to pressure side just after the vane exit and while entering 90° bend. Also the flow is seen to be oriented towards the shroud while entering the L-turn bend. This kind of flow phenomena may be attributed to the flow separation occurring on the suction side near to the trailing edge.

7.2.4 Variation of meridional velocity and swirl angle at the L-turn exit

The circumferentially averaged meridional velocity distribution from hub to shroud at various operating conditions is shown in Fig. 7.9. All the curves are showing first increasing and then decreasing trend from hub to casing. The peak meridional values are observed to occur close to the hub wall. It is very much evident that the flow is concentrated more towards the hub than shroud.

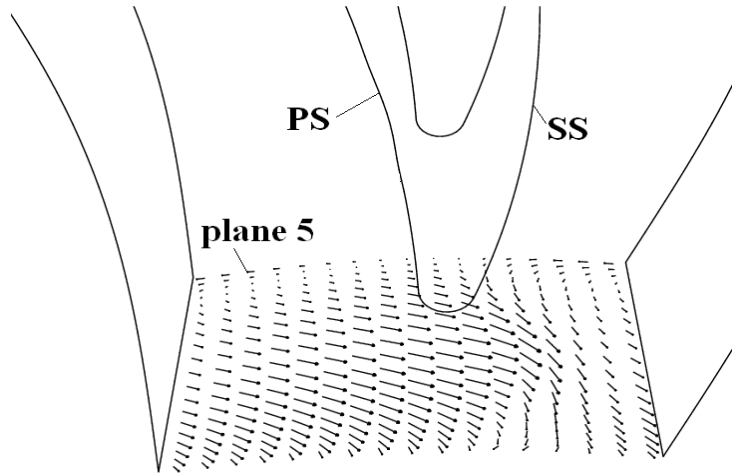


Fig. 7.8 Calculated cross flow velocity vector plot on plane 5 ($\alpha_1 = 29^\circ$)

The design point meridional velocity distribution in the circumferential direction at different non-dimensional distances (x_4/b_4) at the L-turn exit is shown in Fig. 7.10(a). The meridional velocity is observed to be uniform in the circumferential direction near the hub. The meridional velocity is varying in a wavy fashion away from the hub. The trailing edge of the return channel configuration seems to influence the meridional velocity variation from hub to shroud at the L-turn exit. As the flow is more concentrated towards the hub as can be seen from the figure the trailing edge effect is smoothed out while it is not the case towards the shroud. The averaged swirl angle distribution from hub to shroud at all the operating conditions is shown in Fig. 7.10(b). The averaged swirl angles are seen to vary from 98° to 112° throughout the operating range. The filled contour plots of meridional velocity on the L-turn exit plane at all the studied operating conditions are shown in Fig. 7.11. It is observed

that at 70% of design flow rate i.e., when the average flow angle at the inlet of U-bend is 21° the meridional velocity is not much prone to fluctuations in the circumferential direction. As the flow rate through the system is increased i.e. with the increase in average flow angles at the U-bend inlet, the wavy nature of meridional velocity distribution in the circumferential direction is much pronounced. The trailing edge effect of RCV1 on the meridional velocity distribution is clearly visible at the L-turn exit which shows higher values towards the pressure side and lower values towards the suction side.

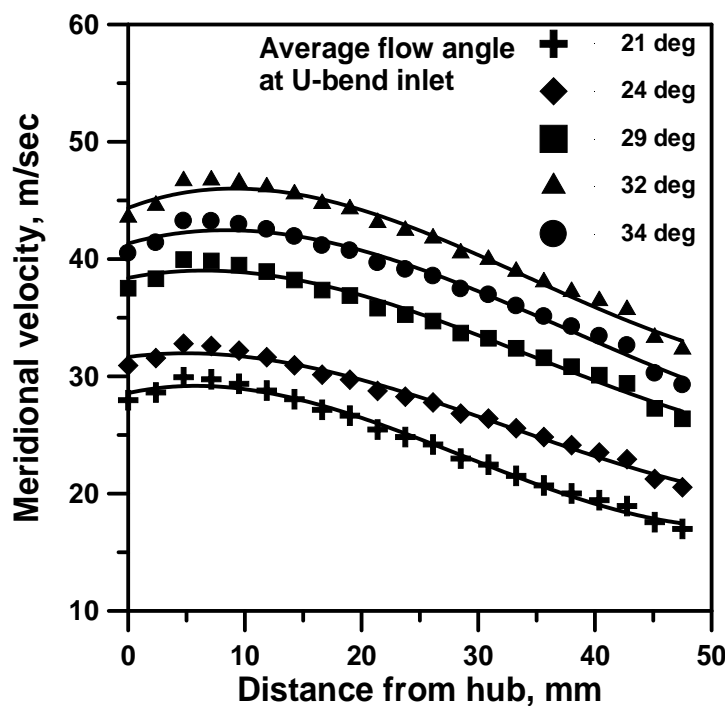


Fig. 7.9 Variation of meridional velocity at the L-turn exit
(Circumferential average)

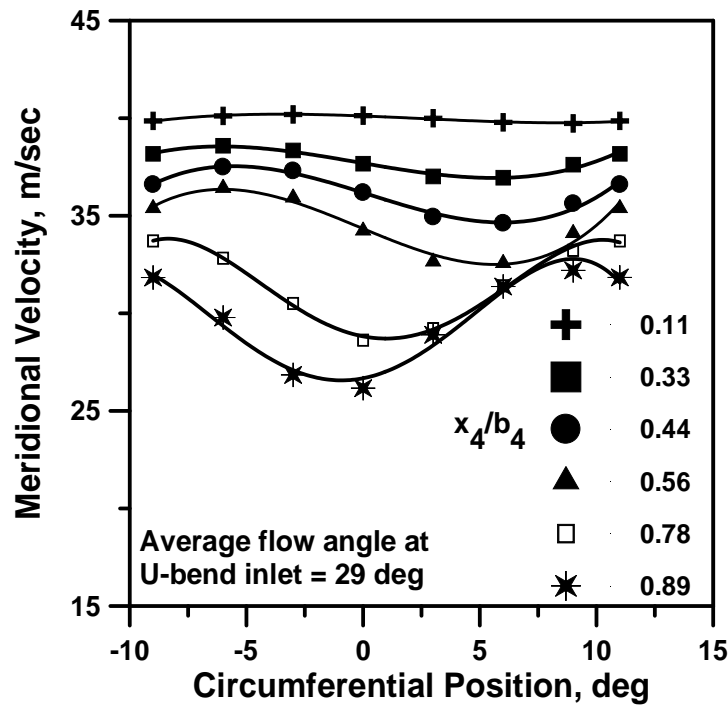


Fig. 7.10(a) Variation of meridional velocity at the L-turn exit

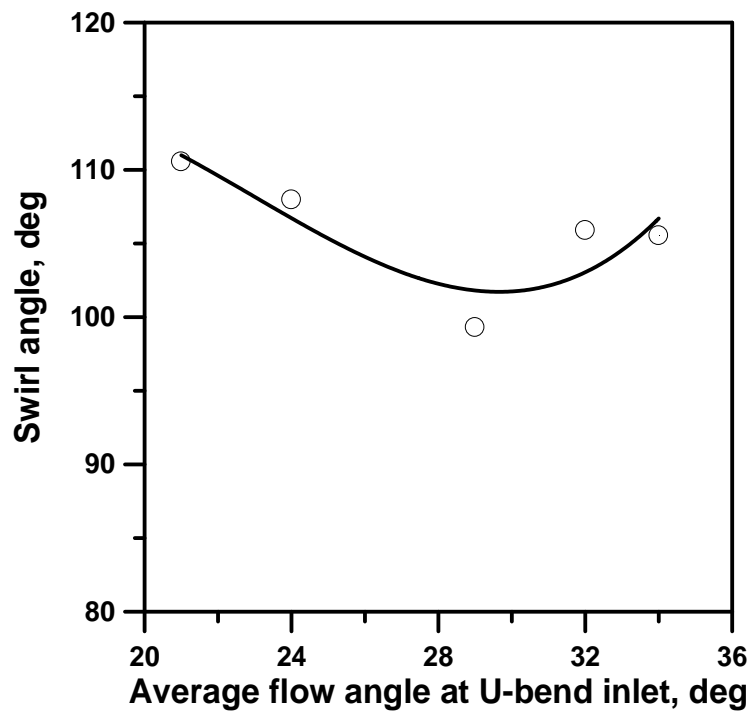


Fig. 7.10(b) Variation of average swirl angle at the L-turn exit

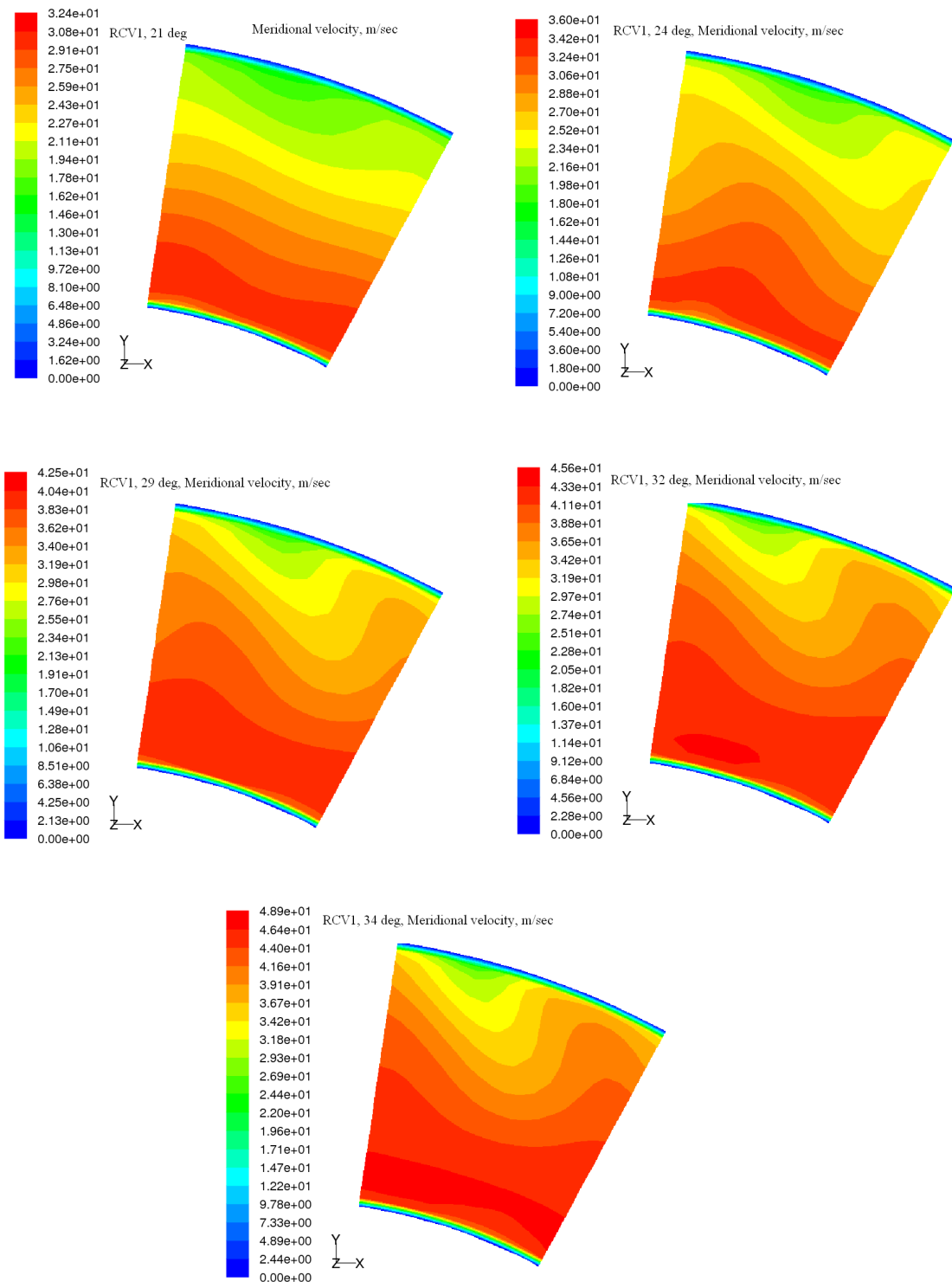


Fig. 7.11 Contours of meridional velocity at L-turn exit

7.2.5 Performance of the stage and U-bend

The variation of total pressure loss coefficient plotted against the average flow angle at the U-bend inlet is shown in Fig. 7.12. The total pressure loss should be minimized before the flow is passed on to the subsequent stage in an actual centrifugal compressor. In the present study it is observed that the total pressure loss is seen to be minimum at an average U-bend inlet flow angle of 23° . With the increase in flow angle further the total pressure loss coefficient is seen to increase rapidly. However with the decrease in flow angle from 23° to 21° a slight increase in total pressure loss is noted. The reason for higher total pressure loss at higher mass flow rate may be attributed to the increased skin friction losses due to increased velocities of fluid. Though the total pressure loss observed in the present study appears to be acceptable, an attempt can further be made to reduce its magnitude, particularly at the lower flow angles by eliminating the flow separation problem on the suction side of the vane in the downstream direction. The variation of static pressure recovery coefficient with average flow angle at U-bend inlet is shown in Fig. 7.13. The static pressure is recovered well at lower average flow angles of U-bend inlet. There is no static pressure recovery at higher flow angle of U-bend inlet. The performance of crossover bend in terms of total pressure loss and static pressure recovery coefficients is shown in Fig. 7.14 (a) and (b) respectively.

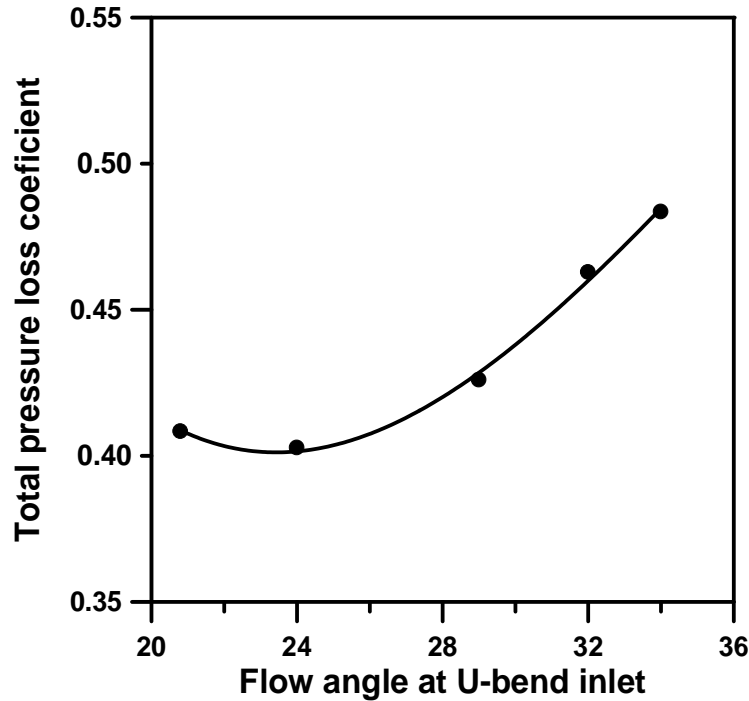


Fig. 7.12 Variation of total pressure loss coefficient (stage)

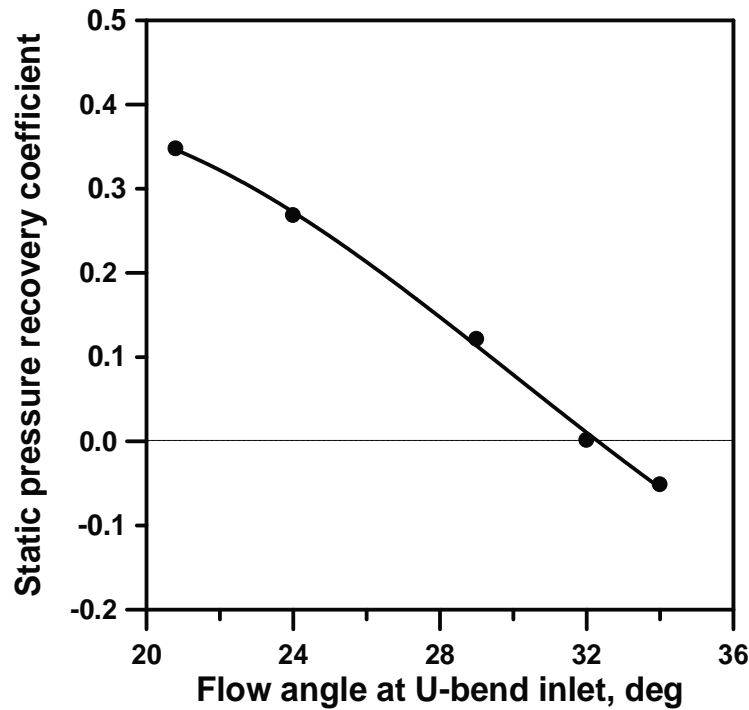


Fig. 7.13 Variation of static pressure recovery coefficient (stage)

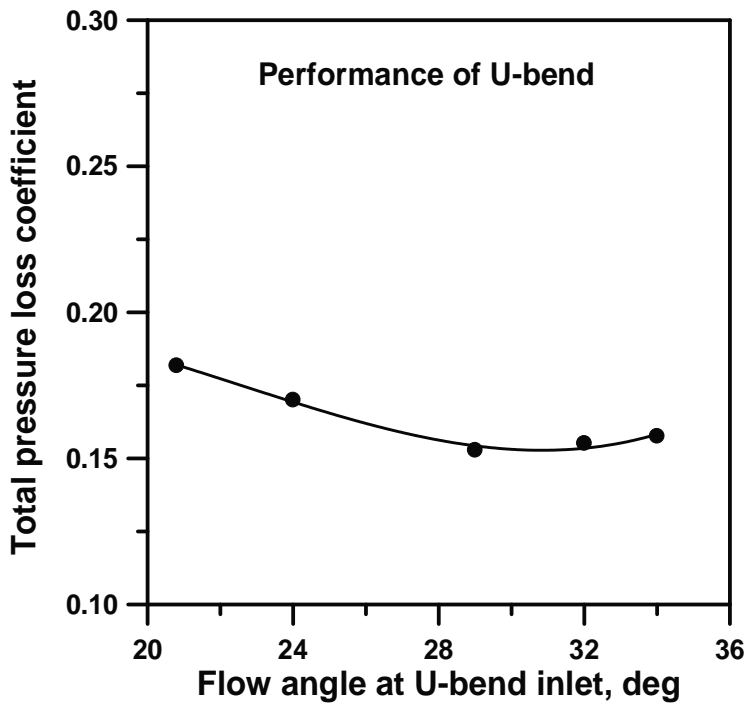


Fig. 7.14(a) Variation of total pressure loss coefficient for U-bend

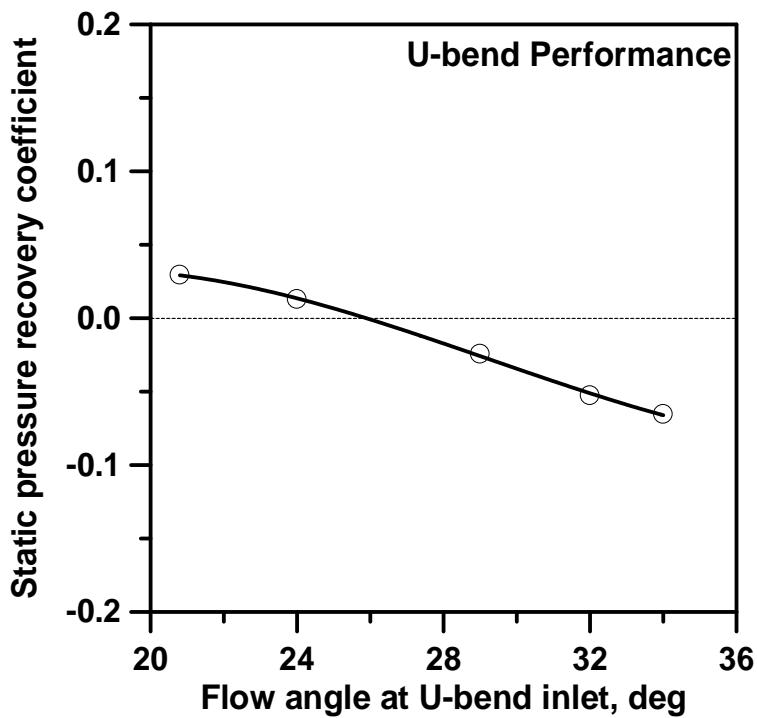


Fig. 7.14(b) Variation of static pressure recovery coefficient for U-bend

7.3 COMPARISON OF EXPERIMENTAL AND NUMERICAL RESULTS IN RCV1 CONFIGURATION

The numerical results obtained with RCV1 are compared with the corresponding experimental results in this chapter. The numerical and experimental results for the RCV1 configuration are presented at the design flow rate and 70% and 120% of design flow rate operating conditions. The comparison is made for the meridional velocity distributions at the U-bend exit, L-turn exit, vane surface pressure distribution, swirl angle distribution at the L-turn exit.

7.3.1 Comparison of meridional velocity and flow angle at U-bend exit

The comparison of experimental and numerical results for the meridional velocity and flow angle distributions at the U-bend exit are shown in Fig 7.15. The calculated flow angle distribution from hub to shroud is seen to be closer to the measured values near the hub than towards the shroud. The present numerical model predicted the meridional velocity and flow angle distributions closer to the experimentally measured values. The similar type of agreement was observed at the off-design conditions also.

7.3.2 Comparison of Vane surface Pressure Distribution

The comparison between CFD and the experimental values for the vane surface pressure coefficient at the all studied operating conditions is shown in Fig. 7.16. A good agreement is observed between the values

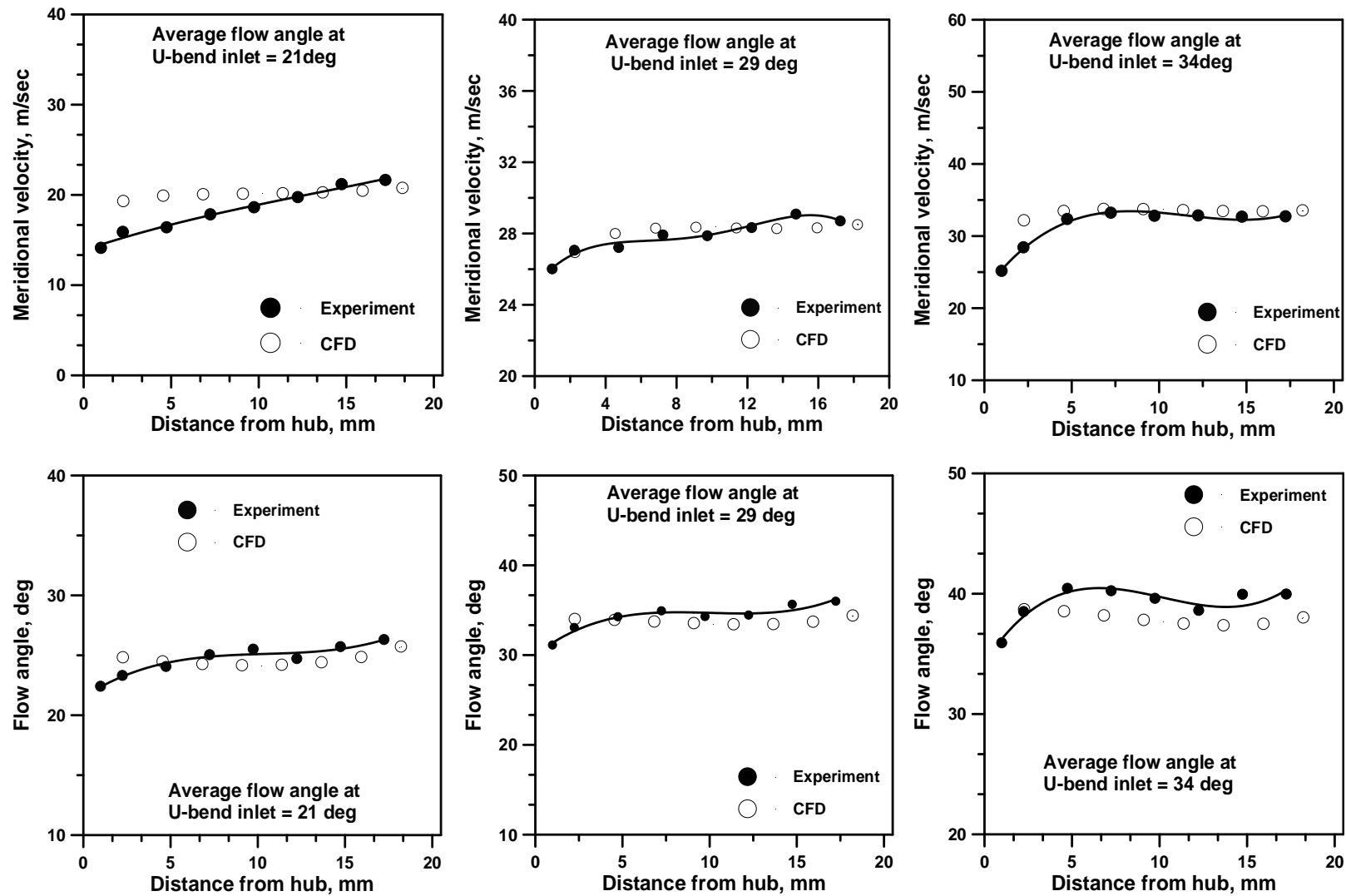


Fig. 7.15 Variation of meridional velocity and flow angle at U-bend exit

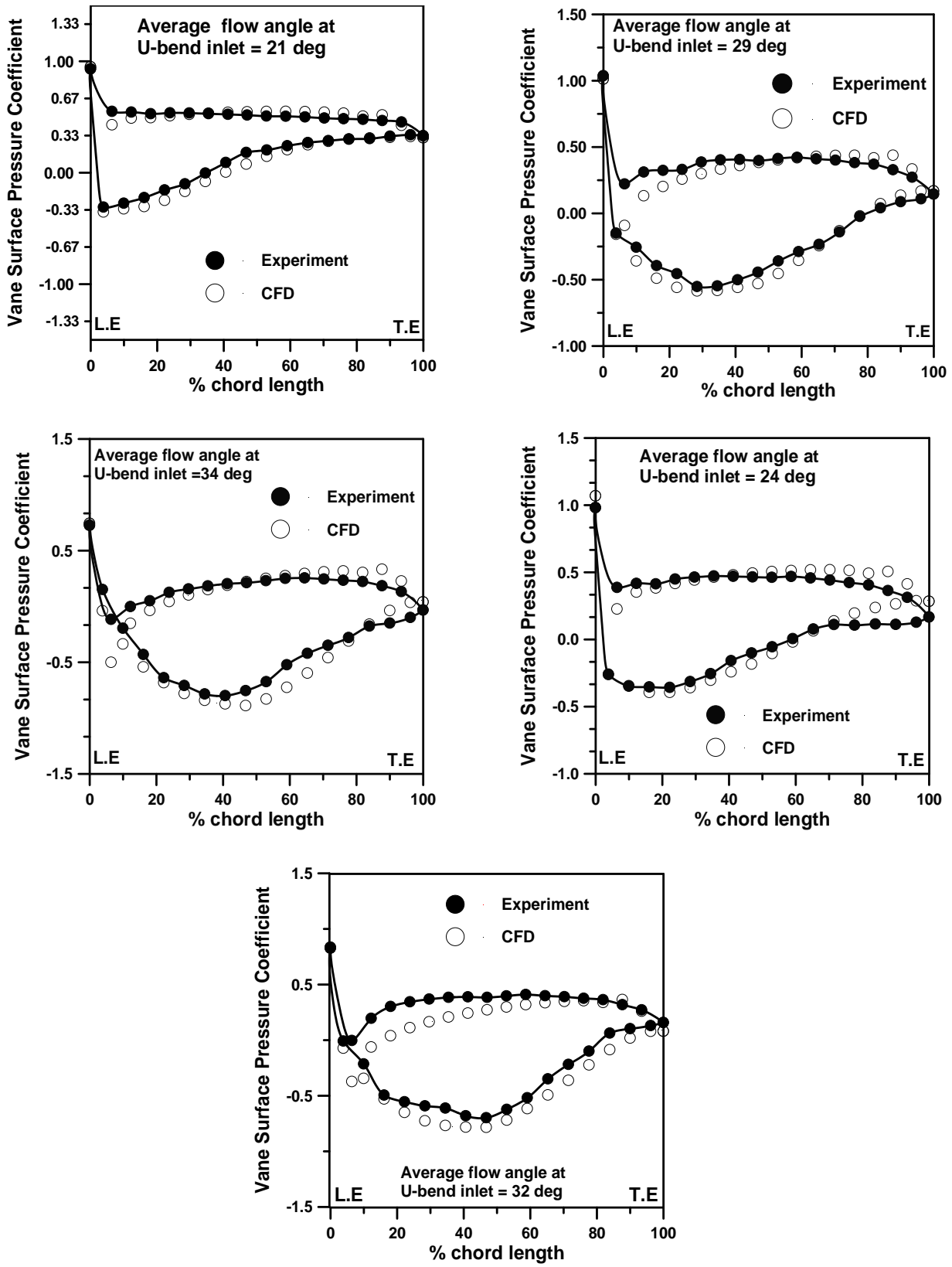


Fig. 7.16 Comparison of Vane surface pressure distribution (RCV1)

except for the portion on pressure side up to 20% chord length. The standard k- ϵ turbulence model used in the present study is seen to predict the flow in near agreement with the experimental values at the design point. At the off-design operating conditions also a qualitative agreement between the predicted and measured values is observed.

7.3.3 Comparison of Meridional Velocity and Swirl Angle at the L-Turn Exit

The comparison of experimental values of circumferentially averaged meridional velocity at L-turn exit with the CFD results is shown in Fig. 7.17(a) to (c). The meridional velocity is seen to be higher towards the hub and is gradually decreasing towards the casing of the L-turn ducting. The experimental values and the calculated CFD values are observed to be in good agreement at this location. At off-design operating conditions also the same kind of agreement is observed.

The comparison of average swirl angles obtained through measurements and CFD calculations at all the operating conditions are shown in Fig. 7.18. It is seen from the figure that the calculated average swirl angle at the design point is 106.8° , while the experimentally measured value is 101.4° . The present CFD model is able to predict the swirl angle distribution in qualitative agreement with experimental values at the 110% and 120% of design flow rate operating conditions while some deviation is observed at the 70%, 80% and 100% of design flow operating conditions. In the present CFD study the standard k- ϵ

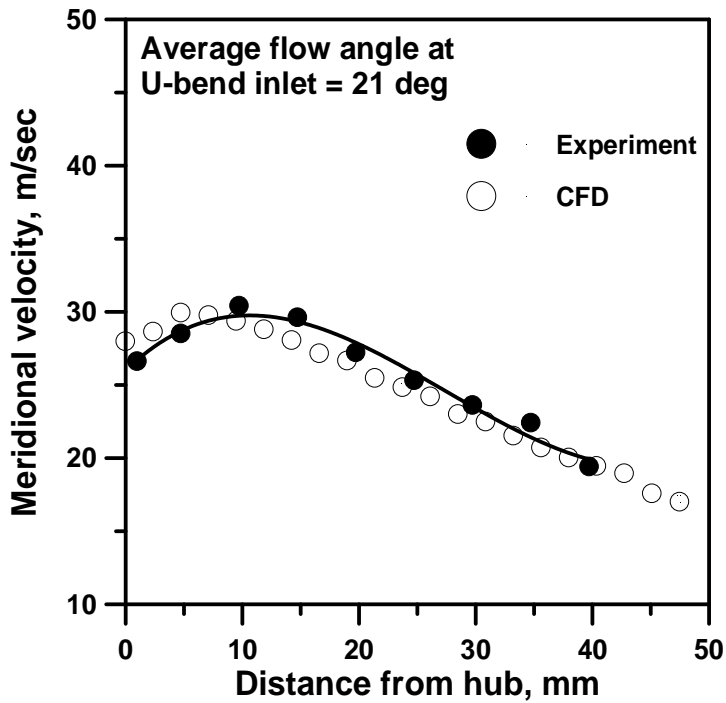


Fig. 7.17(a) Meridional Velocity distribution at the L-turn exit
(70% of design flow)

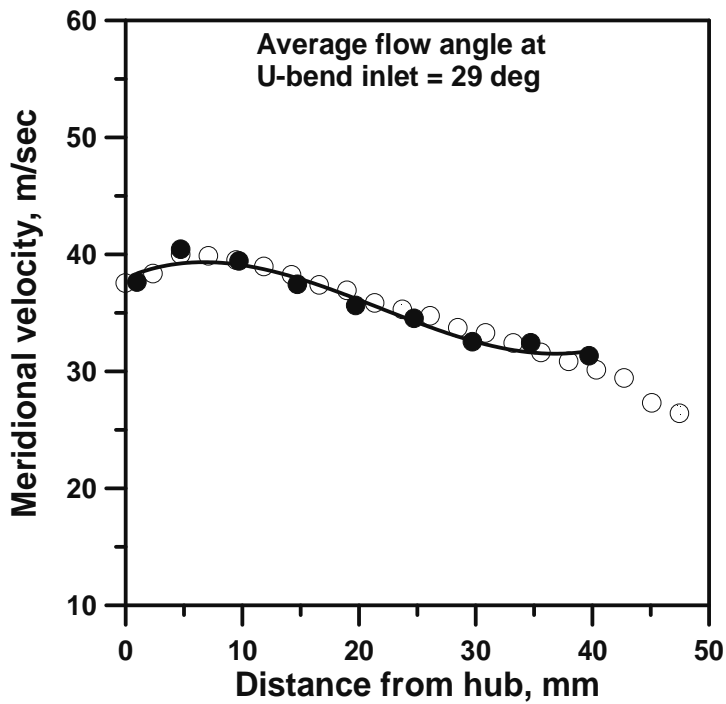


Fig. 7.17(b) Meridional Velocity distribution at the L-turn exit
(100% of design flow)

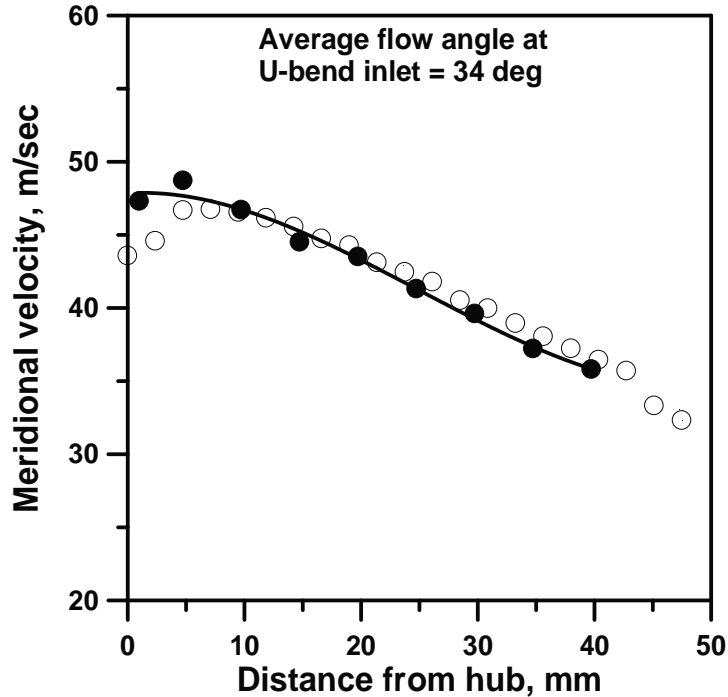


Fig. 7.17(c) Meridional Velocity distribution at the L-turn exit
(120% of design flow)

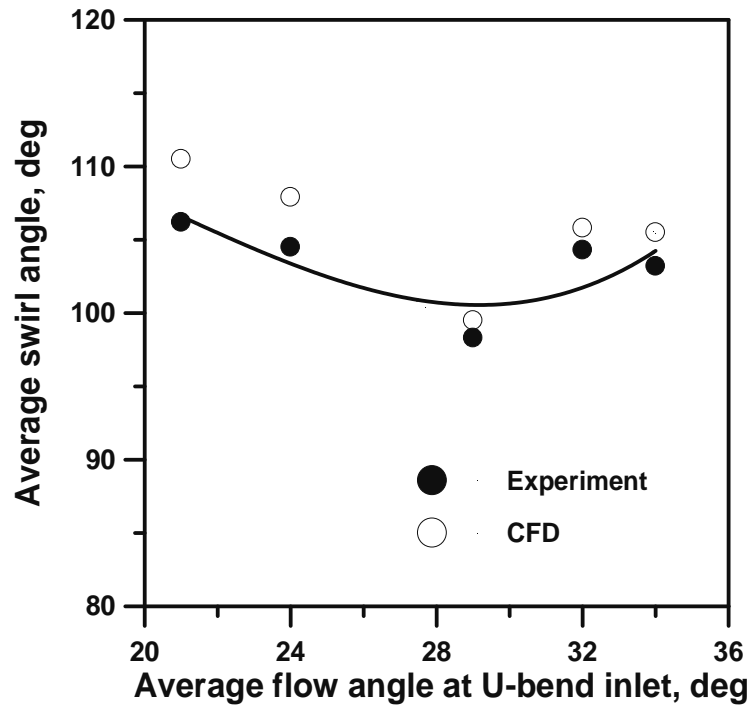


Fig. 7.18 Comparison of average swirl angle distribution

turbulence model was used to predict the flow details. This model was reported to give qualitative agreement between CFD and measured values in situations involving flow through U-bend by Oh et.al. (2005). Lenke and Simon (2000) in their numerical study in return channel passages reported that the k-epsilon turbulence model underestimates the separation length at extremely low flow coefficients. In the present study the present numerical model could not predict the exit swirl angle close to the experimental values particularly with positive incidence on the L.E of the RCV1 vane.

7.3.4 Comparison of Performance of the stage and U-bend

The performance of the whole stage in terms of total pressure loss coefficient and static pressure recovery coefficient is shown in Fig. 7.19 and 7.20 with comparison made between the CFD and experimental values. A good agreement is seen between the predicted and measured values, particularly near the design point while some a little deviation is observed at the off-design operating conditions... Similar kind agreement was reported in literature by Lenke and Simon (2000). The performance of crossover bend in terms of total pressure loss and static pressure recovery coefficients is shown in Fig.7.21 and Fig. 7.22 respectively. A good agreement has been observed between the experimental and CFD values.

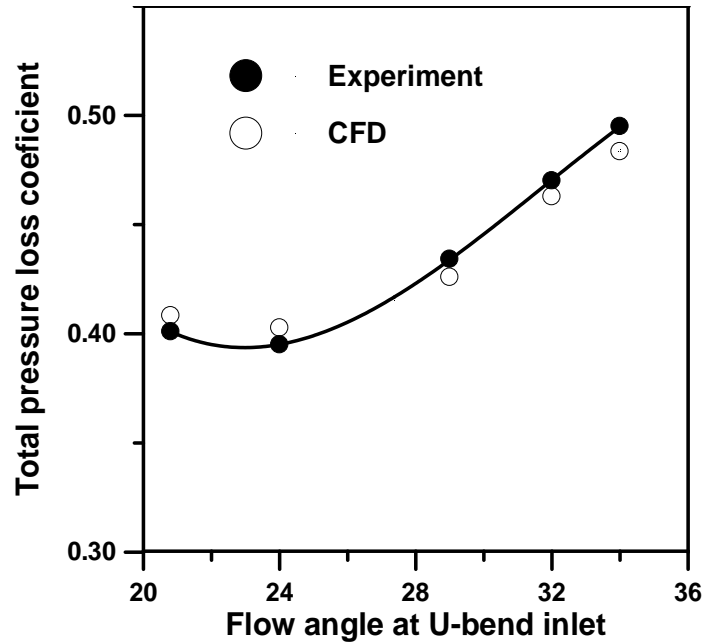


Fig. 7.19 Variation of total pressure loss coefficient (stage)

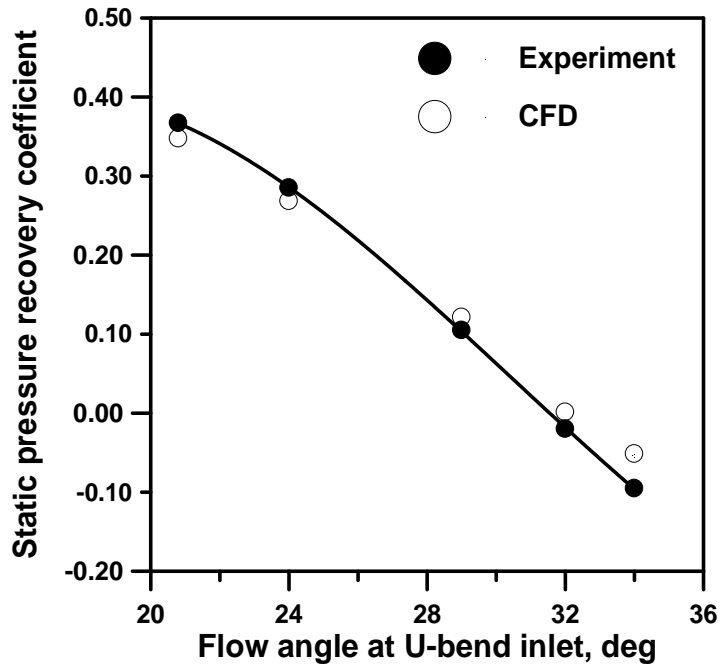


Fig. 7.20 Variation of static pressure recovery coefficient (stage)

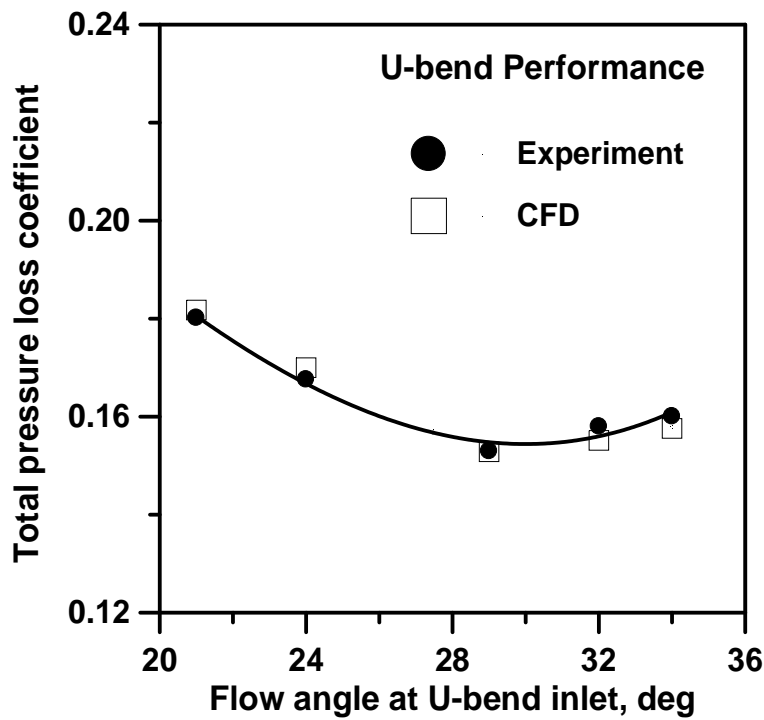


Fig. 7.21 Variation of total pressure loss coefficient for U-bend

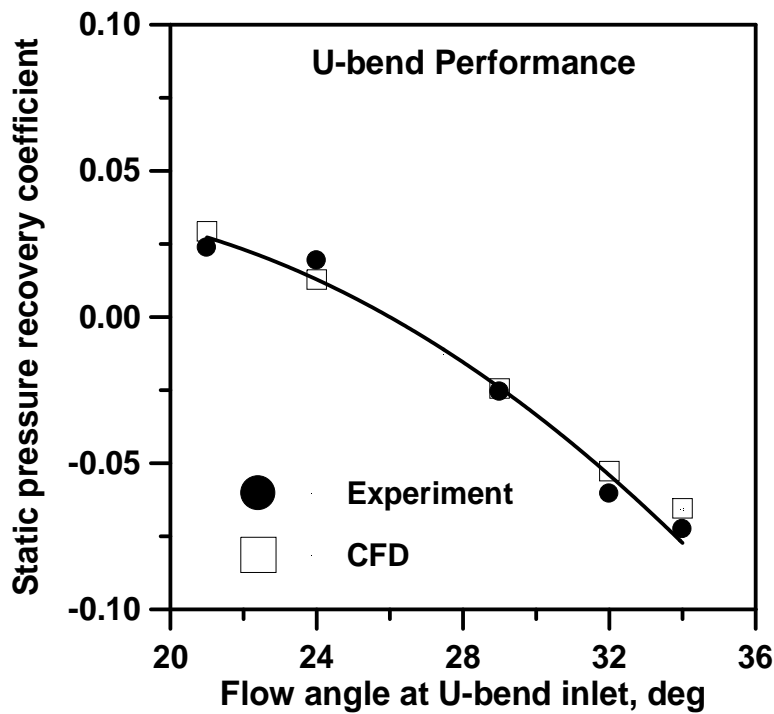


Fig. 7.22 Variation of static pressure recovery coefficient for U-bend

7.4 NUMERICAL RESULTS IN RCV2 CONFIGURATION

The numerical solution procedure used in the study of RCV1 configuration is followed in obtaining the numerical results of RCV2 configuration also. The flow angles obtained through experimental measurements at the inlet of crossover bend in the RCV2 configuration and the corresponding total pressure were specified as the inlet boundary condition. At the L-turn exit the mass flow rate and static pressure were specified. The numerical results obtained in the RCV2 configuration are discussed in the form of quantitative and qualitative plots in the following sections.

7.4.1 Variation of meridional Velocity and flow angle at U-bend exit

The meridional velocity variation from hub to shroud wall for all the operating conditions at the U-bend exit are shown in Fig. 7.23(a). The curves are showing a uniform meridional velocity distribution though an increase in magnitude is observed towards the shroud. Obviously an increase in magnitude is also seen with the increase in the average flow angle at the U-bend inlet due to increasing mass flow rate. The flow while taking 180° turn is likely to be concentrated more towards the shroud wall. The flow path width at U-bend exit is also becoming narrow due to which there is an increase in average meridional velocity at U-bend exit than at the inlet for all the studied operating conditions. The variation of circumferentially averaged flow angles at the exit of U-bend is shown in Fig. 7.23(b). The flow angle is measured with respect to tangential

direction at the exit of cross over bend. The calculated and circumferentially averaged flow angles are plotted against the distance from hub in mm for all the studied operating conditions. When the averaged flow angle at U-bend inlet is 21° , the cross over bend exit flow angle is seen to increase monotonically from 25° near the hub to 29° at the shroud. Similar trend is observed at the other operating conditions but with an increase in the magnitude of flow angles. Figure 7.23(c) shows the meridional velocity contour plot at the exit of U-bend for the design flow rate operating condition. The variation shows uniform meridional velocity distribution from hub to shroud.

7.4.2 Vane Surface Pressure Distribution

The vane surface pressure coefficient, C_{pv} for RCV2 configuration is plotted against the percentage chord length from the L.E and is shown in Fig.7.24. The vane is seen to be uniformly loaded for the 70% of the design flow operating condition (21° flow angle at U-bend inlet). With increase in the flow angle at U-bend inlet there seem to be sudden drop in static pressure on the pressure side immediately after the L.E and thereafter sudden raise to positive static pressure there by indicating possible flow separation at that location. A negative vane surface pressure coefficient is observed throughout the pressure side at the 120% operating condition i.e, when the average flow angle at U-bend inlet is 34° . The average flow angles at U-bend exit and their incidence on the L.E of the vane is shown in the Table 7.2.

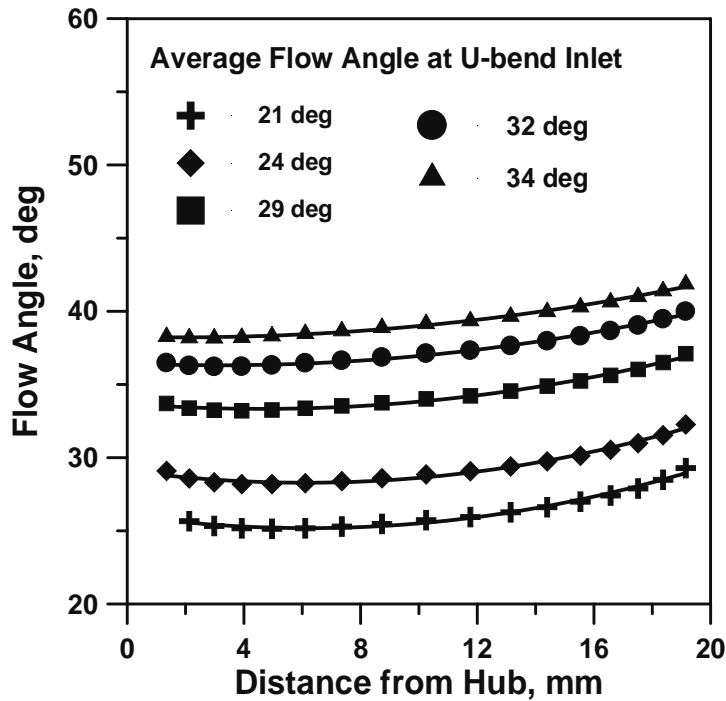


Fig. 7.23(a) Variation of meridional velocity at U-bend exit

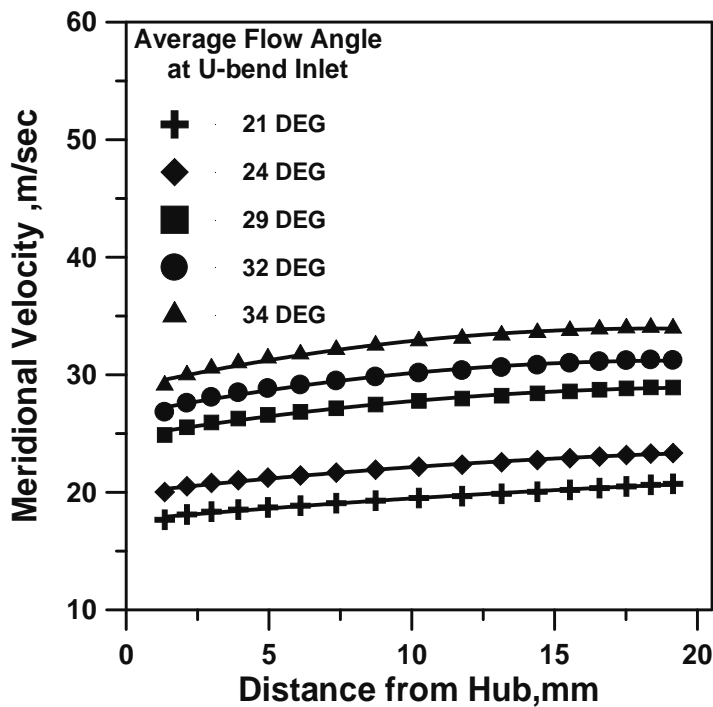


Fig. 7.23(b) Variation of flow angle at U-bend exit

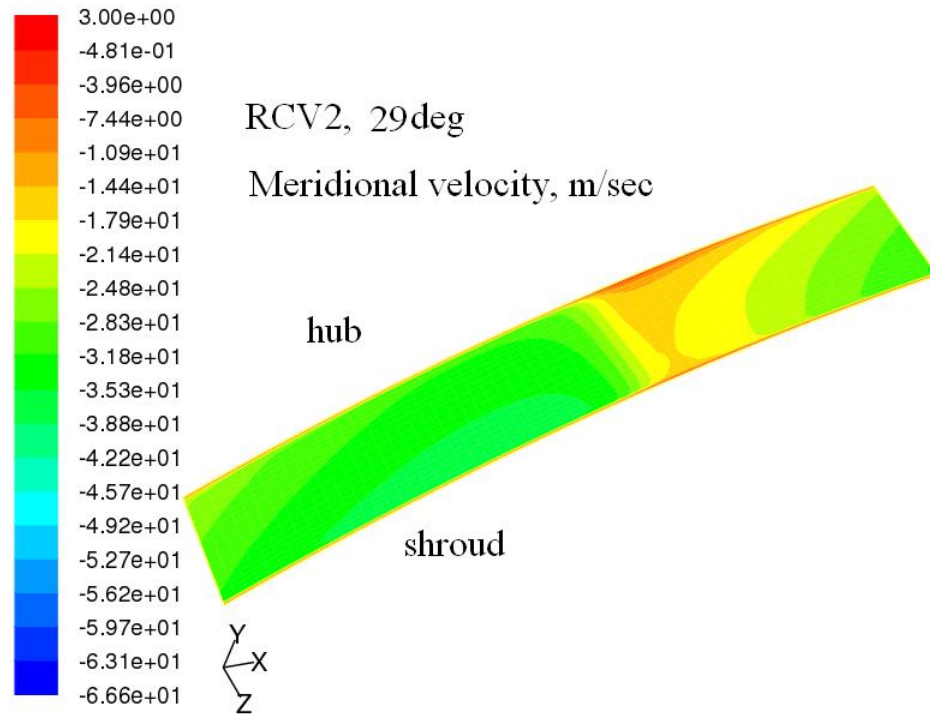


Fig. 7.23(c) Contour plot of meridional velocity distribution at the U-bend exit

Table 7.2 Incidence angles on RCV2 vane

S.No	Average flow angle at U-bend inlet, deg	Average flow angle at U-bend exit, deg	Incidence on the L.E of RCV2,deg
1	21	26.36	+0.64
2	24	29.4	-2.4
3	29	34.4	-7.4
4	32	37.4	-10.4
5	34	39.43	-12.43

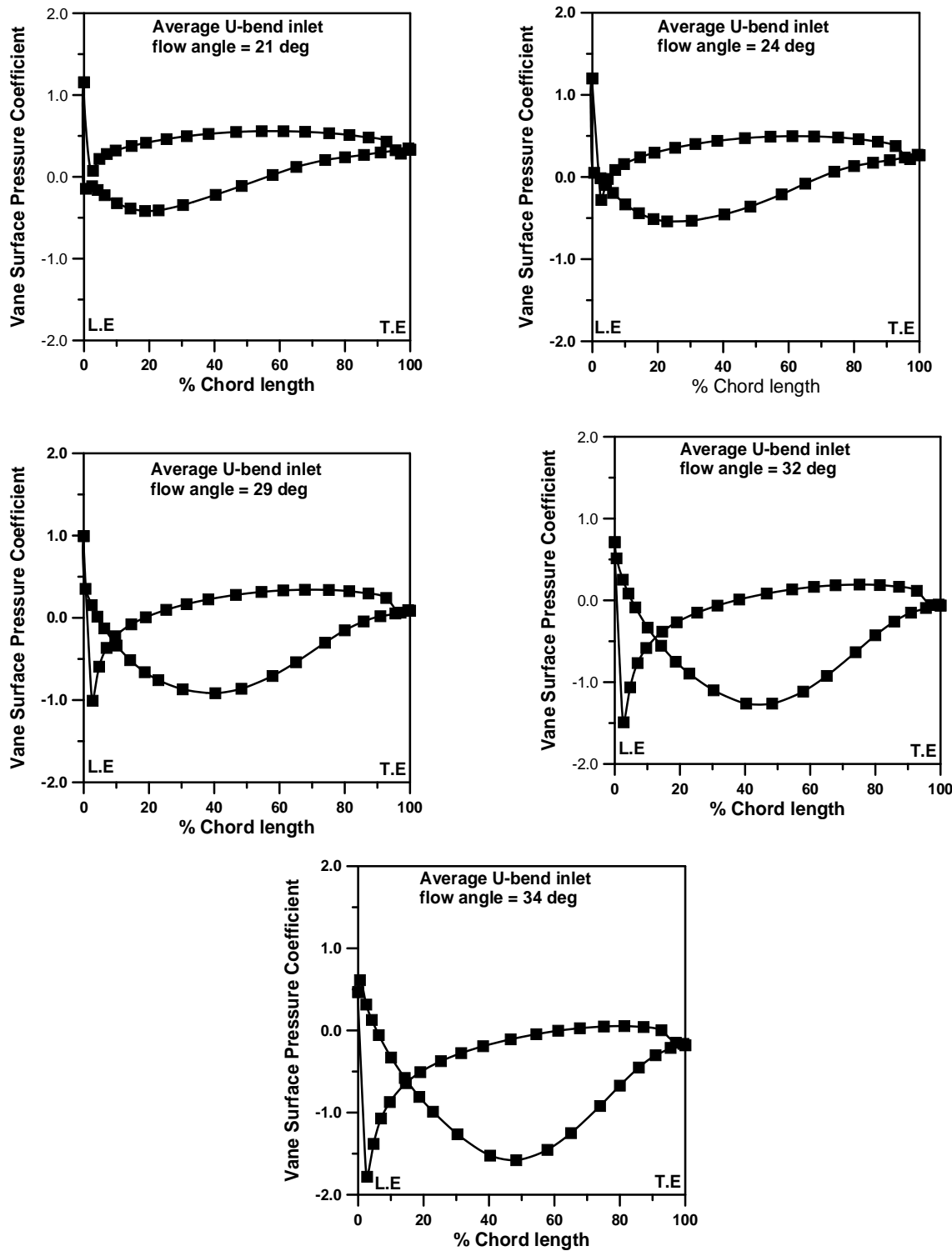


Fig. 7.24 Vane surface pressure distribution (RCV2)

The average flow angle at U-bend exit is observed to be approximately 5.4° higher than the corresponding average flow angle at U-bend inlet. The inlet vane angle of RCV2 is 27° . Therefore it is very much clear that at high negative incidence angles like -10.4° and -12.43° , the vane loading patterns tend to become non-uniform, leading to higher pressure losses. The non-uniform loading patterns occurring at 110% flow and 120% flow can be clearly seen in Fig. 7.24.

Figure 7.25 shows the filled velocity contour plots at all the operating conditions for RCV2 configuration on a plane passing through the mid span of the return channel vane. The flow separation zones on the suction side towards the T.E are clearly seen from the figure. The separation zone got shrunk as the incidence angle on the negative side is increased.

7.4.3 Variation of meridional velocity and Swirl angle at L-turn exit

The variation of circumferentially arranged meridional velocity (axial velocity) at the L-turn exit for RCV2 configuration is shown in Fig.7.26 (a). The flow is seen to be concentrated more towards hub. The meridional velocity is observed to decrease towards the shroud for all operating conditions. However a uniform meridional velocity distribution is seen when the average flow angle at U-bend inlet is 21° . The flow while taking 90° turn is migrating towards the hub due to sharp turning which is the reason for the observed lower meridional velocities near the shroud.

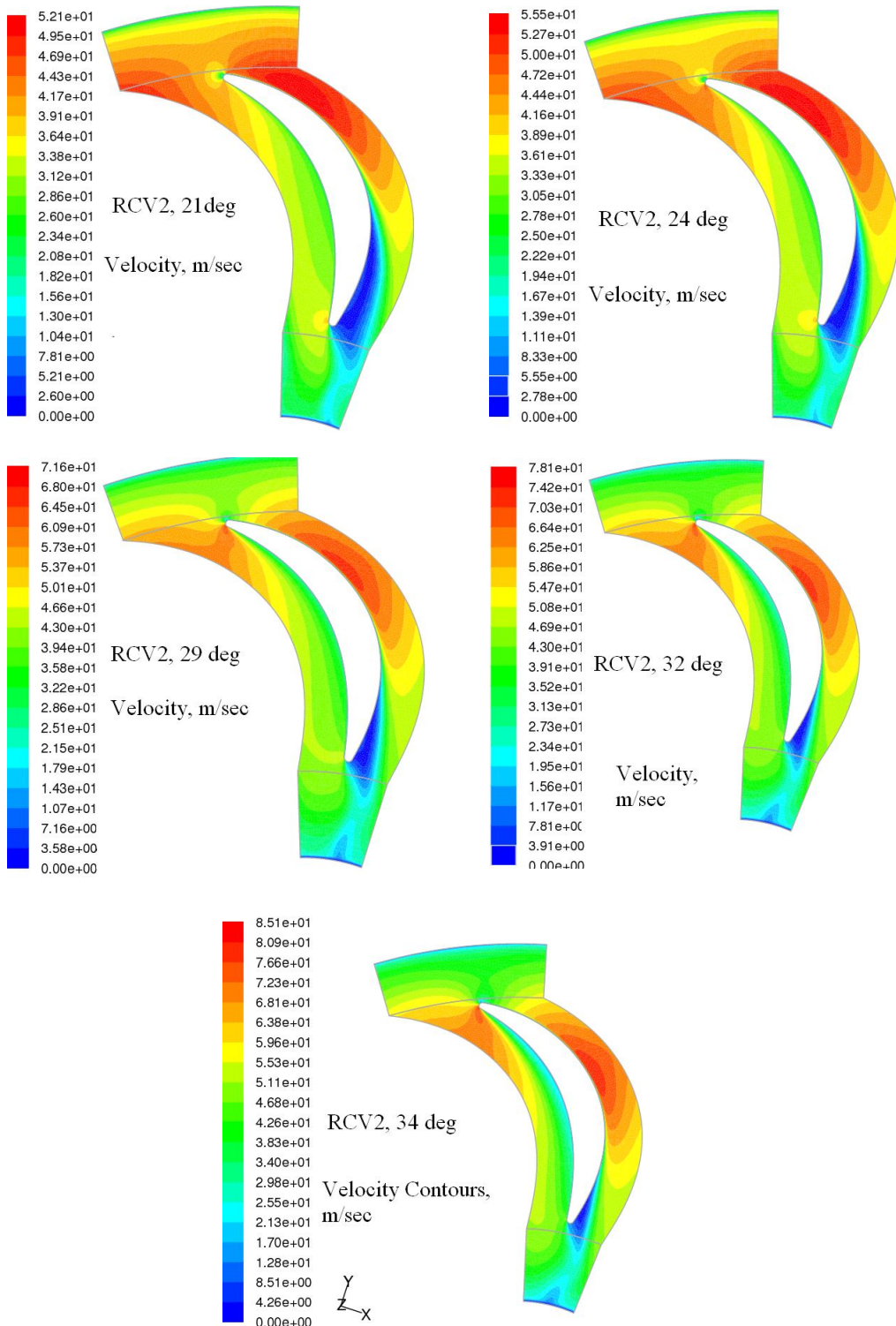


Fig. 7.25 Velocity contours on a plane passing through the mid span of RCV2

Figure 7.26(b) shows the variation of meridional velocity in the circumferential direction for design flow rate at the L-turn exit. A very uniform meridional velocity distribution is observed near the hub. With the increase in distance from the hub, the meridional velocity is seen to decrease in magnitude and also to vary in a wavy fashion. The wavy nature observed reduce towards the hub. The L-turn bend appears to cause the flow to migrate towards the hub. The RCV2 trailing edge wake appears to have an effect on the meridional velocity distribution in causing the wavy nature of variation. The variation of swirl angle at the design point in the circumferential direction at different non-dimensional distances is from hub is shown in Fig 7.27(a). Lower swirl angles are observed near the hub and shroud while higher swirl angles are observed in the mid-region. The variation of average swirl angle at the L-turn exit for all the operating conditions is shown in Fig. 7.27(b). The average swirl angle is seen to be about 94° at the design flow rate operating condition while it is increasing on either side of this design point. Higher swirl angles are observed when the average flow angle at U-bend inlet is 21° and 24° .The filled contour plots of meridional velocity distribution at the L-turn exit are shown in Fig. 7.28. Higher magnitudes of meridional velocities are seen in the contour plots near the hub. The magnitude of meridional velocity is seen to decrease towards the shroud. The wavy nature of variation in meridional velocity is much pronounced when the average flow angle at U-bend inlet is 21° and 24° .

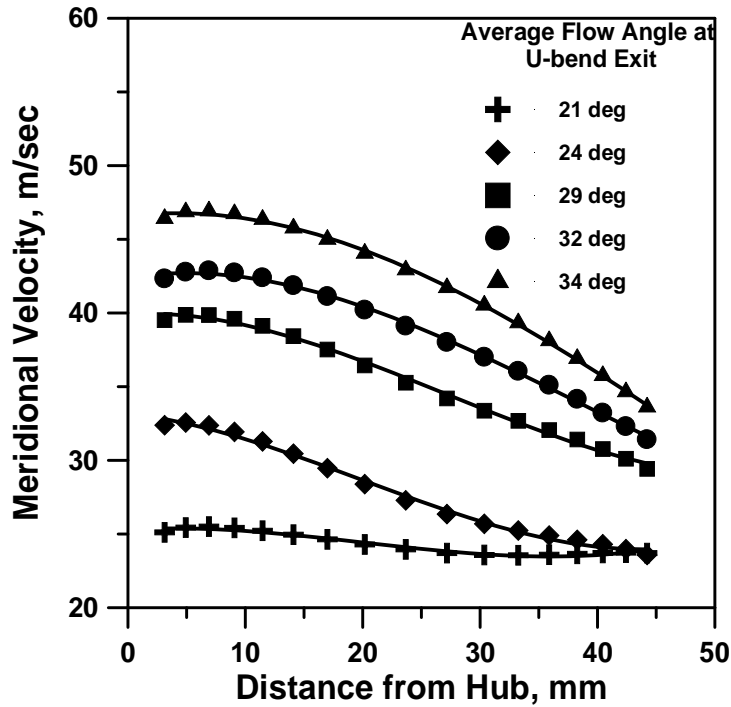


Fig. 7.26(a) Variation of meridional velocity at the L-turn exit
(Circumferential average)

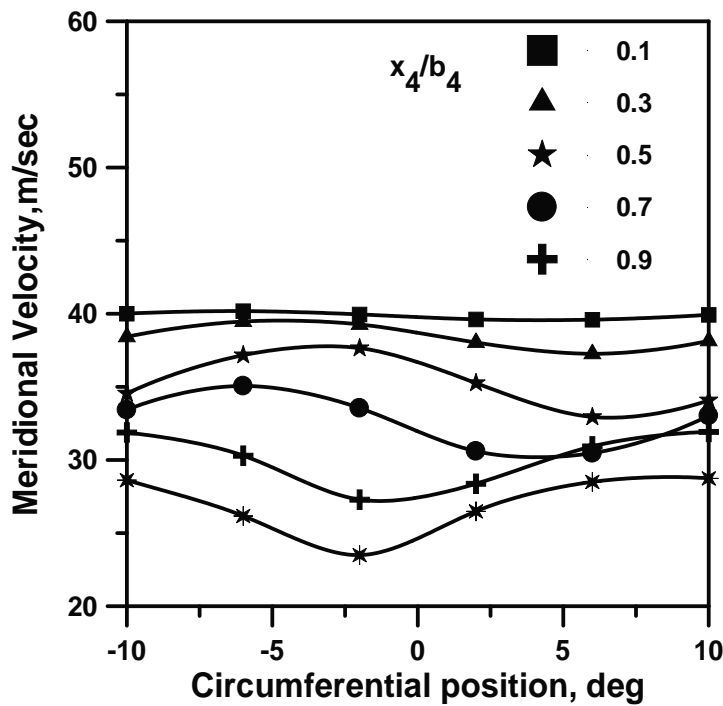


Fig. 7.26(b) Variation of Meridional velocity at the L-turn exit
(Design flow rate)

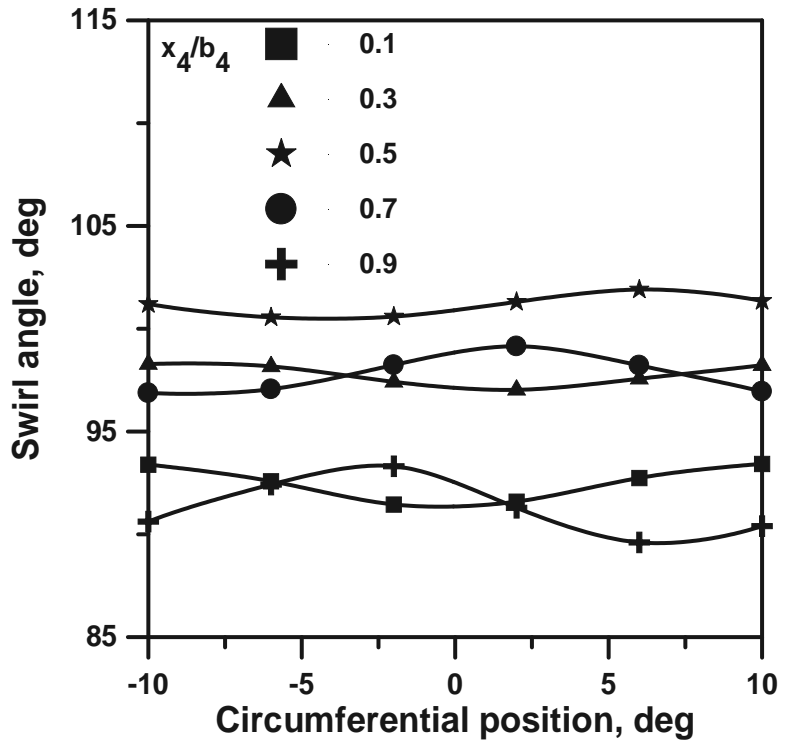


Fig. 7.27(a) Variation of swirl angle at the L-turn exit
(Design flow rate)

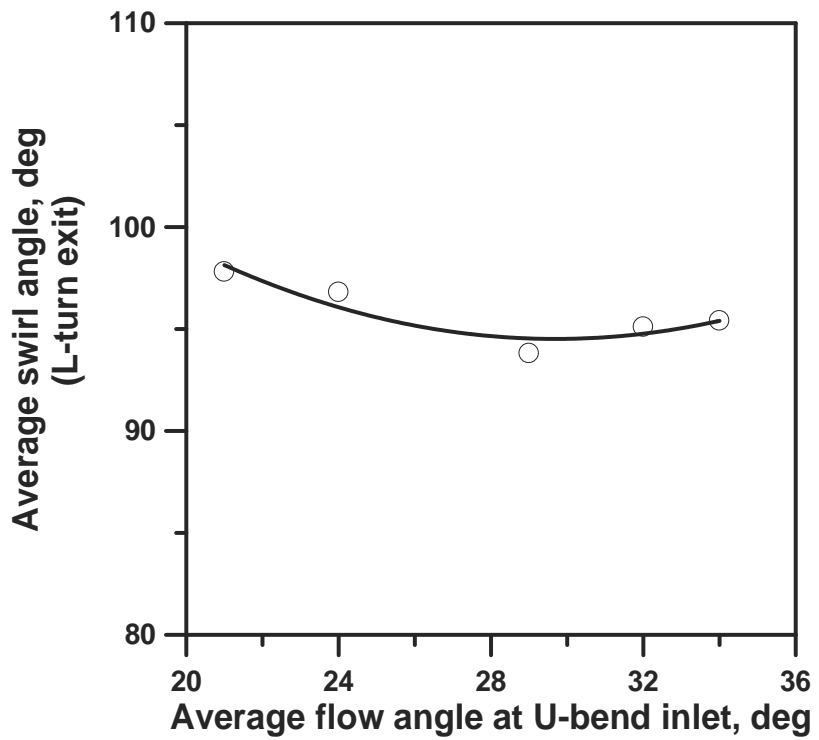


Fig. 7.27(b) Variation of average swirl angle at the L-turn exit

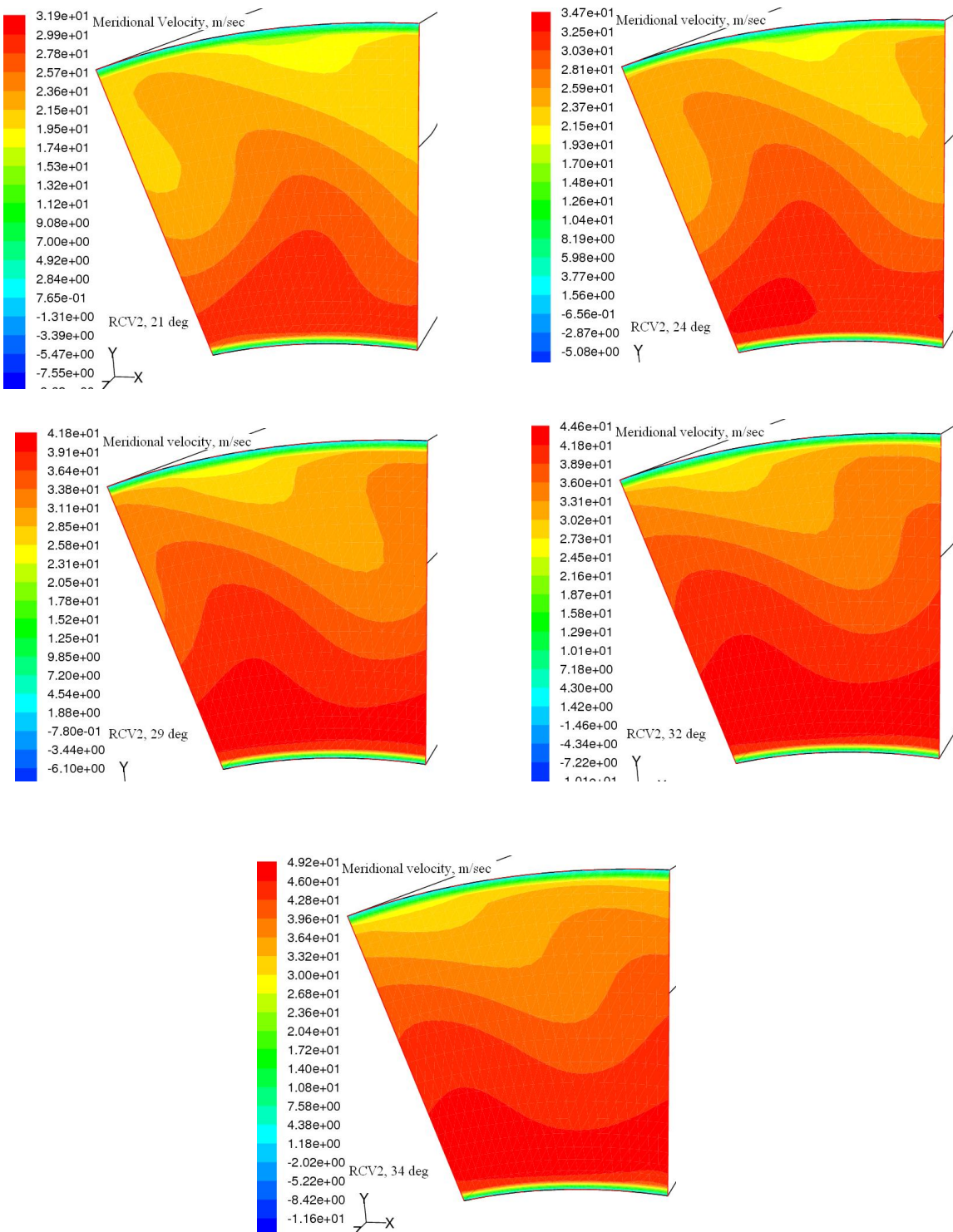


Fig. 7.28 Contour plots of Meridional velocity at the L-turn exit

7.4.4 Performance of the stage and U-bend

The variation of total pressure loss coefficient for the stage with average flow angle at U-bend inlet for the whole stage is shown in Fig.7.29 (a). The total pressure loss coefficient is observed to be minimum when the average flow angle at U-bend inlet is 21° . With the increase in average U-bend inlet flow angle the total pressure loss is observed to increase steeply. The reason for increased total pressure loss with increase in average flow angle at U-bend inlet may be attributed to increased frictional losses and presence of secondary flow. The variation of static pressure recovery coefficient for the stage with average flow angle at U-bend inlet is shown in Fig. 7.29(b). Some recovery in static pressure is observed when the average flow angles at U-bend inlet are 21° , 24° and 29° . However with increase in flow angle beyond 29° the static pressure recovery is seen to be negative. When the flow angle at U-bend inlet is less, the tangential component is more and in the process of removing the swirl the flow is decelerated towards the downstream direction and hence the recovery in static pressure taken place.

The performance of the U-bend expressed in terms of total pressure loss coefficient and static pressure recovery coefficient is shown in Fig. 7.30(a) and 7.30(b) respectively. The total pressure loss in the U-bend is seen to be very less when compared to the total stage pressure loss. This indicates that the return channel passage losses are predominant in the present case with RCV2 configuration.

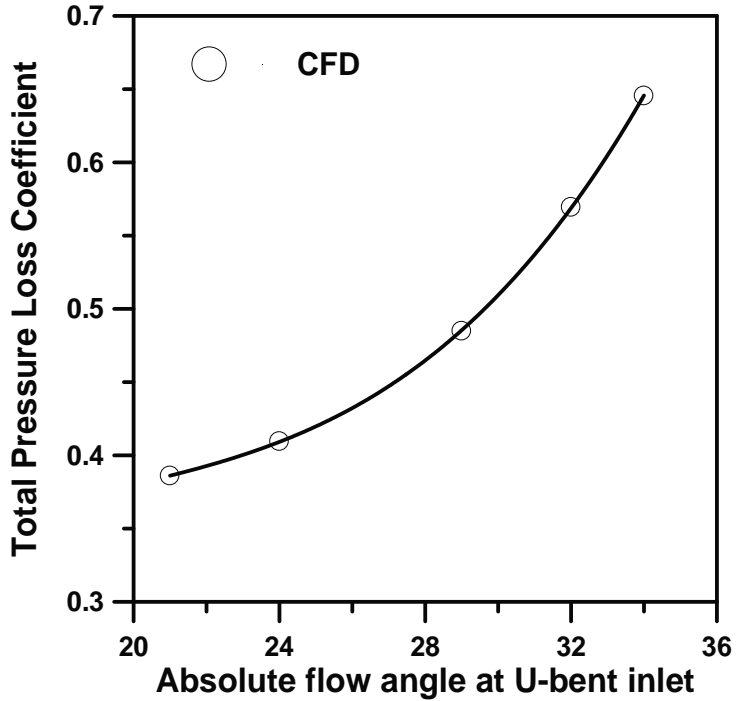


Fig. 7.29(a) Variation of total pressure loss coefficient

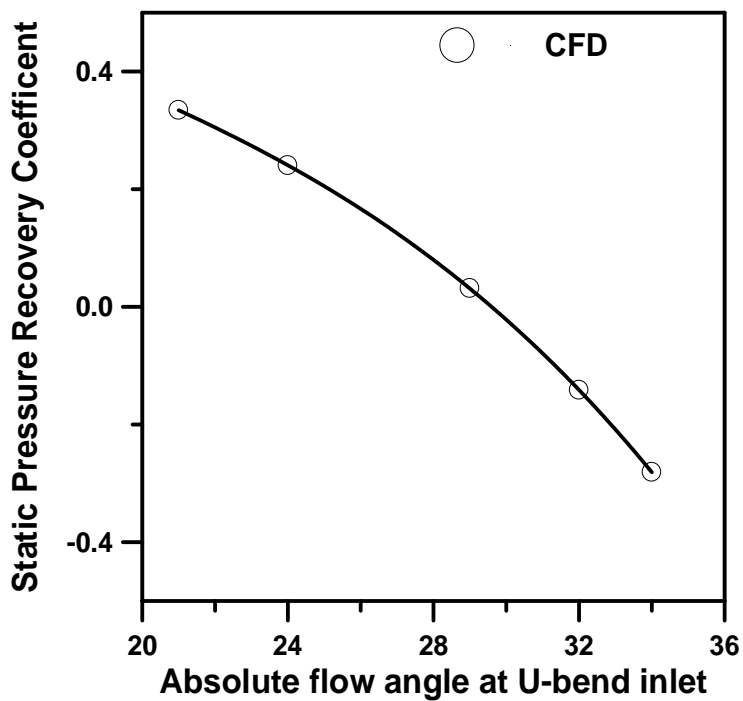


Fig. 7.29(b) Variation of static pressure recovery coefficient

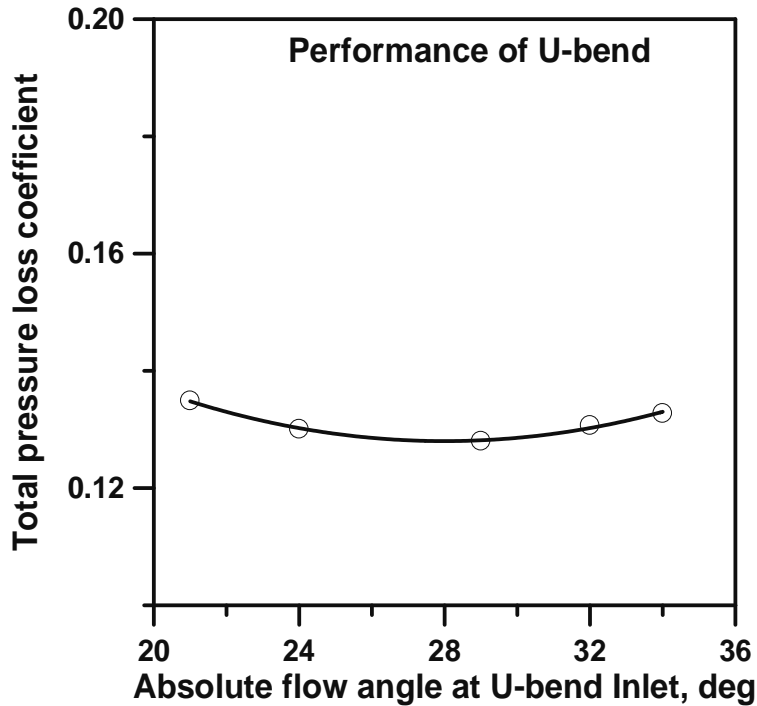


Fig. 7.30(a) Variation of total pressure loss coefficient (U-bend)

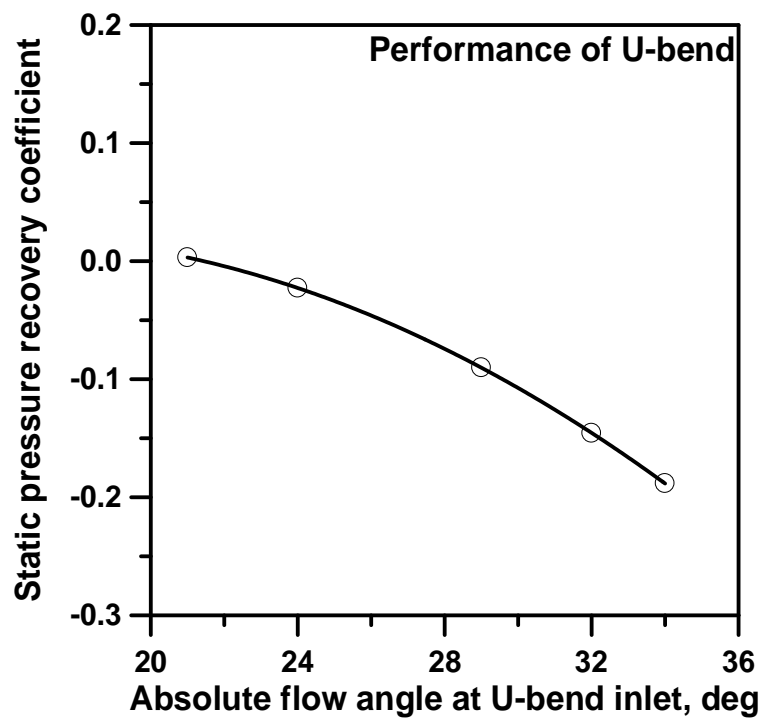


Fig. 7.30(b) Variation of static pressure recovery coefficient (U-bend)

7.4.5 Iso-Mach Contour Plots

The fluid flow simulation in the computational domain was carried out for the five different operating conditions corresponding to 120%, 110%, 100%, 80% and 70% of design flow rate exactly similar to the values used for the experiments. After post processing, the results are presented in the form of iso contours of Mach number in the return channel passage as well on the vane surface. The results corresponding to 100% flow rate, at an average U-bend inlet absolute flow angle of 29° are shown. Figure 7.31 shows the planes and their nomenclature on which iso-Mach contour plots are plotted. Figure 7.32 shows the Iso-Mach number contour plots on different planes along the flow path. Plane 1 corresponds to radius ratio (ratio of radius at which the plane is selected to the radius at which *L.E* is placed) of 0.99, which is very near to the leading edge. The iso-contours of Mach number at this plane indicate acceleration of flow towards the suction surface of the vane. Deceleration is seen to occur at Plane 2 which corresponds to a radius ratio of 0.9, as the flow progresses within the vane passage from Plane 1. Considerable pressure gradient has been observed at Plane 3 (radius ratio of 0.7) from suction side(SS) to pressure side(PS). Region of low flow is seen to occur at plane 3 near the suction surface represented by iso-Mach contours of low magnitude. The iso-contour plot at the trailing edge upstream region of the vane is shown in Plane 4, which is at a radius ratio of 0.52. It is observed that near the SS the low flow regions are widened as

represented by iso-Mach contours of low magnitude. The flow at the downstream region of the vane is represented in Plane 5 (inlet of 90° bend). The region of flow separation is clearly seen on the suction side of plane 5. The region of flow separation is indicated by the low magnitude of Mach number. The flow is seen to be concentrated towards the shroud at this plane. The spread of the low velocity region at inlet to 90° bend is seen on this plane. Figure 7.33(a) shows the iso-Mach contours on a plane through the mid span of the flow channel width in which the low Mach number contours are clearly seen on the downstream of suction side of the vane. It may be noted that the low velocity region which is spreading from the trailing edge of the vane into the 90° bend might be inducing some cross flow from pressure side to suction side. Figure 7.33(b) shows the calculated secondary flows on plane 5 of RCV2.

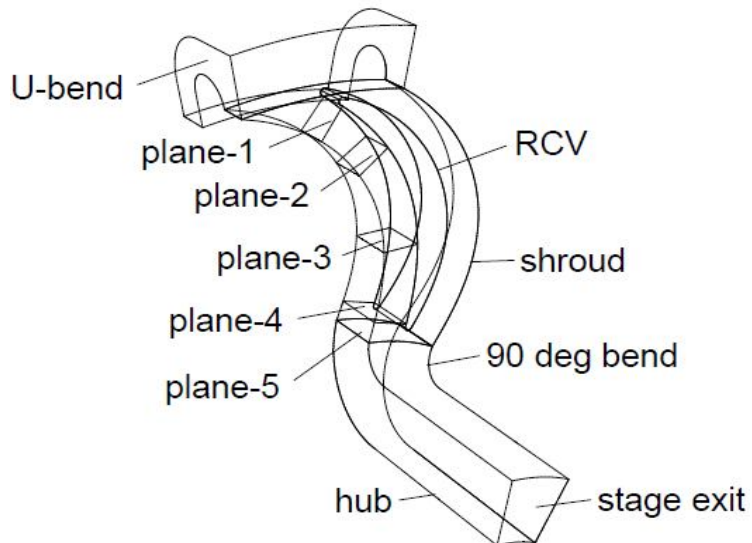


Fig. 7.31 Plane nomenclature used for iso-Mach contour plots

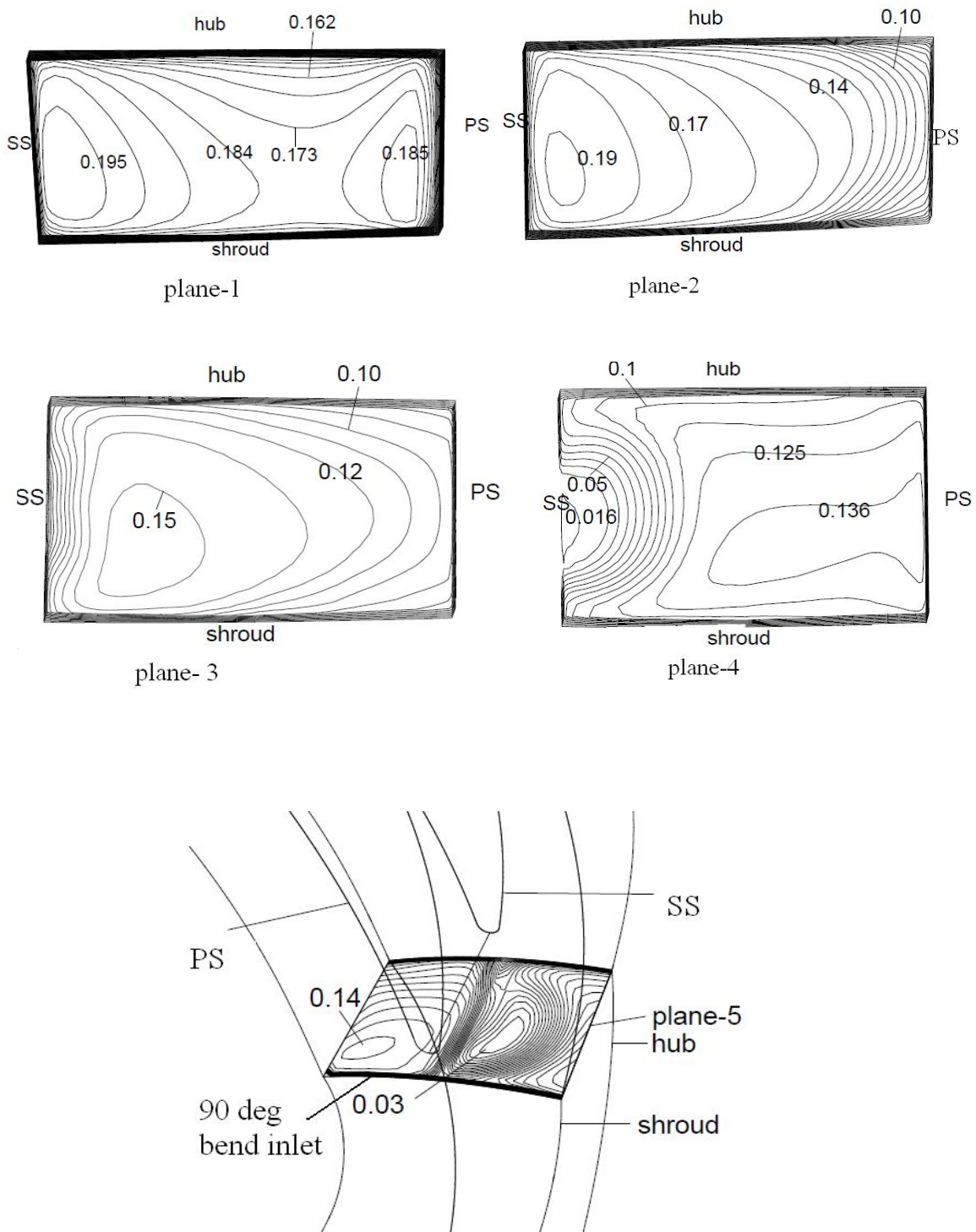


Fig. 7.32 Iso-Mach contour plots on different planes

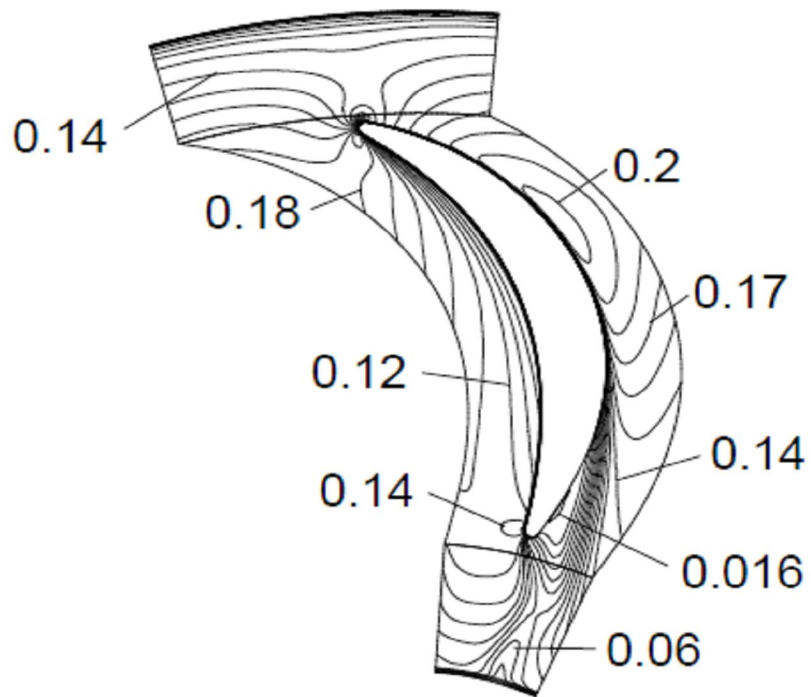


Fig. 7.33(a) Iso-Mach contour plot on a plane passing through mid-span of RCV2

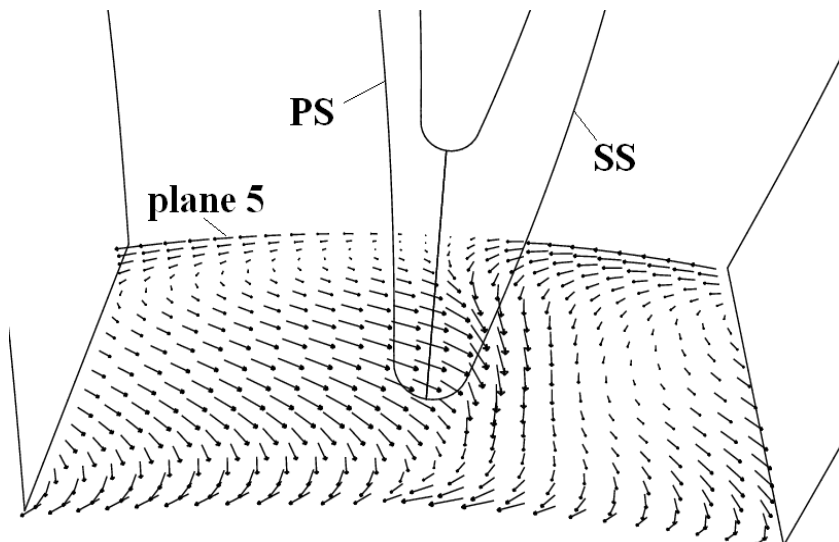


Fig. 7.33(b) Secondary flow pattern on plane- 5

7.5 COMPARISON OF EXPERIMENTAL AND NUMERICAL RESULTS IN RCV2 CONFIGURATION

The experimental and results with RCV2 configuration are compared and discussed in the following sections. The results obtained at the design point ($\alpha_1 = 29^\circ$) and two other off-design points ($(\alpha_1 = 21^\circ \text{ and } \alpha_1 = 34^\circ)$) are presented with comparison. The meridional velocity distributions at the U-bend exit and L-turn exit, vane surface pressure distributions on RCV2, swirl angle distributions at the L-turn exit and performance of the stage are discussed in detail.

7.5.1 Comparison of Meridional velocity and Flow angle at U-bend exit

The comparison of meridional velocity and flow angle distributions at the exit of U-bend for the design point ($\alpha_1 = 29^\circ$), and off-design operating conditions (70% flow and 120% flow) is shown in Fig.7.34. At the design flow rate, the measured and calculated meridional velocity is observed to be in close agreement. The meridional velocity is seen to be increasing from 20 m/sec near the hub to 26 m/sec near the shroud. The flow is observed to be more concentrated towards the shroud as it takes U-turn in the crossover bend. The meridional velocity distributions at $\alpha_1 = 21^\circ$ and 34° are also seen to be in qualitative agreement. The flow angles are observed to increase in magnitude with increase in distance from hub. The numerical results are observed to be in near agreement with the experimentally obtained values.

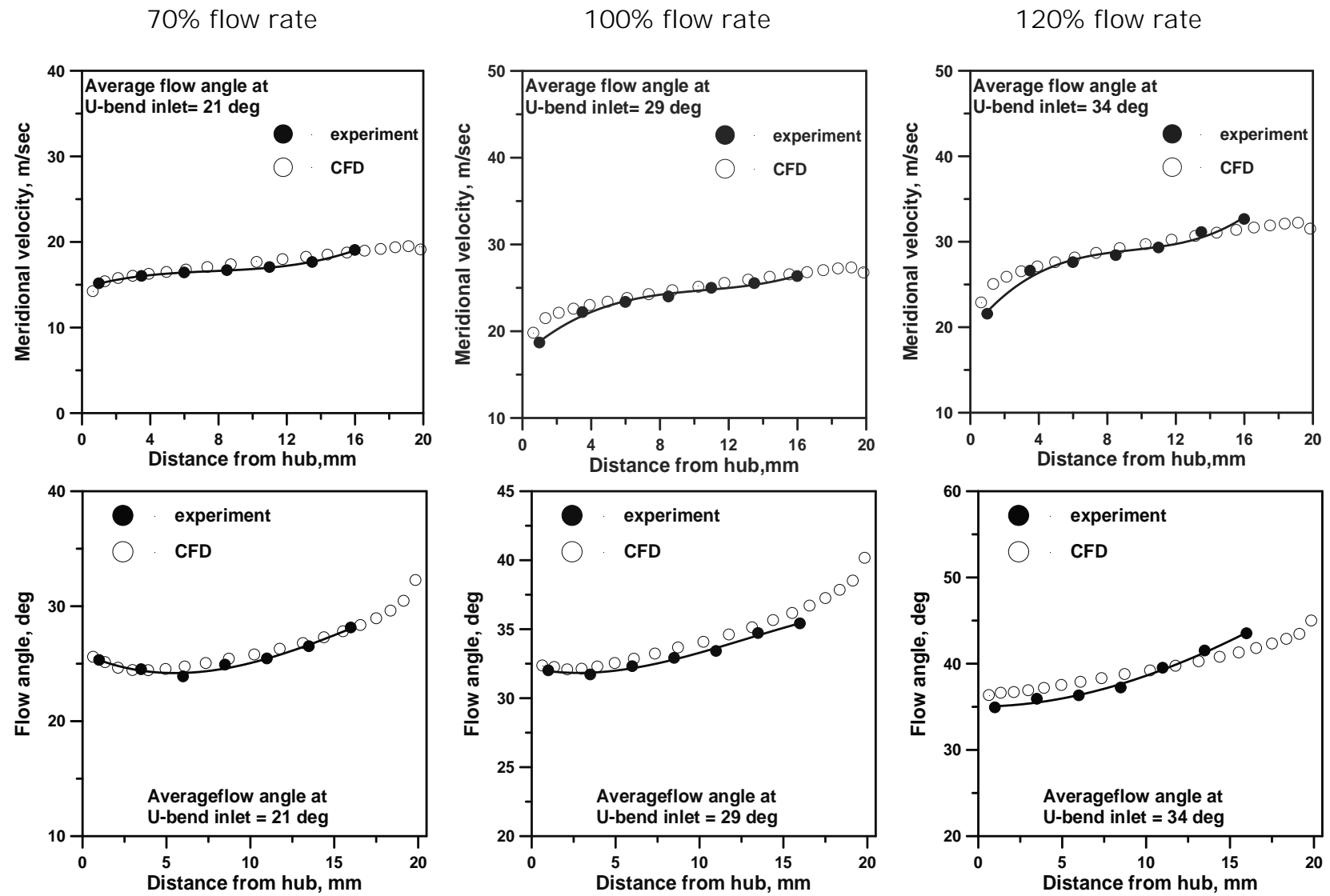


Fig. 7.34 Comparison of meridional velocity flow and angle at U-bend exit ($\alpha_1 = 29^\circ$)

7.5.2 Comparison of Vane Surface Pressure Distribution

The static pressure coefficient on the mid span of RCV2 vane surface plotted against the %chord length from the leading edge of the vane for the design off-design flow angles at U-bend inlet are shown in Fig.7.35. The present numerical solution is seen to predict the vane surface pressure distribution in qualitative agreement with the experimental measurements. The critical region is the suction side trailing edge where flow separation is likely to occur.

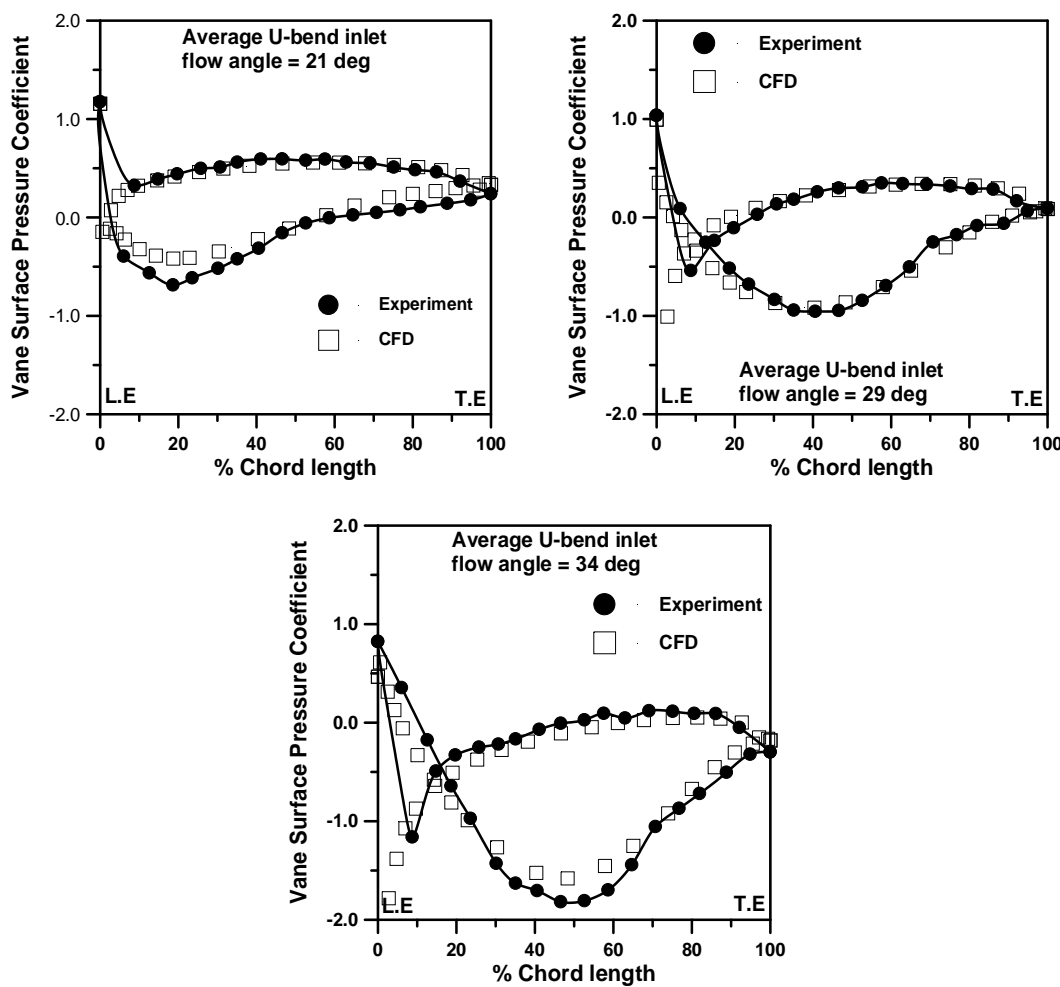


Fig.7.35 Comparison of Vane Surface Pressure Distribution

7.5.3 Comparison of Meridional Velocity at L-turn Exit

The circumferentially averaged meridional velocity distribution at the L-turn exit obtained through numerical solution is compared with experimental results as shown in Fig.7.36(a) to (c). The meridional velocity is observed to be more towards the hub and is decreasing towards the shroud. The 90° turn (L-turn) is causing the flow to migrate towards the hub. The present numerical study predicted the meridional velocity distribution at the L-turn exit in near agreement with the experimental results. For the reasons of brevity the comparison is shown for U-bend inlet flow angles of $\alpha_1 = 21^{\circ}$, 29° and 34° .

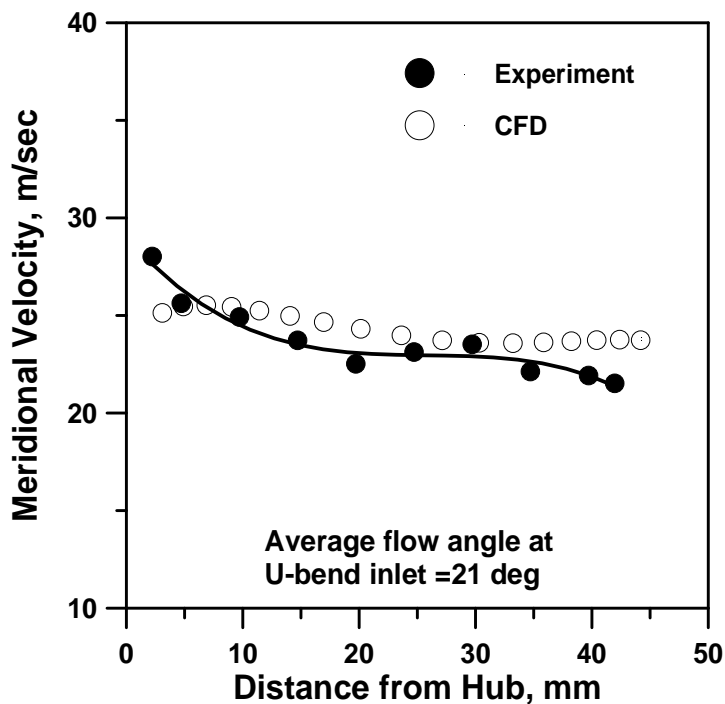


Fig.7.36 (a) Circumferentially averaged meridional velocity at the L-turn exit ($\alpha_1 = 21^{\circ}$)

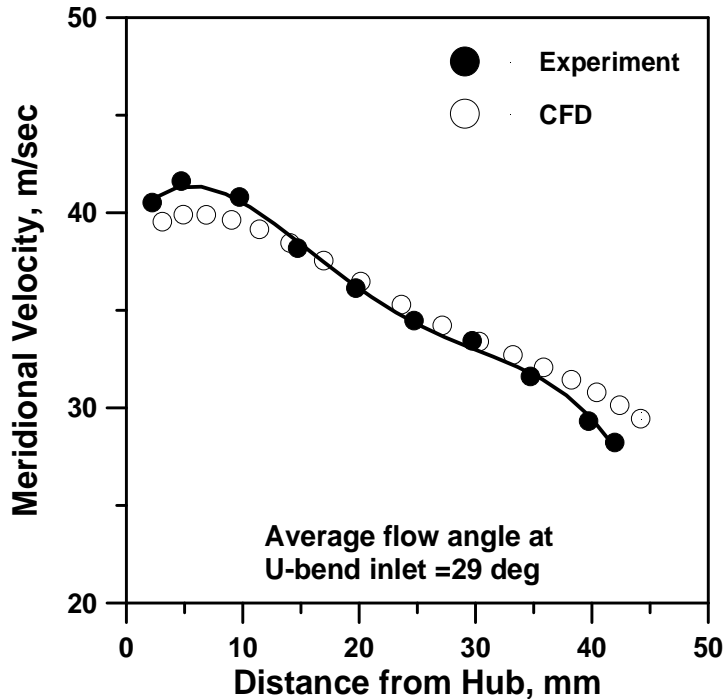


Fig.7.36 (b) Circumferentially averaged meridional velocity at the L-turn exit ($\alpha_1 = 29^\circ$)

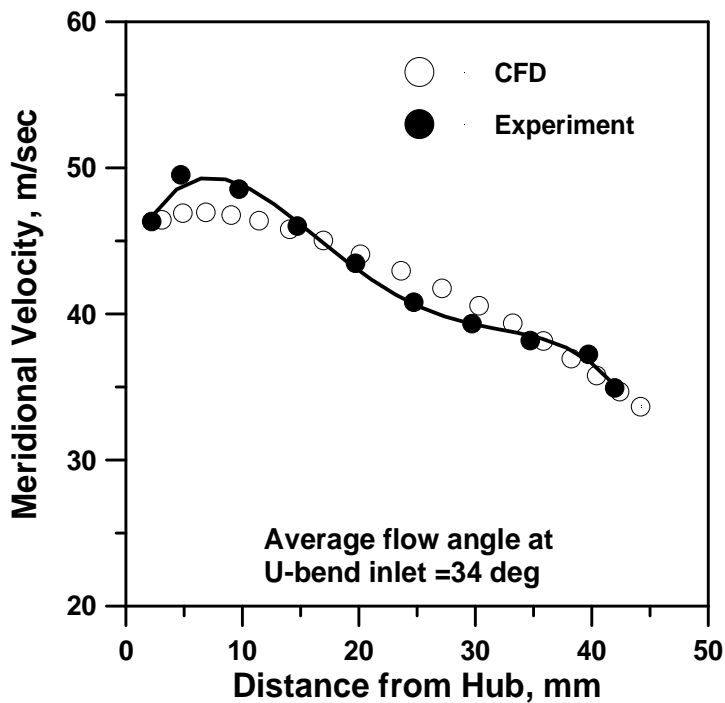


Fig.7.36 (c) Circumferentially averaged meridional velocity at the L-turn exit ($\alpha_1 = 34^\circ$)

7.5.4 Comparison of Average Swirl Angle at the L-turn exit

The average swirl angle distribution obtained from experimental and numerical results at the L-turn exit with RCV2 configuration is compared as shown in Fig. 7.37. It is seen from the figures that the averaged swirl calculated from the numerical results is in qualitative agreement with the experimentally measured values. There is somewhat closer agreement at 110% and 120% of design flow conditions, while the present numerical model could not predict the exit swirl angles close to the measured values at the 70%, 80% and 100% of design flow operating conditions.

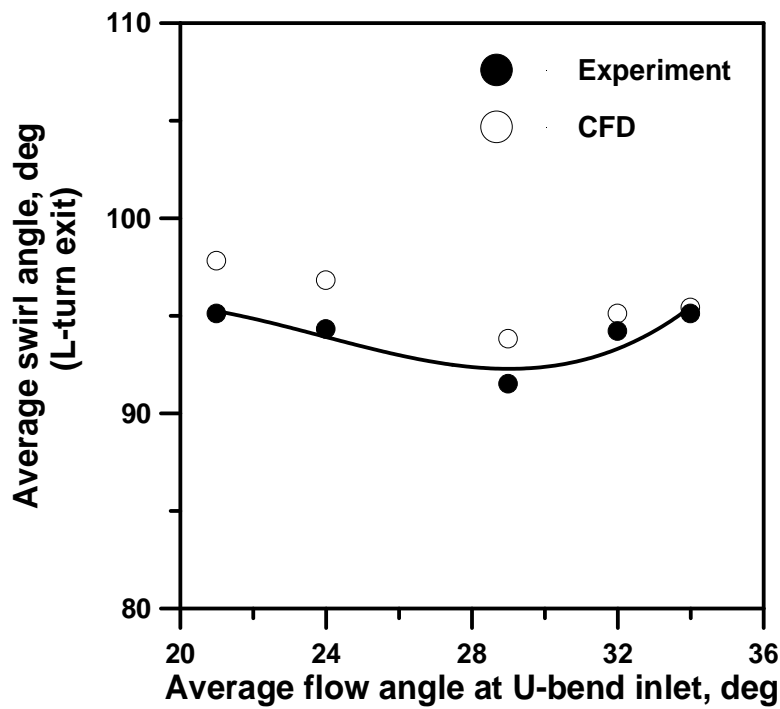


Fig. 7.37 Average swirl angle at the L-turn exit

7.5.5 Comparison of Stage and U-bend Performance

The performance of the stage in terms of total pressure loss coefficient, static pressure recovery coefficient with comparison of experimental and numerical values is shown in Fig. 7.38(a) and (b) respectively. The present numerical study predicted the total pressure loss coefficient in close agreement with the experimental values.

The performance of U-bend is in terms of total pressure loss coefficient and static pressure recovery coefficient is shown in Fig.7.39(a) and (b) respectively. A good agreement between the experimental and numerical values is seen from the figures shown above. The total pressure loss in the U-bend is relatively lower when compared to the return channel passage total pressure losses.

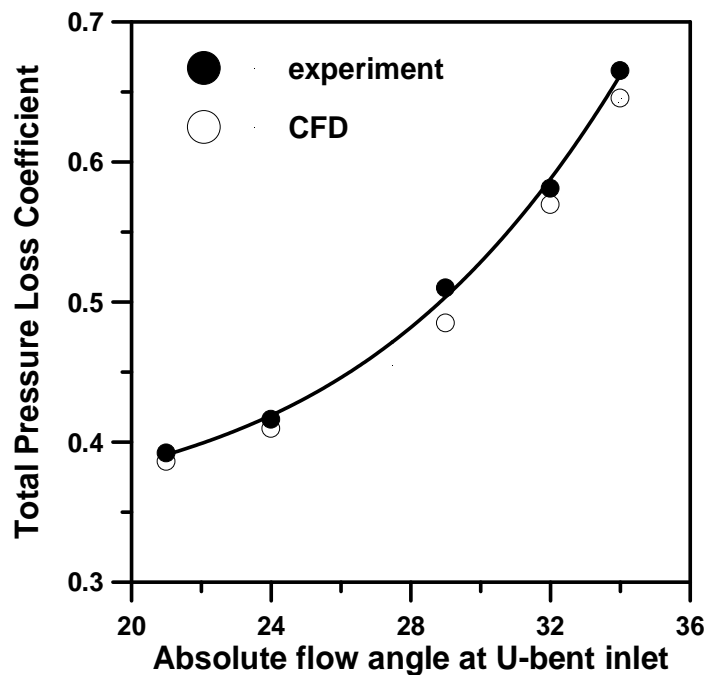


Fig. 7.38(a) Variation of total pressure loss coefficient (stage)

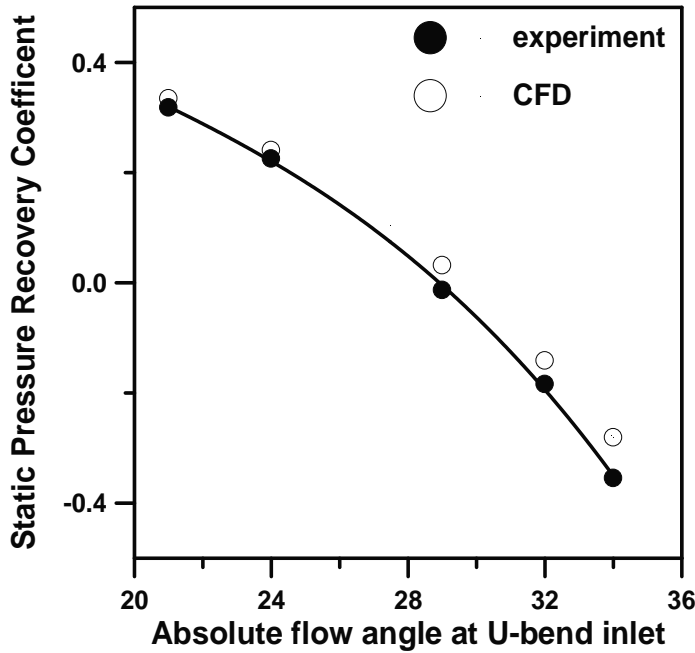


Fig. 7.38(b) Variation of total static pressure recovery coefficient (stage)

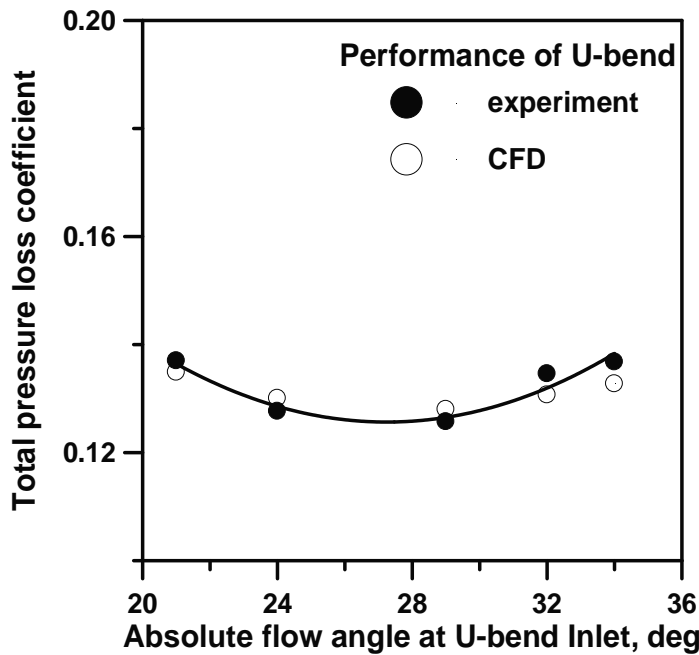


Fig. 7.39(a) Variation of static pressure recovery coefficient (U-bend)

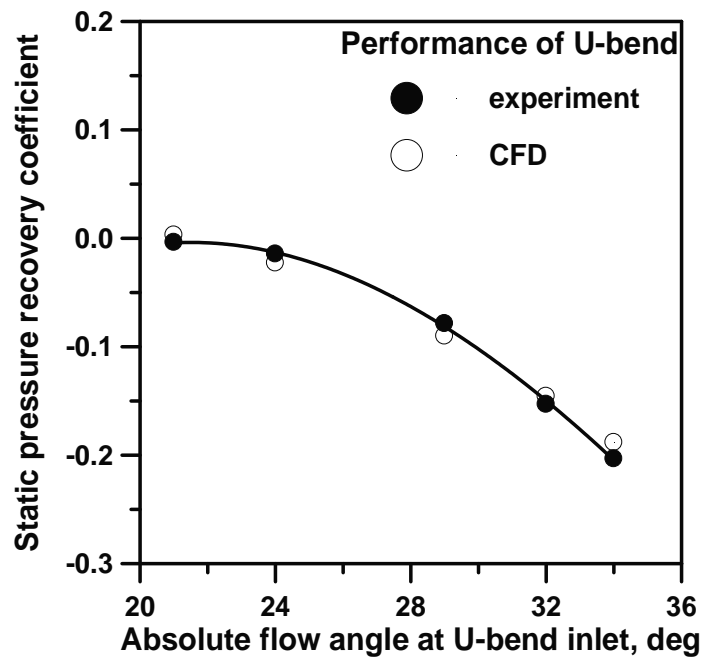


Fig. 7.39(b) Variation of static pressure recovery coefficient
(U-bend)

7.6 NUMERICAL RESULTS IN RCV3 CONFIGURATION

Based on the experiences from the experimental and numerical results of RCV1 and RCV2, a new return channel vane profile RCV3 is designed and its performance is studied numerically. The RCV3 vane profile geometrical details and the variation flow angle along the mean stream line curvature for RCV1, RCV2 and RCV3 are shown in Fig. 7.40(a) and 7.40(b) respectively. The flow angle variation along the mean streamline path is maintained with lesser slope up to 2/3 of the total length and thereafter with higher slope. The variation of meridional velocity, contour plots at U-bend exit, total velocity and static pressure contour plots in the mid-span plane of the return channel vanes and exit swirl angle contour plots are presented in the following sections. The inlet and exit vane angles for RCV3, chord length are tabulated and shown in Table 7.3. The overlapped return channel vane profiles RCV1, RCV2 and RCV3 are shown in Fig. 7.41(a) and (b).

Table 7.3 Vane design parameters for RCV3

S.No	Vane Parameter	Magnitude
1	Inlet vane angle, deg	25°
2	Exit vane angle, deg	82°
3	Chord length, mm	178

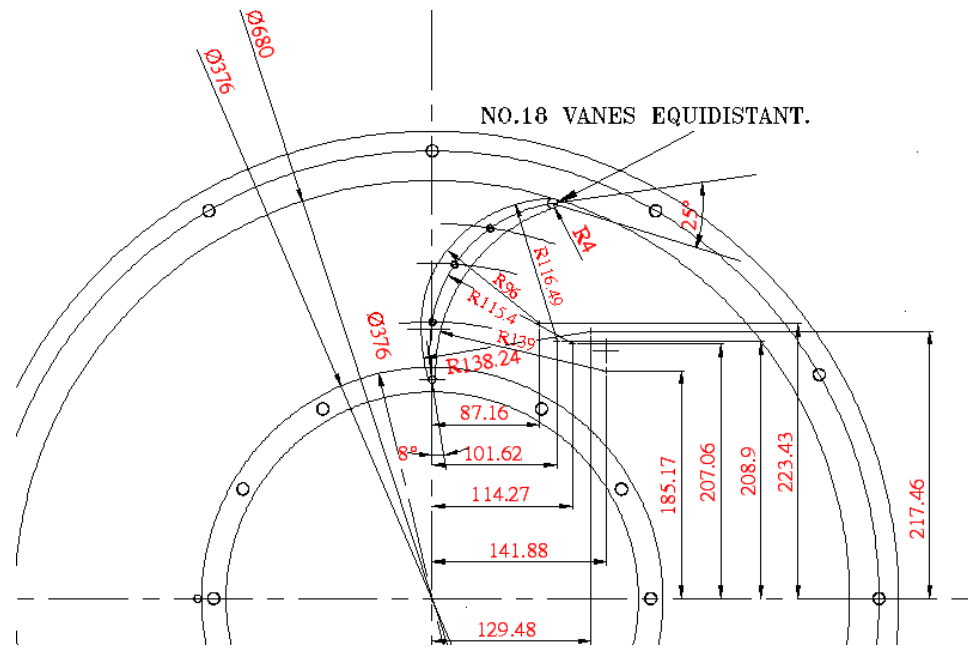


Fig. 7.40(a) Geometrical details of RCV3 configuration

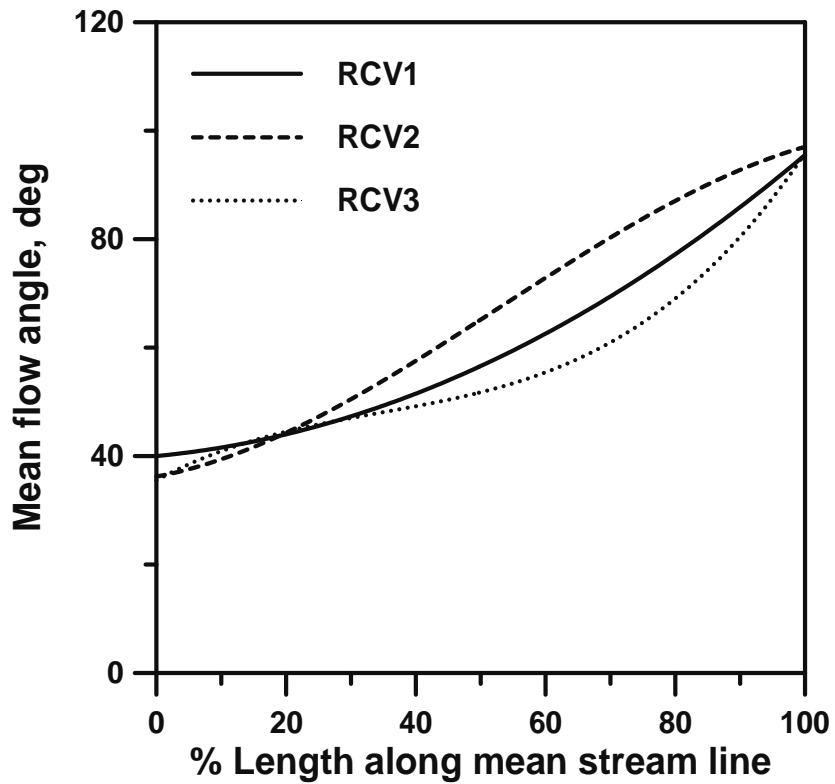


Fig. 7.40(b) Variation of flow angle along the mean stream line (RCV3)

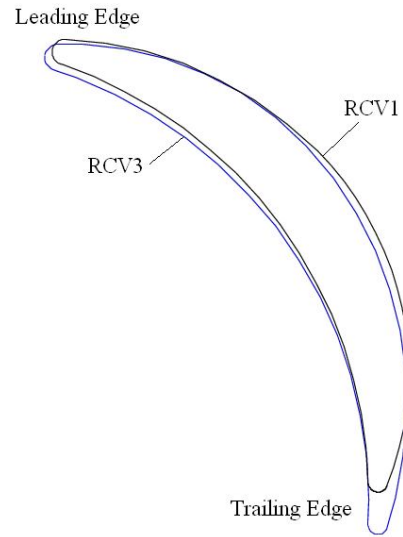


Fig. 7.41(a) Comparison of return channel vane profiles RCV1 and RCV3

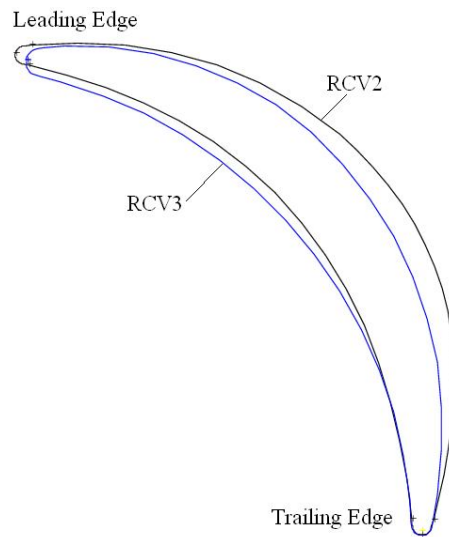


Fig. 7.41(b) Comparison of return channel vane profiles RCV2 and RCV3

7.6.1 Variation of Meridional Velocity and Flow Angle at U-bend Exit

The distribution of circumferentially averaged meridional velocity and flow angle at the exit of U-bend with RCV3 configuration is shown in Fig. 7.42(a) and 7.42(b) respectively. The meridional velocity distribution is observed to be almost uniform from hub to shroud at all operating conditions. The average meridional velocities observed at the U-bend exit are increasing with increase in average flow angle at U-bend inlet due to increasing mass flow rate. The meridional velocity filled contours at the exit of U-bend for design point are shown in Fig. 7.43. The flow angle at the exit of U-bend is also seen to be uniform from hub to shroud at all operating conditions. The average flow angles observed at the U-bend exit at each operating condition are higher than those at the U-bend inlet, due to increased meridional velocity resulting from the decreased flow path width.

7.6.2 Vane Surface Pressure Distribution

Figure 7.44 shows the vane surface static pressure distribution expressed as static pressure coefficient on the mid span of RCV3 configuration at all operating conditions. Table 7.4 shows the vane incidence angle information at all the operating conditions. At 70% of design flow rate i.e. when the U-bend inlet flow angle is 21° the vane is seen to be more loaded on the pressure side and non-uniformly loaded on the suction side. When the incidence angle on the vane L.E is 24° , i.e. at 80% of design flow rate condition the vane appears to be uniformly

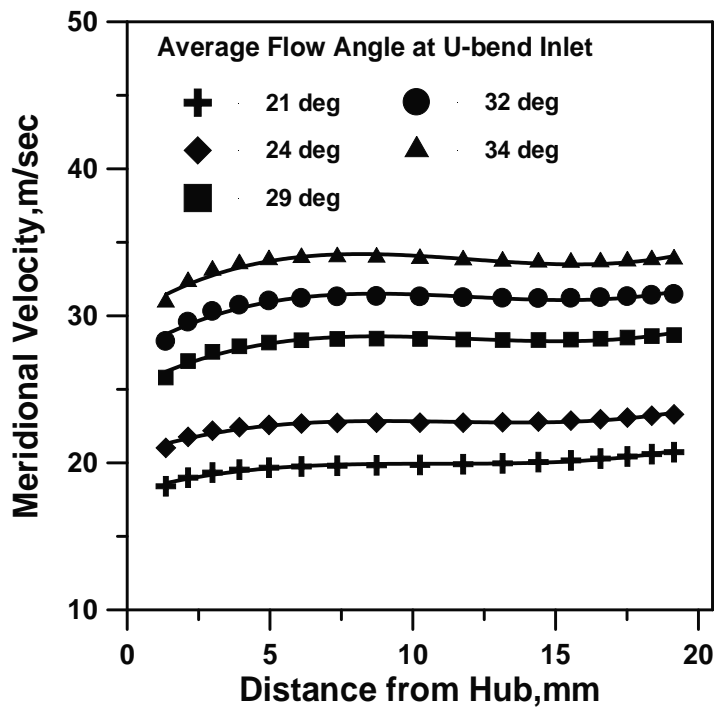


Fig. 7.42 (a) Meridional Velocity Distribution at U-bend exit

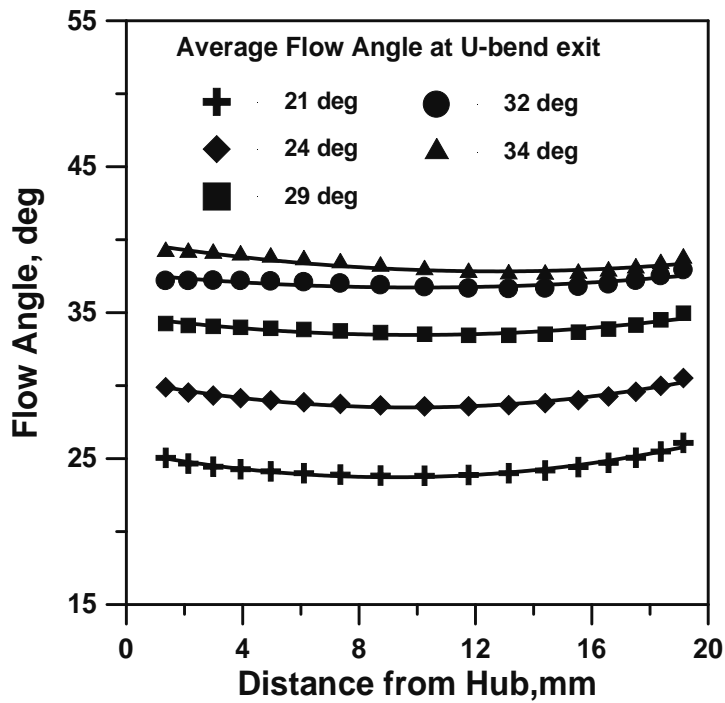


Fig. 7.42(b) Flow Angle Distribution at U-bend exit

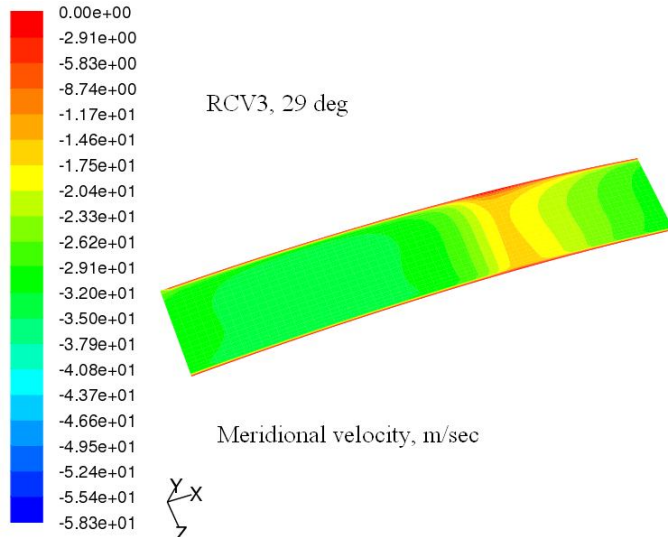


Fig. 7.43 Contour plot of meridional velocity at U-bend exit

Table 7.4 Incidence angle information on the L.E of RCV3

S.No	Average flow angle at U-bend inlet, deg	Average flow angle at U-bend exit, deg	Incidence on the L.E of RCV1,deg
1	21	24.46	+0.54
2	24	29.18	-4.1
3	29	33.93	-8.98
4	32	37.05	-12.05
5	34	38.35	-13.35

loaded. The same pattern of uniform loading is observed at the design flow rate condition. However at 110% and 120% of design flow conditions the vane is more loaded on suction side than pressure side. This is evident from the higher negative flow incidence angle on the L.E of RCV3.

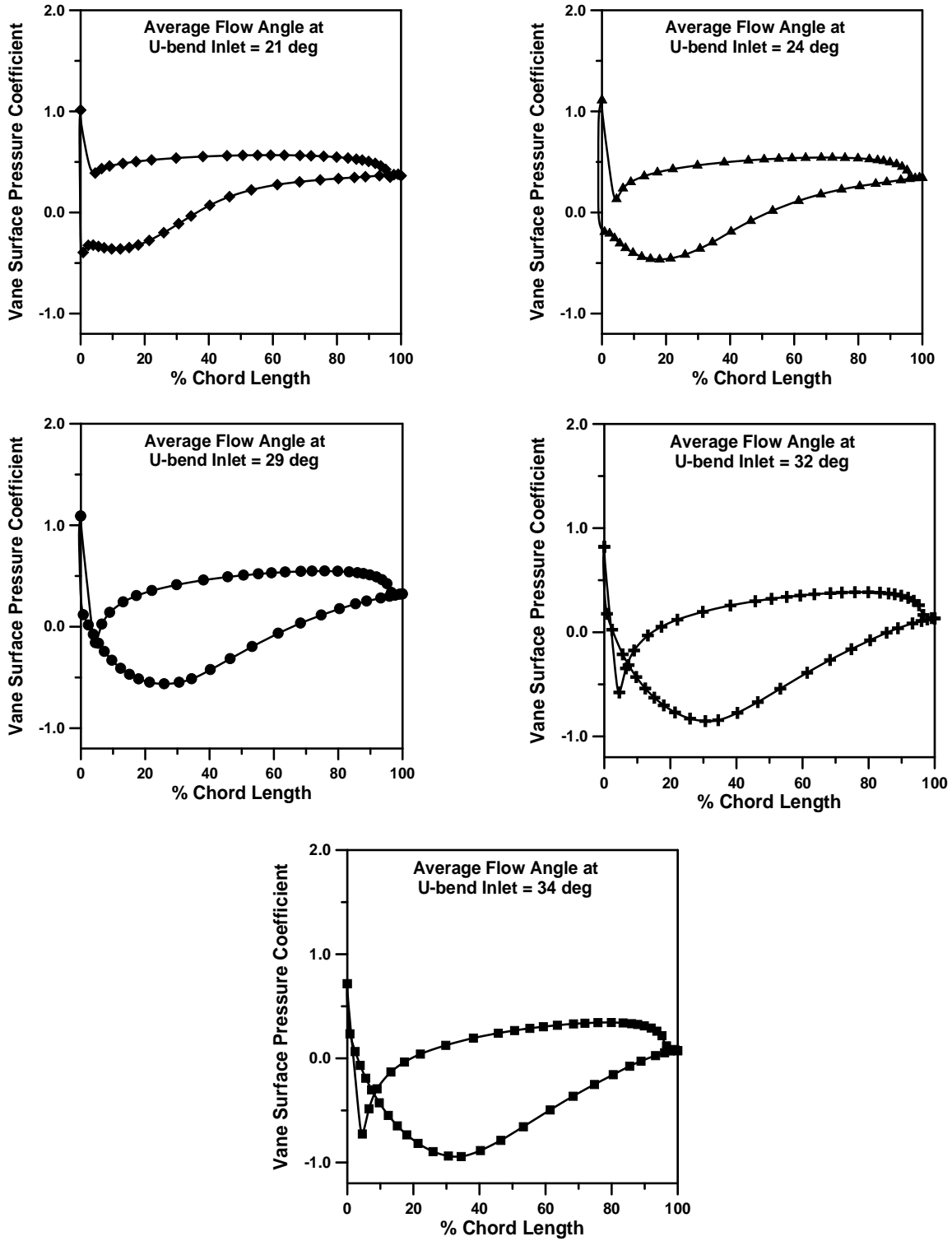


Fig. 7.44 Vane surface pressure distribution for RCV3 configuration

7.6.3 Variation of meridional velocity and flow angle at the L-turn exit

The circumferentially averaged meridional velocity at the L-turn exit with RCV3 configuration from hub to shroud is shown in Fig. 7.45(a). The design point meridional velocity variation in the circumferential direction is shown in Fig. 7.45(b). The circumferentially averaged meridional velocity is seen to be more concentrated towards the hub due to the L-turn 90° bend effect. It is showing a peak value near the hub and thereafter decreasing towards the shroud. The meridional velocity distribution at the design point in the circumferential direction is showing lower magnitudes towards the shroud while highest magnitude is seen near the hub. Also the trailing edge of RCV3 is seen to influence the meridional velocity towards the shroud to vary in a wavy fashion. However as the magnitude of meridional velocity is increasing towards the hub, the wavy nature of variation is observed to subside.

The swirl angle distribution at the design point in the circumferential direction as a function of distance ratio from the hub is shown in Fig. 7.46(a). It is observed to vary in a wavy fashion near the shroud. The magnitude of swirl angle measured with respect to tangential direction is seen to be highest in the mid region of the flow path. The average swirl angle variation with average flow angle at U-bend inlet is shown in Fig. 7.46(b). The average swirl angle is observed to vary from 98° at 70% of design flow operating condition to 97° at the 120% flow condition.

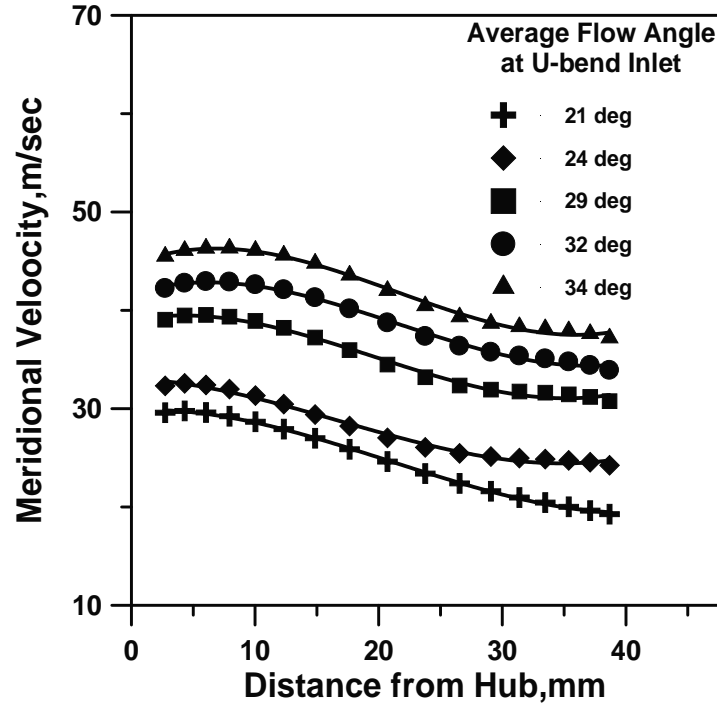


Fig. 7.45(a) Meridional Velocity Distribution at L-turn exit
(Circumferential average)

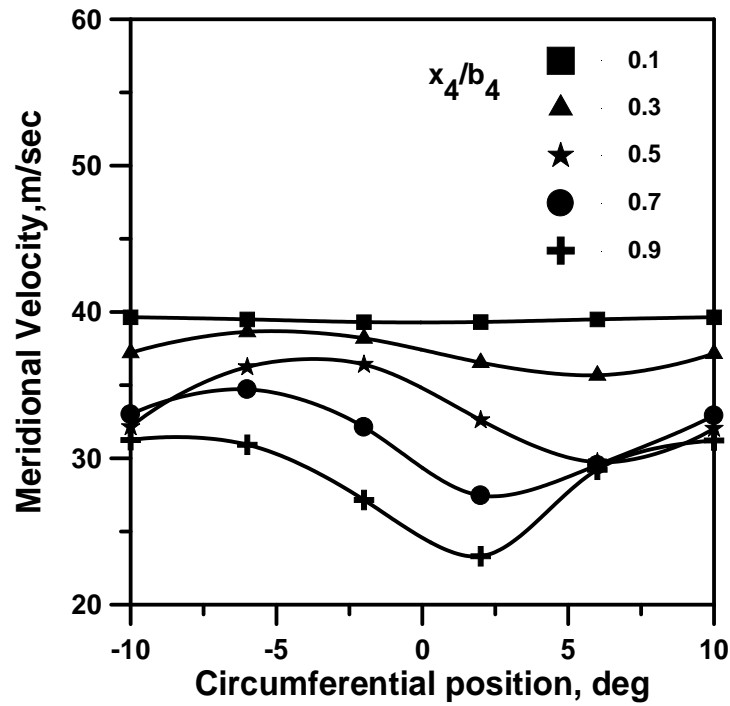


Fig. 7.45(b) Meridional Velocity Distribution at L-turn exit
(Design flow rate)

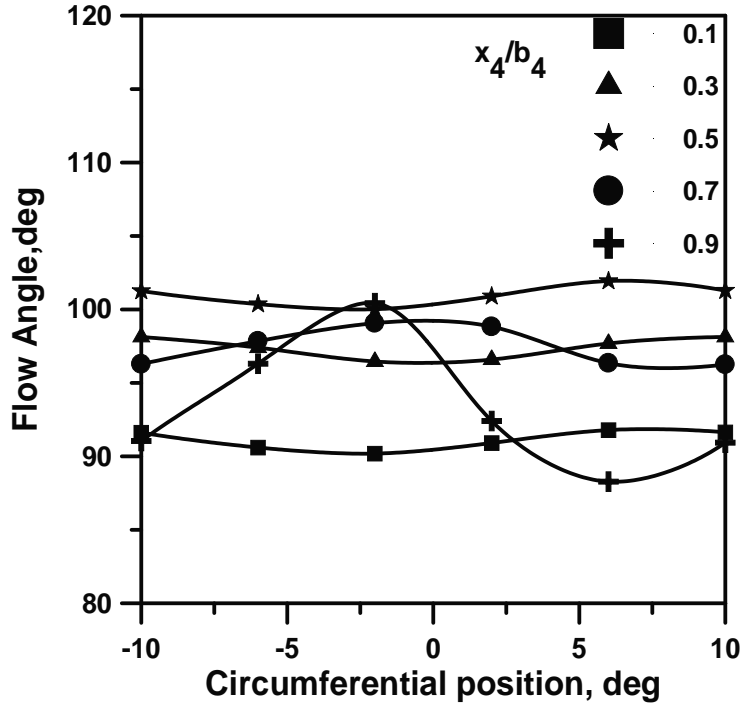


Fig. 7.46(a) Swirl angle distribution at L-turn exit
(Design flow rate)

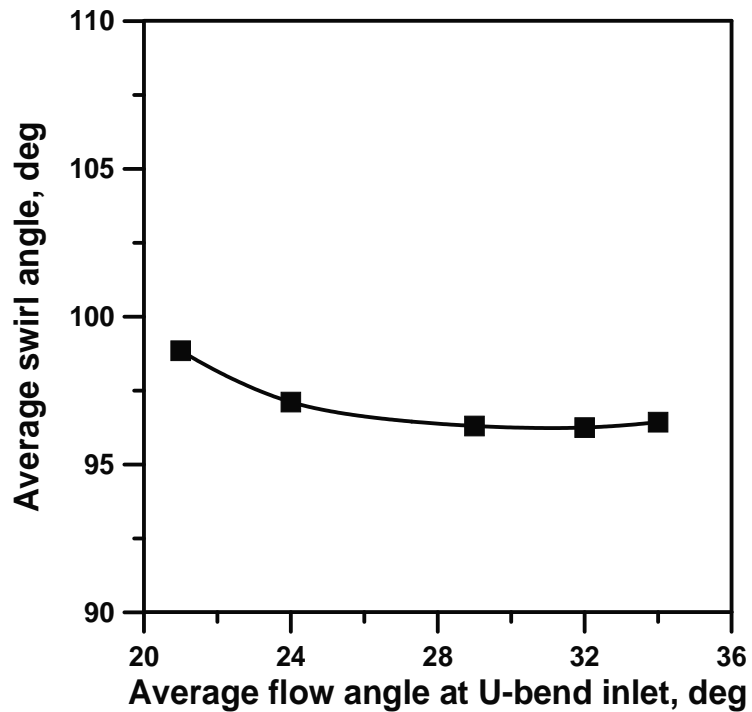


Fig. 7.46(b) Average Swirl angle distribution at L-turn exit

The filled contour plots of meridional velocity and swirl angle distributions at the L-turn exit for RCV3 configuration at all the operating conditions is shown in Fig. 7.47 and 7.48 respectively. It is seen from Fig. 7.47, that the meridional velocity is becoming uniform with highest magnitude towards the hub while it is showing wavy nature towards the shroud at all of the operating conditions studied. The swirl angles are seen be higher in the mid region of flow path and decreasing towards the hub and shroud at all the operating conditions as seen from Fig. 7.48.

7.6.4 Stage Performance with RCV3 Configuration

The performance of the stage in terms of total pressure loss coefficient, static pressure recovery coefficient with RCV3 return channel configuration is shown in Fig. 7.49(a) and (b) respectively. The total pressure loss coefficient is observed to be minimum at 80% of design flow rate condition. It is seen to increase on either side of this operating condition. It is observed to increase more with increase in U-bend inlet flow angle. The total pressure loss coefficient is also increasing with decrease in flow angle at U-bend inlet but with less rate of increase. The reason for the minimum total pressure loss at 80% flow condition may be attributed to the near zero incidence angle of flow on the L.E of the return channel vane RCV3. Also the mass flow rate is increasing with increase in the average U-bend inlet flow angle due to which skin frictional losses are also increasing.

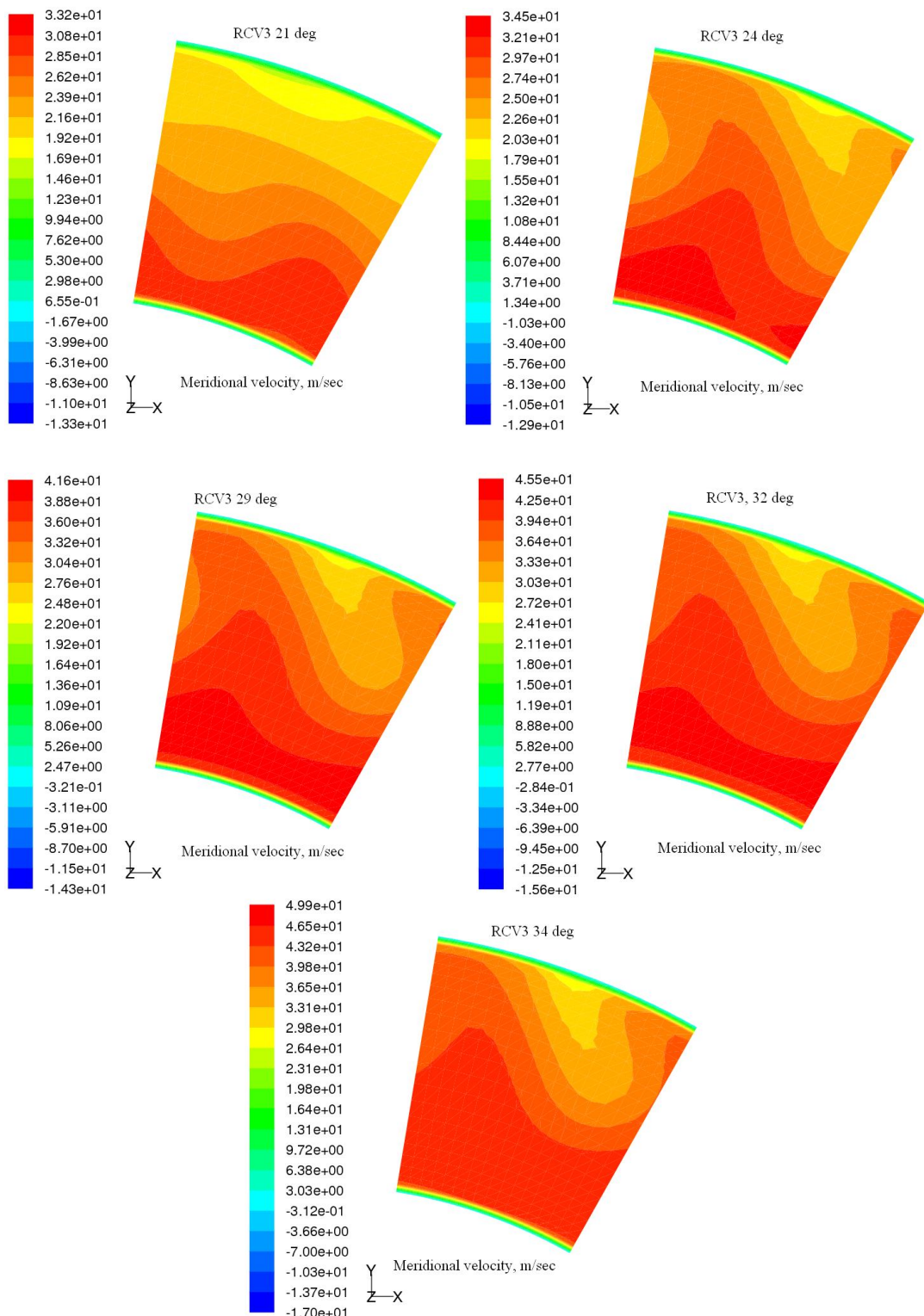


Fig. 7.47 Contours of meridional velocity at L-turn exit

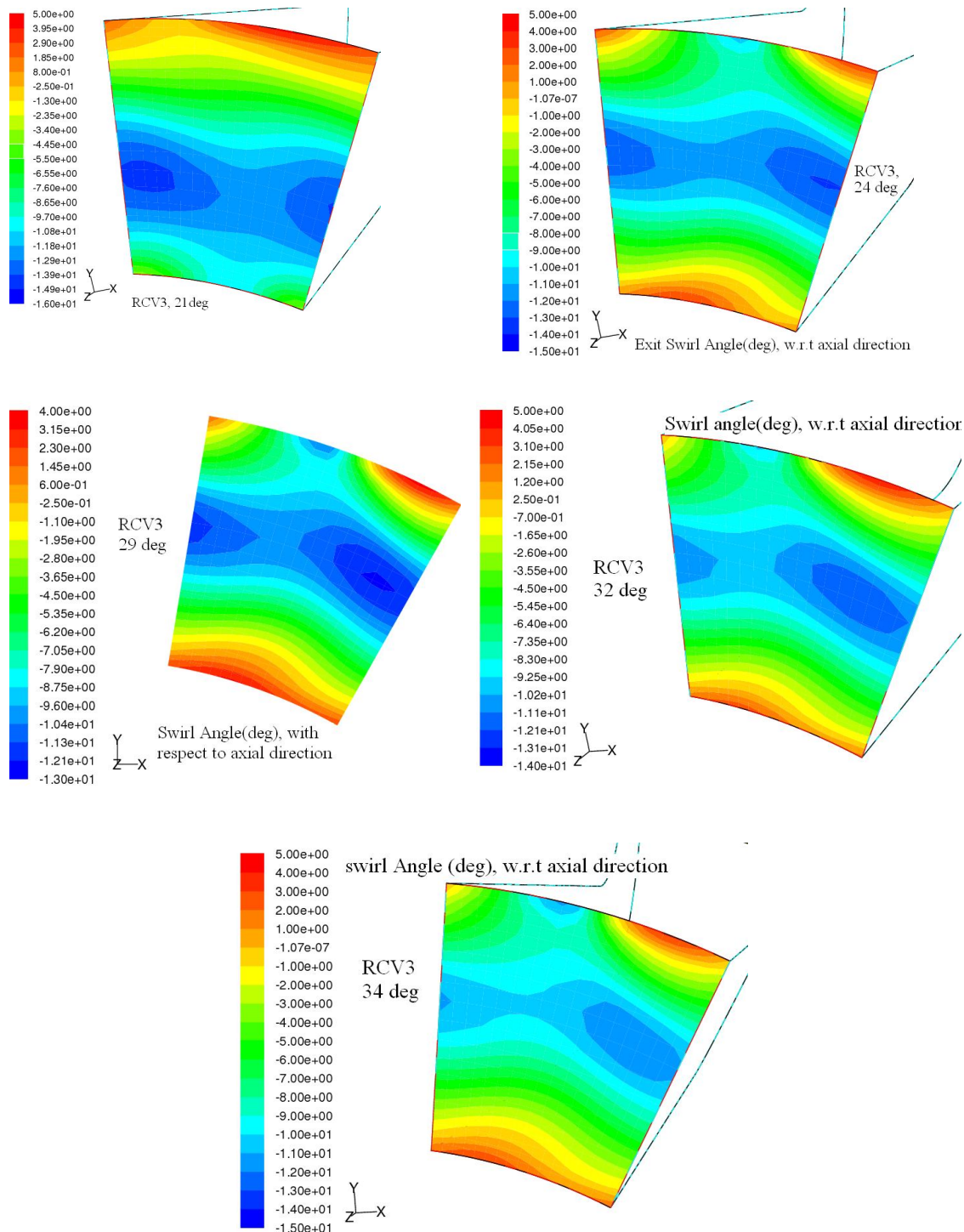


Fig. 7.48 Contours of swirl angle at L-turn exit

The static pressure recovery is observed to be quite favourable with the lower average flow angles at U-bend inlet. Since the tangential component is high at lower flow angles during the deceleration of flow while removing the swirl, static pressure recovery takes place which can be seen from Fig. 7.49(b). Only at the 120% of design flow rate condition the static pressure recovery coefficient is observed to be negative. At 110% of design flow rate it is nearly equal to zero.

7.6.5 Performance of U-bend

The performance of the crossover bend (U-bend) is also expressed in terms of total pressure loss coefficient and static pressure recovery coefficient as shown in Fig. 7.50(a) and (b) respectively. The total pressure loss coefficient is observed to vary from 0.15 to 0.18. The lowest value is observed at 100% flow condition and the highest value is observed to occur at 70% of design flow operating condition. This kind of total pressure loss is considered as desirable and is seen to be within the range specified by Ludke (2004). However looking at the performance of the whole stage, it is seen that the return channel passages are contributing to higher total pressure losses particularly at 100%, 110% and 120% of design flow operating conditions. The static pressure recovery is seen to occur only at the 70% of design flow and thereafter with increase in mass flow and hence the average flow angle at inlet of the U-bend no recovery is observed.

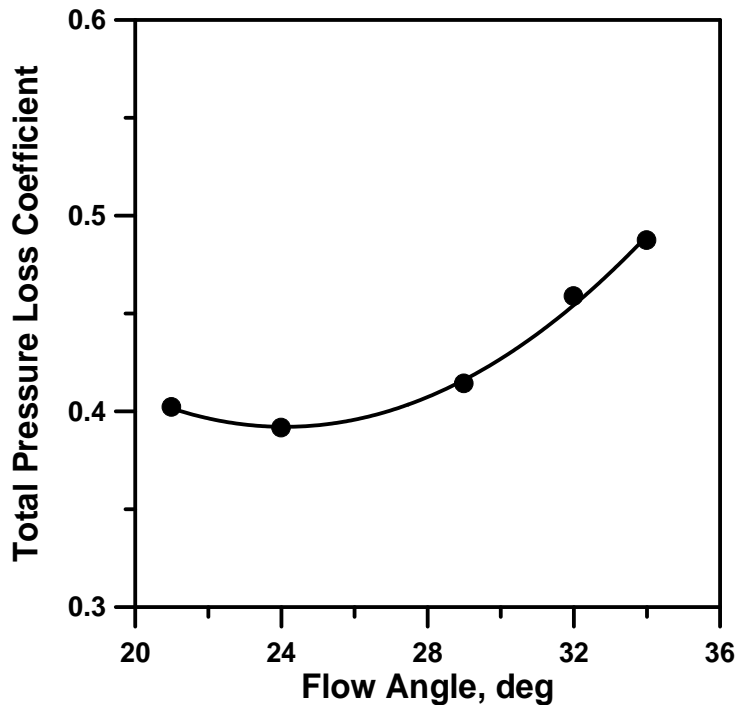


Fig. 7.49(a) Variation of total pressure loss coefficient (RCV3) (stage)

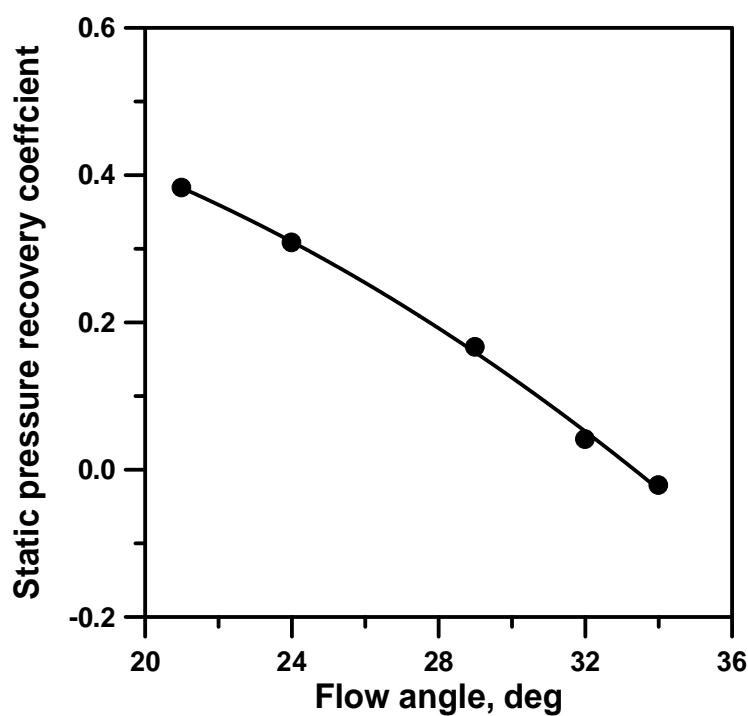


Fig. 7.49(b) Variation of static pressure recovery coefficient (RCV3)(stage)

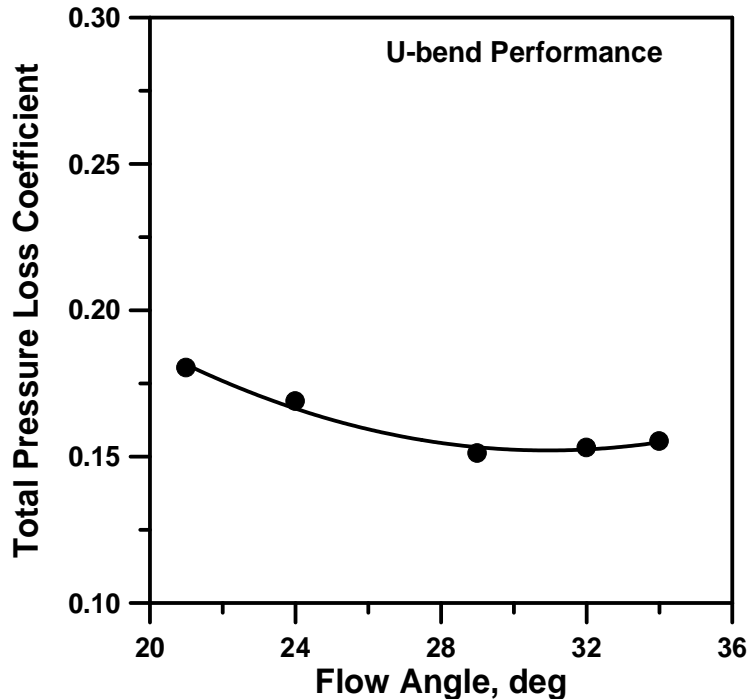


Fig. 7.50(a) Variation of total pressure loss coefficient (U-bend)

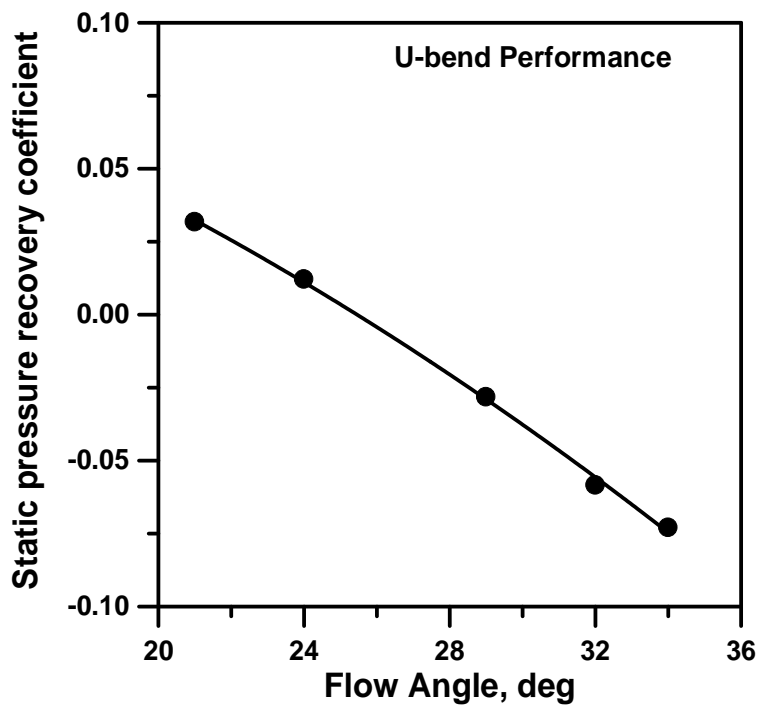


Fig. 7.50(b) Variation of static pressure recovery coefficient (U-bend)

7.7 COMPARISON OF NUMERICAL RESULTS OF RCV1, RCV2 AND RCV3 CONFIGURATIONS

The numerical results of RCV3 are presented comparing with the numerical results of RCV1 and RCV2. The variation of meridional velocity contour plots, at U-bend exit, total velocity and static pressure contour plots in the mid-span plane of the return channel vanes, exit swirl angle contour plots and secondary flows vector plots at the inlet region of L-turn bend are presented case wise in the following sections.

7.7.1 Variation of Meridional Velocity at U-bend exit

The numerical study with RCV3 is carried out with the same inlet and outlet boundary conditions that were used with RCV1 and RCV2. The variation of circumferentially averaged meridional velocity at U-bend exit for an average flow angle of 29° at U-bend inlet is shown in Fig. 7.51(a). The filled iso-contours of meridional velocity for RCV1, RCV2 and RCV3 at the U-bend exit for the design flow operating condition is shown in Fig. 7.51(b). Though there is a change in meridional velocity in the circumferential direction, a uniform trend is observed from hub to shroud at a given circumferential position. Smaller values of meridional values are observed above the vane leading edge on the suction side. However higher values of meridional velocity are noted towards the pressure side of the vane. For RCV2 configuration on the suction side of the vane a gradient in meridional velocity is observed from hub to shroud where as for RCV1 and RCV3 uniform values are observed.

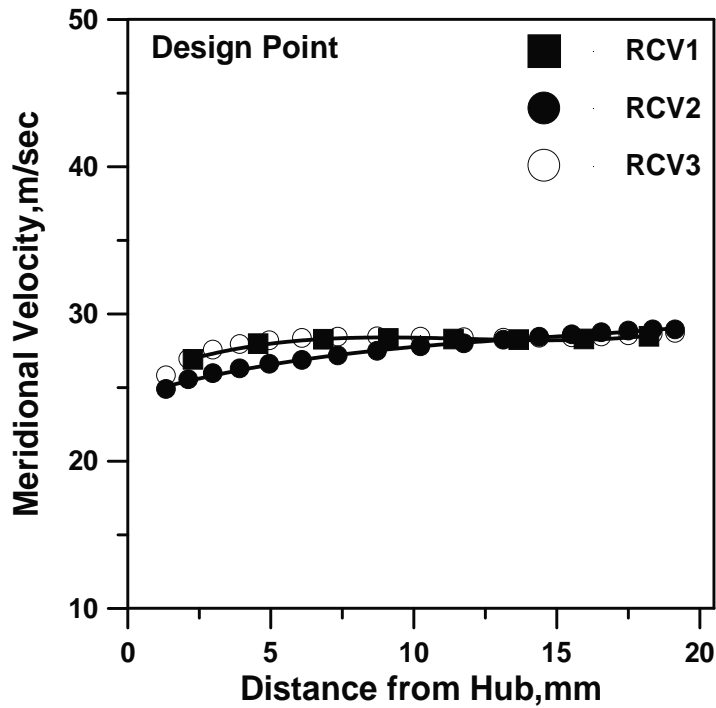


Fig. 7.51(a) Contours of meridional velocity at U-bend exit

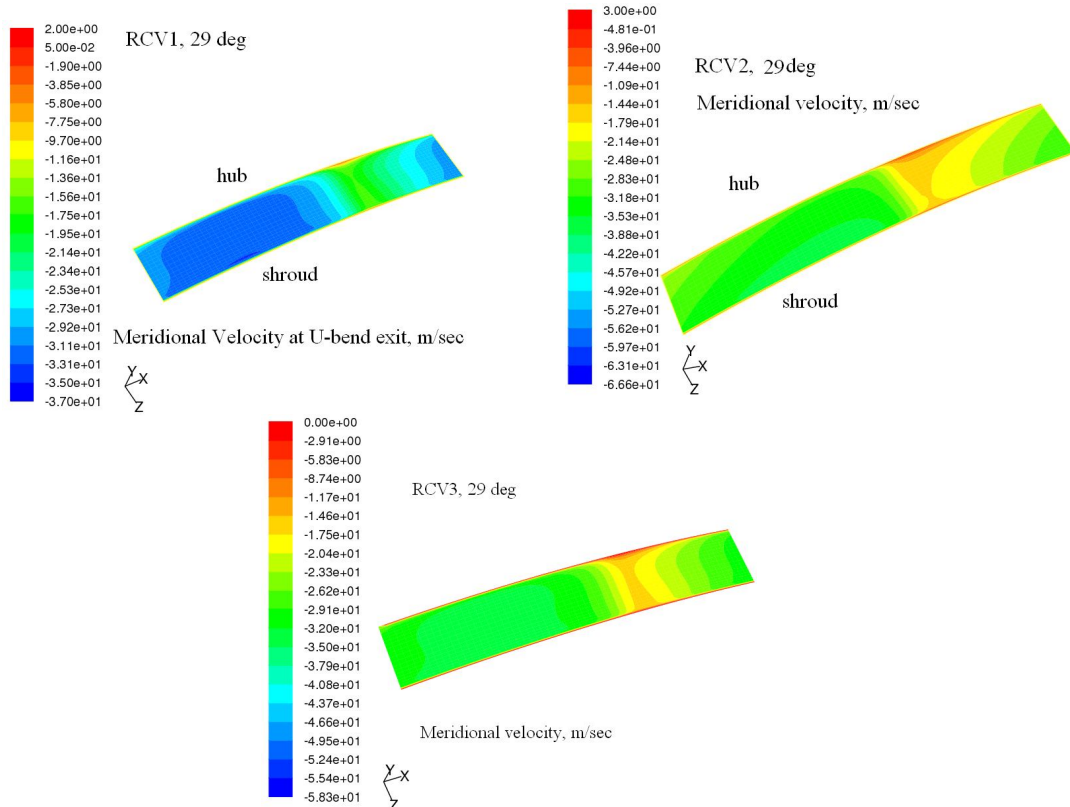


Fig. 7.51(b) Contours of meridional velocity at U-bend exit

Obviously the meridional velocity is seen to increase from hub to shroud as the flow is concentrated more towards the shroud due to 180° turning in the U-bend.

7.7.2 Vane Surface Pressure Distribution at the Design flow Rate

The vane surface pressure distribution obtained through CFD calculations for RCV1, RCV2 and RCV3 configurations is shown in Fig.7.52. The flow incidence angle at the L.E of the three studied configurations namely RCV1, RCV2 and RCV3 at the design point are shown in Table7.5. RCV1 appears to be more loaded on the pressure side due to the lower negative flow incidence angle on its L.E.

Table 7.5 Comparison of angle of flow incidence at the design point

Vane	Inlet vane angle at the L.E	Average flow angle at the L.E, deg	Incidence on the L.E of RCV1,deg
RCV1	28.5	33.75	-5.25
RCV2	26	34.4	-8.4
RCV3	25	33.93	-8.98

7.7.3 Variation of Total Velocity in the RCV mid-span plane

The filled contour plots of total velocity in a plane passing through the mid-span of the RCV are presented and explained in this section. Figure 7.53 shows such contour plots for the 70% operating range i.e. for a U-bend inlet flow angle of 21°.

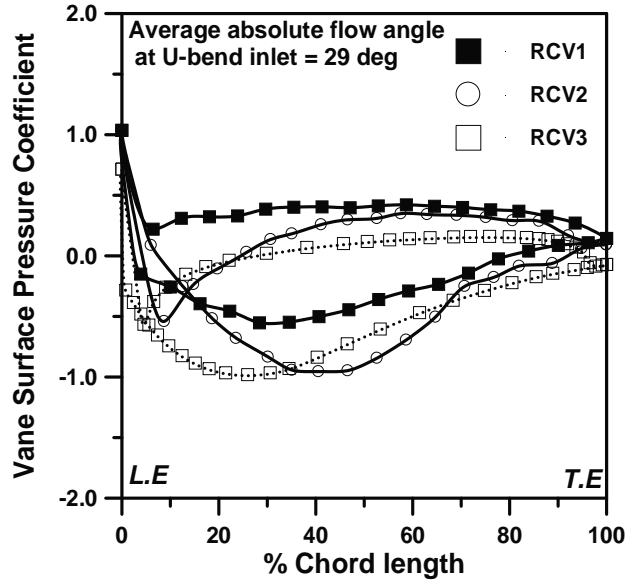


Fig. 7.52 Vane surface pressure distribution at the design point

Initial acceleration of the fluid up to one-third of the flow path length is observed followed by a deceleration in the later flow path length. A low-velocity zone started developing from about two-thirds of the flow path length on the suction side and is observed to widen further in the downstream direction. The magnified vector plots of low velocity regions are also shown against the corresponding contour plots. The flow separation and the reverse flow occurring in the said zone is clearly seen for RCV1 and RCV2. Though a low velocity zone is observed for RCV3 on the suction side, No significant reverse flow is observed in that zone. The incidence angle at this operating condition is $+4^{\circ}$, which means an imminent flow separation on the downstream side of the suction surface. The contour plots of total velocity for other operating conditions on the plane passing through the RCV mid span are shown in Fig. 7.54 to 7.57.

At all the operating conditions even with negative incidence on the leading edge, the flow separation and reverse flow could not be avoided for RCV1 and RCV2. No significant reverse flow is observed for RCV3 at all the five operating conditions of the compressor stage. Therefore RCV3 is seen to eliminate the flow separation and reverse flow problems.

7.7.4 Meridional Velocity Distribution at the Stage Exit

The circumferentially averaged meridional velocity distributions for RCV1, RCV2 and RCV3 calculated at the design point are shown in Fig. 7.58. For all the studied configurations the meridional velocity variation from hub to shroud is observed to be the same. A peak value of meridional velocity of about 40 m/sec is observed near the hub region. It is seen to decrease towards the shroud to about 27 m/sec.

7.7.5 Secondary Flow Pattern at the L-turn inlet

The secondary flows develop due to local pressure gradients and sharp turning of the direction of flow in the flow field. The presence of secondary flows causes internal fluid friction losses and increased swirl at the stage exit. The presence of secondary flows at the L-turn inlet at the design flow rate is presented in the form of vector plots as shown in Fig. 7.59. The L-turn inlet plane is located immediately after the exit of return channel vane. The secondary flow vectors for RCV1 on the L-turn inlet plane are seen to be oriented strongly towards the suction side of the vane. For RCV2 and RCV3 the influence of secondary flows is seen to be less when compared with RCV1.

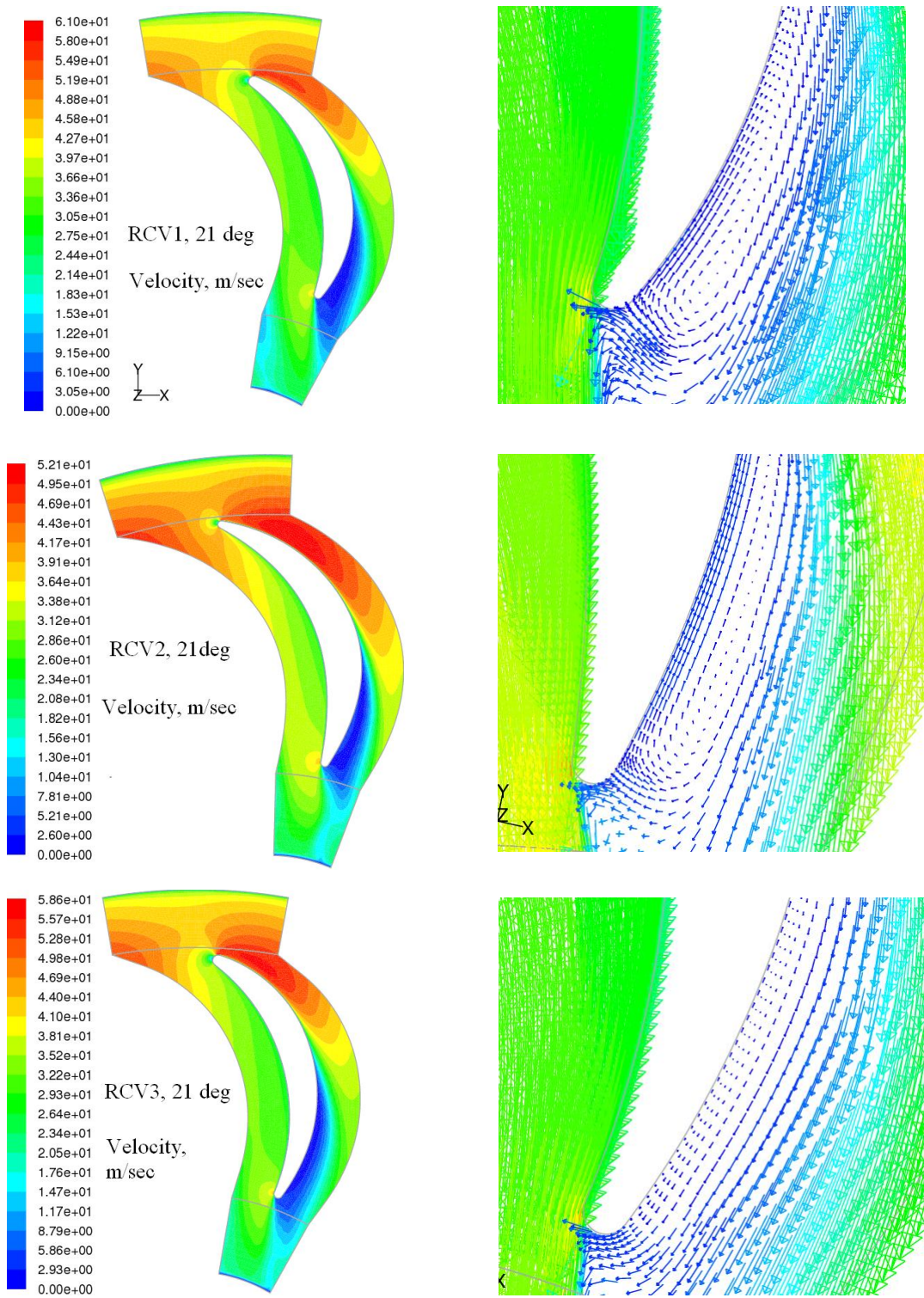


Fig. 7.53 Variation of total velocity in a plane passing through the mid-span of the RCV (flow angle at U-bend inlet = 21 deg)

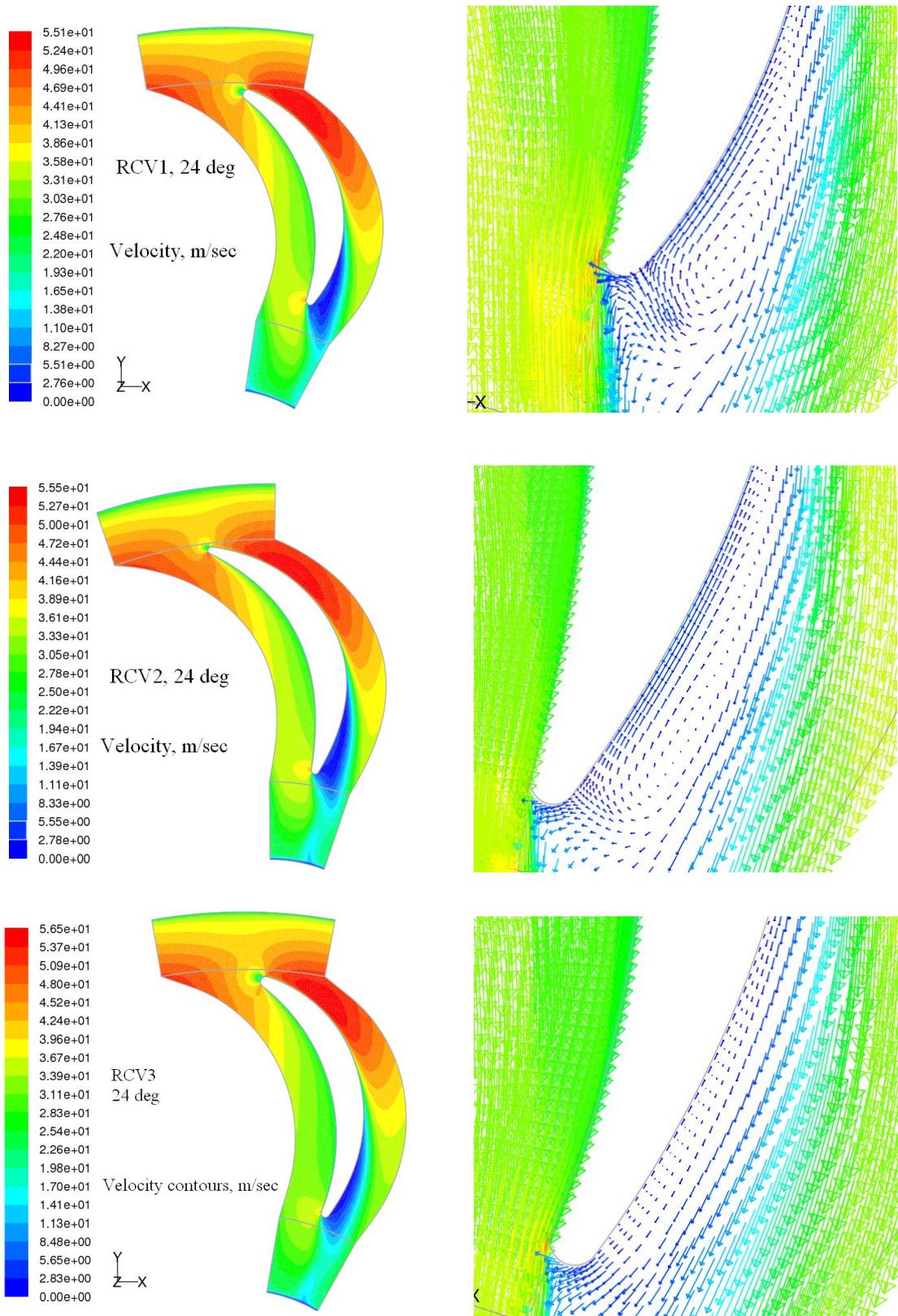


Fig. 7.54 Variation of total velocity in a plane passing through the mid-span of the RCV (flow angle at U-bend inlet = 24 deg)

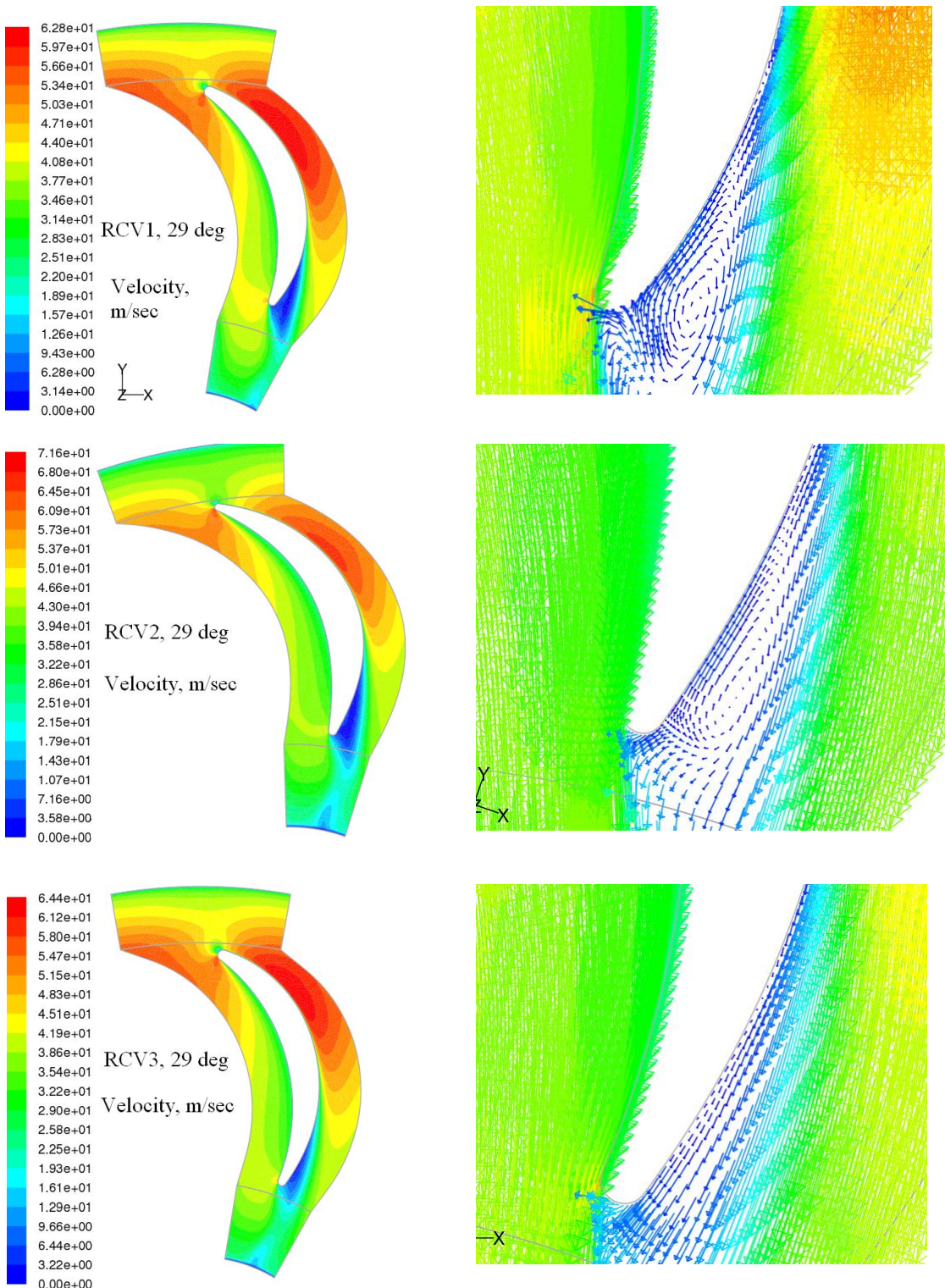


Fig. 7.55 Variation of total velocity in a plane passing through the mid-span of the RCV (flow angle at U-bend inlet = 29 deg)

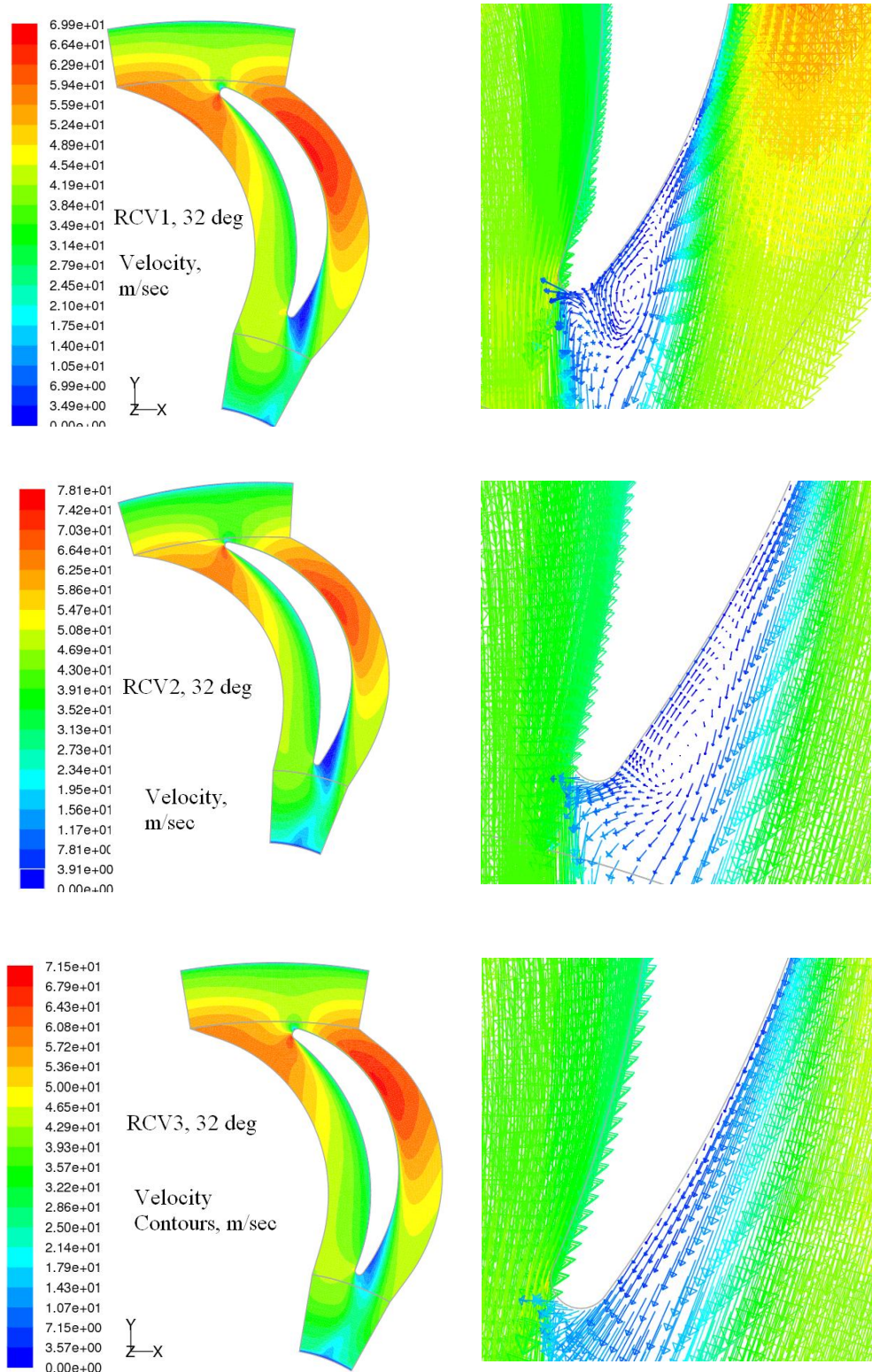


Fig. 7.56 Variation of total velocity in a plane passing through the mid-span of the RCV (flow angle at U-bend inlet = 32 deg)

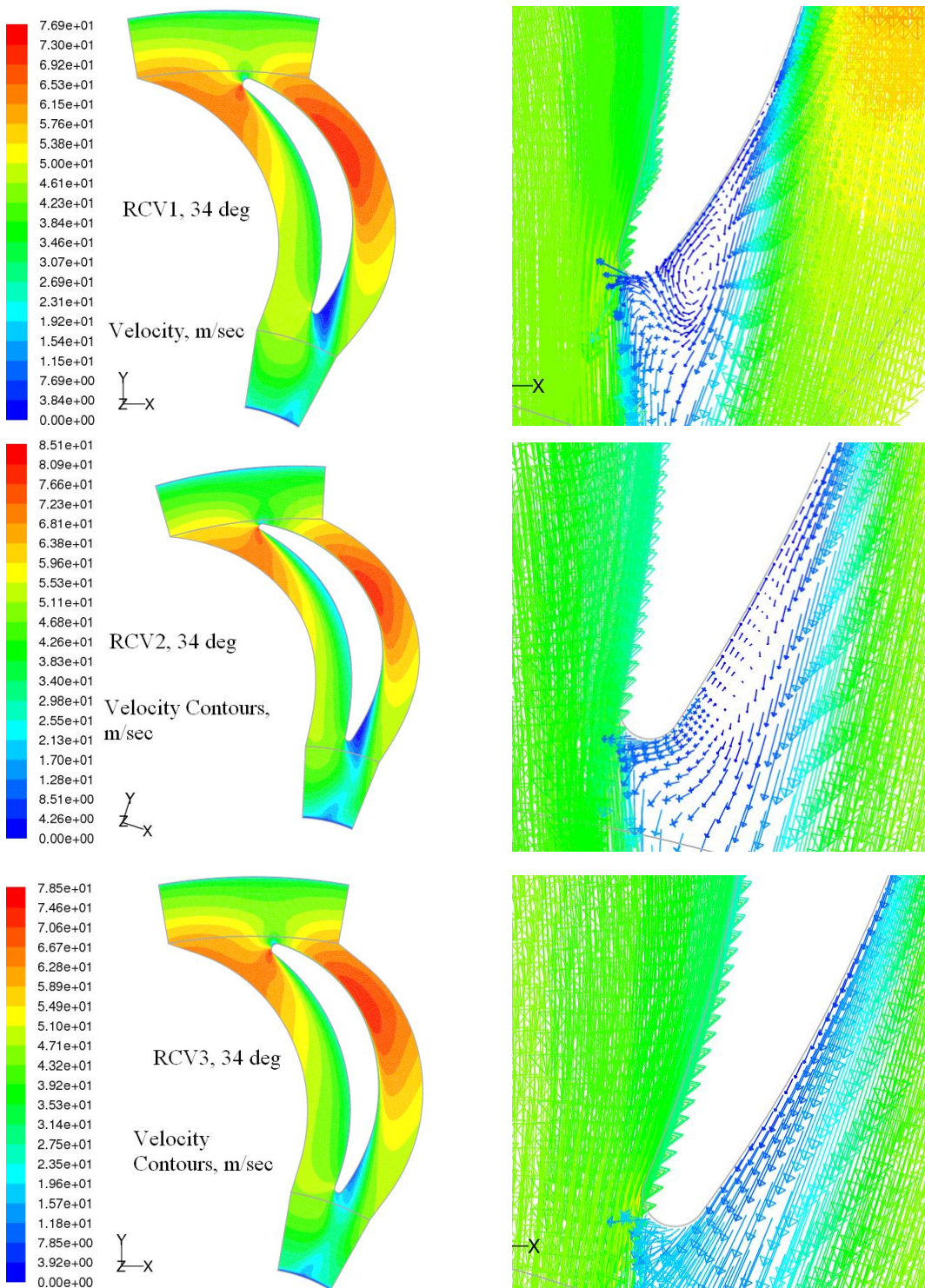


Fig. 7.57 Variation of total velocity in a plane passing through the mid-span of the RCV (flow angle at U-bend inlet = 34 deg)

7.7.6 Variation of Exit Swirl Angle

The filled iso-contours of swirl angle on the stage exit plane calculated with respect to axial flow direction at the off-design flow rate for RCV1, RCV2 and RCV3 are shown in Fig. 7.60 . For RCV1 and RCV3 the maximum flow deviation (swirl angle) is observed to shift towards the shroud with the increase in the average flow angle at U-bend inlet while for RCV2 it is observed to occur consistently at the mid region of the flow path height irrespective of the operating conditions.

7.7.7 Performance of the Stage

The calculated values of total pressure loss coefficient for the stage over the entire operating range for all studied configurations is compared and shown in Fig. 7.61(a). The performance of the stage with RCV3 in terms of total pressure loss coefficient is seen to be better than RCV1 and RCV2. Though the total pressure loss coefficient of RCV1 is closer to RCV3, the swirl angle distribution at the stage exit was observed to be unfavorable. The swirl angle distribution for RCV2 was found to be favorable but the total pressure loss coefficient is observed to be higher than RCV1 and RCV3. The variation of static pressure recovery coefficient of the stage for all the studied RCV configurations is shown in Fig. 7.61(b). The performance of RCV3 in terms of static pressure recovery coefficient is observed to be superior to RCV1 and RCV2.

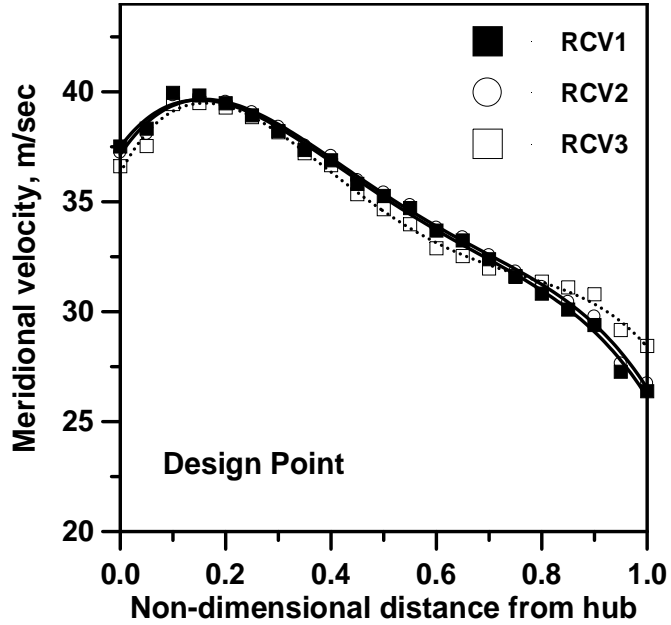


Fig. 7.58 Variation of Meridional Velocity at the Stage Exit (100% flow)

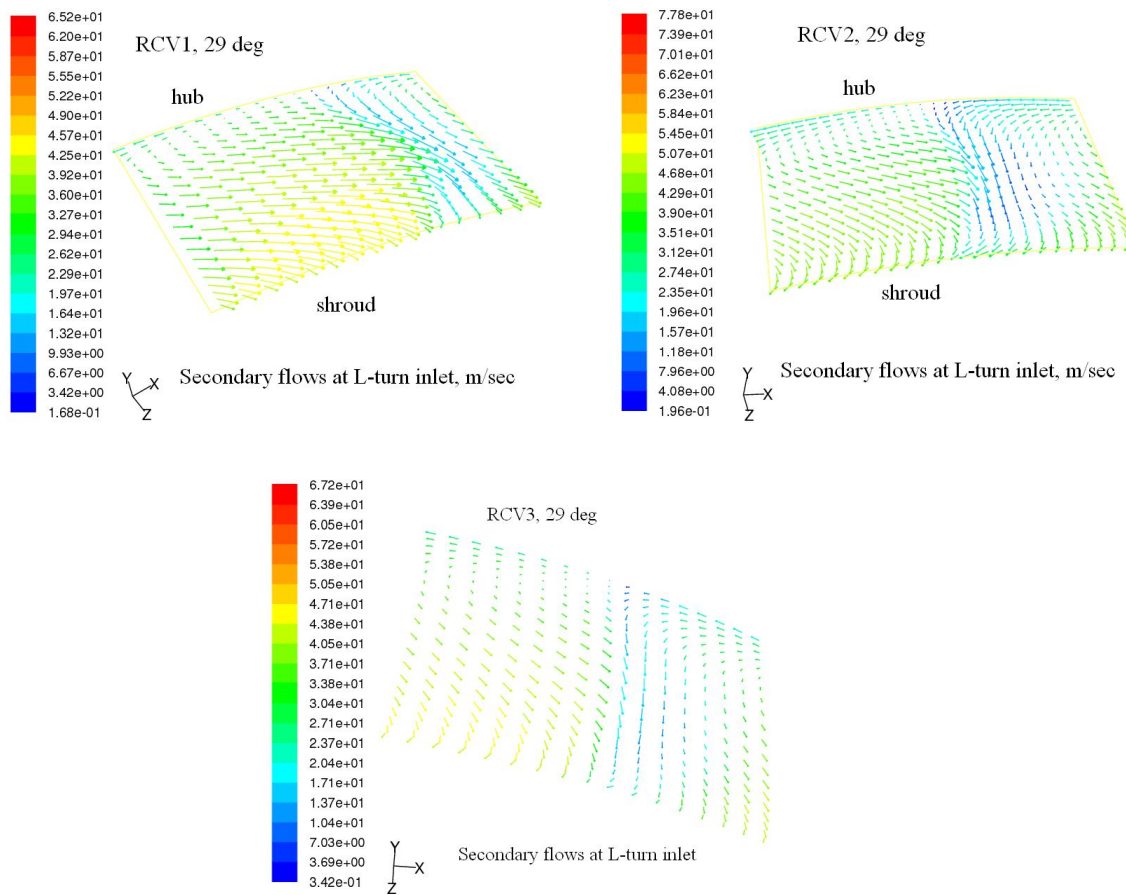


Fig. 7.59 Secondary flow pattern on the L-turn inlet plane (design point)

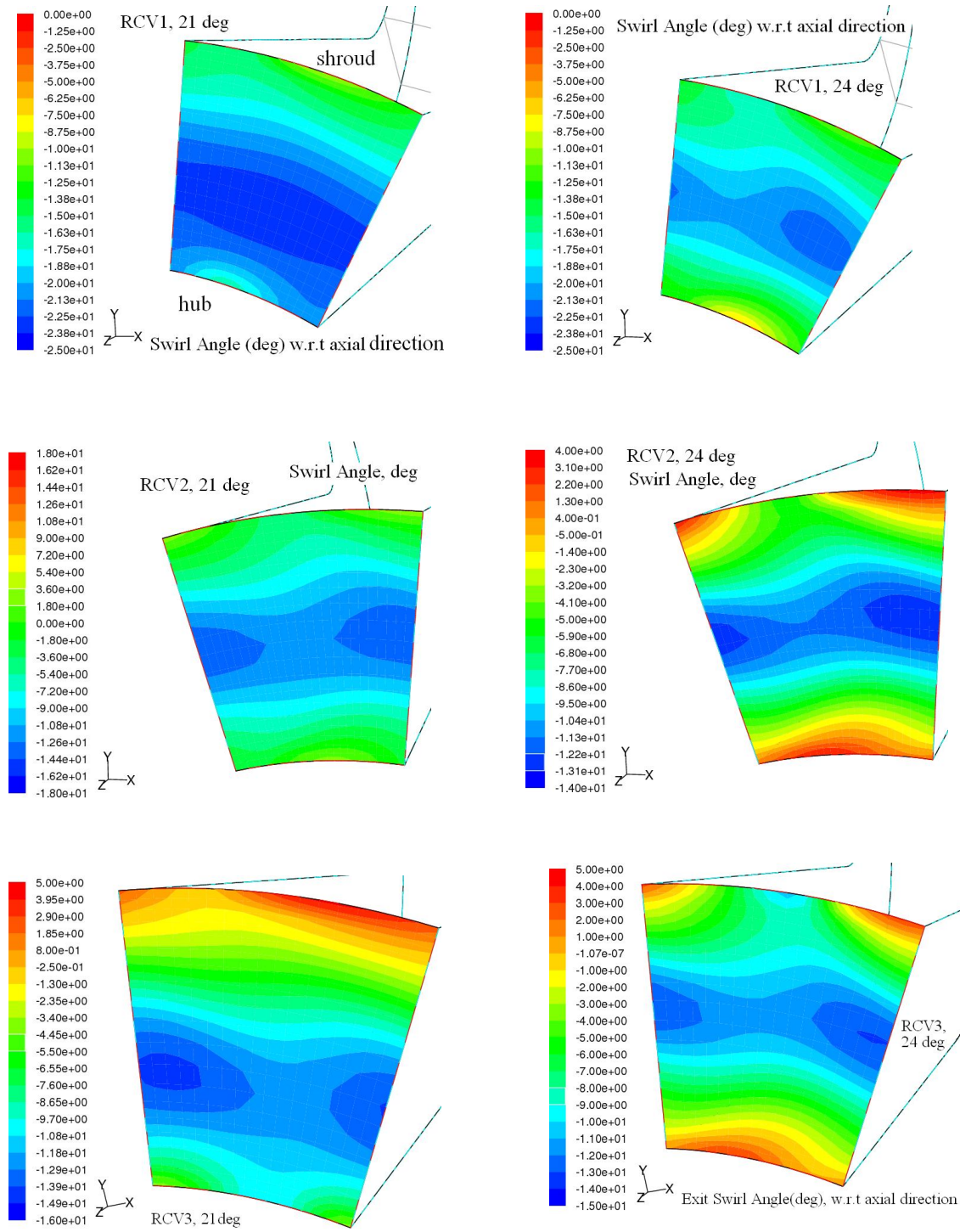


Fig. 7.60 Variation swirl angle at the stage exit (off-design conditions)

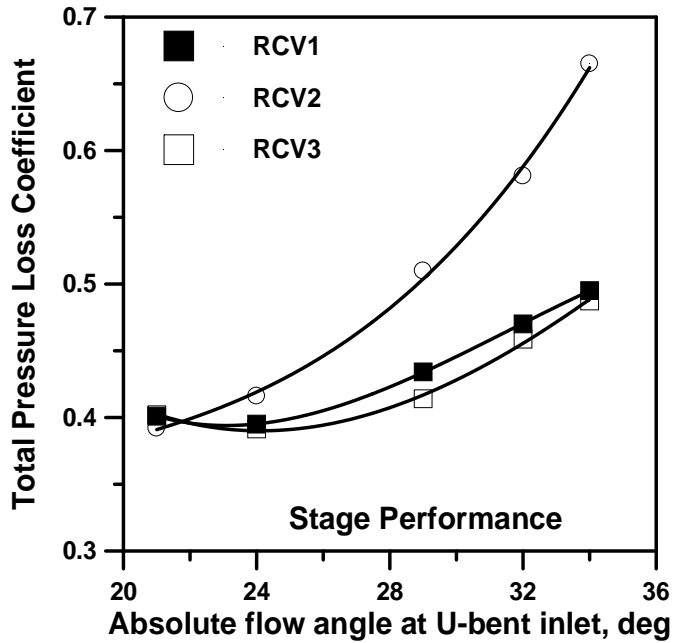


Fig. 7.61(a) Variation of total pressure loss coefficient

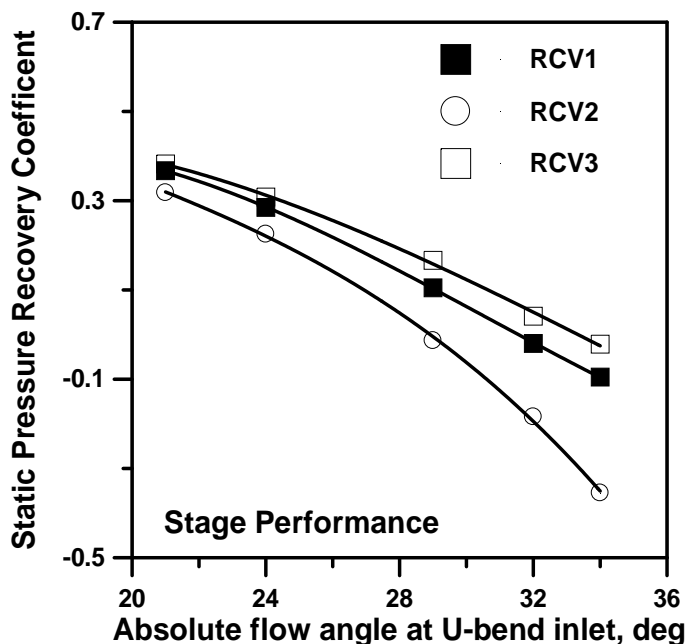


Fig. 7.61(b) Variation of static pressure recovery coefficient

7.7.8 Performance of the U-bend

The variation of total pressure coefficient in the U-bend for the three configurations is shown in Fig. 7.62(a). The total pressure loss coefficient is observed to be minimum for RCV2 configuration compared to RCV1 and RCV3. The variation of static pressure recovery coefficient for the three configurations is shown in Fig. 7.62(b). The static pressure recovery is seen to be better for RCV1 and RCV3 configuration when compared to that of RCV2. A very poor performance is noted in the RCV2 channel in terms of static pressure recovery coefficient. It is understood from the results that the return channel path configuration installed in the downstream direction influences the total pressure loss coefficient and static pressure recovery coefficient. Though RCV3 is showing lesser total pressure losses than RCV1 and RCV2, its static pressure recovery is seen to be poor. However the performance of the whole stage i.e. performance of U-bend coupled with return channel passages is to be seen. The stage performance as discussed in the previous section indicated higher total pressure losses and lower static pressure recovery in RCV2 than the other two configurations RCV1 and RCV3.

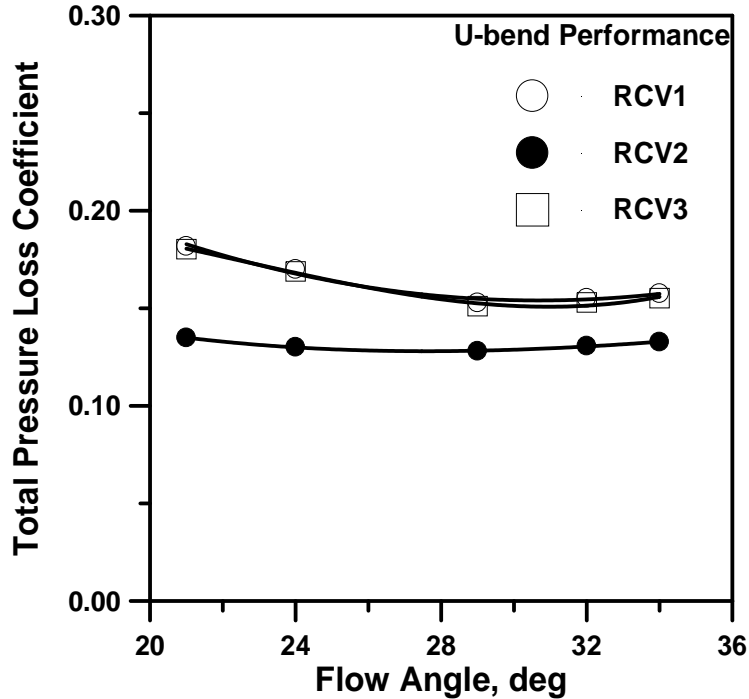


Fig. 7.62(a) Variation of total pressure loss coefficient (U-bend)

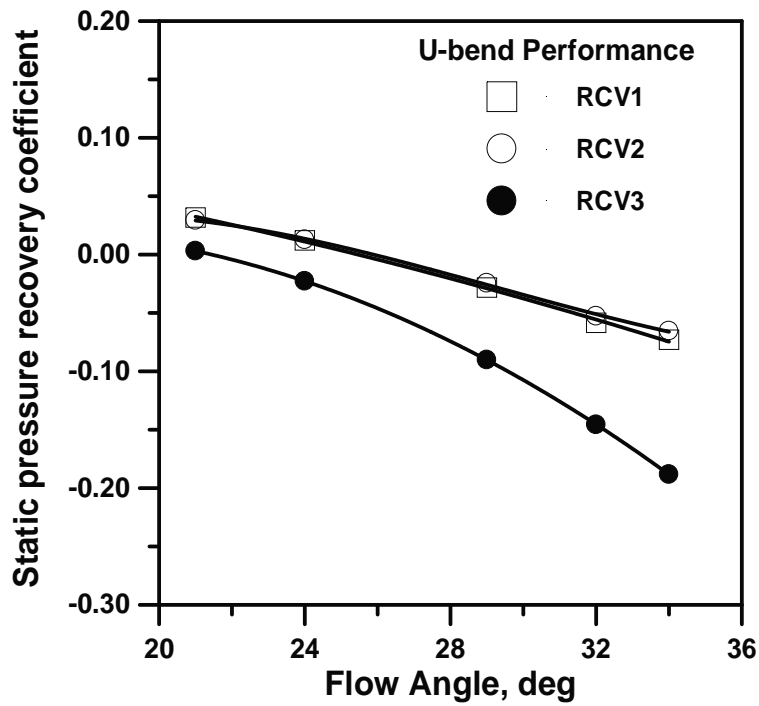


Fig. 7.62(b) Variation of static pressure recovery coefficient (U-bend)

7.8 FURTHER NUMERICAL STUDIES IN RCV3 CONFIGURATION

The improvement in the aerodynamic performance of the stage with RCV3 configuration as reported in section 7.7 was obtained by changing only the vane design parameters. It is estimated that further improvements might be possible by altering the U-bend flow path geometry, return channel vane height variation, number of return channel vanes. Further numerical studies are conducted by varying the flow path parameters with RCV3 configuration installed in the vane passages. The results are discussed in the following sections.

7.8.1 Effect of U-Bend Exit Flow Path Width on the Stage

Performance

The flow path width at the exit of U-bend is expressed in the non-dimensional form (b_2/b_1) . So far the ratio (b_2/b_1) was kept equal to 0.836. Further numerical studies are conducted for two more configurations; $(b_2/b_1) = 1.163$ and 1 by increasing only the b_2 value. In turn the change in (b_2/b_1) is affecting the shroud wall divergence angle, φ . The divergence angle influences the deceleration process in the return channel section. Higher divergence angle causes the area of flow to increase. The shroud wall divergence angle data maintained in the present study is shown Table 7.6. The geometries of U-bend and the return channel wall divergence angle are shown in Fig.7.63. Since the L-turn inlet flow path width is dictated by the subsequent stage inlet width, it is kept constant while only the U-bend exit flow path width is altered.

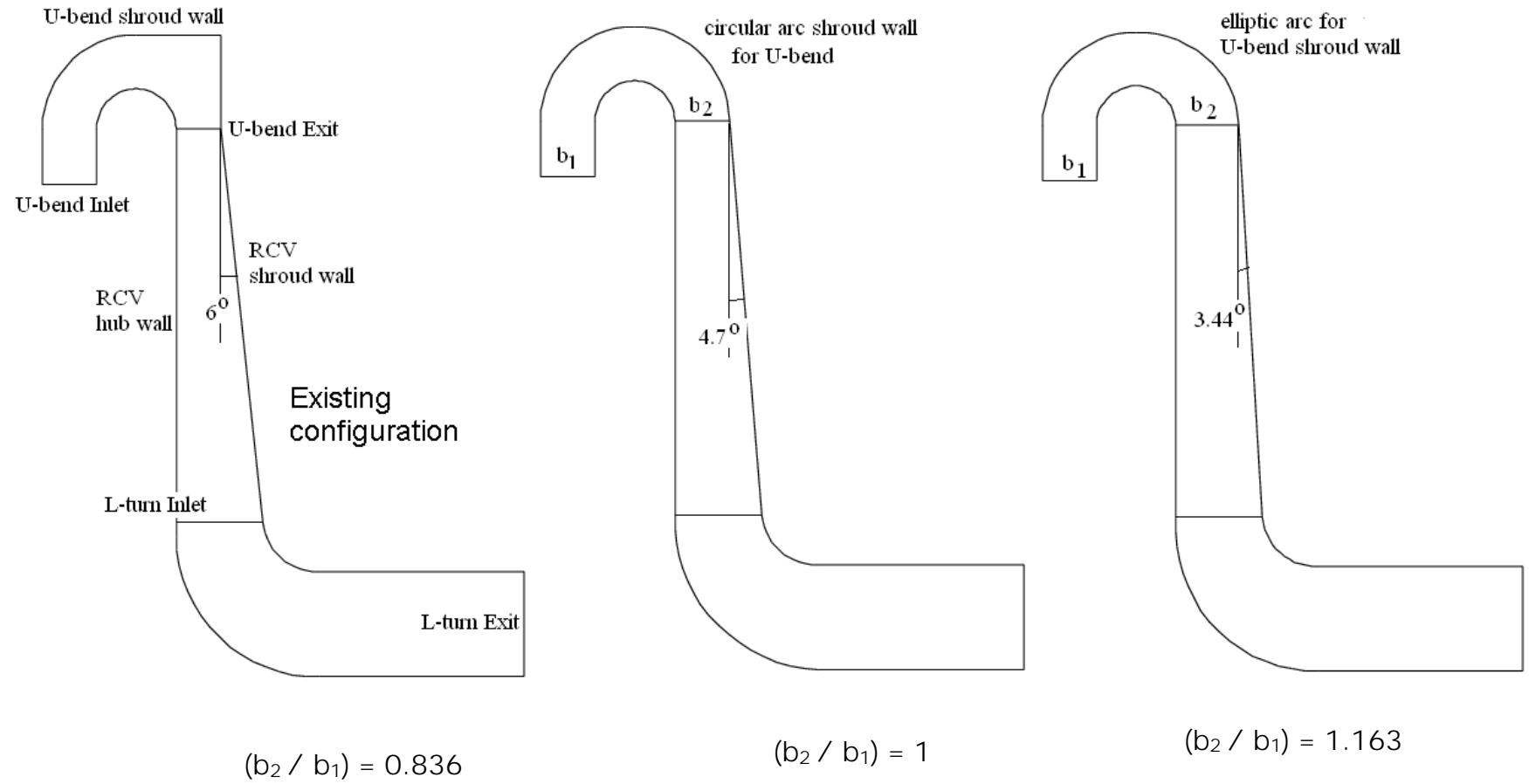


Fig.7.63 Geometrical details of the flow path modifications with varying (b_2 / b_1) ratios
 $(\phi = \text{RCV shroud wall divergence angle})$

Table 7.6 U-bend flow path parameters

S.No	(b_2/b_1)	φ (deg)
1	0.836	6
2	1	4.7
3	1.163	3.44

The altering of U-bend exit caused the U-bend shroud wall curvature to change. For $(b_2/b_1) = 0.836$ and 1.163 , the U-bend shroud wall is joined with an elliptic arc. The same inlet and exit boundary conditions were given for the altered flow path studies. The same numerical solution methodology is adapted in these cases also. Figure 7.64 (a) shows the variation of total pressure loss coefficient for the stage with altered flow path configurations. A drastic improvement in the aerodynamic performance for width ratio of 1.163 is observed in terms of reduced total pressure losses. The variation of static pressure recovery coefficient with different (b_2/b_1) ratios is shown in Fig.7.64(b). The static pressure recovery observed to be better for the case of $(b_2/b_1) = 1.163$. To know the U-bend total pressure losses alone the total pressure loss coefficient for the crossover bend is plotted and shown in Fig.7.65(a). It is very interesting to see that the U-bend total pressure loss coefficient is reduced for the crossover bend with $(b_2/b_1) = 1.163$, which is contributing to some extent in the overall improvement of stage performance. The reason for improved performance may be also be attributed to the changed average flow angles at the U-bend exit.

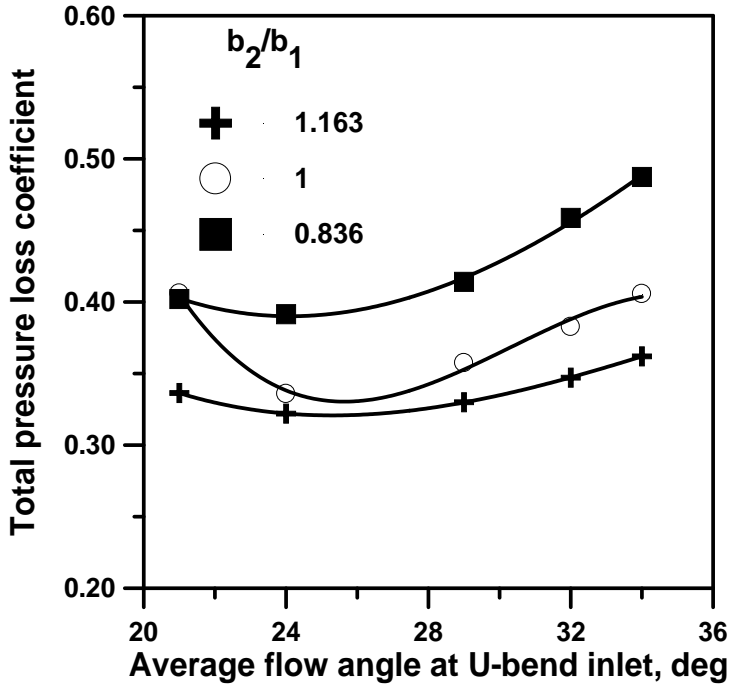


Fig. 7.64(a) Variation of total pressure loss coefficient for the stage for different b_2/b_1 ratios

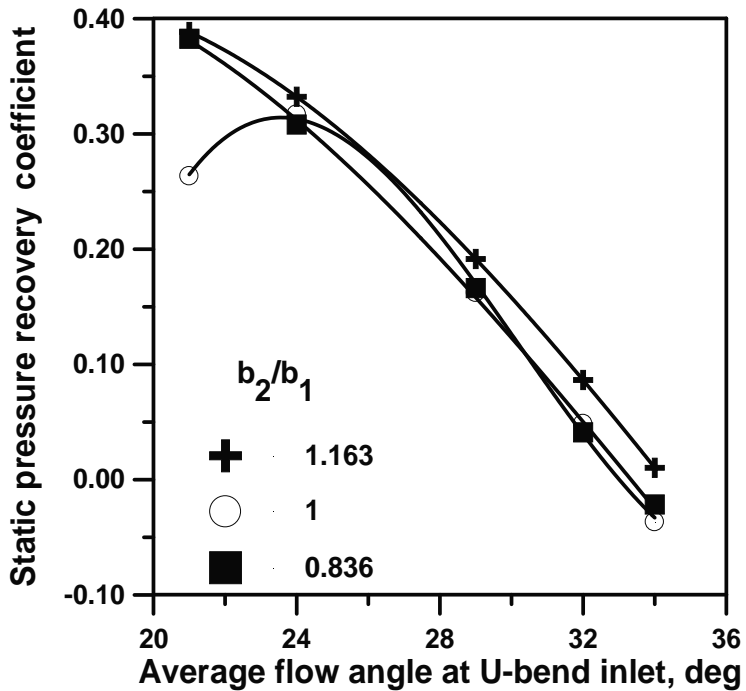


Fig. 7.64(b) Variation of static pressure recovery coefficient for the stage for different b_2/b_1 ratios

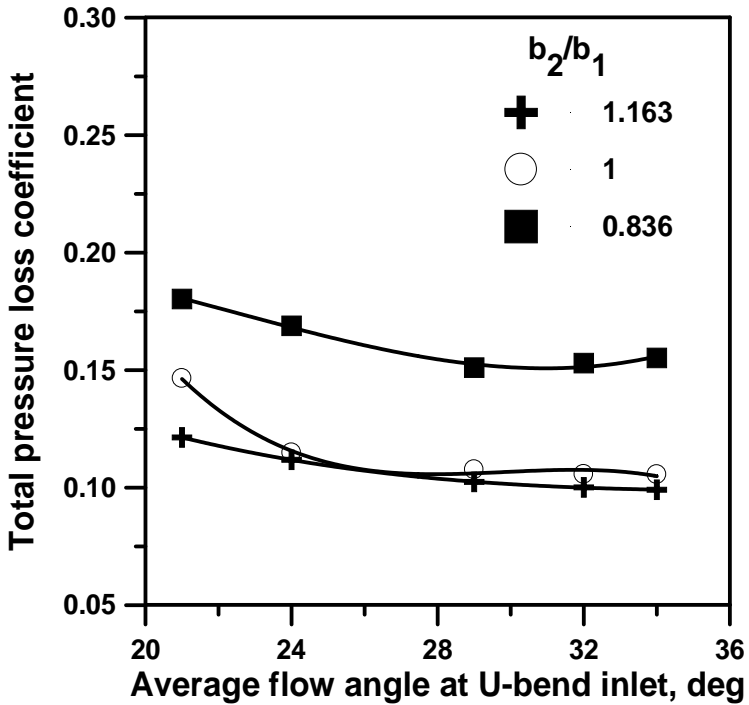


Fig. 7.65 (a) Variation of total pressure loss coefficient for U-bend for different b_2/b_1 ratios

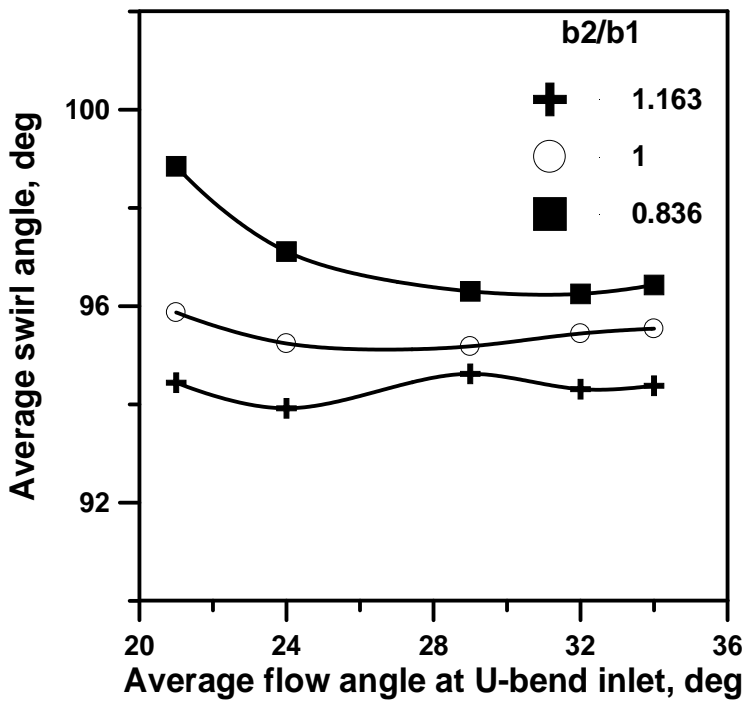


Fig. 7.65(b) Variation of average swirl angle at the stage exit for different b_2/b_1 ratios

The grand average values of flow angles measured with respect to the tangential direction at the U-bend exit for the design flow rate condition are shown in Table 7.7. The average flow angle at the U-bend exit is seen to be decreasing with increase in the flow path width at the exit section. This is expected as per the continuity equation causing a decrease in radial velocity. The average flow angles observed at the U-bend exit throughout the operating range appears to be more favorable when $(b_2/b_1) = 1.163$. The average swirl angle distribution at the exit of the L-turn for varying (b_2/b_1) ratios is shown in Fig.7.65(b) The average swirl angle at the stage exit for $(b_2/b_1) = 1.163$ is observed to be the least. The average swirl angle for the case with $(b_2/b_1) = 1.163$ has a maximum exit swirl angle of 94° (-4° with respect to axial direction). This is quite lower in magnitude when compared to the other two cases and is closer to the ideal requirement of zero-swirl. The swirl angle distribution appears to have improved considerably at the 70% and 80% of design flow rate conditions when the average flow angles at the U-bend inlet were maintained equal to 21 and 24 degrees respectively. The filled contour of velocity on the mid plane passing through RCV3 is shown in Fig. 7.66.

Table 7.7 Average flow angles at the U-bend exit for design flow rate

S.No	(b_2/b_1)	α_2	i
1	0.836	33.93°	-8.93°
2	1	31.92°	6.92°
3	1.163	28.55°	-3.55°

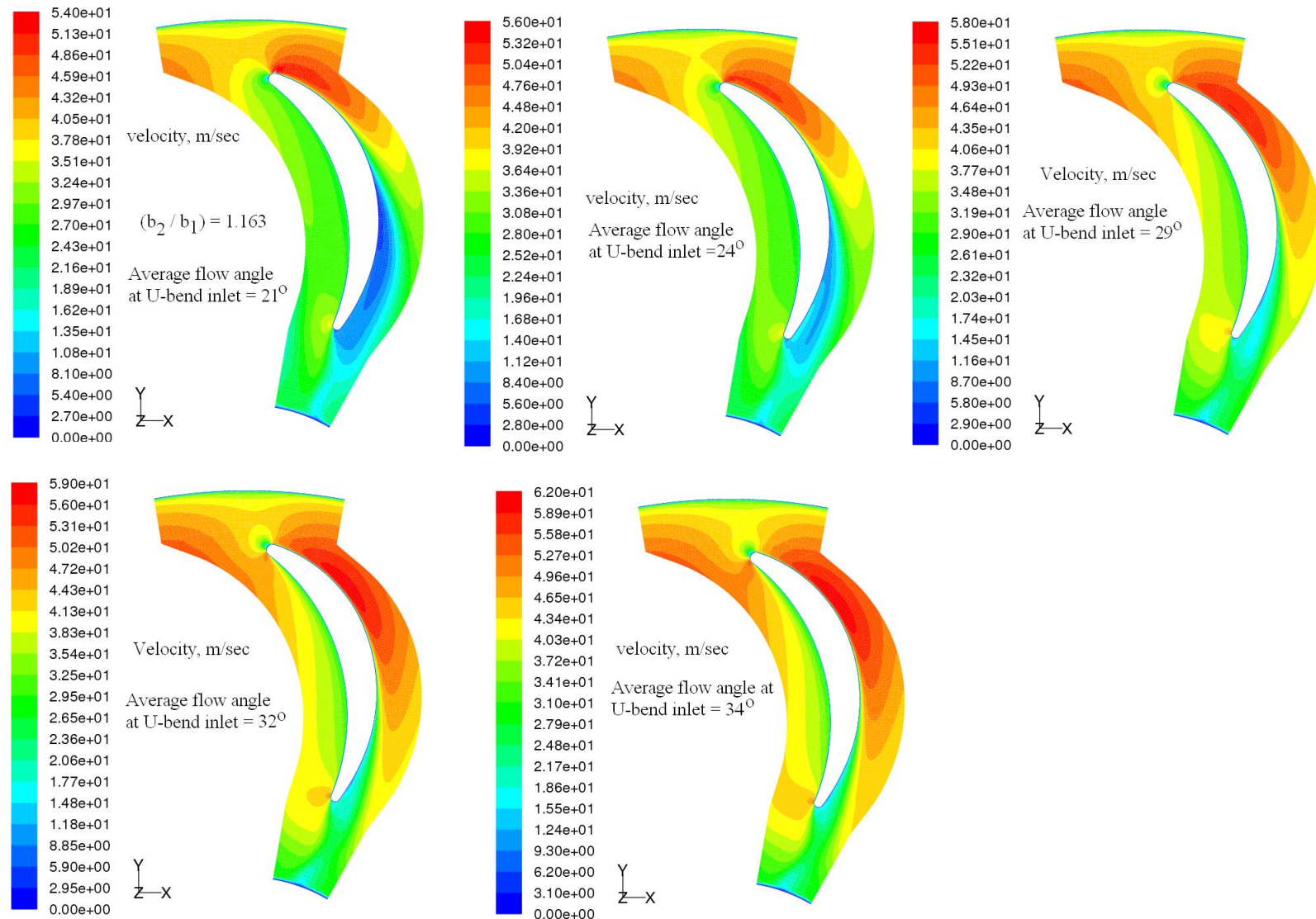


Fig. 7.66 Velocity contour plots on a plane passing through the mid-span of RCV3 for $(b_2/b_1) = 1.163$

7.8.2 Effect of Varying the U-Bend Radius of Curvature on the Stage Performance

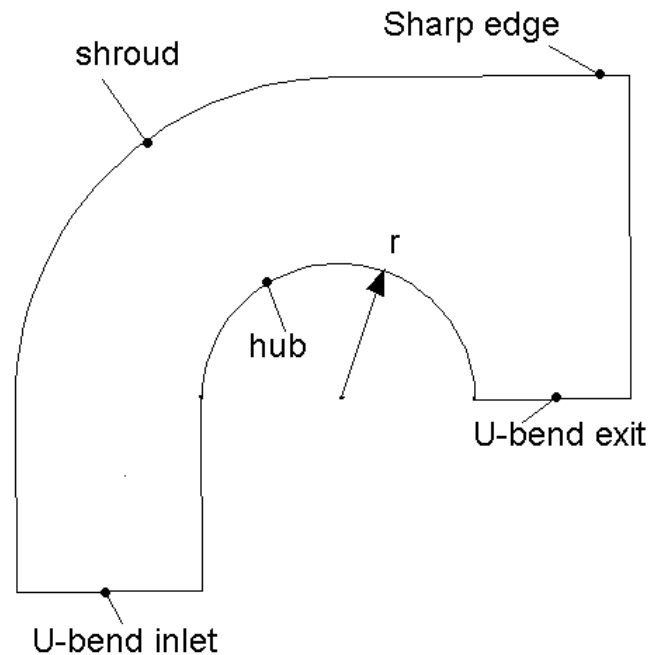
The crossover bend in the existing configuration has a sharp edge on the shroud wall. The curvature of U-bend is expressed with a parameter called curvature factor, R^* as given below.

$$R^* = \frac{2r}{(b_1 + b_2)}$$

Further numerical studies are carried out by varying the R^* value while keeping the U-bend inlet and exit flow path widths and all other parameters the same as in the existing case, i.e., $(b_2/b_1) = 0.836$. Only the radius of the U-bend hub arc, r is altered to get new value of R^* . Table 7.8 shows the modified U-bend parameters for which the numerical study results are presented in this section. It may be noted that in all these configurations, the hub curve of U-bend is always a circular arc while the shroud wall arc is either a sharp or elliptic type. The geometrical details of the U-bend are shown in Fig. 7.67

Table 7.8 Existing and modified U-bend parameters

S.No	b_2/b_1	R^*	Shroud wall arc type
1	0.836	0.8	Sharp edge (existing)
2	0.836	0.8	Elliptic
3	0.836	0.7	Elliptic
4	0.836	0.97	Elliptic



$R^* = 0.8$ (with sharp edge)

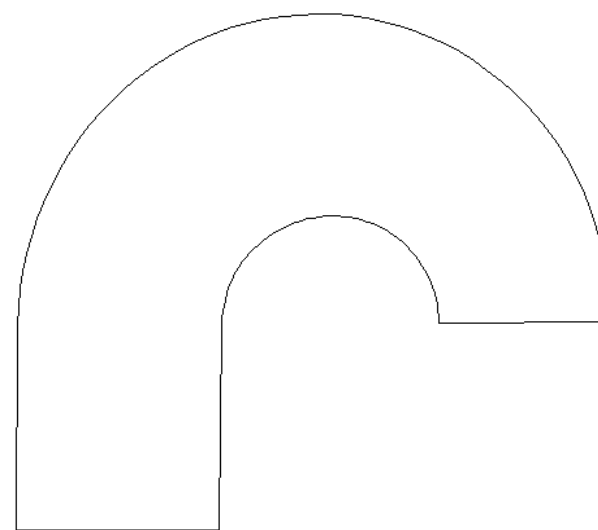
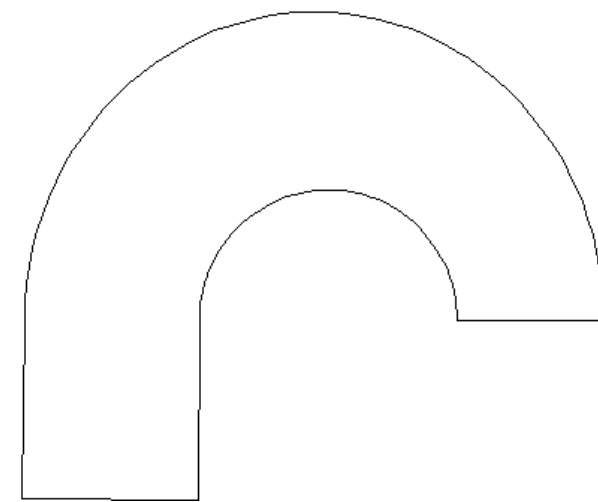
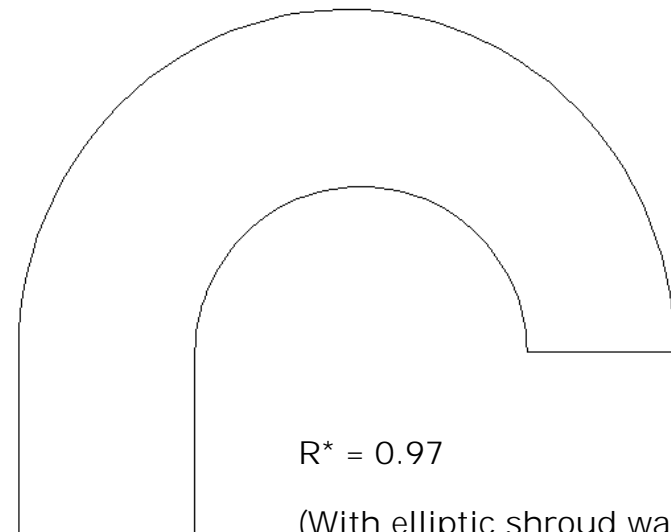


Fig. 7.67 Modified U-bend geometry configurations

The numerical studies in the RCV3 return channel configuration with the modified U-bend configurations as shown above were carried out with the same boundary conditions used in the earlier studies. Figure 7.68(a) and 7.68(b) shows the aerodynamic performance of the stage in terms of total pressure loss coefficient and static pressure recovery coefficient. The total pressure loss coefficient is seen to be higher for the existing configuration of U-bend with sharp edge at 70% and 80% of design flow rate conditions. At the design flow rate condition, i.e. for an average U-bend inlet flow angle of 29° , the total pressure loss is observed to be the same. However at the 110% and 120% of design flow rate conditions, the existing configuration is showing lower total pressure losses when compared with the other modified U-bend curvatures. The static pressure recovery coefficient is seen to be higher throughout the operating range for the existing U-bend configuration.

The calculated L-turn exit swirl angle distribution for the studied cases is shown in Fig.7.69. The modified configurations are showing relatively lower swirl angles at the 70% and 80% of design flow rate conditions while the existing configuration is showing lower swirl angles at the 110% and 120% of design flow rate conditions. From the above observations it may be said that altering the U-bend curvature without changing inlet and exit flow path widths of U-bend is influencing the stage performance to a very little and the existing configuration appears to be the better choice.

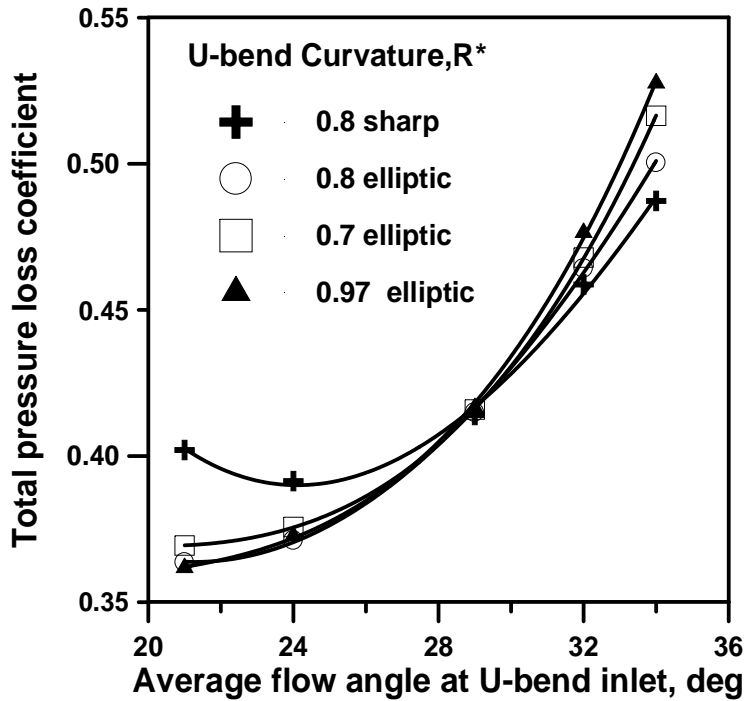


Fig. 7.68(a) Variation of total pressure loss coefficient for varying R^*

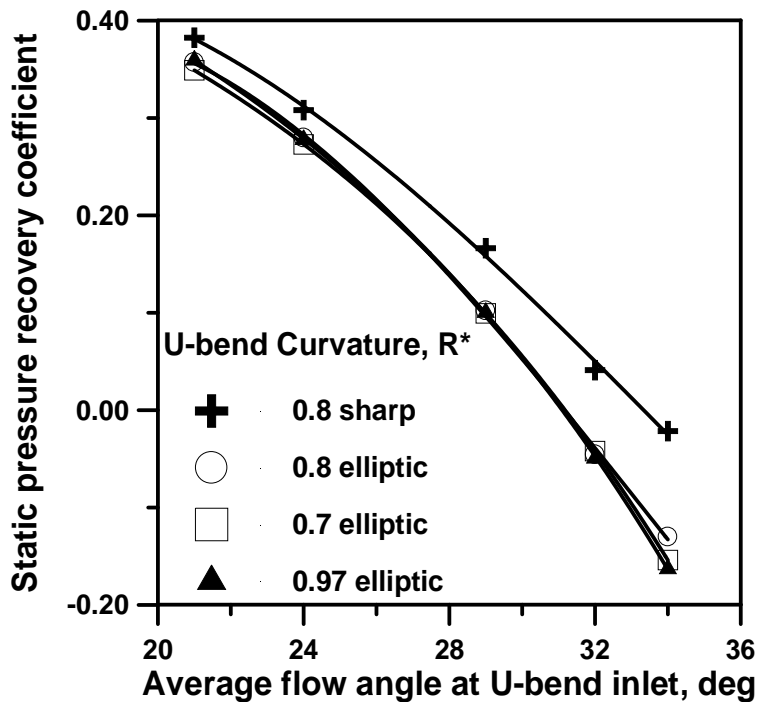


Fig. 7.68(b) Variation of static pressure recovery coefficient for varying R^*

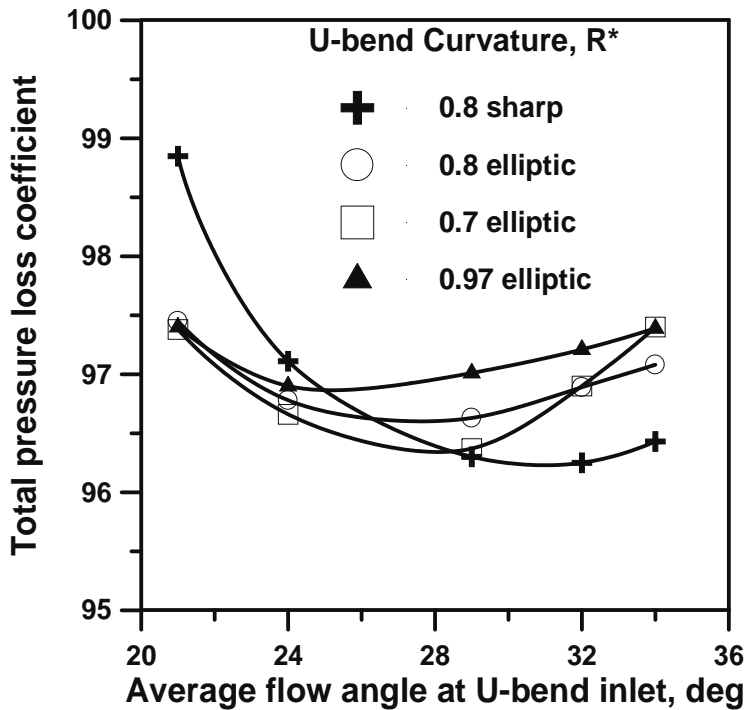


Fig.7.69 Variation of swirl angles for varying R^* values

7.8.3 Effect of Varying the Number of Vanes on the Stage Performance

The existing return channel passages have 18 vanes. Increasing the number vanes ensures better turning of the fluid but at the cost of increased frictional losses which may add to the total pressure losses. At the same time a decrease in the number of vanes might reduce frictional losses but the turning of the fluid may not be proper. To know the effect of varying the number of return channel vanes on the aerodynamic performance of the stage, further numerical studies were conducted with 16 and 20 vanes. The stage performance is compared with the existing

configuration. The variation of total pressure loss coefficient and static pressure recovery coefficient with number of vanes is shown in Fig 7.70(a) and (b) respectively. As expected the total pressure loss coefficient is observed to increase with increase in number of vanes to 20 and is seen to decrease with decrease in number of vanes. However in terms of static pressure recovery the existing case with 18 vanes is seen to be superior to other configurations with 16 and 20 vanes. The variation of average swirl angle at the L-turn exit with varying number of vanes is shown in Fig. 7.71. Due to the stringent flow path direction with increased number of vanes the average swirl angle at the L-turn exit is seen to be the least for 20 vanes among the studied variants. Though the swirl angle distribution at the stage exit is favorable with 20 vanes, because of the increased total pressure losses and poor static pressure recovery, the existing configuration with 18 vanes is considered to be superior to the other cases.

7.8.4 Summary on Modifications of Flow Path

From the above studies described in 7.8.1 to 7.8.3, it may be concluded that the RCV3 configuration with increased flow path width (b_2) at the exit of U-bend gives the best aerodynamic performance in terms of lower total pressure losses and higher static pressure recovery and reduced swirl angles at the L-turn exit whose details are compared with experimental results of RCV1 as shown Table 7.9.

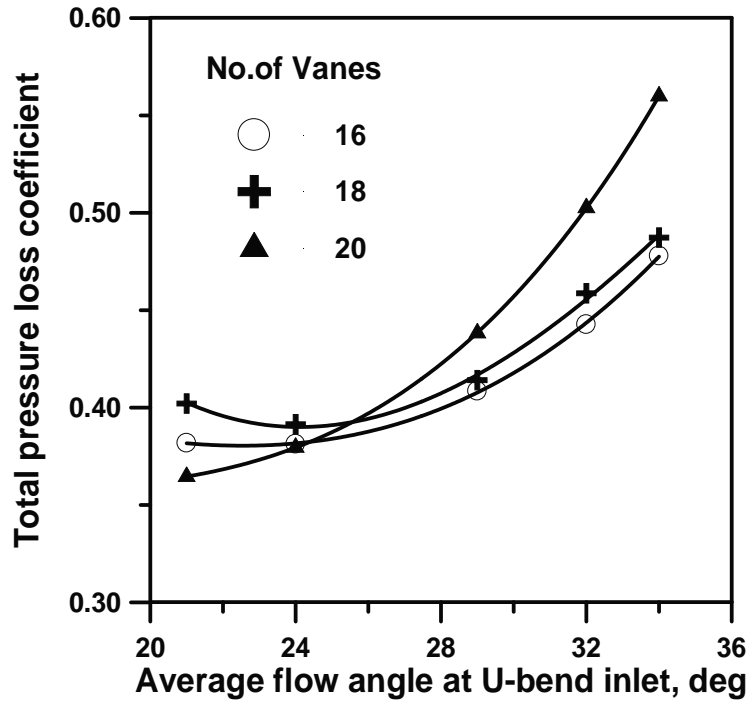


Fig. 7.70 (a) Variation of total pressure loss coefficient with number of vanes

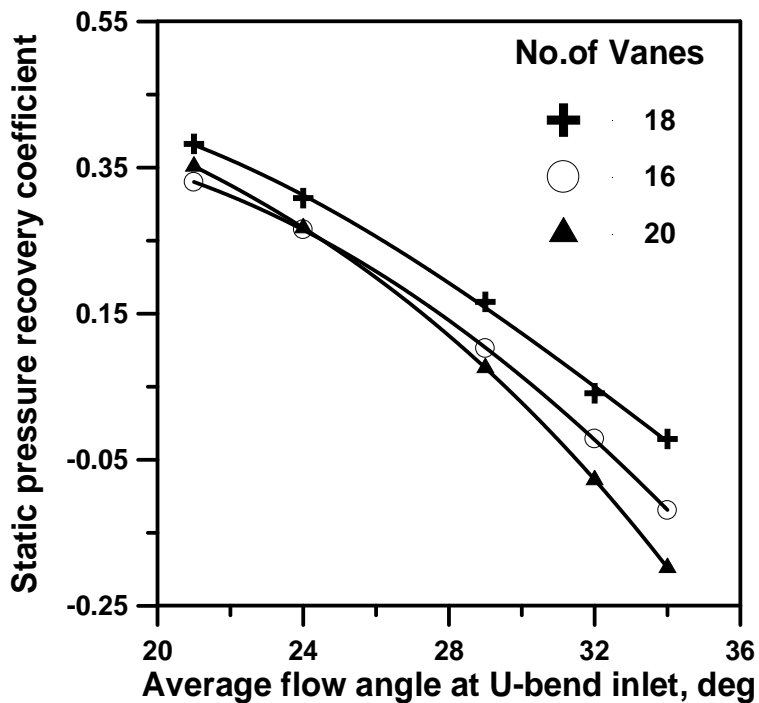


Fig. 7.70(b) Variation of static pressure recovery coefficient with number of vanes

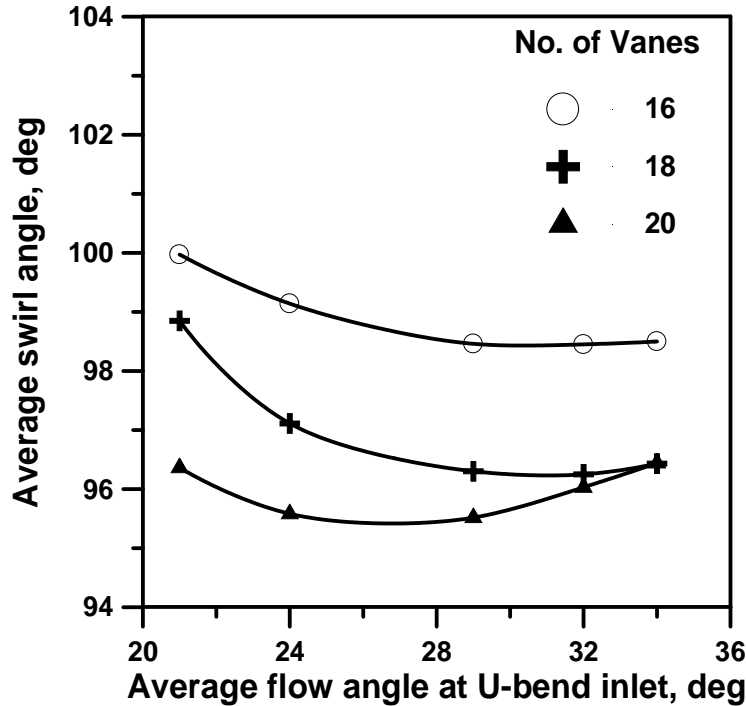


Fig. 7.71 Variation of average swirl angle with number of vanes

It is noted from the Table 7.9 that RCV3 with $(b_2/b_1) = 1.163$ is showing consistently reduced total pressure loss coefficient throughout the operating range. The maximum reduction of 27% is noted at 120% of design flow condition while least reduction of 16% is observed at 70% of design flow operating condition. At the 100% of design flow a reduction of 24% in total pressure loss coefficient is observed.

In the static pressure recovery coefficient of RCV3 with $(b_2/b_1) = 1.163$, an increase of 140% is noted at 110% of design flow operating condition, while a minimum of 5.7% increase is observed at 70% of design flow operating condition when compared with the corresponding values of RCV1.

Table 7.9 Comparison of aerodynamic performance for RCV1 and RCV3 [$(b_2/b_1) = 1.163$]

a_1	RCV1(exp)		RCV3 ; $b_2/b_1= 1.163$		% decrease in ζ for RCV3	% increase in C_p for RCV3
	ζ	C_p	ζ	C_p		
21	0.4	0.367	0.336	0.388	16%	5.7%
24	0.395	0.285	0.321	0.332	18.7%	16.5%
29	0.434	0.104	0.329	0.191	24%	83.6%
32	0.47	-0.02	0.347	0.008	26.2%	140%
34	0.495	-0.09	0.361	0.001	27%	101%

Chapter 8

CONCLUSIONS AND SUGGESTIONS

8.1 SUMMARY

- The experimental and numerical studies in the crossover system of a centrifugal compressor stage consisting of 180^o U-bend, radial cascade of return channel passages and exit L-turn ducting were carried out on a test rig with static swirl vanes for determining the aerodynamic performance of the stage. The performance of the stage was assessed with two different configurations of return channel vanes namely RCV1 and RCV2 and the results were compared.
- Based on the conclusions from the above studies a new return channel vane configuration RCV3 was designed for reducing the stage losses and was assessed for its aerodynamic performance through CFD studies.
- Further numerical studies were conducted with the improved RCV3 configuration by varying the parameters pertaining to U-bend curvature, U-bend exit flow path width (return channel vane height variation) and the number of return channel vanes, with the objective of reducing the total pressure losses and exit swirl.

8.2 CONCLUSIONS

- From the experimental results, the total pressure loss coefficient for RCV1 is observed to decrease first and then increase with increase in the U-bend inlet flow angle. It is found to be minimum when average flow angle at U-bend inlet (α_1) is 23° . The total pressure loss coefficient for RCV2 is seen to increase continuously with increase in α_1 and is found to be much higher than RCV1. The static pressure recovery coefficient for both RCV1 and RCV2 is observed to decrease with increase in α_1 and the recovery is better in RCV1. The aerodynamic performance of RCV1 is observed to be superior to RCV2 except for the average exit swirl angle.
- The average swirl angle distribution at the L-turn exit for RCV1 is observed to vary from 98° to 106° with respect to tangential direction indicating more turning in the L-turn ducting. The average swirl angle at the L-turn exit in RCV2 configuration is observed to vary from 92° to 96° , indicating lesser turning in the L-turn ducting.
- The numerical results found to be in qualitative agreement with the experimental results for both the chosen RCV1 and RCV2 configurations. The flow pattern was visualized on different planes across the flow path by means of Iso-Mach contour plots, which revealed the flow getting separated on the suction side of both the RCV1 and RCV2 configurations near to the trailing edge. This low

pressure region extending into the 90° bend inlet is observed to cause migration of flow from pressure side to suction side resulting in secondary flow phenomenon and contributing to the addition of swirl to the exiting flow. However the less turning of flow in the L-turn ducting with RCV2 configuration is attributed to the less intense secondary flow phenomena than in RCV1.

- A new configuration RCV3, whose inlet vane angle is 25°, is seen to give better aerodynamic performance in terms of reduced total pressure losses and increased static pressure recovery and reduced average swirl angle at the L-turn exit than RCV1 and RCV2. The improved performance may be attributed to the improved design with lesser rate of turning of flow along the mean stream line curvature in the return channel passages for the first 2/3 of the length and then followed by a sharp turning when the velocities are considerably reduced.
- The further numerical simulations carried out in RCV3 configuration by varying the U-bend exit flow path width has resulted in drastically reduced total pressure loss coefficient, improved static pressure recovery and reduced average exit swirl angle; when the $(b_2/b_1) = 1.163$ was maintained. This configuration changed the RCV3 shroud wall divergence angle to $\varphi=3.44^\circ$. This configuration is the best one that is evolved finally

with an average reduction in total pressure loss coefficient by 22%, increase in average static pressure recovery by 69%.

- Further numerical studies carried out in RCV3, by changing only the U-bend curvature factor, R^* without altering the U-bend exit flow path width, did not show any further improvement in the aerodynamic performance.
- Similarly, when the number return channel vanes are changed to 16 and 20, no significant improvement in the overall aerodynamic performance is observed.
- The details of finally evolved best flow path configuration with improved aerodynamic performance of the return channel passages in the present study is given below:

Vane inlet angle = 25°

Vane exit angle = 82°

Chord length = 178 mm

b_1 = 24.5 mm

b_2 = 28.5 mm

b_4 = 47.5 mm

R^* = 0.8.

Number of vanes = 18.

8.3 SUGGESTIONS FOR FUTURE WORK

- The present work dealt with a single stage starting from the inlet of crossover bend to the exit of L-turn ducting of the first stage. The numerical analysis may be further extended to multiple stages.
- The numerical study of return channel passages with vaned diffusers may be carried out to assess the aerodynamic performance of the stage.
- The analysis may be carried out with a rotating impeller by simulating the flow from the inlet of the compressor to the L-turn exit.

Appendix – A1

ERROR ANALYSIS

1. GENERAL

Uncertainty or error analysis is the forecast of the error limit, which is associated with an experimental result, based on the observation of scatter in the data used in the calculation of the result. Measurement errors occur in the process of gathering the data and in the data acquisition system. These errors are spread through the data reduction, resulting in uncertainty. Measurement error can be defined as the maximum error, which might be expected between a measured and the true value of the measured parameter. Authors like, Moffat (1982 and 1985), Holman and Gajda (1984), and Govardhan (1997), have recommended strategies to calculate the two sources of errors namely, precision (random) and bias (fixed) errors, which together have considered as total error. Precision error is the spread observed in the measurement that fall into a Gaussian distribution about a mean value in a many samples. Bias error is defined as the difference between the mean value and the true value. All measuring instruments have both the bias and precision errors. The errors are calculated for entire data path from the measurement source to the output device.

Overall, system measurement error is estimated by combining each individual components using the following equations,

$$B = \sqrt{\sum_{k=1}^N (B_k)^2} \quad (\text{Eq. A1})$$

$$P = \sqrt{\sum_{k=1}^N (P_k)^2} \quad (\text{Eq. A.2})$$

Where, N = Number of readings of the sample population

k = variable under consideration

B = Bias error of the variable under consideration

P = Precision error of the variable under consideration

The precision and bias errors are combined and represented as total uncertainty,

$$U = \pm \sqrt{(B^2 + t_{95} P^2)} \quad (\text{Eq. A.3})$$

Where, U = Uncertainty

t_{95} =95th percentile point for the two tailed student 't' distribution.

In a single sample experiment, the result R is a function of k variables x_i ,

$$R = R(x_1, x_2, \dots, x_k) \quad (\text{Eq. A.4})$$

The equation (A.4) is the data reduction equation used for determining R from the measured values of the variables, x_i . It is assumed that the relationship given in the above equation is continuous and has continuous derivatives in the domain of interest, that the measured

variables x_i , are independent of one another. Then the uncertainty in the result is given by,

$$U_R = \sqrt{\left(\frac{\partial R}{\partial x_1} U_{x_1}\right)^2 + \left(\frac{\partial R}{\partial x_2} U_{x_2}\right)^2 + \dots + \left(\frac{\partial R}{\partial x_k} U_{x_k}\right)^2} \quad (\text{Eq. A.5})$$

Where, the U_{x_i} are the uncertainties in the measured variables x_i . In equation (A.5), all of the uncertainties U_{x_i} should be expressed with the same odds or coverage. In most cases, 95% coverage (20:1 odds) is used with the uncertainty in the result then also being at 95% coverage.

2. Error Estimation in Flow Parameters

The errors were calculated based on the accuracy of the instrumentation used in measurements. Following the procedure (Issac 2003) the uncertainties in various parameters are calculated and given hereunder.

Measured variable	Quantity	Instrument
P_o, P_s	Total and static pressure	Pressure probe, micro manometer
T_a	Ambient temperature	Thermometer
P_a	Ambient pressure	Barometer
N	Rotational speed	Tachometer
α	Flow angle	Pressure probe, micro manometer, protractor
ΔP	Pressure rise	Micro manometer

The bias and precision errors for the above instruments, except for the pressure probes, are given in the table.

Instrument	Bias error	Precision error
Thermometer	0.2° C	0.05° C
Barometer	0.2 mm of Hg	0.05 mm of Hg
Protractor	0.5°	0.125°
Micro manometer	0.2mm of water	0.05 mm of water

2.1 Uncertainty in Pressure Measurement

From the errors mentioned above the chief sources of errors in pressure probe measurements were identified as those caused by turbulence, wall vicinity and blockage effects. These errors are considered as bias errors caused by installation effects.

Error Source	Bias error
Turbulence	0.35%
Wall vicinity	0%
Probe blockage	0.4%
Micro manometer	0.2 mm of water

As mentioned earlier, the wall vicinity effect is negligible beyond two probe thickness normal to the wall. By neglecting this effect, the total bias error in the pressures for the remaining region is calculated:

$$\frac{U_p}{P} \left[\left(\frac{B_p}{P} \right)^2 + \left(\frac{P_p}{P} \right)^2 \right]^{\frac{1}{2}} = \pm 2.08\%$$

This magnitude of the bias error in the pressures is taken for the calculation of the bias errors in the other dependant variables.

The precision error by the unsteadiness in the pressures was obtained by sampling. 20 magnitudes of pressures were taken and the precision error was seen to be 2%. Considering the precision error in the micro manometer, which was given as 0.025%, the total precision error involved in pressure measurement is

$$\frac{B_p}{P} = \left[(0.35)^2 + (0.4)^2 + (0.2)^2 \right]^{\frac{1}{2}} = 0.57\%$$

The total error in pressure is

$$\frac{P_p}{P} = \left[(2)^2 + \left(0.05 \times \frac{78}{200} \right)^2 \right]^{\frac{1}{2}} = \pm 2.00\%$$

2.2. Errors in Angle Measurement

The main sources of errors in the measurements angle and the related bias errors are given in the following table.

Source of error	Bias error in angle
Wall vicinity	0.27%
Micro manometer	0.2mm of water
Protractor angle count of traverse mechanism	0.5°

Hence the bias error in the measurement of angle is

$$= \frac{B_\alpha}{\alpha} = \left[(0.27)^2 + \left(\frac{0.2 \times 100}{200} \right)^2 + \left(\frac{0.5 \times 100}{90} \right)^2 \right]^{\frac{1}{2}} = \pm 0.860\%$$

The precision errors, for angle are obtained by sample and is found to be 2%. Considering the precision errors in the micro manometer and protractor, which are 0.05 mm of water and 0.125° and nominal values are 200 mm of water and 90° respectively. So, the total precision errors involved in angle measurements are

$$\frac{P_\alpha}{\alpha} = \left[(2)^2 + (0.025)^2 + \left(\frac{0.125 \times 100}{90} \right)^2 \right]^{\frac{1}{2}} = \pm 2.01\%$$

The total uncertainty in α is $\frac{U_\alpha}{\alpha} = \left[\left(\frac{B_\alpha}{\alpha} \right)^2 + \left(\frac{P_\alpha}{\alpha} \right)^2 \right]^{\frac{1}{2}} = \pm 2.10\%$

2.3. Error in Velocity Measurement

The expression for velocity and its consequent simplification is given below. Also the bias B_C in the velocities is given in terms of the biases in the other variables. The expression for the precision error P_C is the same as that for the bias error with B being replaced by P with the corresponding suffixes.

$$C(\text{velocity}) = \left[\frac{2(\text{dynamic pressure})}{\text{density}} \right]^{\frac{1}{2}} = \left[\frac{2(\Delta P)}{\rho} \right]^{\frac{1}{2}} \quad (\text{Eq. A6})$$

$$\rho(\text{density}) = \frac{(\text{ambient pressure})}{(R)(\text{ambient Temperature})} = \frac{P_a}{RT_a} \quad (\text{Eq. A7})$$

$$C = (\text{constant}) \left[\frac{\Delta P T_a}{P_a} \right]^{\frac{1}{2}} \quad (\text{Eq. A8})$$

$$\frac{B_c}{C} = \left[\frac{1}{4} \left(\frac{B_{\Delta p}}{\Delta P} \right)^2 + \frac{1}{4} \left(\frac{B_{T_a}}{T_a} \right)^2 + \frac{1}{4} \left(\frac{B_{P_a}}{P_a} \right)^2 \right]^{\frac{1}{2}} \quad (\text{Eq. A9})$$

Variable	Bias error	Precision error
ΔP	0.2mm water	0.05 mm of H ₂ O
T_a	2°C	0.5°C
P_a	0.2mm of Hg	0.05mm of Hg

$$\frac{B_c}{C} = \left[\frac{1}{4} \left(\frac{0.2 \times 200}{78} \right)^2 + \frac{1}{4} \left(\frac{0.2 \times 100}{300} \right)^2 + \frac{1}{4} \left(\frac{0.2 \times 100}{950} \right)^2 \right]^{\frac{1}{2}} = \pm 0.259\%$$

$$\frac{P_c}{C} = \left[\frac{1}{4} \left(\frac{0.05 \times 200}{78} \right)^2 + \frac{1}{4} \left(\frac{0.05 \times 100}{300} \right)^2 + \frac{1}{4} \left(\frac{0.05 \times 100}{950} \right)^2 \right]^{\frac{1}{2}} = 0.065\%$$

The total error in velocities is $\frac{U_c}{C} = \left[\left(\frac{B_c}{C} \right)^2 + \left(\frac{P_c}{C} \right)^2 \right]^{\frac{1}{2}} = \pm 0.267\%$

Uncertainties in the velocity components are varying with the angle α .

REFERENCES

1. Arpad Veress., and Vanden Braembussche, R., 2004, "Inverse Design and Optimization of a Return Channel for a Multistage Centrifugal Compressor," ASME Journal of Fluids Engineering, Vol. 126, pp. 799-806.
2. Aungier, R. H, "Aerodynamic Design and Analysis of Vaneless Diffusers and Return Channels." Paper No. 93-GT-101, ASME, New York, 1993a.
3. Aungier, R. H, Centrifugal Compressors, ASME Press, 2000, PP 187-194.
4. B.S. 848, "Fans for general Purposes – Part I: performance testing using standardized airways 1997 (British Standards).
5. Casey, M.V., and Dalbert, P., and Roth, P., "The Use of 3D Viscous Flow Calculations in the Design and Analysis of Industrial Centrifugal Compressors," ASME Journal of Turbomachinery, 1992, Vol.114, PP 27-37.
6. Dean, R.C.Jr., 1974, "The Fluid Dynamic Design of Advanced Centrifugal Compressors," Creare TN-185.
7. Edward S Taylor, "Film Notes for Secondary Flow." Encyclopedia Britannica Educational Corporation, 1968, PP 1-8.
8. Engeda, A., Yunbae Kum, Ronald Aungier, Gregory Direnzi, 2003, "The Inlet Flow Structure of a Centrifugal Compressor Stage and

- its Influence on the Compressor Performance", ASME Journal of Fluids Engineering, Vol.125, pp.779-785.
9. Govardhan, M., 1997, "Uncertainty analysis of experimental data, QIP Short Term Course on Modern Measurement Techniques of Turbomachinery, Indian Institute of Technology, Madras, India, July 1997.
10. Holman, J.P., and Jr. Gajda, "Experimental Methods for Engineers, Mc Graw Hill, 1989.
11. Hathaway, M.D., Chriss, R.M., Wood, J.R., and Strazisar, A.J., 1993, "Experimental and Computational Investigation of the NASA Low Speed Centrifugal Compressor Flow Field," ASME Journal of Turbomachinery, Vol.115, pp.527-542.
12. Inoue, Y., and Koizumi, T., 1983, "Experimental Study on Flow Patterns and Losses in Return Passages for Centrifugal Compressor," ASME Fluids Engineering Division, Vol. 3, Return Passages of Multistage Turbo machinery, pp. 13-21.
13. Inoue, M., and Cumpsty, N.A., 1984, "Experimental Study of Centrifugal Impeller Discharge Flow in Vaneless and Vaned Diffusers," ASME Journal of Engineering for Gas Turbine and Power, Vo.106, pp.455-467.
14. Issac, J.M., 2003, "Performance and flow field measurements in different types of diffusers of centrifugal compressors, PhD. Thesis, Indian Institute of Technology, Madras.

15. Japike D, "Turbomachinery Performance Modeling." Concepts NREC, 2009-01-0307.
16. Klaus Brun and Rainer Kurz, "Analysis of Secondary Flows in Centrifugal Impellers." International Journal of Rotating Machinery, 2005:1, PP 45-52.
17. Lenke, L.J., and Simon, H., 2000, Aerodynamic Analysis of Return Channels of Multi-Stage Centrifugal Compressors," ASME PID-Vol. 5, Challenges and Goals in Industrial and Pipeline Compressors, pp. 117-126
18. Lüdtke, K. H., Process centrifugal compressors, Springer, Berlin, 2004, PP 86-88.
19. Meng, S. Y., and Jackson, E. D., 1983, "The continuous Diffusion Crossover System Design," ASME FED-Vol. 3, Return Passages of Multistage Turbomachinery.
20. Oh, J M., Engeda, A., and Chung, M K., 2005, "A Numerical Study of the U-turn Bend in Return Channel Systems for Multistage Centrifugal Compressors," Proc. I Mech E Vol. 219, part C: J. Mechanical Engineering Science, pp. 749-756.
21. Pazzi S, Martelli F, Michelassi V and Giachi M, "The Use of Artificial Neural Networks for Performance Prediction of Return Channels for Industrial Centrifugal Compressors." Proceedings of ASME-Turbo Expo 2002, PP 1-9.

22. Simon, H., and Rothstein, E., 1983, "On the Development of Return Passages of Multistage Centrifugal Compressors," ASME Fluids Engineering Division, Vol. 3, Return Passages of Multistage Turbo machinery, pp. 1-11
23. Siva Reddy T. Ch "Flow Investigations on Low Solidity Vaned Diffusers of a Centrifugal Compressor Stage", May, 2007, PhD thesis submitted to the faculty of Mechanical Engineering, Osmania University, Hyderabad, India.
24. Sorokes J.M, Kuzdzal M.J, Sandberg M.R and Colby G.M, "Recent experiences in Full Load, Full Pressure Shop Testing of a High Pressure Gas Injection Centrifugal Compressor" TP100prt, Dresser Rand Company, 2000.
25. Sorokes J M , Hutchinson B R, "The Practical Applications of CFD in the Design of Industrial Centrifugal Compressors", ASME PID-Vol. 5, Challenges and Goals in Industrial and Pipeline Compressors, pp. 47-54.
26. Sorokes J.M, Nye D.A, D'Orsi N and Broberg R, "Sidestream Optimisation Through the Use of Computational FluidDynamics and Model Testing" Proceedings of the 29th Turbomachinery Symposium, PP 21-29.
27. Suping WEN, Xiaowen HU, Yong ZHANG, Jun WANG, Tingbin LI, "Optimal r/b Ratio of Bend Channel in Centrifugal Compressor" Front. Energy Power Eng. China 2008, 2(4), PP 381-385

28. Tomitaro Toyokura and Toshiaki Kanemoto, September 1986,
"Studies on Circular cascades for Return Channels of Centrifugal
Turbomachinery" 1st report-Inverse Method and Cascade Design,
Bulletin of JSME, Vol. 29, No. 255, paper: 255-22.
29. Tomitaro Toyokura and Toshiaki Kanemoto, September 1986,
"Studies on Circular cascades for Return Channels of Centrifugal
Turbomachinery" 2nd report-Flows and Performances of Cascades,
Bulletin of JSME, Vol. 29, No. 255, paper: 255-23.